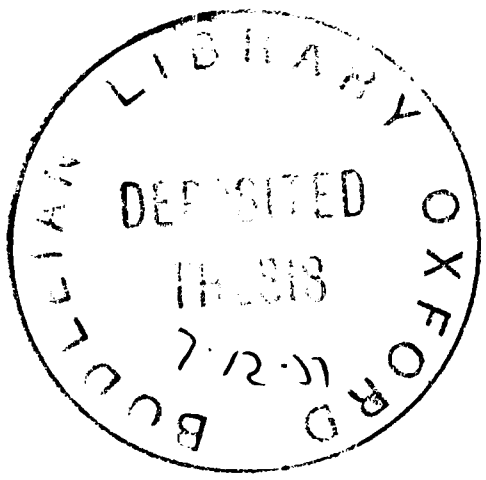
DEVELOPMENT OF AN INTENSE OPTICALLY PUMPED LASER OF NARROW BANDWIDTH IN THE FAR INFRARED

GARY TAYLOR

Keble College



This thesis is submitted in partial fulfilment of the requirements for the Degree of Doctor of Philosophy in the University of Oxford

Department of Engineering Science,
Parks Road, Oxford

September, 1977

TO MY FAMILY

CONTENTS

		Page
	CHAPTER I	
	INTRODUCTION	1
1.1	THE IMPORTANCE OF THOMSON SCATTERING IN PLASMA DIAGNOSTICS	1
1.2	THE WAVELENGTH REQUIREMENT	5
1.3	THE POWER REQUIREMENT	6
	1.3.1 The Constraint Imposed by the Detector NEP	6
	1.3.2 The Constraint Imposed by the Plasma Radiation	9
	1.3.3 Minimum Power Requirement	10
1.4	THE BANDWIDTH REQUIREMENT	10
1.5	SUMMARY OF THE REQUIREMENTS FOR COLLECTIVE THOMSON SCATTERING	11
	CHAPTER II	
	A REVIEW OF PULSED, OPTICALLY PUMPED F I R LASERS: THEIR DISCOVERY AND DEVELOPMENT	13
2.1	THE DISCOVERY OF OPTICALLY PUMPED F I R LASERS	13
2.2	THE OPERATING PRINCIPLES OF AN OPTICALLY PUMPED F I R LASER	14
2.3	THE PUMP LASER MATCHING CONDITION	15
2.4	CAVITY LASERS	18
2.5	SUPER-RADIANT LASERS	22
2.6	OSCILLATOR-AMPLIFIER SYSTEMS	24
	CHAPTER III	
	THE CO_2 LASER SYSTEM	28
3.1	CONSTRUCTION AND CIRCUITRY OF THE CO_2 LASER UNITS	28
3.2	THE CO_2 LASER PULSE SHAPE	32
3.3	CO_2 LASER SYSTEM A	32
3.4	CO_2 LASER SYSTEM B	35
3.5	THE TRIGGER DELAY CIRCUIT	35
3.6	THE GAS MIXTURE CONTROL SYSTEM	36
3.7	SUMMARY OF THE CO_2 LASER PARAMETERS	37

CONTENTS

(continued)

		Page
	CHAPTER IV	
	THE F I R CAVITY LASER	38
4.1	THE MULTIMODE CAVITY	38
4.2	THE 496 μm, CH_3F MULTIMODE CAVITY LASER	41
4.3	THE SINGLE MODE CAVITY	45
4.4	THE 496 μm, CH_3F SINGLE MODE CAVITY LASER	47
4.5	SUMMARY OF THE PROPERTIES OF THE 496 μm, CH_3F CAVITY LASER	54
	CHAPTER V	
	THE SUPER-RADIANT F I R LASER	55
5.1	THE SUPER-RADIANT LASER	55
5.2	THE 496/452 μm, CH_3F LASER	57
5.3	THE 385/359 μm, D_2O LASER	67
5.4	THE 114 μm, D_2O LASER	72
5.5	THE 66/119/50 μm, D_2O LASER	75
5.6	SUMMARY OF THE PERFORMANCE AND CHARACTERISTICS OF THE CH_3F AND D_2O SUPER-RADIANT F I R LASERS	81
	CHAPTER VI	
	THE F I R OSCILLATOR INJECTED SUPER-RADIANT LASER	85
6.1	DESCRIPTION OF THE OSCILLATOR INJECTED SUPER-RADIANT LASER	85
6.2	THE DEPENDENCE OF THE INJECTION LASER BANDWIDTH ON THE INTENSITY OF THE INJECTED F I R RADIATION	89
6.3	OPTIMIZATION OF THE POWER OUTPUT OF THE F I R INJECTION LASER	93
6.4	CONSTRAINTS ON THE OPERATING PRESSURE IN THE 496 μm, CH_3F INJECTION LASER	94
6.5	SUMMARY OF THE PERFORMANCE OF THE 496 μm, CH_3F INJECTION LASER	95
	CHAPTER VII	
	COMPUTER SIMULATION OF THE 496 μm, CH_3F SUPER-RADIANT LASER	97
7.1	THE SLAB MODEL FOR AN OPTICALLY PUMPED SUPER-RADIANT LASER	99
7.2	THE COMPUTER PROGRAM	103
7.3	COMPARISON OF THE COMPUTER SIMULATION WITH EXPERIMENTAL DATA FROM THE 496 μm, CH_3F SUPER-RADIANT LASER	105

CONTENTS

(continued) Page

CHAPTER VIII

CONCLUSIONS AND SUGGESTIONS FOR FUTURE WORK 110

8.1 SUMMARY OF THE MAIN CONCLUSIONS ARISING FROM THE PRESENT WORK 110

8.2 SUGGESTIONS FOR FUTURE WORK 112

8.2.1 An Improved FIR Oscillator Stage 112

8.2.2 A Two Stage FIR Injection Laser System 116

APPENDICES

App. 'A' CALCULATION OF THE TRANSVERSE MODE SPACING FOR A HEMISPHERICAL LASER CAVITY 118

App. 'B' POSSIBLE MECHANISMS FOR THE PRESSURE DEPENDENT FREQUENCY SHIFT IN THE 496 μm, CH_3F LASER 119

App. 'C' THE METAL MESH FABRY-PEROT INTERFEROMETER 122

App. 'D' POSSIBLE PROCESS FOR THE ABSORPTION OF OFF-RESONANT P(20) CO_2 PUMP RADIATION IN CH_3F 124

App. 'E' THE SPECTROSCOPY OF THE OPTICALLY PUMPED D_2O AND CH_3F FIR LASERS 127

App. 'F' THE SPECTROSCOPY OF THE CO_2 LASER 133

REFERENCES 136

ACKNOWLEDGEMENTS

I debated with myself for some time over the order in which I should present the names of those I wished to thank. In the end I made a compromise and decided to list them alphabetically.

My sincerest thanks to Drs D.E. Evans, R.N. Franklin, S.M. Hamberger, D.A. Huckridge, B.W. James, W.A. Peebles and L.E. Sharp, for their encouragement, help, criticism, and for tolerating me during the past three years.

I would also like to express my thanks to Mr A.S. Furzer, who introduced me to the Culham computer and helped to resolve some of my programming problems, and Mr R.A. Guinee, who supplied and operated the gallium doped germanium detector. I extend my thanks also to the many others, both at Oxford and Culham, who have assisted me at various times and helped to keep me moderately sane.

I gratefully acknowledge the Science Research Council who have given me financial support during the period of this work.

Finally, as so many have done before me, I thank Ina Godwin for typing and laying out my thesis.

"I could have done it in a much more complicated way"
said the red Queen, immensely proud.

Lewis Carroll

There is something fascinating about science, one
gets such wholesale returns of conjecture out of
such a trifling investment of fact.

Mark Twain.

DEVELOPMENT OF AN INTENSE OPTICALLY PUMPED LASER OF NARROW BANDWIDTH IN THE FAR INFRA-RED

G. Taylor, Keble College

A thesis submitted for the degree of Doctor of Philosophy
in the University of Oxford, September, 1977.

ABSTRACT

This thesis describes an experimental study of high intensity, pulsed, optically pumped, far-infrared (F I R) lasers. The work was motivated by the need for a radiation source for the measurement of the ion temperature in magnetically confined, high temperature plasmas (e.g. tokamak plasmas), using Thomson scattering. Constraints imposed by the plasma parameters, the scattering geometry and available detector sensitivities lead to the requirement of a radiation source wavelength between 30 μm and 1 mm and a source power $\geqslant$ 1 MW in a bandwidth $\leqslant$ 60 MHz.

Results are presented for a 496 μm, 500 watt, methyl fluoride (CH_3F) cavity laser, with a bandwidth of < 30 MHz, which was optically pumped by a 9.55 μm CO_2 laser. Results are also presented for an optically excited mirrorless, super-radiant, CH_3F laser, which generated over 0.6 MW of F I R radiation within a bandwidth of about 300 MHz. The performance of this laser has also been simulated by a computer model, which allows the optimum operating parameters to be predicted.

An assembly constructed on the principle of the injection laser, in which low power narrow-band oscillator radiation is used to control the output of a super-radiant system, has been used to generate 250 kW of 496 μm radiation, with a bandwidth of < 60 MHz.

Investigations of the F I R output from heavy water vapour (D_2O) in a super-radiant laser assembly, optically excited by several different CO_2 laser wavelengths, have resulted in the generation of 60 ns (F W H M) pulses of F I R radiation with average powers of 1.3, 9.2 and 15.8 MW, at wavelengths of 385, 119 and 66 μm, respectively. All these lasers were found to have a higher CO_2 to F I R photon conversion efficiency than the 496 μm CH_3F laser. In addition, the energy level spacing in D_2O is such that the molecule can generate narrow bandwidth radiation more readily than the CH_3F molecule. From this work it is concluded that an injection laser assembly, similar to that used with CH_3F, but containing D_2O vapour, optically pumped by a 9.26 μm CO_2 laser and generating several megawatts of 385 μm radiation, would satisfy the source requirements mentioned above.

CHAPTER I

INTRODUCTION

The work presented in this thesis is an experimental study of high intensity, pulsed, optically pumped far-infrared lasers[†]. This research was motivated by the need for a suitable far-infrared (F I R)[*] source for the investigation of magnetically confined high temperature plasma by Thomson scattering. In this introductory chapter we will derive the power, bandwidth and wavelength requirements which a diagnostic of this kind must fulfil.

1.1 THE IMPORTANCE OF THOMSON SCATTERING IN PLASMA DIAGNOSTICS

One important plasma parameter, the ion temperature (T_i), is at present deduced from the energy distribution of neutrals emitted from the plasma following charge exchange interactions. Doppler line broadening due to plasma impurities has also been used to infer T_i, although this is generally considered to be somewhat unreliable, requiring confirmation by neutral particle detection methods. Neutral particle detection is a line of sight method and cannot therefore give information concerning local variations in T_i. In future fusion plasma devices the neutral particles which escape will have made many charge exchange collisions as a result of the higher plasma densities and greater dimensions of the next generation of machines (BERRY et al, 1976 and T F R Group, 1976). A different method of ion temperature measurement is therefore required.

The spatial distribution of ion temperature can be determined, in principle, from the spectrum of radiation scattered from a collimated beam

---

† In this thesis we will only discuss optically pumped F I R lasers: for brevity we will refer to these devices as 'F I R lasers'.

* In the present work the far-infrared region is defined as referring to electromagnetic radiation with a free space wavelength between 30 μm and 2 mm.

of electromagnetic radiation, by electron density correlations in the plasma (DeSILVA and GOLDENBAUM, 1970; EVANS and KATZENSTEIN, 1969 and SHEFFIELD, 1975). This method also allows the measurement of other details of the ion distribution. For example it has been suggested (EVANS and YEOMAN, 1974) that the degree of impurity could be determined, since the spectrum of radiation Thomson scattered by ion-acoustic fluctuations in the plasma, depends on the relative concentration of all the ions, including impurities. However, the Thomson scattering cross-section (σ) per electron is very small ($\sim 5 \times 10^{-26}\ cm^2$) and thus necessitates the use of an intense, well collimated, radiation source.

The power scattered in the frequency interval ω to $\omega + \Delta\omega$, when radiation of power I_0 is incident on a volume of plasma, V, is given by:

$$I(\underset{\sim}{k},\omega)\Delta\omega = \frac{I_0}{\pi r^2}\,\sigma\, n_e\, V\, \Omega\, S(\underset{\sim}{k},\omega)\Delta\omega \qquad \ldots (1.1)$$

where r is the radius of the incident radiation beam,

n_e is the electron density and Ω is the solid angle over which the scattered radiation is collected.

$I(\underset{\sim}{k},\omega)$ can be conveniently divided into two components, commonly known respectively as the electron feature and the ion feature, because of their great disparity in frequency width, the former being associated purely with the electron motions and the latter being affected by the ion parameters The total profile, including both the electron and ion features is represented by the dynamic form factor $S(\underset{\sim}{k},\omega)$, illustrated in Fig.1.1. $\underset{\sim}{k}$ is the scattering wave vector, which can be most readily defined by the vector diagram of the scattering interaction shown in Fig.1.2. From the geometry of this figure and for a non-relativistic plasma†

---

† For a non-relativistic plasma the electron thermal velocity is much less than the velocity of light, thus the Doppler shift due to the electron velocity is much less than the incident radiation frequency and $|\underset{\sim}{k}_0| \approx |\underset{\sim}{k}_s|$.

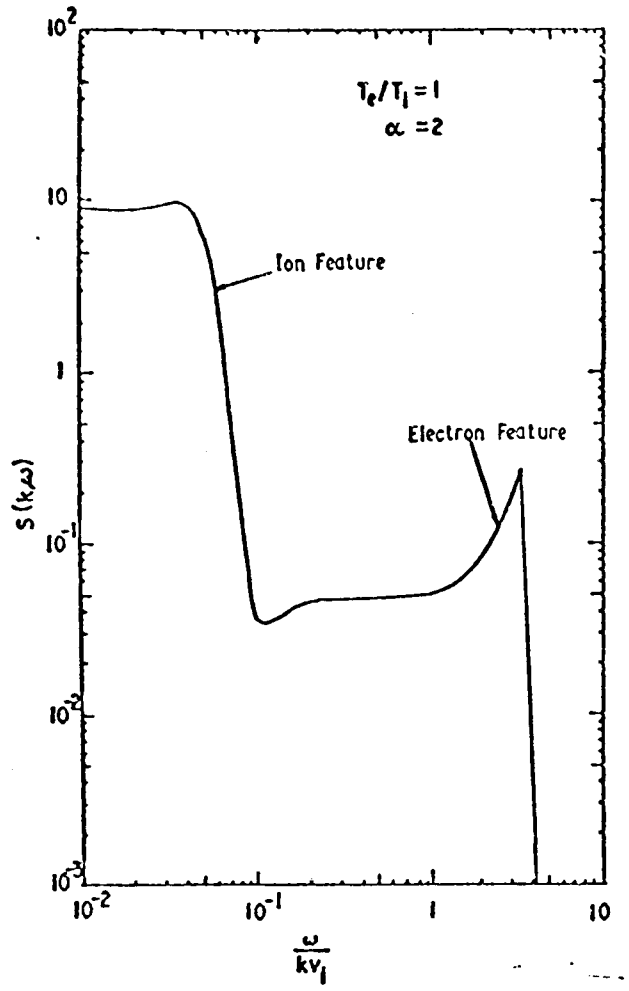


Fig.1.1
The scattered radiation intensity as a function of ω/kv_i

$$|\underset{\sim}{k}| = |\underset{\sim}{k}_s - \underset{\sim}{k}_0| = 2|\underset{\sim}{k}_0|\sin(\theta/2)$$
$$= \frac{4\pi}{\lambda_0}\sin(\theta/2) \qquad \ldots (1.2)$$

where λ_0 is the wavelength of the incident radiation, θ is the scattering angle, $\underset{\sim}{k}_0$ is the incident wavevector and $\underset{\sim}{k}_s$ is the wavevector of the radiation after scattering has taken place.

The shape of the scattered radiation profile is produced by Doppler shifts in the incident radiation frequency, due to the motion of electrons in the plasma. But the ions can also influence the scattered radiation spectrum since the electrons form charge clouds about the ions with dimensions of the order of the Debye length (λ_D) given by:

$$\lambda_D = \left(\frac{k_B T_e}{4\pi n_e e^2}\right)^{\frac{1}{2}} \qquad \ldots (1.3)$$

where k_B is Boltzmann's constant, T_e is the electron temperature and e is the electronic charge. The contribution of these clouds to the Fourier components of the spatial electron density fluctuations, strongly influences the scattered radiation spectrum for incident radiation wavelengths greater than λ_D, and this is referred to as the 'collective' regime.

We now define a dimensionless quantity, α, such that

$$\alpha = \frac{\text{scattering scale length}}{\text{Debye length}} = \frac{1}{k\lambda_D} \quad . \qquad \ldots (1.4)$$

Combining (1.2) and (1.4) we obtain:

$$\alpha = \frac{\lambda_0}{4\pi\lambda_D \sin(\theta/2)} \qquad \ldots (1.5)$$

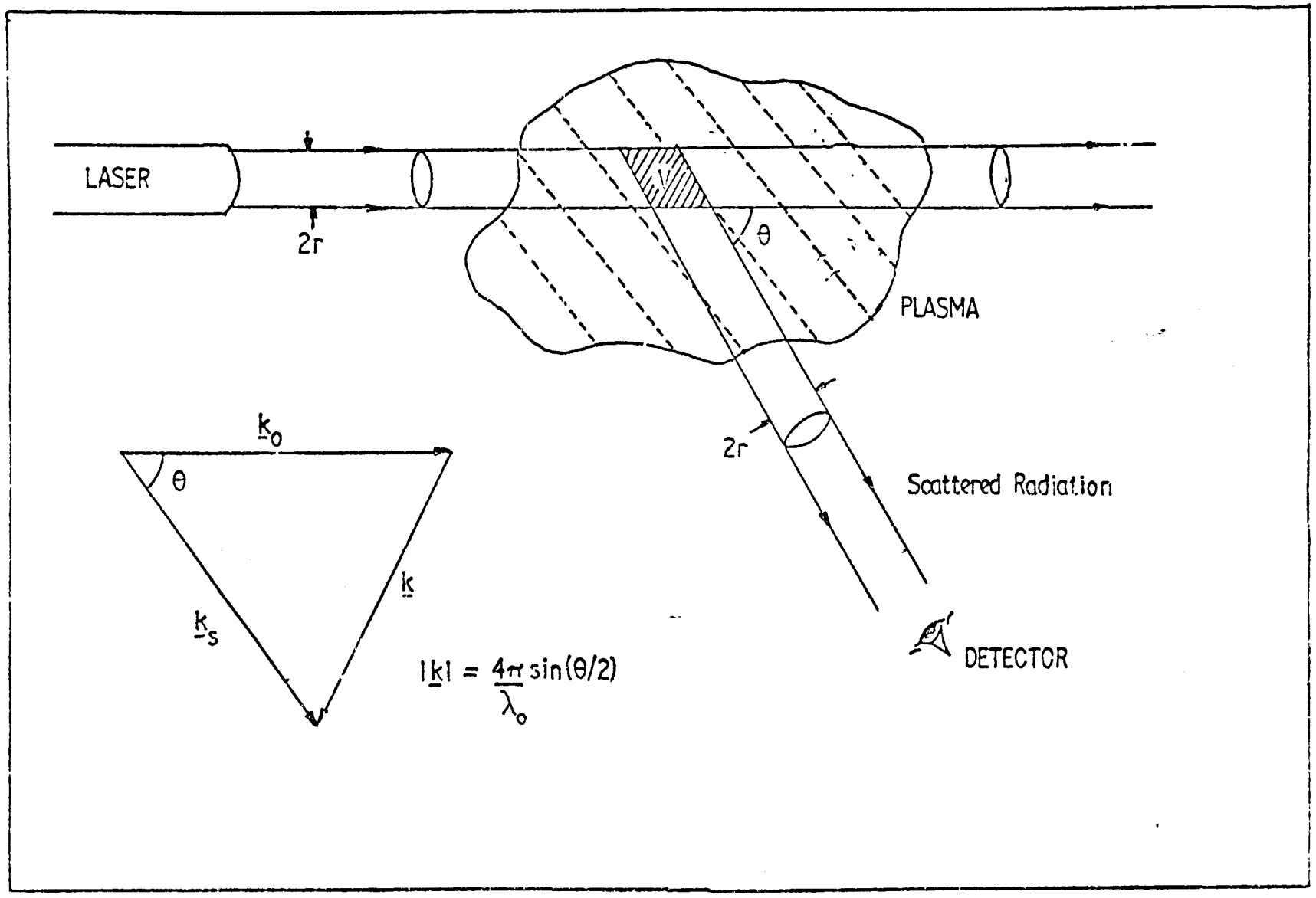


Fig.1.2
The geometry of a Thomson scattering experiment

The fraction of light scattered into the ion feature is given by:

$$F_i = \frac{\alpha^4}{(1+\alpha^2)^2} \qquad \ldots (1.6)$$

so that for $\alpha \ll 1$ the ion term of $S(\underset{\sim}{k},\omega)$ is negligibly small, whilst for $\alpha \gtrsim 1$ the ion motion influences the spectrum, and contributes about 90% of the scattered radiation for $\alpha \gtrsim 3$. Therefore by arranging the radiation wavelength and the scattering angle so that $\alpha \gtrsim 1$ it is possible, in principle, to determine the plasma ion temperature.

In the following sections we derive the requirements which must be satisfied by a radiation source which would be suitable for the measurement of T_i. In order to obtain these requirements we must consider the constraints imposed by the plasma parameters, the scattering geometry and the available detector sensitivites.

1.2 THE WAVELENGTH REQUIREMENT

It can be seen from equation (1.5) that α depends on both λ_0 and θ, so that it would appear possible to obtain any value of α for a given λ_0 by making θ small enough. However, for small θ (i.e. $\theta \leqslant 1^\circ$) the resolution is poor both spatially and in k, and the angular spread of the beam, due to diffraction effects in the input optics and refraction in the plasma, results in the incident radiation reaching the detector. In addition the necessarily small collection solid angle results in less radiation reaching the detector than is possible at large scattering angles. It is therefore generally advantageous to work at scattering angles larger than 1° and if possible greater than 10°.

For a typical tokamak plasma in which $T_e \approx 1$ keV and $n_e \approx 5 \times 10^{13}\,\mathrm{cm}^{-3}$ equation (1.3) gives $\lambda_D \approx 30\,\mu\mathrm{m}$. Therefore for the constraints on θ and α discussed above (namely $\theta \gtrsim 10^\circ$ and $\alpha \gtrsim 1$) equation (1.5) gives a minimum incident radiation wavelength $\sim 30\,\mu\mathrm{m}$.

The long wavelength limit for the radiation source is set by the electron plasma frequency (ω_{pe}), since electromagnetic radiation with a frequency lower than this value will not propagate in the plasma. ω_{pe} is given by the expression:

$$\omega_{pe} = \left(\frac{4\pi n_e e^2}{m_e}\right)^{\frac{1}{2}} \qquad \ldots (1.6)$$

where m_e is the electron mass. For a plasma with a peak electron density of $5 \times 10^{13}\,cm^{-3}$ equation (1.6) gives a long wavelength limit of 5 mm. However refraction effects in the plasma can be serious even at frequencies several times higher than ω_{pe} (BROSSIER and BLANKEN, 1974), so that in practice the long wavelength limit is ~ 1 mm.

To summarize, therefore, we may give the wavelength requirement for a radiation source as:

$$\boxed{1\,mm \gtrsim \lambda_0 \gtrsim 30\,\mu m} \quad \text{The Wavelength Requirement}$$

1.3 THE POWER REQUIREMENT

We now derive the minimum power requirement, this can be determined by imposing the condition that the scattered radiation reaching the detector must adequately exceed both the noise equivalent power (NEP) of the detector and the plasma emission near the source wavelength.

1.3.1 The Constraint Imposed by the Detector NEP

The scattered power falling on the detector must be greater than the minimum detectable power, which leads to the condition:

$$I(\underset{\sim}{k},\omega)\Delta\omega > \frac{N_d}{2\pi}\,\Delta\omega\,\rho \qquad \ldots (1.7)$$

where ρ is the signal-to-noise ratio of the receiver and N_d is the NEP of the detector. Combining equations (1.1) and (1.7) we have the condition:

$$I_0 > \frac{N_d \rho r^2}{2\sigma n_e V \Omega S(\underset{\sim}{k},\omega)} \qquad \ldots (1.8)$$

From the scattering geometry of Fig.1.2 it can be shown that the scattering volume, taken as the intersection of two circular cylinders, radius r, is

given by:

$$V = \frac{16}{3} \frac{r^3}{\sin\theta} \qquad \ldots (1.9)$$

Two other constraints must be imposed. First, V must be sufficiently large to contain several scalelengths, otherwise $\underset{\sim}{k}$ will be ill-defined, since a broadband of Fourier components of the spatial distribution of electron density will be observed simultaneously†. From geometry, the number of scale lengths in the scattering volume, η, is given by:

$$\eta = \frac{4r}{\lambda_0} \tan(\theta/2). \qquad \ldots (1.10)$$

Second, if a heterodyne detection system is employed Ω must satisfy the van Cittert-Zernicke theorem in order that the scattered beam should be coherent across the detector. This imposes the condition $\pi r^2 \Omega \leqslant \lambda_0^2$, so we have the constraint:

$$\pi r^2 \Omega = \lambda_0^2 \qquad \ldots (1.11)$$

For video detection this condition need not be satisfied and the maximum Ω is determined by the size limit for aberration free optics. However, in the calculations which follow we shall consider only heterodyne detection, since the NEP for this type of detection system can be reduced by many orders of magnitude, in the FIR regime, provided sufficient local oscillator signal is used.

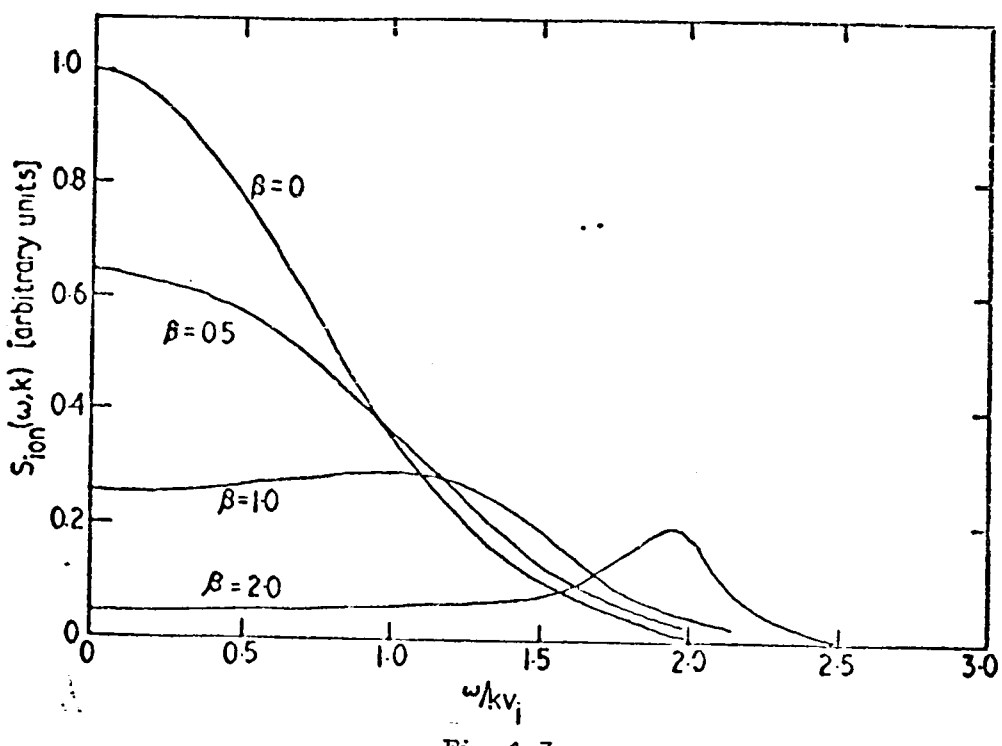


Fig.1.3
The dynamic form factor for the ions, $S_{ion}(\omega,k)$ against (ω/kv_i) for various values of β

Figure 1.3 shows the ion feature, $S_{ion}(\omega,\underset{\sim}{k})$, for various values of the parameter β given by:

---

† The theoretical analysis used to derive $S(\underset{\sim}{k},\omega)$ actually assumes many collective wavelengths in the scattering volume.

$$\beta^2 = \frac{\alpha^2}{(1+\alpha^2)}\, Z\, \frac{T_e}{T_i} \qquad \ldots (1.12)$$

where Z is the ionic charge. From this figure it can be seen that $S_{ion}(\omega,\underset{\sim}{k})$ can be approximated to a rectangular function for $\beta \approx 1$, with a width $\approx 2kv_i$, where v_i is the ion thermal velocity. Therefore:

$$S_{ion}(\omega,\underset{\sim}{k}) \approx \frac{S_i(\underset{\sim}{k})}{2\,k\,v_i} \qquad \ldots (1.13)$$

where $v_i = (2\,k_B\,T_i/M_i)^{\frac{1}{2}}$, M_i being the ionic mass,

and $S_i(\underset{\sim}{k}) = \int S_{ion}(\underset{\sim}{k},\omega)\,d\omega$. Thus substituting equations (1.9), (1.10), (1.11) and (1.13) into equation (1.8) gives the condition $I_0 \geq I_{min}$ where:

$$I_{min} = \frac{3\pi}{8n_e} \cdot \frac{\eta}{\lambda_0^2 \sigma} \cdot \frac{N_d \rho}{S_i(\underset{\sim}{k})} \sqrt{\frac{2k_B T_i}{M_i}} \cos^2\left(\frac{\theta}{2}\right) \sin\left(\frac{\theta}{2}\right) \qquad \ldots (1.14)$$

and

$$S_i(k) = \frac{Z\,\alpha^4}{(1+\alpha^2)\left\{1+\alpha^2\left(1+Z\,\frac{T_e}{T_i}\right)\right\}}$$

I_{min} has been evaluated from equation (1.14) for a plasma with $T_i = 1$ keV and $n_e = 5 \times 10^{13}\,cm^{-3}$ and the calculated values for I_{min} are tabulated in Table 1.1 for $\theta = 10°$, $30°$ and $90°$. The value of λ_0 used in this table is 500 μm, which is well within the wavelength range suggested in section 1.2. A value of $10^{-17}\,W\,Hz^{-1}$ was used for N_d which is a typical NEP for Schottky diodes working at this wavelength and η was set arbitrarily equal to 10.†

TABLE 1.1

THE MINIMUM POWER FOR $\theta = 10°, 30°$ AND $90°$

θ	$10°$	$30°$	$90°$
α	14	5	1.7
$S_i(k)$	0.5	0.47	0.32
I_{min}	0.4 MW	1.2 MW	2.6 MW
$T_e = T_i = 1$ keV		$N_d = 10^{-17}\,W\,Hz^{-1}$	
$\rho = 4$		$\eta = 10$	
$n_e = 5 \times 10^{13}\,cm^{-3}$		$\lambda_0 = 500$ μm	

† For ruby laser scattering measurements of T_e, η can be as large as 10^4, so that $\eta = 10$ should be taken as a minimum practical value.

1.3.2 *The Constraint Imposed by the Plasma Radiation*

From Table 1.1 it is clear that powers $\geqslant 1$ MW are required for $\theta \sim 30°$. The above calculation only considers the limitation imposed by the detector sensitivity; however a further constraint is set by the plasma emission at the radiation source wavelength.

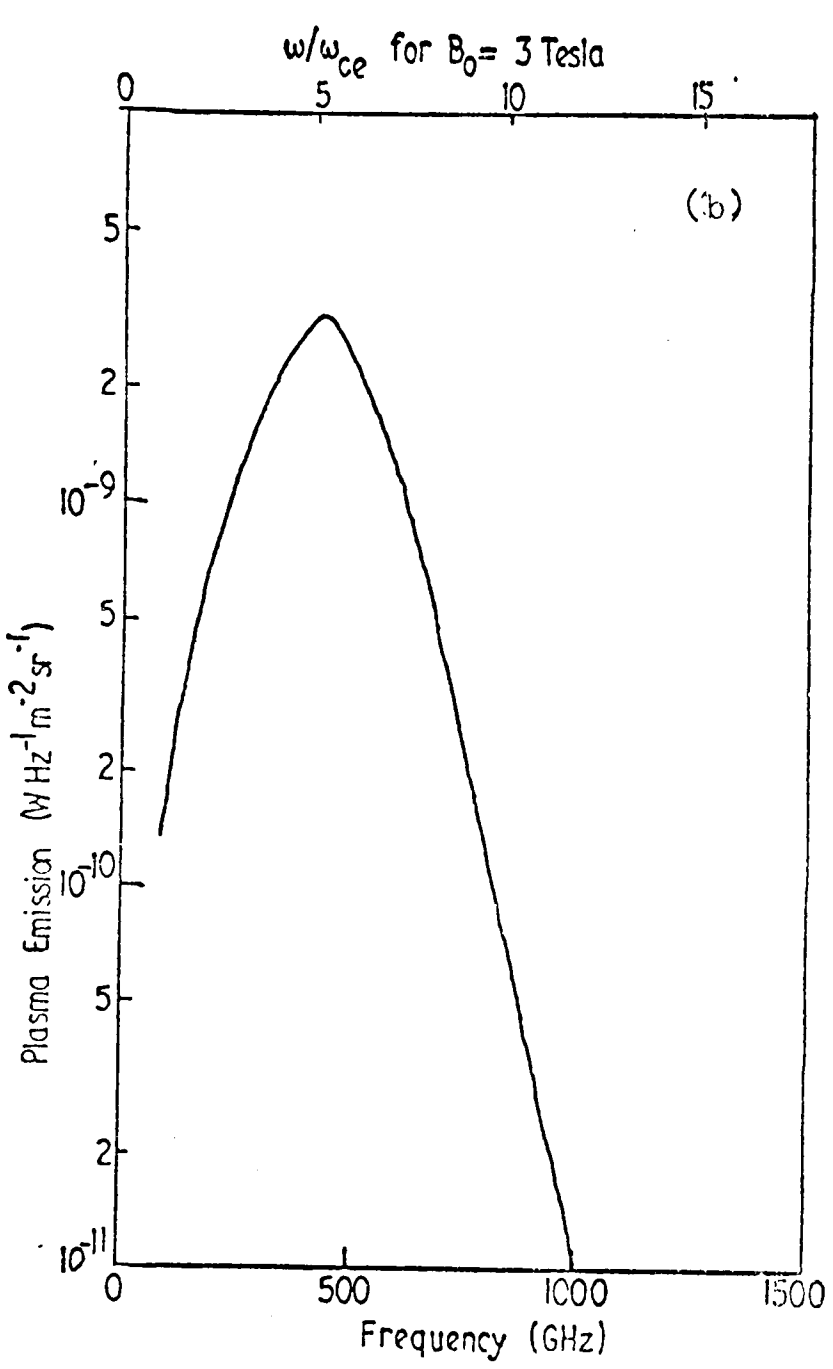
When $I_0 = I_{min}$, so that equation (1.14) is satisfied, the power density of the radiation scattered by the plasma is given by:

$$I_p = \frac{N_d \rho}{\pi r^2 \Omega} \, W\,m^{-2}\,Hz^{-1}\;\; sr^{-1}$$

and so imposing the coherence condition in equation (1.11) we obtain:

$$I_p = \frac{N_d \rho}{\lambda_0^2}$$

When this expression is evaluated for the values of N_d, ρ and λ_0 used in Table 1.1 we obtain a value of $I_p \approx 10^{-10}\,W\,m^{-2}\,Hz^{-1}\,sr^{-1}$. BROSSIER et al, (1976) have measured the emission from several tokamak devices, in particular they measured the emission spectrum from plasma in TFR for $n_e \sim 5 \times 10^{13} m^{-3}$, $T_e \sim 1.8$ keV and a magnetic field of 3.9 Tesla, their results are summarized in Fig.1.4(a). The plasma emission peaks at harmonics of the electron cyclotron frequency, the maximum of the cyclotron emission envelope being about $2 \times 10^{-10}\,W\,m^{-2}\,Hz^{-1}\,sr^{-1}$, comparable to the scattered power calculated above. This behaviour has been predicted by a computational model and calculations by COSTLEY et al (1975) for the proposed JET device, which will be considerably larger than present tokamaks, are shown in Fig. 1.4(b). The plasma emission at 600 GHz is seen to be around $10^{-9}\,W\,m^{-2}\,Hz^{-1}\,sr^{-1}$, which would require an order of magnitude increase in the calculated minimum power shown in Table 1.1. However, the actual plasma emission at the frequency of the source will depend where the source frequency falls relative to the harmonics of the electron cyclotron frequency, so that $10^{-9}\,W\,m^{-2}\,Hz^{-1}\,sr^{-1}$ represents the worst case condition.



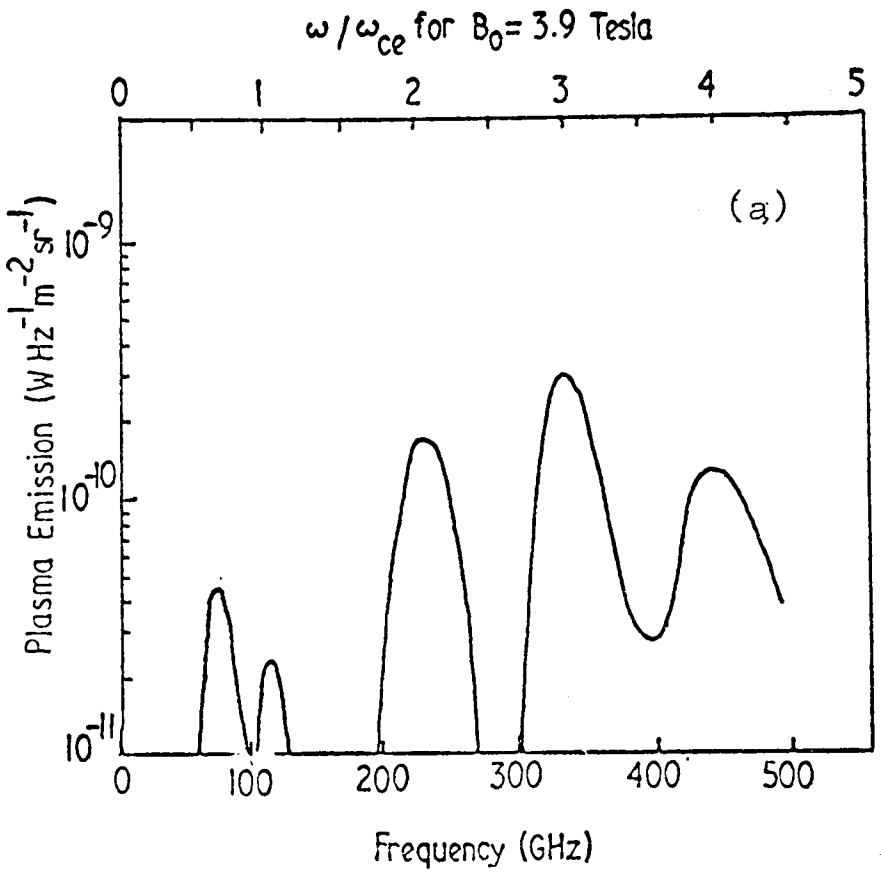


Fig.1.4

(a) Cyclotron emission results for TFR, $T_e = 1.8\,keV$, $n_e = 5 \times 10^{13}\ cm^{-3}$

(b) Predicted cyclotron emission for JET.

1.3.3 *Minimum Power Requirement*

In summary then, calculations for the minimum source power which only include the NEP of the detector suggest powers of around 1 MW for $\theta \sim 30°$. When plasma emission is also included, this power level is found to be only just adequate to allow the scattered power to exceed the plasma cyclotron emission in the present generation of tokamaks. In the next generation of tokamaks the minimum laser power requirement is determined almost entirely by the cyclotron emission level and this will become especially true as the sensitivity of available fast FIR detectors improves. We therefore have an estimate of the minimum power requirement, namely:

$$\boxed{I_{min} > 1 \text{ MW}} \quad \text{The Power Requirement}$$

1.4 THE BANDWIDTH REQUIREMENT

Since the measurement of T_i depends on adequately resolving the ion feature of $S(\underset{\sim}{k},\omega)$, the radiation source bandwidth, $\Delta\nu_0$, must be significantly narrower than the ion feature, given roughly by

$$\Delta\nu_{ion} \approx \frac{kv_i}{2\pi}$$

(see section 1.3.1 and Fig.1.3). Typical values of $\Delta\nu_{ion}$ for $T_i = 1$ keV and $\lambda_0 = 500\,\mu m$ are given in Table 1.2.

TABLE 1.2

CALCULATED ION FEATURE WIDTHS FOR $T_i = 1$ keV AND $\lambda_0 = 500\,\mu m$

θ	10°	30°	90°
α	14	5	1.7
$\Delta\nu_{ion}$	110 MHz	290 MHz	880 MHz

It should be possible to obtain $\Delta\nu_{ion}$ and hence T_i for $\Delta\nu_0 \leqslant \Delta\nu_{ion}/2$, however to determine the proportion of impurities in a plasma would require the measurement of the shape of the ion feature (EVANS and YEOMAN,

1974) and this would require $\Delta\nu_0 \leqslant \Delta\nu_{ion}/5$. Thus from Table 1.2, $\Delta\nu_0$ must satisfy the condition:

$\Delta\nu_0 \leqslant 60$ MHz	The Bandwidth Requirement

1.5 SUMMARY OF THE REQUIREMENTS FOR COLLECTIVE THOMSON SCATTERING

The radiation source requirements for collective Thomson scattering can be summarized as shown in Table 1.3.

TABLE 1.3

THE RADIATION SOURCE REQUIREMENTS

Wavelength: Requirement	1 mm $\geqslant \lambda_0 \geqslant$ 30 μm
Power Requirement	$I_{min} >$ 1 MW
Bandwidth Requirement	$\Delta\nu_0 \leqslant$ 60 MHz

To generate the narrow linewidths and high powers required it is, in practice, necessary to use a laser source, but until recently there were very few laser sources in the F I R wavelength region to which we are constrained.† Optically pumped F I R lasers, the subject of the present work, have however made considerable progress in the last few years and they are now close to meeting the requirements in Table 1.3. The value of high power optically pumped F I R lasers for plasma diagnostics in nuclear fusion research has already been stressed by several authors (JASSBY et al, 1974 and LAX and COHN, 1974), and it is in this field that these devices might well find their most important application in the near future.

We review the development of these devices, in the seven years since their discovery, in Chapter II. Chapter III describes the CO_2 laser system

† H C N discharge excited lasers being the most powerful up to about 1973. These devices produced less than 1 kW of pulsed 337 μm laser radiation (SHARP and WETHERALL, 1972)

used to pump the F I R lasers investigated in the present work, and the performance of a 500 watt narrow line width, methyl fluoride (CH_3F), F I R cavity laser is presented in Chapter IV. In Chapter V, experimental investigations of multimegawatt, D_2O (heavy water) and CH_3F, super-radiant laser systems are discussed. Chapter VI describes an oscillator injected, super-radiant CH_3F configuration, which combines the narrow bandwidth characteristics of the cavity laser with the high power of the super-radiant laser. In Chapter VII we describe a computer model of a 496 μm , CH_3F, super-radiant laser. Finally, in Chapter VIII, the degree to which presently developed F I R lasers can fulfil the requirements for a F I R scattering system will be discussed, together with suggestions for future work.

CHAPTER II

A REVIEW OF PULSED, OPTICALLY PUMPED F I R LASERS: THEIR DISCOVERY AND DEVELOPMENT

Until recently the F I R region of the electromagnetic spectrum has suffered from a dearth of good radiation sources with a wide spectral coverage. This is despite attempts to extend microwave techniques into the submillimetre regime via harmonic generation, and the development of various discharge excited lasers (e.g. HCN, H_2O), which suffer from problems due to chemical decomposition and poor stability (SHARP and WETHERALL, 1972, CROCKER et al, 1964 and GEBBIE et al, 1964).

This chapter reviews the recently developed pulsed optically pumped F I R lasers which offer, for the first time, the ability to produce laser action at hundreds of different wavelengths throughout the F I R regime with powers of many megawatts.

2.1 THE DISCOVERY OF OPTICALLY PUMPED F I R LASERS

The operation of a pulsed optically pumped F I R laser was first reported by CHANG and BRIDGES in 1970. They discovered laser action in methyl fluoride (CH_3F) whilst investigating the use of the gas in a saturable absorber (CHANG, WANG and CHEO, 1969), for a CO_2 laser working at a wavelength of 9.55 μm .

The CH_3F molecule was found to produce passive Q-switching of the CO_2 laser at comparitively low gas pressures ($\sim$ 0.1 torr), which suggested a rapid saturation of the resonant absorption in CH_3F . The ν_3 vibrational mode (Appendix E, Fig.E.1), excited in CH_3F by the absorption of CO_2 laser photons, is sparsely populated at room temperature and thus selective excitation of molecules to the J = 12 rotational level in this vibrational band is a possible mechanism for population inversion.

Chang and Bridges observed laser radiation at three wavelengths, namely 452, 496 and 541 μm. The 452 μm line arises from the depopulation of the J = 12 level of the vibrational ground state and corresponds to the J = 13→12 transition (see Fig.E.2(a)). The 496 μm and 541 μm lines are emitted as a result of the J = 12→11 and J = 11→10 transitions in the ν_3 vibrational band, respectively.

Chang and Bridges used a relatively small, 1.5 kW peak power, Q-switched CO_2 laser which produced a laser pulse with a duration of about 0.3 μs. However, despite the low pump power, their cavity F I R laser (Fig.2.2(a)) produced ~ 0.1 watts in a pulse of approximately 1 μs duration. Indeed, the 496 μm CH_3F laser is still one of the most efficient and powerful F I R lasers discovered in the past seven years.

2.2 THE OPERATING PRINCIPLES OF AN OPTICALLY PUMPED F I R LASER

In this section we give only a simplified outline of the principles on which optically pumped F I R lasers operate. A more detailed and specific description of the CH_3F and D_2O optically pumped F I R lasers investigated in this thesis, together with their spectroscopy, is given in Appendix 'E'.

The operation of an optically pumped F I R laser can most readily be illustrated by a partial energy level diagram, such as that shown in Fig.2.1. The lower vibrational state in this figure is either a low lying vibrational level or the vibrational ground state of a molecule in the laser medium. Each vibrational state has a number of rotational levels which are characterised by the total rotational quantum number, J, which can take values of 0, 1, 2, ... Each J level is then further subdivided into a series of K levels, which arise from the orientation of the dipolar axis with respect to the axis of rotation of the molecule, where K can take the

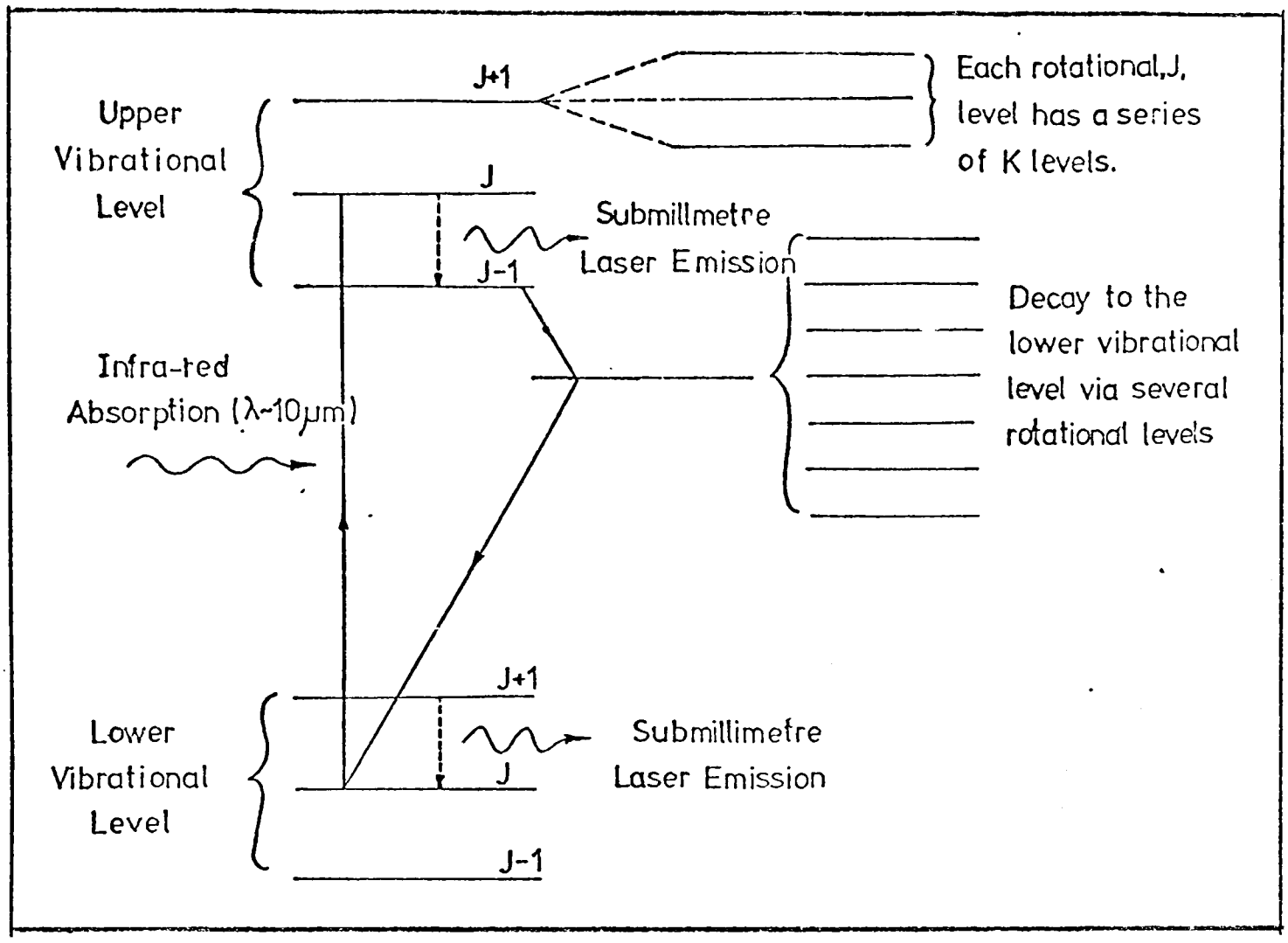


Fig.2.1
Partial energy level diagram to illustrate the operation of an optically pumped F I R laser

values $0, \pm 1, \pm 2, \ldots \pm J$. A near infrared laser is used to excite the molecular gas from some rotational level in the lower vibrational state to another rotational level in the upper vibrational state. Inversion between rotational levels in the upper vibrational manifold is thus readily established if this level has a small thermal population with respect to the lower vibrational manifold. If the molecule has a permanent dipole moment, laser action can then be obtained between rotational levels in the upper vibrational manifold. Population inversion can also arise between rotational levels in the lower vibrational state, as a result of the selective depopulation of the rotational levels by the near infra-red pump radiation.

2.3 THE PUMP LASER MATCHING CONDITION

Over the last six years about 600 different F I R laser lines have been generated by optically pumped lasers. Their wavelengths range from 30 to 2000 μm, (YAMANAKA, 1976; ROSENBLUH et al, 1976; CHANG, 1974 and

GALLAGHER et al, 1977), the large majority of these lines being generated by optically pumping molecular gases with a CO_2 laser. However many of these laser lines have been generated with comparatively low efficiencies, this being due to a mismatch between the pumping and absorption frequencies.

Several different processes have been inves igated which bring the pump and absorption lines into resonance. FETTERMAN et al (1972) have optically pumped the Q(5,3) transition of NH_3 with the P(32) (10.6 μm band) CO_2 laser line even though the separation between the pump and absorption lines is about 950 MHz and the CO_2 laser, which was operated at 30 torr, had a frequency width of only 250 MHz. They interpret this 'off resonant optical pumping' (OROP) effect as resulting from saturation broadening of the absorbing transition by the intense pump radiation.

If the pump laser frequency (ω_0) is several linewidths from the frequency of the absorbing transition (ω) in the optically pumped medium, then the population difference (ΔN) between the upper and lower states in the absorbing transition is given by †

$$\Delta N \approx \frac{N_0}{\left(1 + \left(\frac{\mu E}{\hbar(\omega-\omega_0)}\right)^2\right)} .$$

Where E is the electric field associated with the pump radiation, N_0 is the population of the lower state in the absence of the laser pump, and μ is the dipole matrix element for the absorbing transition. For $\mu E \geqslant (\omega-\omega_0)\hbar$ $\Delta N \leqslant N_0/2$ and thus an appreciable proportion of the population resides in the upper state.

The dipole matrix element for the Q(5,3) absorption line of NH_3 is approximately 0.12 Debye (0.39×10^{-30} Cm) and for the pump intensities used by FETTERMAN et al (1972), namely 7 GW/m^2, $\mu E/h \approx 1.4$ GHz. Thus with

---

† Off resonant pumping is discussed in several publications and in particular by PANTELL and PUTHOFF (1969) and SHIMODA and SHIMIZU (1972).

experimentally realisable pump intensities a frequency mismatch of several GHz is tolerable.

Recently it has been suggested (PETUCHOWSKI et al, 1977 and CHANG and McGEE, 1976) that the Q (5,3) transition, and several other laser lines in optically pumped NH_3, and other gases, may result from stimulated Raman emission. PETUCHOWSKI et al (1977) have investigated optically pumped 66 and 50.3 μm D_2O lasers, and they found that the CO_2 pump laser detuning was equal to the frequency difference between the molecular absorption transition in D_2O and the frequency of the FIR radiation. This is a strong indication of a Raman effect. In addition, CHANG and McGEE (1976) have operated optically pumped NH_3 and C_2H_4 lasers involving molecular transitions whose populations cannot be inverted. They explain the operation of these lasers in terms of a Raman type two quantum process. Since the CO_2 lasers used to pump these Raman lasers also have a linewidth of several GHz it is, in principle, possible to tune the FIR laser emission through several GHz, simply by tuning the CO_2 laser pump frequency.

Finally, FETTERMAN et al (1973) have investigated Stark effect tuning (which does not require high pump intensities) of the NH_3 Q (5,3) transition. Using a Stark electrode plate separation of a few millimetres and an applied voltage of about 5 kV, they succeeded in obtaining laser action on the Q (5,3) $J = 5 \rightarrow 4$ transition and several other lines in NH_3, which required even greater electric fields. INGUSCIO et al (1976) have calculated the performance of a 496 μm Stark tunable FIR CH_3F laser, and they suggest that a tunability of about 1% (~6 GHz) is possible with applied fields of up to 30 kV cm^{-1}. This tunability is due largely to the high J quantum number of the levels involved in the operation of the 496 μm CH_3F laser.

To summarize, saturation broadening, stimulated Raman scattering and Stark effect tuning allow appreciable flexibility in the design of pulsed F I R laser systems. In particular, the use of Raman and Stark effects to produce tuning of up to 1% in the F I R emission frequency is of considerable practical importance.

2.4 CAVITY LASERS

Studies of pulsed F I R lasers have led to the development of two types of laser, the cavity laser and the mirrorless or 'super-radiant'[†] laser. (The latter will be discussed in section 2.5). F I R cavity laser design is constrained by the necessity of arranging the optical components so that optimum use is made of the near infrared pump photons, whilst retaining a reasonably high efficiency of extraction for the F I R radiation. In the six or seven years of F I R laser development five distinguishable cavity configurations have evolved. The first of these, the hole coupled cavity, is shown schematically in Fig.2.2(a). This configuration was originally used by CHANG and BRIDGES in 1970, and it is now one of the most widely used configurations. A major disadvantage of this cavity arises from the use of the small coupling aperture, although diffraction of the F I R radiation passing through this aperture can be reduced by using a small cylindrical horn after the coupling hole.

The use of a coupling aperture is avoided entirely in the Transverse Optically Pumped (T O P) cavity used by BROWN et al in 1974 (Fig.2.2(b)). With this T O P scheme Brown et al obtained pulses of 496 μm radiation from CH_3F, which had powers of about 300 watts within a bandwidth of less than 30 MHz and a pulse width (FWHM) of approximately 60 ns. Because of the high

---

[†] The use of the term 'super-radiance' in the present work refers to all travelling wave amplification phenomena observed in F I R mirrorless lasers. It does not specifically refer to Dicke Super-radiance (DICKE, 1954) - although evidence for this process occurring within mirrorless F I R lasers has been obtained on several occasions (PLANT et al, 1974).

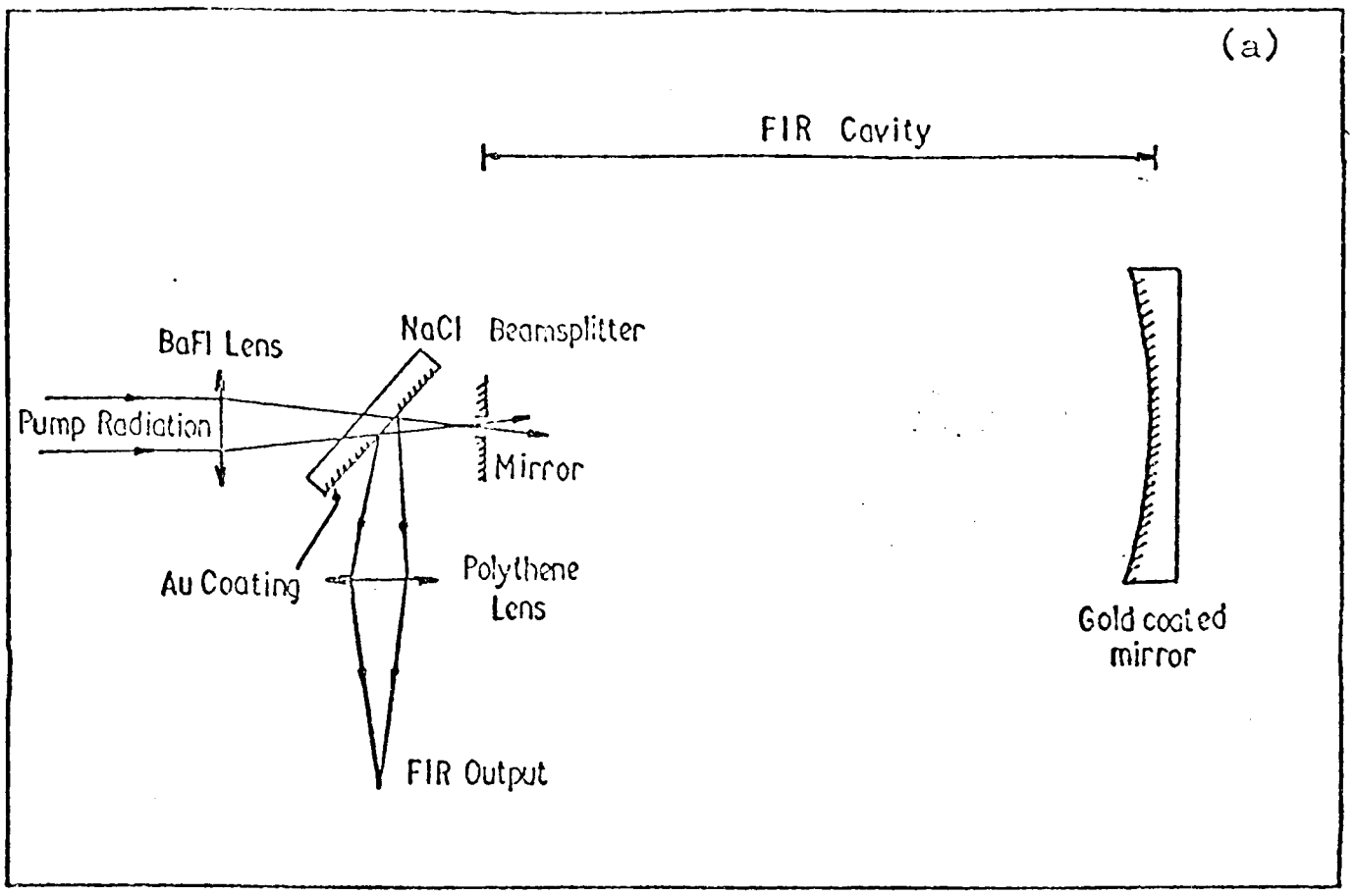


Fig.2.2
(a) Hole coupled cavity; after Chang and Bridges (1970)
(b) Transverse optically pumped (TOP) oscillator; after Brown et al (1974).

pumping intensities used in this experiment, which result from the production of a line focus by the cylindrical mirrors, operating pressures of about 8 torr could be used. This produced a considerable broadening of the fluoresence line so that tuning was accomplished over a significantly wide spectral range (~500 MHz in this case). However, one disadvantage of the system is the need to use a large salt (NaCl) window which is hygroscopic and easily damaged by the pump radiation. Another problem arises from the short pump radiation path length in the gas, which results in a significant proportion of the pump photons not being absorbed and hence to low pump to F I R photon conversion efficiencies.

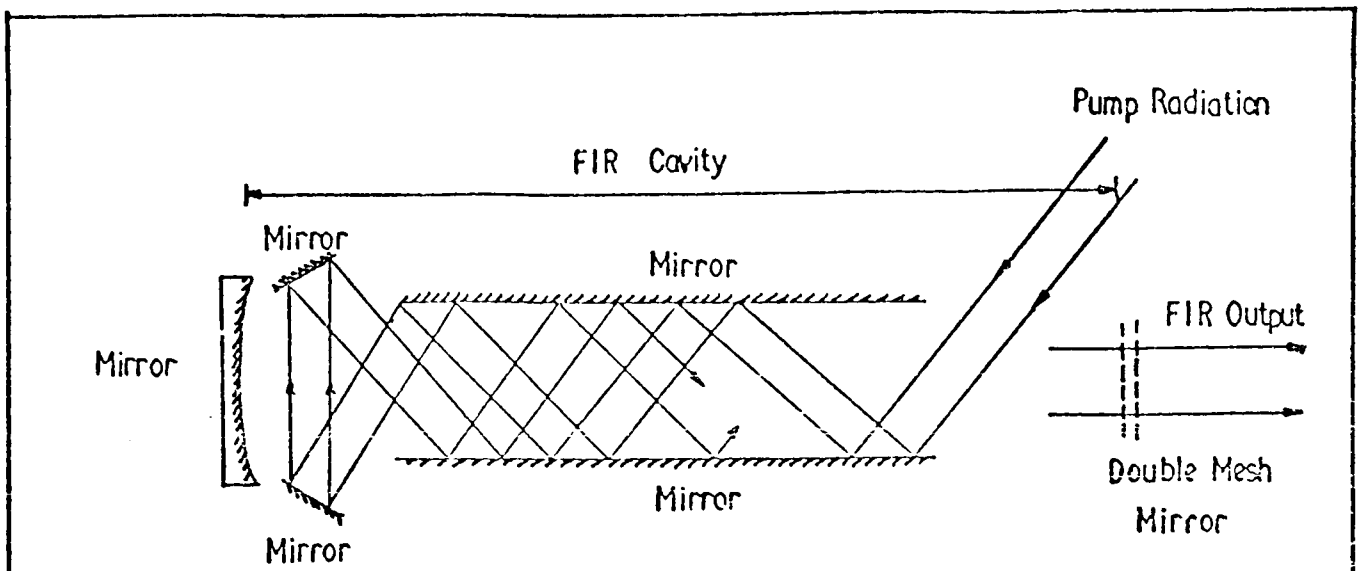


Fig.2.3 Zig-Zag pumped cavity; after Cohn et al (1975)

COHN et al (1975) have employed a zig-zag pumping system for a 496 μm CH_3F oscillator (Fig.2.3) which has a conversion efficiency over seven times greater than that obtained by BROWN et al (1974). By using a zig-zag configuration the pump radiation (~ 0.6 J) could be totally absorbed at the optimum operating pressure of 2 torr. The 60 ns long F I R ouput pulse had an average power in excess of 9 kW, within a bandwidth of less than 30 MHz.

A fourth configuration, used by SHARP et al (1975), employed an off axis pumped configuration (Fig.2.4) for a CH_3F oscillator. (This configuration is discussed in greater detail in Chapter IV.) This oscillator was found to produce comparatively long F I R output pulses (~ 1 μs) with peak powers in excess of 10 kW. Although the off-axis geometry is considerably

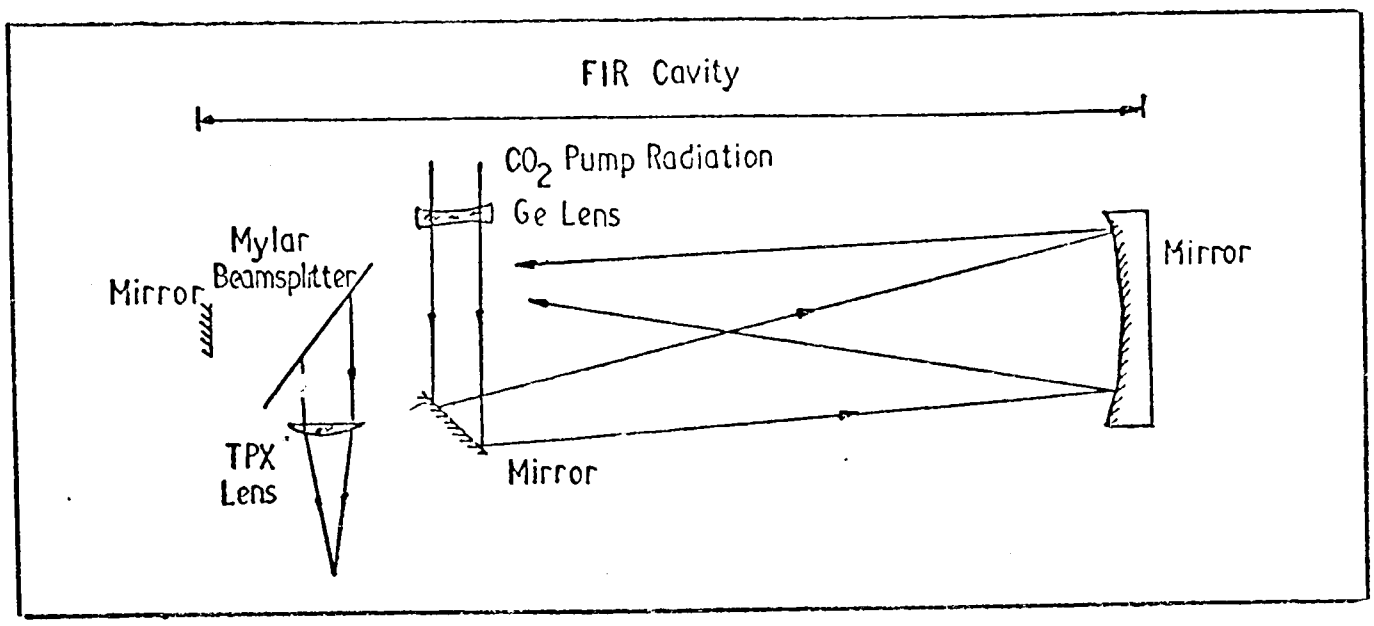


Fig.2.4 Off axis pumped oscillator; after Sharp et al (1975)

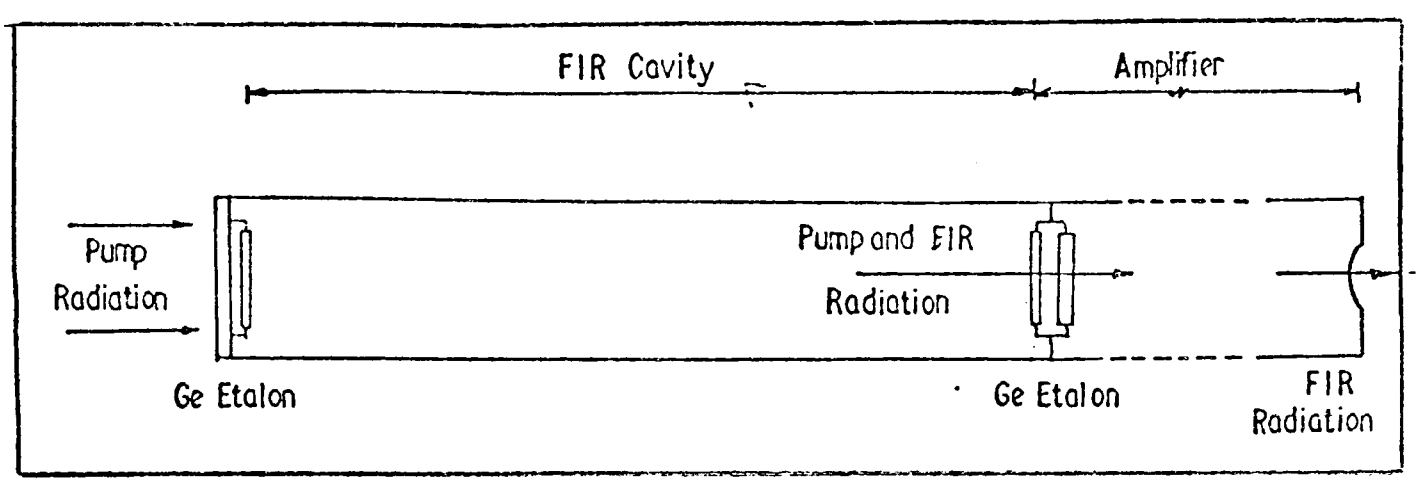


Fig.2.5 Linearly pumped oscillator-amplifier; after Brown et al (1976)

simpler than the zig-zag pumping system, a significant proportion of the mode volume near the optical axis is left unexcited.

BROWN, HISLOP and KRONHEIM (1976) have operated a linearly pumped CH_3F oscillator (Fig.2.5) which combines simplicity with good optical pumping near the cavity optical axis. They employed germanium etalons as the cavity mirrors to increase the reflectivity for the FIR radiation whilst still allowing transmission of the near infrared pump radiation. This oscillator produced short, 60 ns pulses with powers of about 2 kW at 496 μm, within a linewidth of 60 MHz. (The use of this cavity in an oscillator-amplifier system will be discussed later in this chapter.) One drawback of this system is, however, that it requires a different germanium etalon for each FIR wavelength.

2.5 SUPER-RADIANT LASERS

Where the laser medium has a sufficiently high gain for F I R radiation, the generation of F I R laser pulses in a travelling wave or 'super-radiant' configuration is possible. The simplicity of the super-radiant laser is particularly appealing as it requires little more than a gas cell, a few metres long, to contain the laser medium.

DeTEMPLE et al reported the operation of the first F I R laser using a super-radiant cell in 1973. They obtained approximately 1 kW of F I R radiation at 496 μm from CH_3F gas pumped by an 0.6 MW CO_2 laser. The super-radiant F I R laser pulses were observed to have a similar duration to the CO_2 pump laser pulse ($\leqslant$150 ns). This is in contrast to the F I R cavity laser, where the pulse duration is also influenced by the Q of the resonator.

In a similar experiment BROWN et al (1973) observed irregular 0.5 mJ, 50-100 ns pulses containing spikes with peak powers of about 30 kW . In 1974 Brown et al measured the spectral content of F I R pulses from a T O P super-radiant, 496 μm, CH_3F laser with a scanning Fabry-Perot interferometer, and found the bandwidth to be approximately 700 MHz. They suggested that this, together with the irregular pulse shape, arose from simultaneous emission on the pure rotational lines $J = 12 \rightarrow 11$, $K = 1$ to $K \sim 7$ which could all be pumped by the 2-3 GHz bandwidth CO_2 laser used in the experiment (Fig.E.2b).

PLANT et al (1974) have investigated several F I R super-radiant lasers, pumped by a CO_2 T E A (transversely excited atmospheric) laser which was capable of producing either self mode-locked or single longitudinal mode pulses. With a CO_2 pulse energy of 300 mJ they produced 496 μm pulses with energies of approximately 0.6 mJ and powers of 100 kW from a 10 metre CH_3F gas cell. They also observed super-radiant laser action in NH_3, D_2O and several other gases which produced emission lines with wavelengths between 50 and 385 μm . In particular they found the 66 μm D_2O laser to have seven

times the pump to F I R energy conversion efficiency of the 496 μm CH_3F laser. The super-radiant F I R output was found to contain a number of nanosecond duration spikes, similar to those observed by BROWN et al (1973), even when the gas cell was pumped by a temporally smooth single mode CO_2 laser pulse. The F I R output therefore appears to depend on rapid processes within the laser medium and not only on the CO_2 laser pulse shape. Plant et al also observed a significant delay (~ 2.5 μs) of the F I R output relative to the CO_2 pump pulse at low (~ mtorr) pressures and a forward to backward intensity ratio of 10^4 in the observed F I R signal, which suggest that Dicke super-radiance (DICKE, 1954) may be the dominant process in these lasers.

TEMKIN et al (1975) have investigated the pumping and emission characteristics of a 4 kW super-radiant CH_3F laser. The saturated absorption coefficient was found to be far higher than that theoretically predicted if only the molecules initially in the $v = 0$ (ground vibrational state), $J = 12$ state are considered. They conclude that a rapid emptying of the $v = 0$ $J = 12$ level by the CO_2 pump radiation, together with continuous refilling of this band, must be taking place during the generation of the 100 ns F I R pulse. A similar investigation of the 66 μm D_2O laser pumped by a 9.7 μm CO_2 laser has been carried out by MAGYAR (1977), which demonstrates the same strong collisional recycling of the rotational manifold.

Even higher peak F I R powers than those obtained by PLANT et al (1974) at 496 μm were obtained by EVANS et al in 1975. F I R output pulses with peak powers of more than 1 MW were measured for a super-radiant laser optically pumped by a CO_2 T E A laser with a 200 MW, 60 ns (F W H M) gain switched spike. They found the bandwidth of the F I R radiation to be approximately 300 MHz, significantly less than that observed by BROWN et al (1974). However, Evans et al operated their super-radiant laser at a pressure of about 2 torr (cf. 5 torr used by Brown et al). At 2 torr the collisional linewidth is only 80 MHz and thus fewer K levels can be excited

simultaneously by the CO_2 pump radiation, resulting in a narrower fluorescence line. EVANS et al (1976) have also investigated megawatt level super-radiance in optically pumped D_2O vapour (see Chapter V). They measured the photon conversion efficiencies of the 385 and 114 μm lines as a function of pump intensity and found that both these lines were much brighter at high pump intensities ($\geqslant 50\,GW/m^2$) than the work of PLANT et al (1974), which was carried out for relatively low pump intensities ($\leqslant 10\,GW/m^2$), had indicated. This disagreement is explained as being possibly due to the OROP or saturation broadening effect described by FETTERMAN et al (1972). Evans et al used a 10 J CO_2 laser pump to produce 120 mJ of 385 μm radiation in a pulse having an average power of about 2 megawatts. Whilst at 114 and 66 μm they measured F I R energies of 240 mJ and 330 mJ, which are the highest F I R energies produced by a pulsed F I R laser so far.

The longest wavelength super-radiant F I R laser operated, up to the present time, is the 1.22 mm wavelength $^{13}CH_3F$ laser which was reported by HACKER et al in 1976. This laser produced over 5 kW of F I R power from a 3 metre long, 38 mm diameter tube filled with 5 torr of CH_3F isotopically enriched to contain 90% of the rare carbon-13 isotope of CH_3F. A mesh mirror Fabry-Perot interferometer was used to produce a high resolution spectral profile which revealed a bandwidth of approximately 100 MHz.

2.6 OSCILLATOR-AMPLIFIER SYSTEMS

In the last chapter we derived the bandwidth and power requirements for a F I R laser which would be suitable for collective Thomson scattering measurements of a high temperature plasma. Neither the cavity lasers described in section 2.4 nor the super-radiant lasers discussed in the last section are able to satisfy both these requirements. It is therefore necessary to design a laser system which combines the narrow bandwidth ($\leqslant 50$ MHz) of the cavity laser and the high power of the super-radiant laser ($\geqslant 1$ MW).

Oscillator-amplifier systems, as described in this final section have produced results which to date indicate a significant advance towards meeting the power and bandwidth conditions.

DROZDOWICZ et al reported the first pulsed F I R oscillator-amplifier system in 1976. A schematic of this configuration is shown in Fig.2.6. Both the CH_3F oscillator and the amplifier section were pumped in the zig-zag mode, the oscillator being a slightly modified version of the cavity reported by COHN et al in 1975. The laser system produced approximately 6 kW of narrow-linewidth ($\leqslant$30 MHz) 496 μm radiation. The bandwidth of the oscillator was found to be maintained after the power had been increased by a factor of three in the 2.1 metre amplifier.

In another experiment using a linearly pumped CH_3F oscillator-amplifier (Fig.2.5) BROWN, HISLOP and KRONHEIM (1976) produced over 30 kW within a line width of < 60 MHz. This represents a power gain of over 15 for the amplifier which was only 1.8 metres long. The authors point out that for a similar gain to be obtained in a zig-zag pumped amplifier (COHN et al, 1975) a factor of 20 increase in amplifier length would be required over that necessary if linear pumping is used.

SEMET and LUHMANN (1976) have operated a CH_3F oscillator-amplifier configuration (Fig.2.7) which typically produced 70 kW of narrow linewidth radiation in a 50 nsec pulse. This corresponds to a power gain of about 6.5 for the 4.5 metre amplifier tube, the oscillator power being ~11 kW. An important fact to note about both this and the system previously discussed in this section is that the oscillator produces a pulse typically 60 ns long, which is comparable to the duration of the CO_2 pump pulse used to excite the amplifier. Semet and Luhmann observed a considerable (~50%) increase in gain if the oscillator pulse is delayed by 45 ns with respect to the CO_2 laser pulse used to pump the amplifier. In the linearly pumped oscillator-amplifier described by BROWN, HISLOP and KRONHEIM (1976) this delay cannot be imposed between the oscillator and the amplifier.

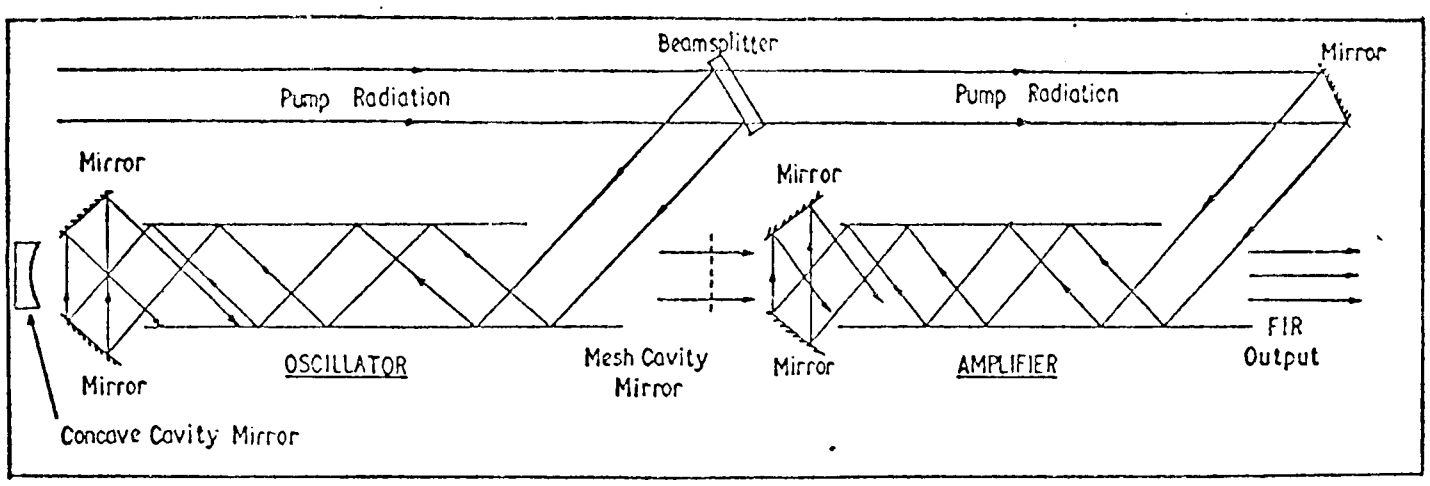


Fig.2.6
Zig-zag pumped oscillator-amplifier system;
after Drozdowicz et al (1976)

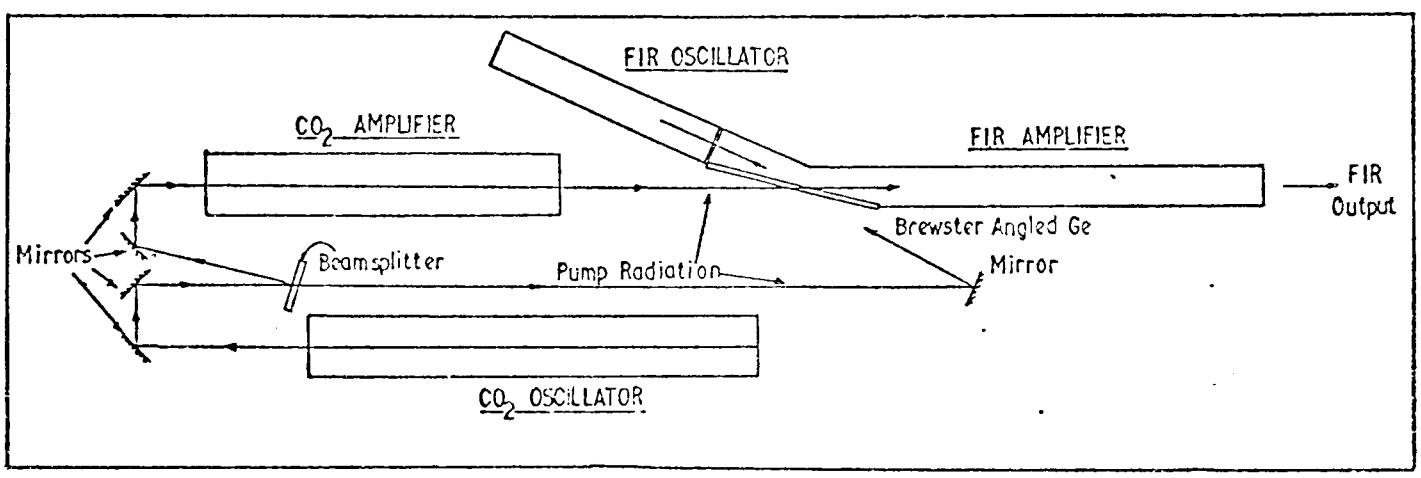


Fig.2.7
Oscillator-amplifier configuration; after
Semet and Luhmann Jr. (1976)

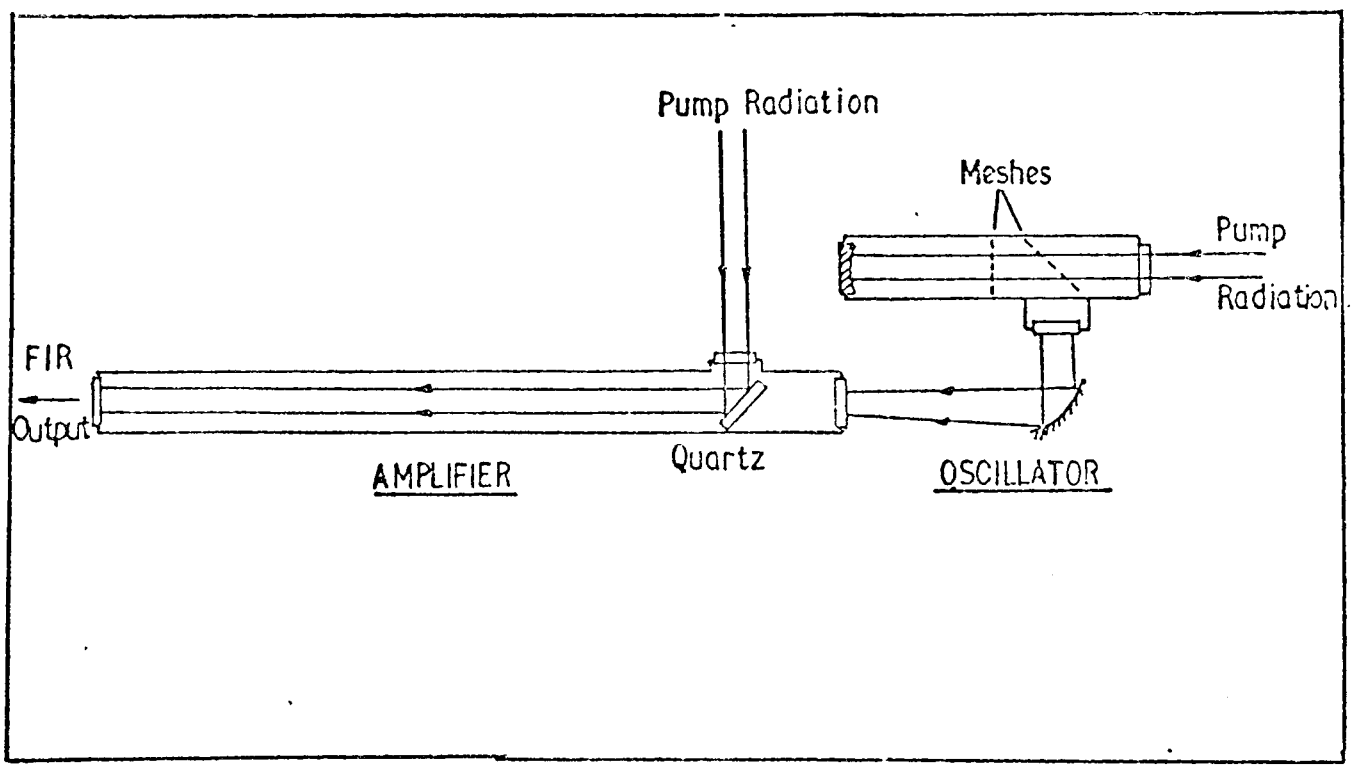


Fig.2.8
D_2O oscillator-amplifier system; after Woskoboinikow et al (1976)

EVANS et al (1977) have used a CH_3F single mode, 500 watt, oscillator with an off axis configuration (SHARP et al, 1975) which produced long ($\sim$ 600 ns) pulses to drive a high power oscillator-amplifier system. (This work will be discussed in more detail in Chapter VI.) The long oscillator pulse and the use of two separate CO_2 laser pumps, which can be fired independently, allows a high degree of control over the synchronization between the F I R oscillator and the 4.2 metre amplifier. This system has produced several hundred kilowatts of 496 μm radiation within a bandwidth of $\leqslant$50 MHz and power gains of $\sim$400. In order to obtain effective gains as high as this strong suppression of super-radiance must occur at the input of the amplifier.

WOSKOBOINIKOW et al (1976) have generated 195 kW at 385 μm within a bandwidth of 70 MHz using an optically pumped D_2O oscillator-amplifier (Fig.2.8). One advantage of using D_2O results from the wide spacing of the K levels (see Appendix 'E') which are nearly degenerate in CH_3F resulting in reduced laser efficiency and line broadening. The D_2O oscillator in this case generated a narrow linewidth (< 20 MHz) pulse with a duration of about 60 ns. This was delayed by 35 ns relative to the CO_2 laser pump for the 8 metre F I R amplifier.

The highest powers reported for a F I R oscillator-amplifier at present are those obtained by BROWN, HISLOP and TURPINIAN (1976) with a linearly pumped CH_3F system, similar to that shown in Fig.2.5 but with a much longer, 7.2 metre amplifier cell. This laser produced approximately 600 kW of F I R radiation within 30 MHz, the bandwidth being inferred from 150 MHz time resolved signals of the F I R amplifier output. The authors suggest that suppression of super-radiance, due to saturation of the F I R transition at the input of the amplifier by the F I R oscillator,† must be occurring in this case.

---

† The saturation of the F I R transition by the F I R oscillator is similar to that observed by EVANS et al (1977).

CHAPTER III

THE CO_2 LASER SYSTEM

The purpose of the present chapter is to give a brief outline of the operation and layout of the CO_2 laser system used in the optically pumped F I R laser experiments to be described later.†

Two separate CO_2 laser systems were used in the present work, both systems being transversely excited atmospheric (TEA) lasers constructed with an electrode geometry similar to that used by DUMANCHIN et al (1972). (The spectroscopy of the CO_2 laser is discussed in Appendix 'F'.) Fig.3.1 shows a schematic diagram of the CO_2 laser modules. For convenience the CO_2 laser used to pump the F I R cavity laser (to be discussed in Chapter IV) will be referred to as system A, whilst that used to pump the F I R super-radiant laser (to be discussed in Chapter V) will be called system B. Both systems produced laser pulses with a bandwidth of about 1 GHz.

3.1 CONSTRUCTION AND CIRCUITRY OF THE CO_2 LASER UNITS

The CO_2 laser system was constructed from almost identical perspex modules (Fig.3.2). Each module contained a flat aluminium anode and an aluminium cathode with ten (for system B) or sixteen (for system A) closely spaced, longitudinal, rectangular grooves. These contained glass capillary tubes inside each of which was a fine tungsten wire. The discharge length in each module was about one metre whilst the electrode separation was about 55 mm. A schematic diagram of the discharge circuit used for each module is shown in Fig.3.3 A 60 kV pressurized (50 p.s.i.) field distortion spark

---

† CO_2 laser technology has advanced rapidly over the past ten years and in this chapter we discuss only those aspects of the field which are relevant to the operation of the CO_2 laser system used here. However several review articles have been written on CO_2 lasers in recent years, for example BEAULIEU (1971), WILLET and GLESSON (1971), FOSTER (1972) and DULEY (1976).

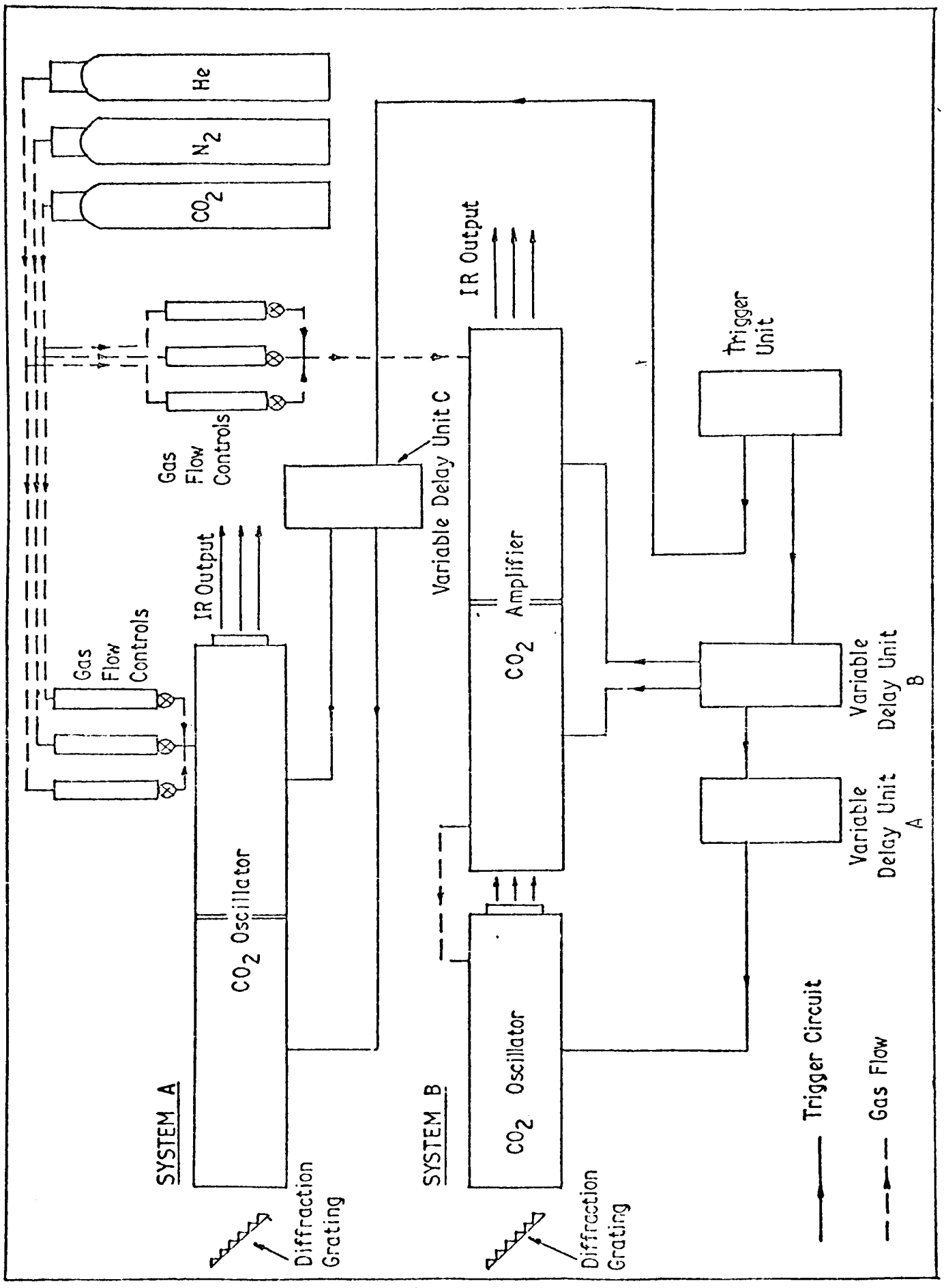


Fig.3.1

Block diagram of the CO_2 laser system. Showing the trigger delay circuit and the gas flow system

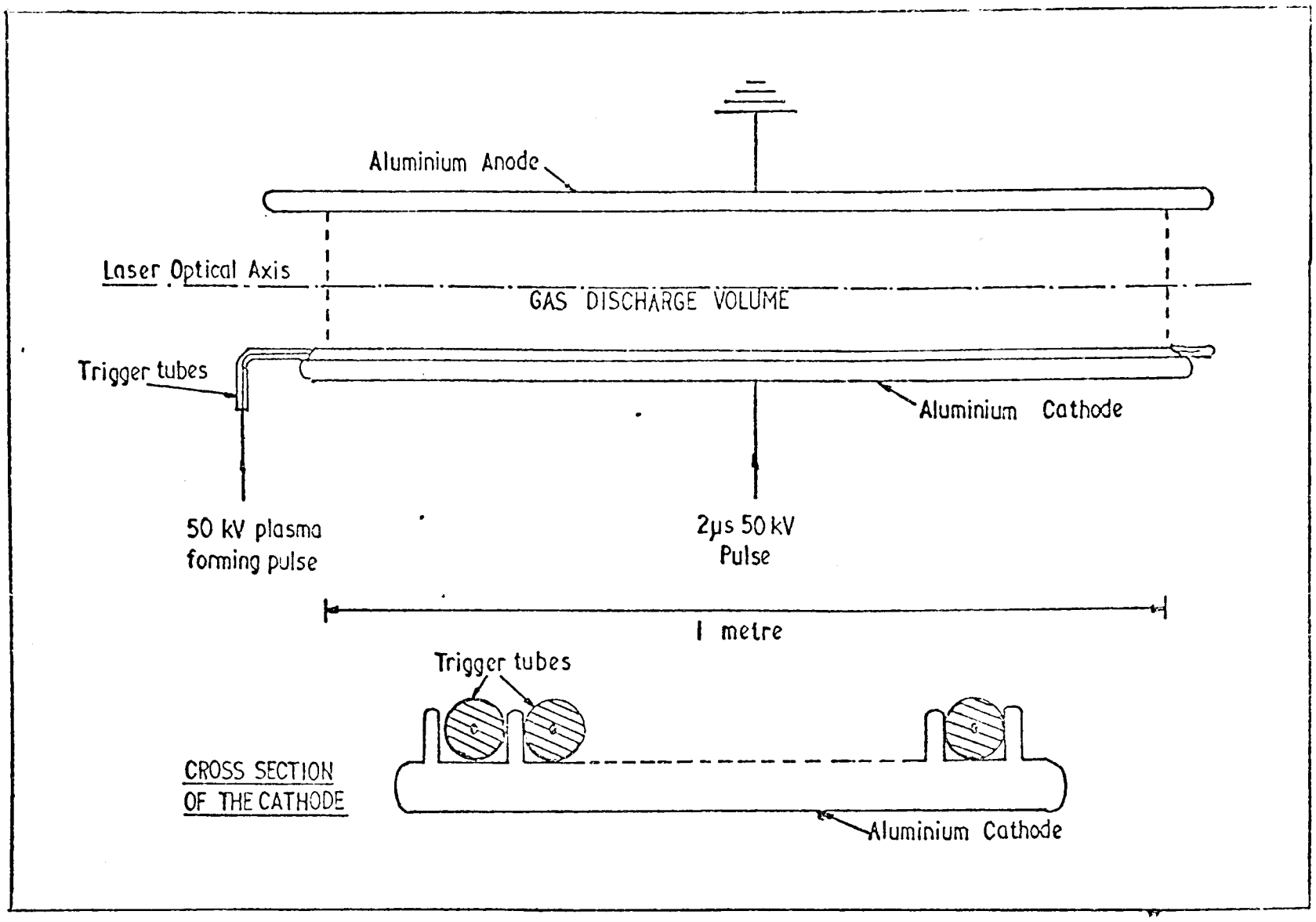


Fig.3.2 Construction of a CO_2 laser module

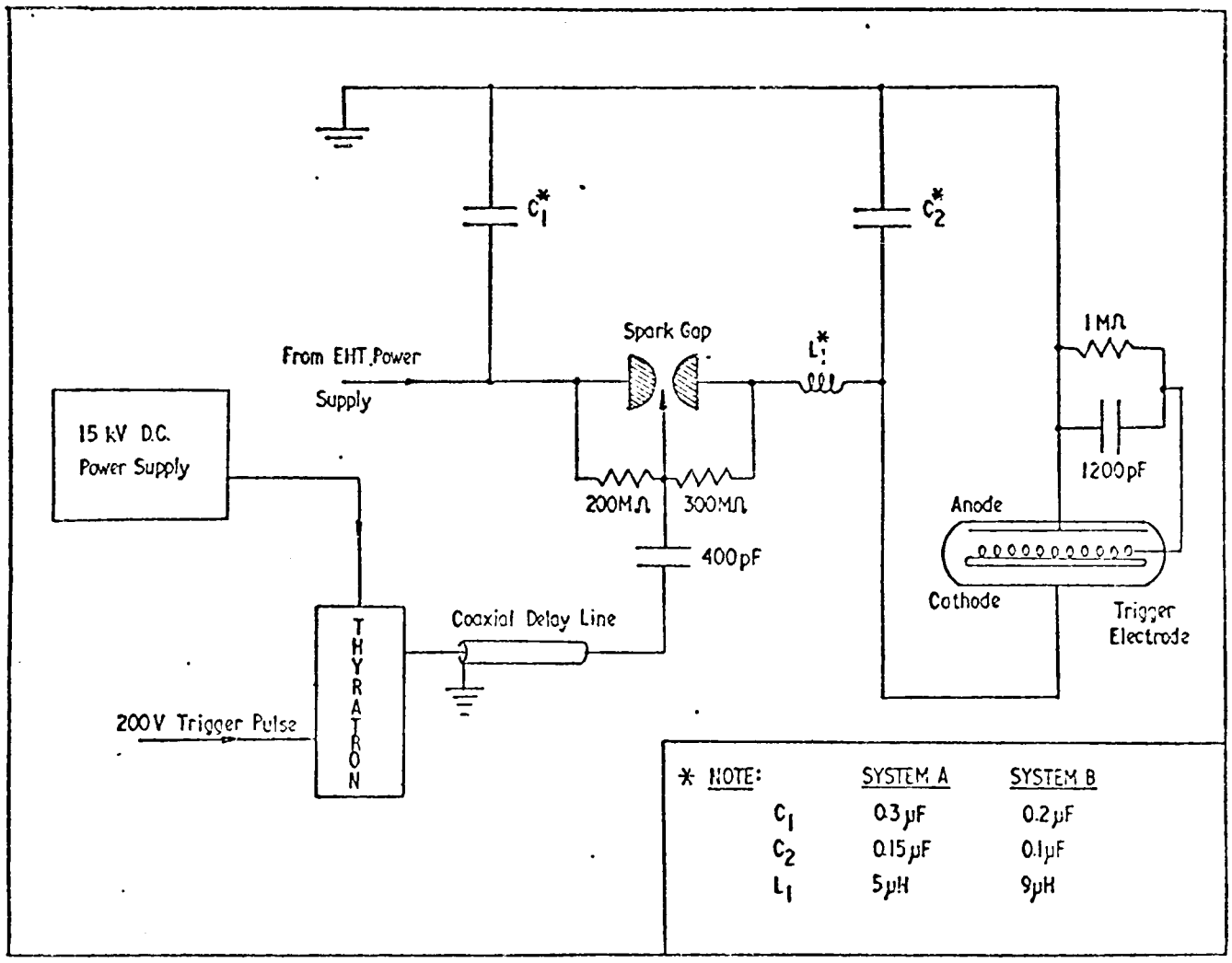


Fig.3.3 The firing circuit for a CO_2 laser module

gap was fired by a, thyratron switched, 15 kV d.c. power supply, connected to the spark gap trigger electrode via a voltage doubling coaxial delay line and a 400 pF capacitor.

The main storage capacitor (C_1) for each module had a capacity of either 0.2 μF (for system B) or 0.3 μF (for system A) and it was charged to between 50 and 55 kV from the EHT power line. This corresponds to an available energy density of about 50 J ℓ^{-1} for the 5.5 litre discharge volume. A low inductance capacitor (C_2) was then pulse-charged via a spark gap and an inductance (L_1). The values of L_1 and C_1 were adjusted, so that the delay in establishing the peak voltage across the laser electrodes matched the time required to establish a corona discharge between the trigger electrode and the cathode. This then initiated a uniform excitation of the laser medium between the main electrodes. Fig.3.4 shows the voltage across the laser electrodes and the resultant discharge current as a function of time. The voltage pulse lasted about 2 μs and the laser medium reached maximum population inversion soon after this pulse had died away. The power supplies

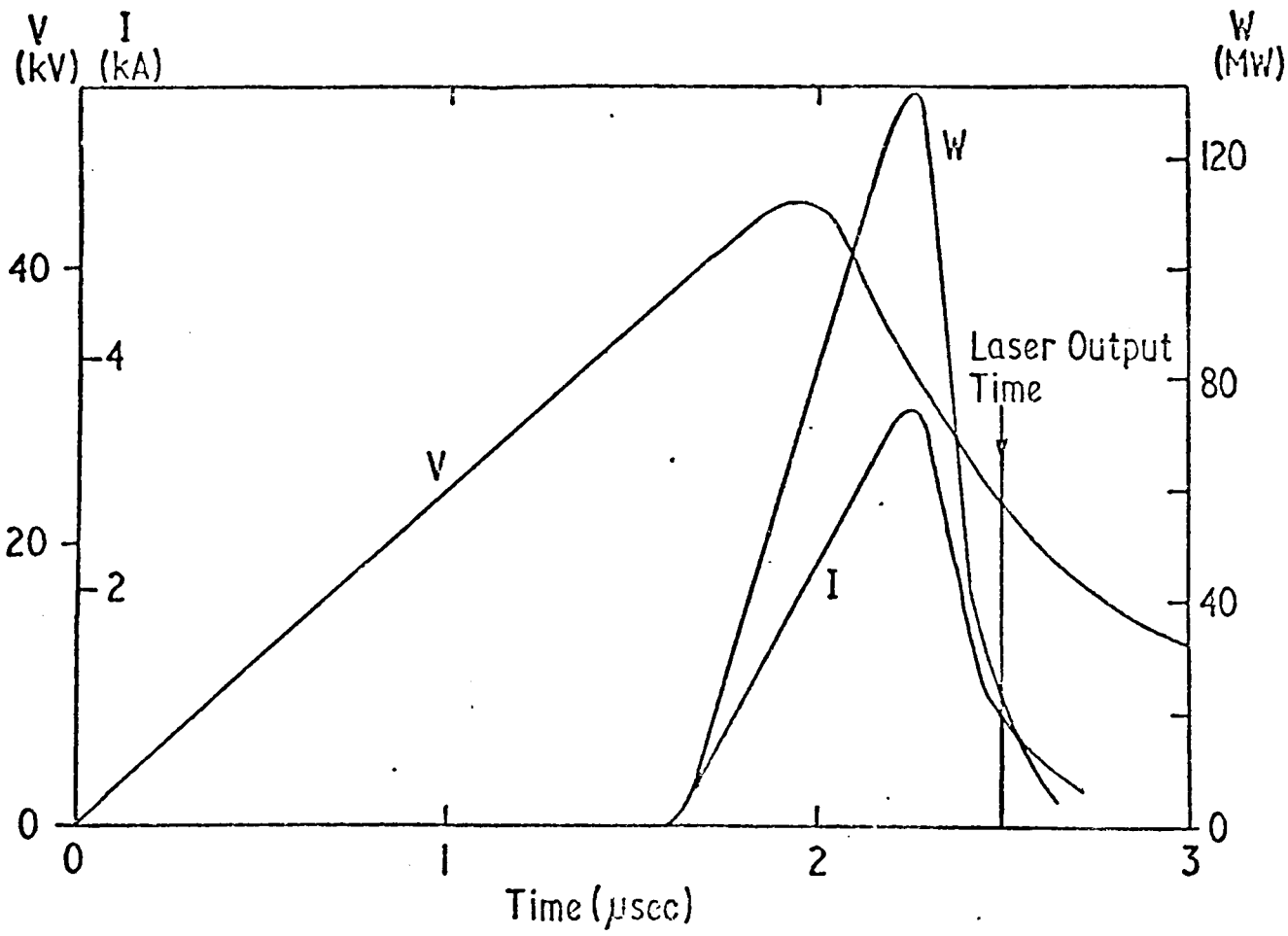


Fig.3.4
Voltage (V) and current (I) waveforms for a CO_2 laser module. The calculated electrical power dissipation (W) is also shown.

limited the charging time for the main capacitors to about 20 seconds, so that the typical pulse repetition period for both system A and B was about 20 to 25 seconds.

3.2 THE CO_2 LASER PULSE SHAPE

The pulse shape produced by both CO_2 laser systems consisted of a gain-switched spike of about 60 ns halfwidth followed by a tail with a duration of several microseconds (Fig.3.5). The proportion of energy in the spike depended on the gas mixture used in the laser medium (see Appendix 'F'), but typically 20% of the total pulse energy was emitted in the spike.† The laser pulse shape was measured with a germanium photon drag detector (GIBSON et al, 1970) which had a response time of less than a nanosecond, while the total pulse energy was measured with a Gentech model ED 500 thermopile calorimeter. Exposed polaroid film was used to determine the spatial structure of the CO_2 laser beam.

3.3 CO_2 LASER SYSTEM A

This laser was constructed from two CO_2 laser modules to produce an oscillator with a cavity length of about 2.5 metres. The cavity was formed between a germanium flat (anti-reflection coated on one side to give a reflectivity of about 35%) and a rectangular (70 mm × 80 mm) gold coated 150 lines mm^{-1} original diffraction grating, which was blazed for 8 μm radiation. The grating had a resolution of 8×10^{-4} μm (more than sufficient to select adjacent emission lines of the CO_2 laser whose separation is ~0.02 μm, see Appendix 'F') and an angular dispersion of 4×10^{-3} μm/mrad. The grating was mounted on a 360° rotational movement with a micrometer control to allow tuning of the CO_2 laser to any one of the laser emission lines between 9 and 11 μm (see Appendix 'F'). The system A laser produced a total pulse

† The spike to tail energy ratio was determined from photon drag signals similar to that shown in Fig.3.5(a).

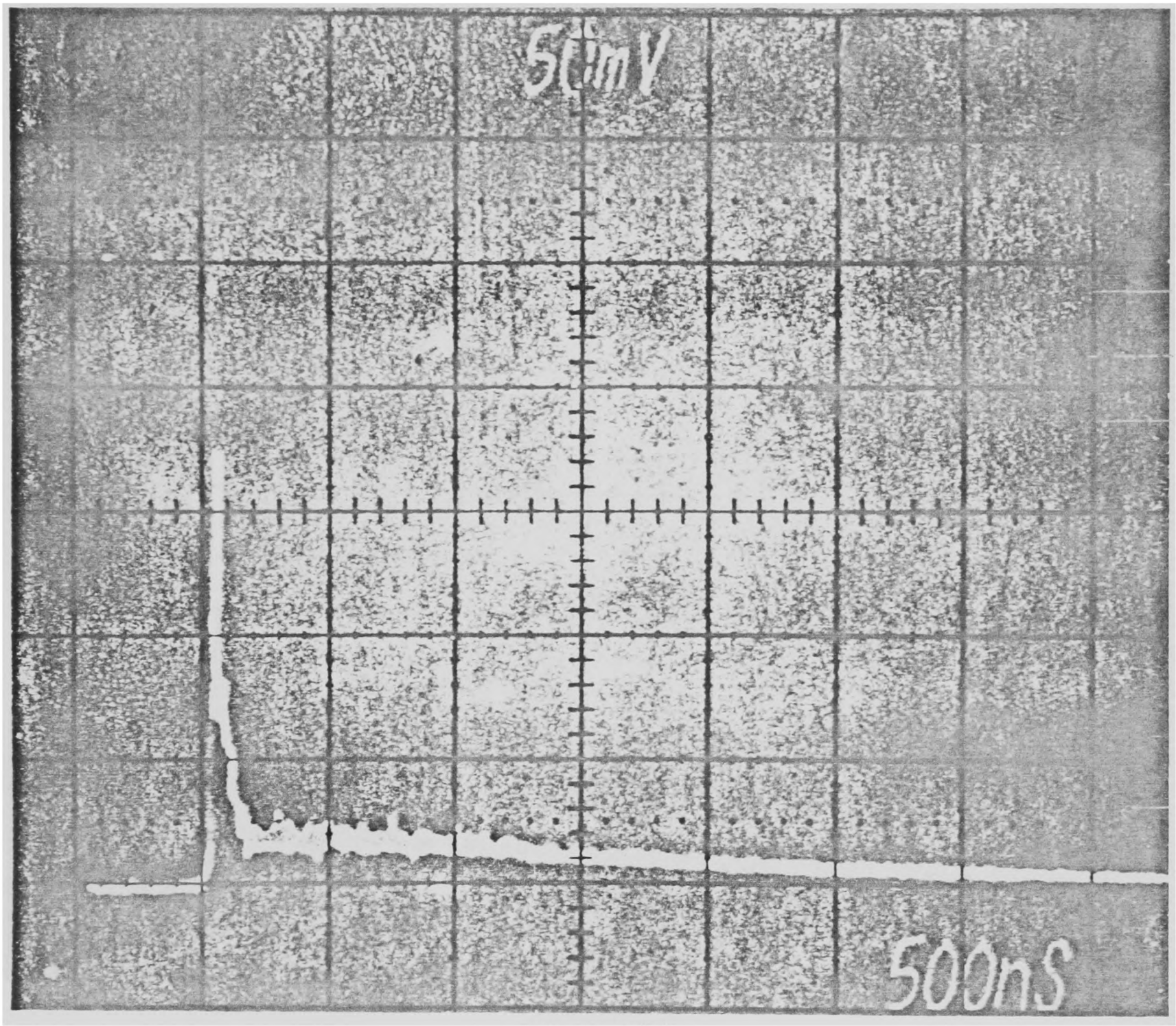


Fig.3.5(a)

CO_2 laser pulse shape showing the 60 nsec gain switched spike and a tail of several microseconds duration (Horizontal scale 500 nsecs/division)

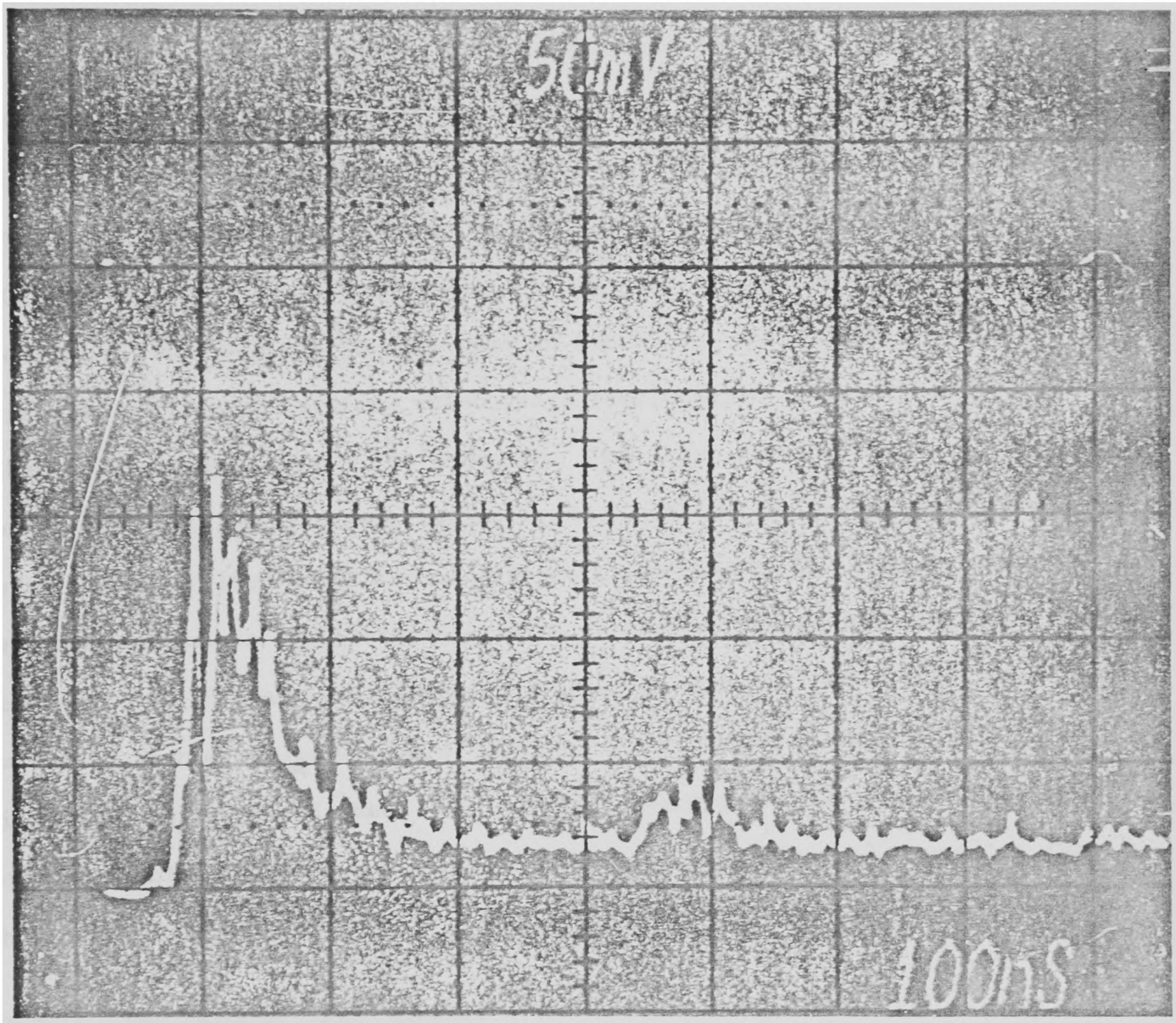


Fig.3.5(b)
Detail of the 60 nsec gain switched spike.
(Horizontal scale 100 nsecs/division)

energy of about 30 J on the 9.55 μm (P(20)) laser line used to pump the F I R cavity.

3.4 CO_2 LASER SYSTEM B

The system B laser was constructed from three CO_2 laser molecules and was operated in one of two configurations. First as a long oscillator (cavity length ≈ 4.5 metres) and second, as a short oscillator (cavity length ≈ 1.5 metres) followed by an amplifier, formed by the remaining two CO_2 laser modules. In both configurations the cavity was formed between a germanium flat, similar to that used in system A, and a 50 mm diameter circular diffraction grating which had a resolution of 1.3×10^{-3} μm and an angular dispersion of 4×10^{-3} μm/mrad. The laser pulse energy for the long oscillator configuration was typically 45 J, whilst the pulse energy obtained with the oscillator-amplifier configuration was about 65 J. When system B was operated as an oscillator-amplifier, a perspex flight tube was used to connect the oscillator module to the amplifier modules, and a KCl salt flat was used as the output window of the amplifier. The 1.5 metre oscillator in system B produced about 15 J of laser energy, so that the overall gain of the double amplifier was about 4. This low amplifier gain suggests that both amplifier modules were well saturated.

3.5 THE TRIGGER DELAY CIRCUIT

To allow flexibility in the relative timing of the various CO_2 laser modules three variable delay units were used in the trigger circuit, these are shown schematically in Fig.3.1. Delay unit A was used to vary the firing time of the oscillator relative to the two amplifier modules in system B, this delay was by-passed when system B was operated as a long, three module, oscillator. Delay units B and C allowed the firing time of system A to be delayed relative to system B or vice versa. The delay units used here were capable of producing delays from 1 to 100 μs. The delay could be

controlled to better than 30 ns , this limit being set largely by the spark gap jitter.† The trigger unit could be operated manually or automatically with a repetition rate between 1 and 10^{-3} Hz.

3.6 THE GAS MIXTURE CONTROL SYSTEM

The gas supply for the CO_2 laser system is shown in Fig.3.1. Helium, carbon dioxide and oxygen-free nitrogen were supplied from separate gas cylinders. Separate sets of calibrated gas flow meters were used to monitor and control the gas mixture to the two CO_2 laser systems.

The total volume of the perspex modules used for the CO_2 laser heads was about 250 litres and this was flushed with the gas mixture at atmospheric pressure. The flow rates of the gases used for each system were:

	System A	System B
H_e	8.0 litres/min	8.0 litres/min
CO_2	1.0 litres/min	1.1 litres/min
N_2	1.0 litres/min	0.7 litres/min.

The higher N_2:CO_2 ratio used in system A was employed in order to increase the tail to spike energy ratio in the CO_2 laser pulse for this system, (see Appendix 'F'). This was necessary since the CO_2 laser pulse tail contributed at least 50% of the useful pump energy in the F I R cavity laser, whereas in the super-radiant laser it contributed nothing. (The significance of the tail of the CO_2 laser pulse for the F I R cavity laser will be discussed in Chapter IV.)

Before operating the laser system it was flushed with H_e , CO_2 and N_2 for about 45 minutes to eliminate oxygen from the system. If the total gas flow rate was reduced much below the values quoted here arcing occurred, owing to impurities being evolved after each discharge and not being flushed from the system. When the lasers were fired, air was sucked

---

† The delay accuracy required for the F I R oscillator-amplifier experiments discussed in Chapter VI was ± 50 ns .

in through the gas outlet on each laser. It was therefore necessary to fix a few metres of hose to each outlet to restrict this intake of air, since even a small quantity of oxygen in the discharge caused severe arcing.

3.7 SUMMARY OF THE CO_2 LASER PARAMETERS

The operating parameters for the CO_2 lasers used in the present work are summarized in the following table:

	SYSTEM A	SYSTEM B	
Configuration:	2.5 m Oscillator	4.5 m Oscillator	Oscillator-Amplifier
Number of CO_2 laser modules	2	3	3
Number of trigger tubes per module	16	10	10
Discharge volume (litres)	11	16.5	16.5
Total stored energy in main capacitor (Joules)	900	750	750
Pump energy density (J/litre)	80	45	45
Main capacitor peak voltage (kV)	55	50	50
CO_2 laser pulse energy (J)	30	45	65
Peak laser power in 60 ns gain switched spike (MW)	100	150	220
Capacitance of energy storage capacitor (μF)	0.6	0.6	0.6
He:CO_2:N_2 gas ratio	8 : 1 : 1	8 : 1.1 : 0.7	8 : 1.1 :0.7
bandwidth (GHz)	≈ 1	≈1 *	≈ 1
Polarization of laser radiation	Horizontal	Horizontal	Horizontal
Divergence (mrad)	20	10	20
Active laser volume (litres)	7.2	5.4	5.4

NOTE: * The bandwidth of the System B 4.5 m oscillator was measured with a pressure scanning germanium Fabry-Perot interferometer and was found to be 0.9 GHz.

CHAPTER IV

THE FIR CAVITY LASER

In this chapter we present results for the operation of a 496 μm CH_3F cavity laser. Initially this laser was operated on several transverse and longitudinal modes with no attempt to reduce the bandwidth. This multimode laser is described in section 4.1, and its performance is discussed in section 4.2. The oscillator was later operated on a single cavity mode by inserting a transverse mode limiting aperture and an interferometer to select a single longitudinal mode in the cavity. This single mode cavity is described in section 4.3 and its performance analysed in section 4.4. Finally the properties of the 496 μm CH_3F cavity laser are summarized in section 4.5.

4.1 THE MULTIMODE CAVITY

The multimode cavity used in the experiments presented in this chapter is shown schematically in Fig.4.1. A near-hemispherical cavity was used, since it produces a large mode volume and is comparatively easy to align. It also allows the use of a stretched mesh as the plane cavity mirror, thus facilitating efficient coupling of the FIR radiation out of the cavity. This would not be possible for a cavity, such as a confocal resonator, which uses curved mirrors only. The advantages and disadvantages of this and other FIR cavity laser configurations are treated in Chapter II.

The FIR cavity was formed between a gold coated 30 cm diameter concave mirror with a radius of curvature of 246 cms and a copper or nickel 250 lines/inch electroformed mesh[†]. The mesh mirror was positioned

---

[†] Electroformed mesh can be obtained from either: Buckbee-Mears Co., 245 East 6th Street, Saint Paul, Minnesota 55101, U.S.A. or EMI Electronics Ltd., Electron Tube Division, 243 Blyth Road, Hayes, Middlesex UB3 1HJ, England.

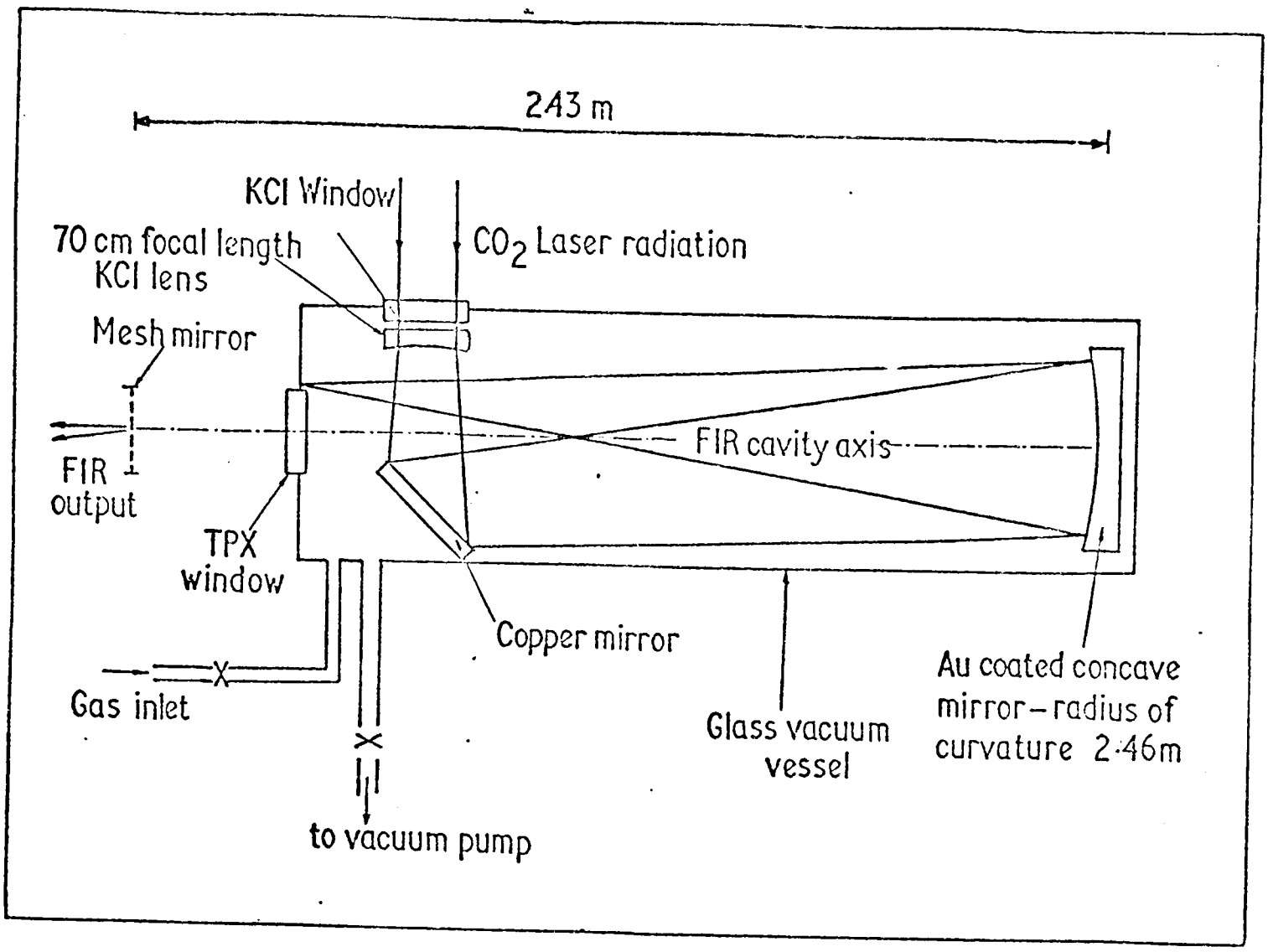


Fig.4.1 Layout of the Multimode Cavity

approximately 243 cms away from the concave mirror. The transmission of the mesh mirror was measured to be about 25% for 496 μm radiation.† Most of the cavity volume was enclosed in a 2 m long glass vacuum vessel of 35 cms internal diameter. The concave cavity mirror was mounted inside this vacuum vessel, but could be adjusted externally by micrometer controls. The mesh mirror was mounted separately outside the glass vacuum vessel and the FIR radiation passed between the mesh mirror and the concave mirror via a TPX≠ window, which was over 95% transparent for 496 μm radiation.

---

† An internal beamsplitter was initially used to couple the FIR radiation out of the cavity but this was found to be inferior to the mesh mirror output coupler described here.

≠ TPX is the trade name for poly-4-methylpent-1-ene which is manufactured by Yarsley Research Ltd., Stokes Poges, Slough, Berks. SL2 4QD, England. It is transparent in the visible and FIR having a refractive index of 1.43, but opaque to CO_2 radiation at 9.55 μm.

9.55 μm CO_2 laser radiation entered the vacuum vessel via a 10 cm diameter, 1 cm thick, KCl, flat and a 10 cm diameter, 0.8 cm thick, KCl, plano-concave lens with a focal length of 70 cms. The CO_2 pump radiation was then directed towards the concave cavity mirror by a plane copper mirror mounted slightly off the optical axis of the F I R cavity. The CO_2 pump beam was about 25 cm in diameter when it reached the concave cavity mirror, which then reflected the CO_2 laser radiation to a focus just in front and to one side of the TPX vacuum window. This arrangement ensured that the volume pumped by the CO_2 laser coincided with the volume of the fundamental, TEM_{00}, mode. The TPX vacuum window, the KCl optics for the CO_2 laser radiation and the plane copper mirror, were all mounted on an aluminium flange, which was bolted to one end of the glass vacuum vessel. The vacuum pump and the gas inlet connections were also made to this flange. The vacuum vessel was evacuated to about 10^{-2} torr by a single stage rotary pump prior to being statically filled with CH_3F gas at pressures between 0.2 and 1.8 torr. The gas pressure in the vacuum vessel was measured with a mercury McLeod gauge.

Alignment of the CO_2 pump optics was carried out with a 6328 Å He-Ne laser, equipped with a beam expanding telescope, which produced a laser beam with a diameter of about 5 cms; this effectively allowed the path of the CO_2 laser radiation to be observed visually. A separate HeNe laser, which was not equipped with a beam expander, was used to align the F I R cavity. This laser was located outside the F I R cavity and was directed through the mesh mirror towards the concave cavity mirror. The mesh mirror produced sufficient reflection and transmission of the red laser light to allow alignment of the mesh mirror via its reflected diffraction pattern and alignment of the concave mirror via the transmitted diffraction pattern.

4.2 THE 496 μm, CH_3F MULTIMODE CAVITY LASER

In this section we discuss the operation of a CH_3F multimode cavity laser, which was optically pumped by the P(20), 9.55 μm CO_2 laser line, using the system A laser described in section (3.4).

The F I R energy emitted by the CH_3F multimode cavity laser was measured with a calorimeter (Laser Instrumentation model 17), which had previously been calibrated at the United Kingdom National Physical Laboratory to an accuracy of 10%. This calorimeter had a sensitive area which was approximately the same size as the F I R output beam from the laser (i.e. about 2.5 cm diameter). Thus it was possible to obtain the total F I R energy in a single laser shot. Fig.4.2 shows the F I R output energy for the multimode cavity as a function of CH_3F gas pressure from 0.1 to 1.8 torr. Several CO_2 laser pump energies were obtained by attenuating the CO_2 laser beam with a number of thin polythene sheets. A Gentech ED 500 calorimeter was used to measure the energy of the CO_2 laser beam for each pump energy. For all the CO_2 pump energies used the F I R output was found

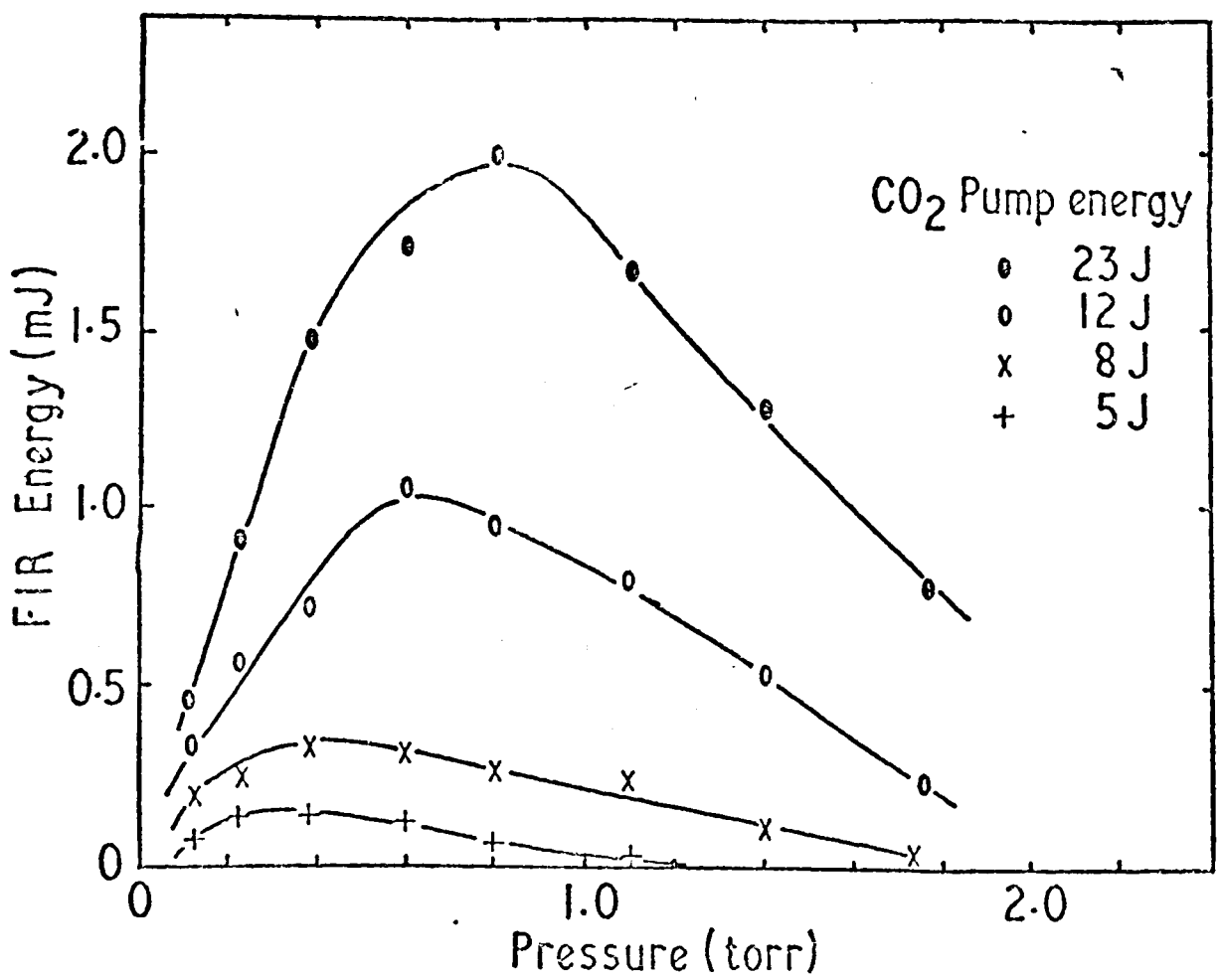


Fig.4.2

Multimode cavity F I R energy against CH_3F gas pressure for several different CO_2 laser pump energies

to peak at CH_3F gas pressures between 0.4 and 0.8 torr. As the pump energy was increased, the CH_3F pressure at which the maximum F I R energy was obtained also increased. The shape of the F I R energy against pressure curves may be explained as the result of competition between radiative and collisional processes in the laser medium. Thus at sufficiently high pressure ($\geqslant 2$ torr) the laser output would be quenched by the rapid collisional depopulation of the $J = 12$, ν_3 level (see Appendix E).

Figure 4.3 shows the F I R output-energy plotted as a function of CO_2 pump energy. The F I R output was found to saturate at CH_3F pressures of less than 0.2 torr and then only for pump energies in excess of 20 J. The pump to F I R energy conversion efficiency was found to decrease with decreasing pump energy, from 8.6×10^{-5} for a CO_2 pump energy of 23 J to 2×10^{-5} for a pump energy of 5 J.

Figure 4.4 shows an oscillogram of the F I R laser pulse shape measured with a Si-W point contact diode[†], amplified by an Avantek 400 MHz bandwidth amplifier and displayed on a 100 MHz bandwidth storage oscilloscope. The multimode F I R output pulse was strongly modulated within a pulse envelope about 600 ns long, this modulation is due to beating between the 30 MHz separated transverse cavity modes (see Appendix 'A'). The measured pulse length combined with the F I R pulse energies of about 2 mJ imply an average power of about 3.5 kW and a peak power of 7 kW. (This calculation ignores the effects of modulation which would approximately double the calculated peak power.)

The F I R pulse duration was found to be shorter at higher pressures, for example at 1.5 torr the F I R pulse was only 400 ns long. However, for all the CH_3F gas pressures used the pulse duration was always much longer

---

† The Si-W point contact diode and its mounting were made to contract by Custom Microwave Components, Orlando, Florida, U.S.A.

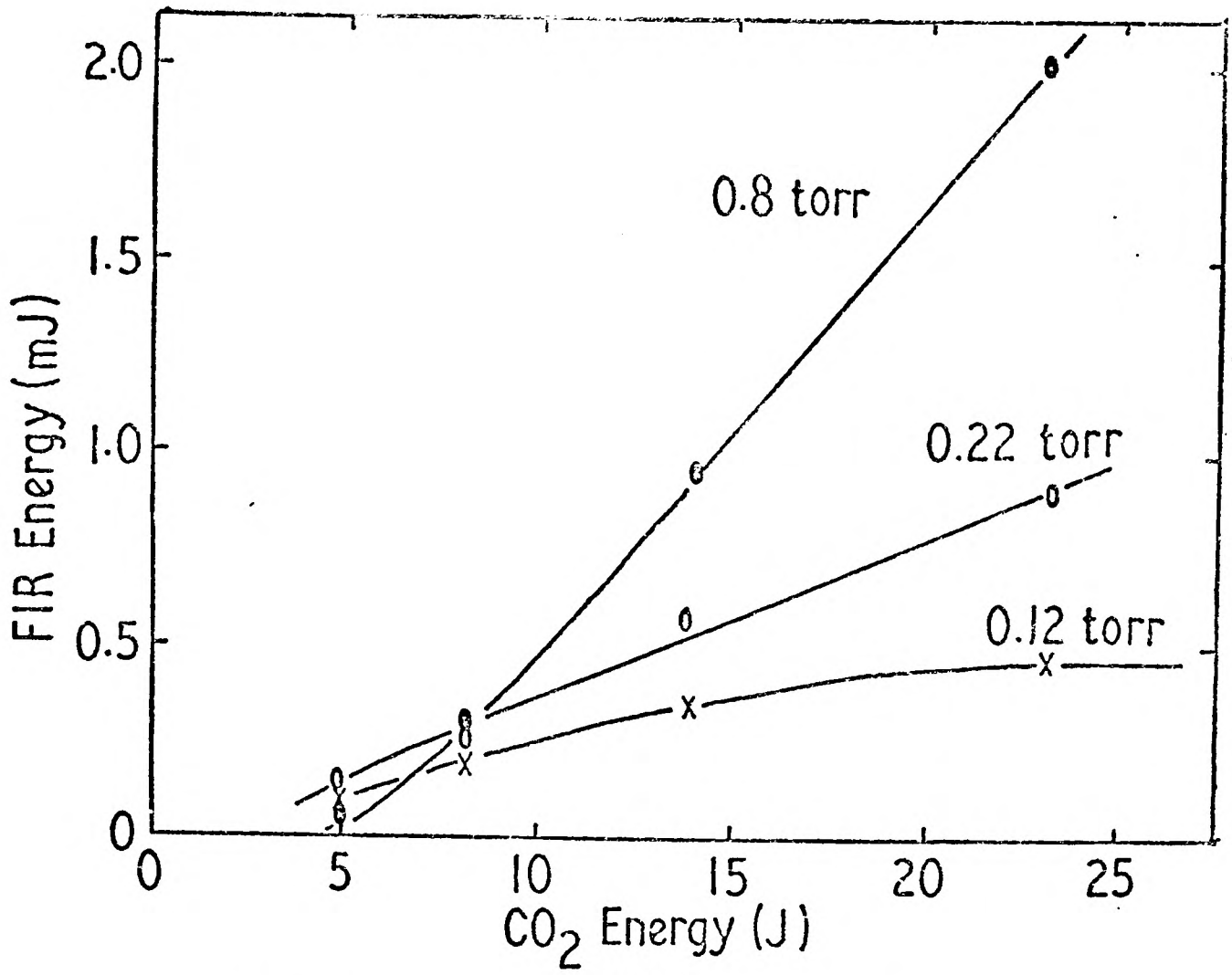


Fig.4.3
Multimode cavity FIR energy against CO_2 laser pump energy for several different CH_3F gas pressures

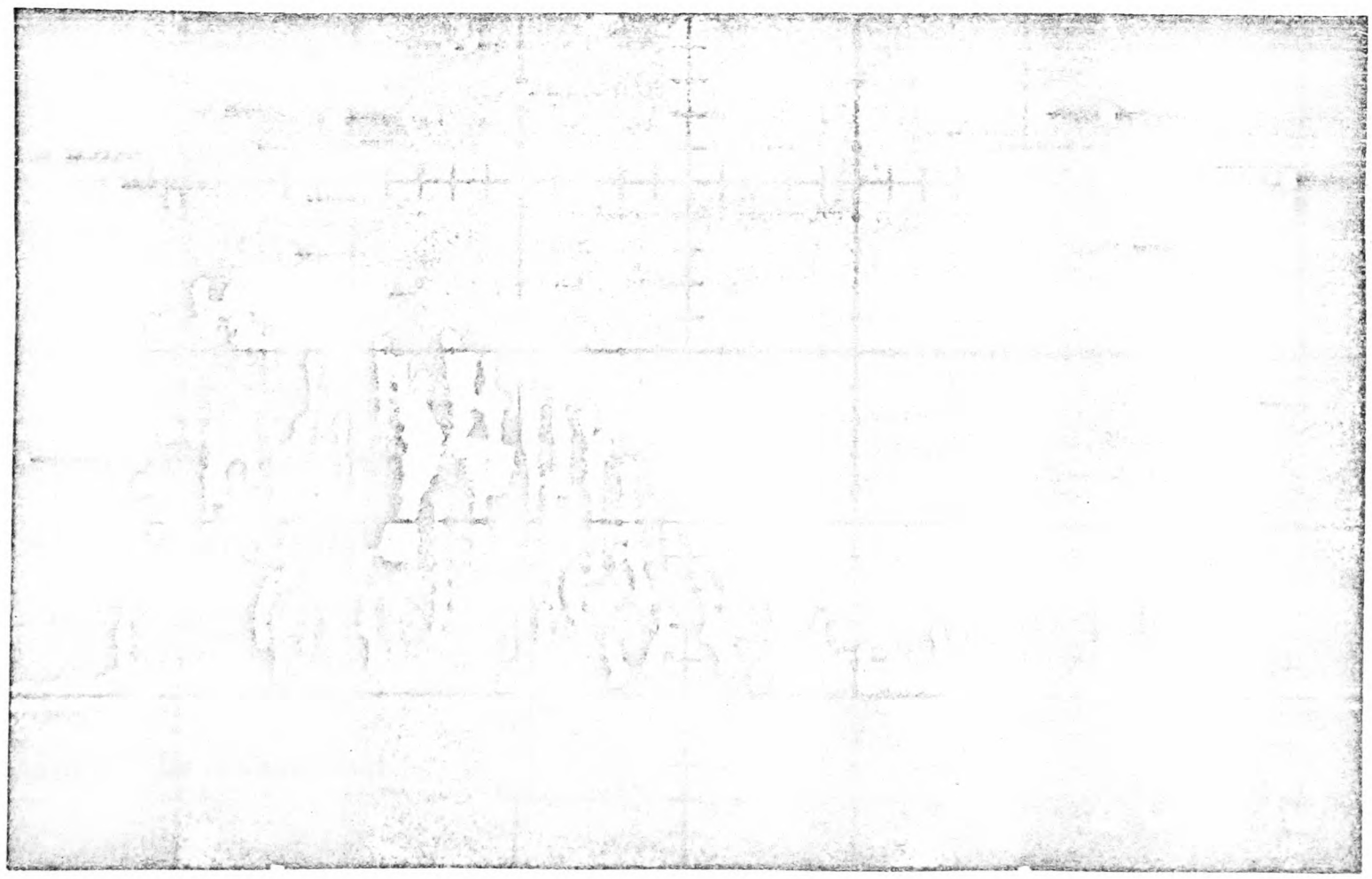


Fig.4.4
Point contact diode trace for the multimode cavity laser (Horizontal scale 200 nsecs/division)

than the, 60 ns halfwidth, gain-switched spike of the CO_2 laser pulse. This suggests that a significant proportion of the useful CO_2 pump energy comes from the CO_2 laser pulse tail. Indeed, this interpretation is supported by the observation that on many occasions the F I R pulse shape was seen to consist of two partially merged peaks of equal height which appeared to correspond to the spike and tail of the CO_2 laser pulse. (An example of this effect can be seen in Fig.4.10(d)). At high pressures ($\geqslant$ 1.5 torr) these double peaks were almost entirely separated.

A scanning metal mesh Fabry-Perot interferometer (see Appendix 'C') with a free spectral range of 10 GHz was used to determine the wavelength of the F I R output which was found to be 496 μm. (This corresponds to the $J = 12 \rightarrow 11$, ν_3 transition discussed in Appendix 'E'.) The Fabry-Perot interferometer spectrum was built up from a sequence of F I R laser pulses. A Fabry-Perot interferometer with a free spectral range of 360 MHz and an instrumental width of about 30 MHz was used to measure the bandwidth of the multimode F I R cavity laser and the results obtained are shown

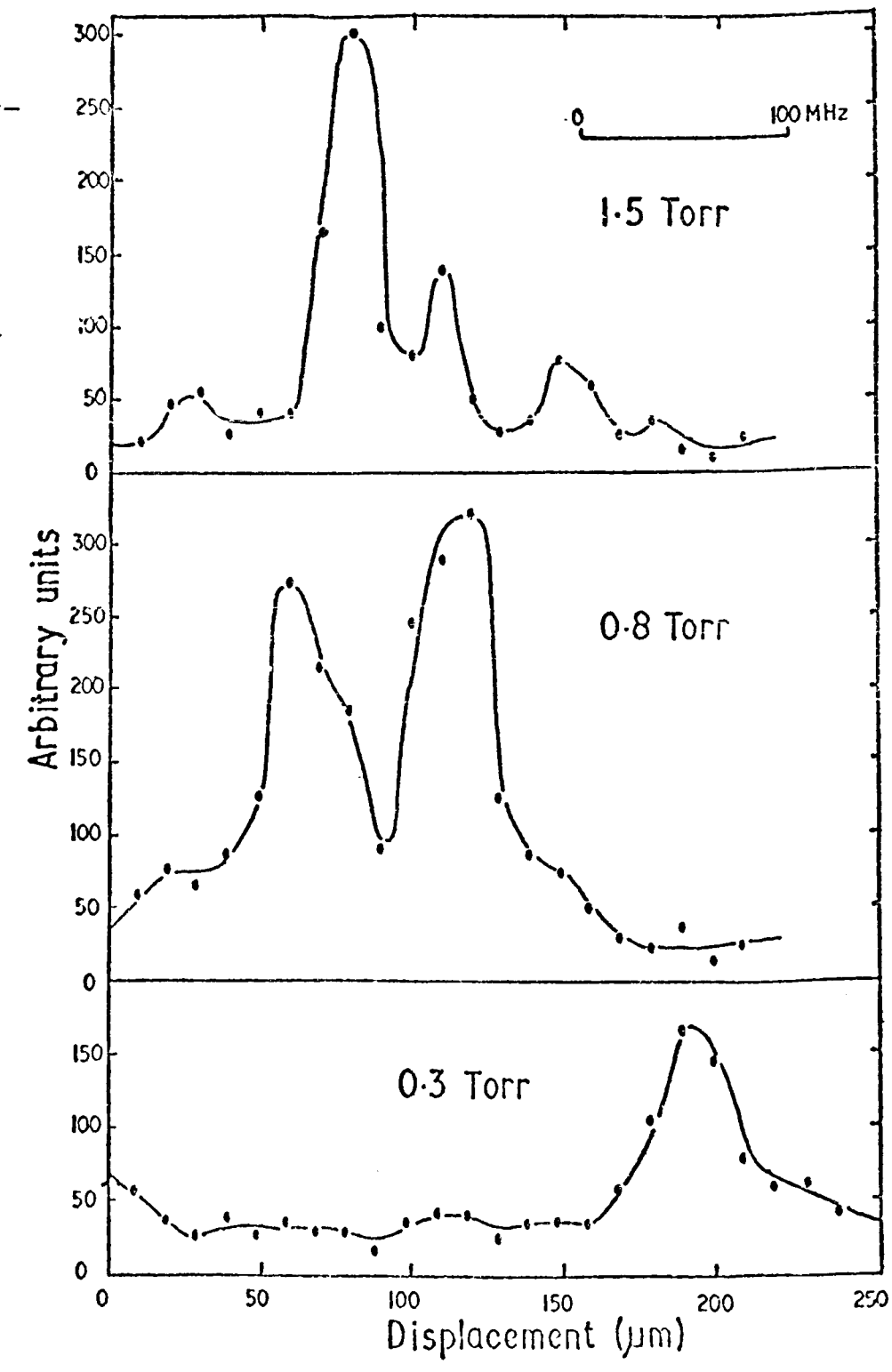


Fig.4.5
Fabry-Perot interferometer scans of the multimode cavity output for CH_3F gas pressures of 0.3, 0.8 and 1.5 torr

in Fig.4.5. The bandwidth increased from about 50 MHz at 0.3 torr to over 130 MHz at 0.8 torr. The bandwidth fell slightly at higher CH_3F pressures, being only 80 MHz at 1.5 torr. It is interesting to note the shift of centre frequency of the laser as the CH_3F pressure was increased. The centre frequency shifted by over 150 MHz when the CH_3F pressure was increased from 0.3 to 0.8 torr, although above this pressure the centre frequency appeared to remain reasonably constant. This effect may result from a change of K level involved in the FIR transition (see Appendix 'E'), although it is complicated here by the superposition of both longitudinal and transverse cavity modes. However, we have also observed this phenomenom in a mirrorless, super-radiant CH_3F laser where there are no cavity modes to complicate the frequency dependence of the laser gain (see Chapter V). We consider a possible explanation for this effect in Appendix 'B'.

A grid polarizer was used to determine the degree of polarization of the FIR laser beam. The FIR radiation was found to be 95% plane polarized perpendicular to the CO_2 pump radiation; this is consistent with absorption by a $\Delta J = 0$, Q-branch, transition (CHANG, 1974 and Appendix 'E').

4.3 THE SINGLE MODE CAVITY

In order to narrow the bandwidth of the FIR cavity laser,† steps were taken to reduce the number of cavity modes for which gain could be obtained in the oscillator. Fig.4.6 shows a schematic diagram of the FIR cavity laser which illustrates the additional optical components required to obtain laser oscillation on a single longitudinal mode.

An iris diaphragm with an aperture which could be varied from 1 to 8 cms in diameter was used to suppress off-axis modes. This aperture was

---

† The objective here was to satisfy the laser bandwidth requirement for collective Thomson scattering derived in Section 1.4, namely $\Delta\nu \leqslant 60$ MHz.

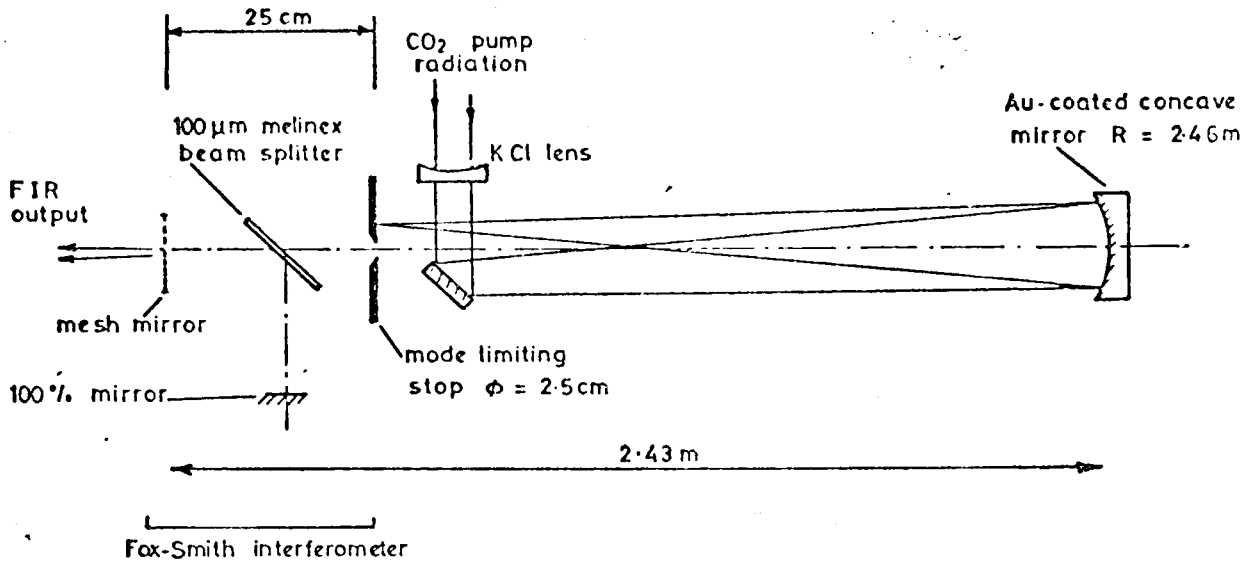


Fig.4.6 Layout of the single mode cavity

mounted inside the vacuum vessel and immediately adjacent to the TPX vacuum window shown in Fig.4.1; the aperture could be adjusted from outside the vacuum system. To be certain of obtaining TEM_{oo} mode operation of the cavity for radiation of wavelength λ, the Fresnel number, N, for the cavity, given by $N = dD/L\lambda$, must satisfy the condition $N \leqslant 1$, where L is the distance between the aperture and the concave mirror, D is the radius of the pump beam on the concave cavity mirror and d is the radius of the aperture. For the cavity geometry shown in Fig.4.6 this implies an aperture diameter of about 2.5 cms, although as we show later, TEM_{oo} operation was obtained for aperture diameters up to 4 cms.

Longitudinal mode selection was obtained by inserting a Fox-Smith interferometer (SMITH, 1965) into the F I R cavity (but outside the vacuum vessel). (Both transverse and longitudinal mode selection methods are discussed by KOGELNIK (1966).) The Fox-Smith interferometer behaves as a frequency selective mirror, and was chosen in preference to a Michelson interferometer since it displays a high reflection finesse. The interferometer consisted of a 100 µm thick Melinex† beam-splitter, a 100% reflecting

† Melinex (or Mylar) is the trade name for polyethylene tetraphthalate which is reasonably transparent in the F I R with a refractive index of about 1.75.

concave copper mirror with a radius of curvature of 100 cms [†] and the metal mesh cavity mirror. The concave copper mirror was mounted on an axially adjustable side-arm with a micrometer movement which allowed the mirror to be scanned through 5 cms. The cavity formed between the mesh mirror and the copper side-arm mirror was about 80 cms long. Thus the principal F I R cavity had a longitudinal mode separation of 61 MHz, whilst the auxiliary cavity had a longitudinal mode spacing of 190 MHz.

4.4 THE 496 μm, CH_3F SINGLE MODE CAVITY LASER

In this section we discuss the performance of a single mode F I R cavity laser. The results presented here were obtained with 0.5 to 0.8 torr of CH_3F gas as the laser medium, optically pumped with about 30 J of 9.55 μm, P(20), CO_2 laser radiation.

Figure 4.7 illustrates the suppression of off-axis transverse modes by the iris diaphragm in the F I R cavity. The three traces shown in the figure were obtained with a Si-W point contact diode, the output signals from the diode being displayed on a 100 MHz storage oscilloscope. Trace (a) was obtained by scanning the Fox-Smith interferometer side-arm mirror to obtain a single longitudinal mode, the aperture diameter was about 4 cms, sufficiently small in this case to select the lowest order, TEM_{oo}, transverse mode. Traces (b) and (c) were obtained for an aperture diameter of 6 and 8 cms , respectively. Beating between low order transverse modes (separated by about 30 MHz, see Appendix 'A') was seen to grow as the diameter of the diaphragm aperture was increased beyond about 4 cms.

---

† Initially a plane copper mirror was used in the side arm of the Fox-Smith interferometer; however this generally resulted in poor longitudinal mode selection. In order to match the spot sizes of the fundamental modes in both the main and interferometer cavities, the use of a concave sidearm mirror was adopted. The formulae for the calculation of the radius of curvature of this mirror, required in order to match the two cavities, are given in BOYD and KOGELNIK (1962).

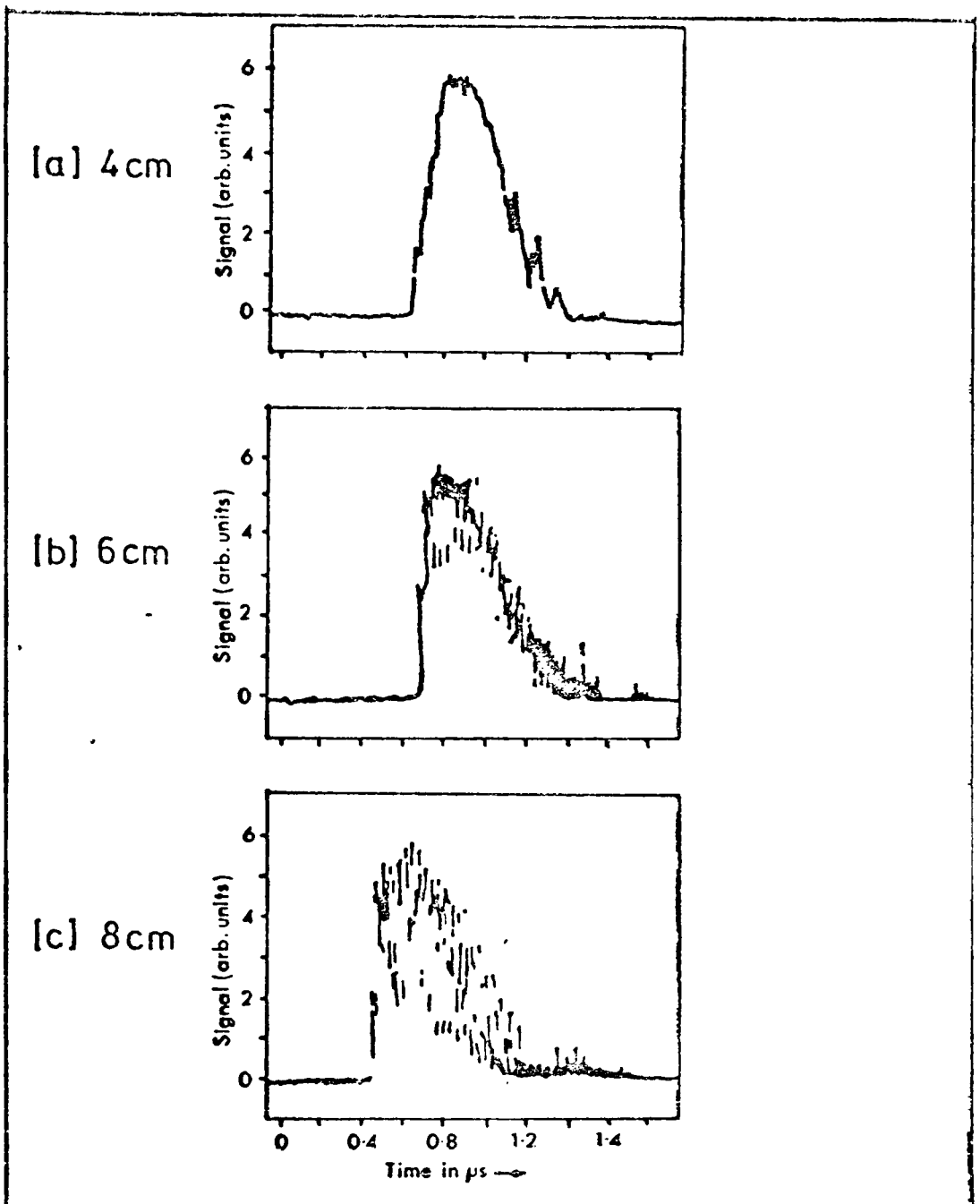
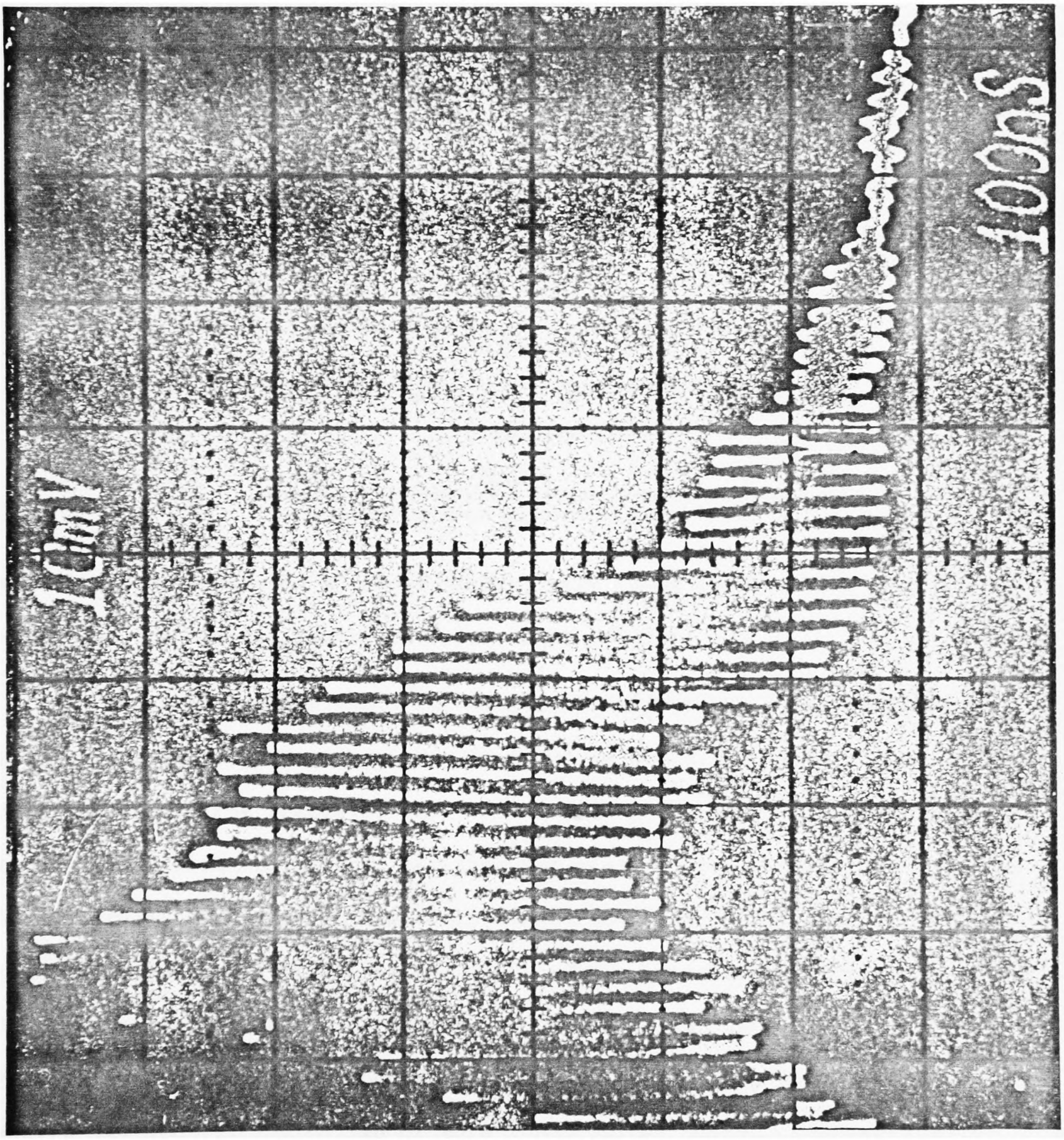


Fig.4.7
Effect of the mode limiting stop the F I R laser output pulse. Point contact diode traces are shown for aperture diameters of (a) 4 cms, (b) 6 cms, (c) 8 cms.

With the interferometer beam splitter removed from the cavity strong 60 MHz modulation was observed on the F I R output pulse, when the aperture in the cavity was reduced to reject all but the TEM_{oo} set of longitudinal modes. Fig.4.8 shows a Si-W point contact diode trace of a F I R output pulse which illustrates strong beating between adjacent longitudinal modes. In order to confirm the presence of two or more longitudinal modes under these conditions a Fabry-Perot interferometer was used to analyse the spectrum of the F I R pulses. Fig.4.9 shows one of these Fabry-Perot interferometer scans obtained with a free spectral range of just over 360 MHz . Three

Fig.4.8
Point contact diode signal showing strong 60 MHz
longitudinal mode beating



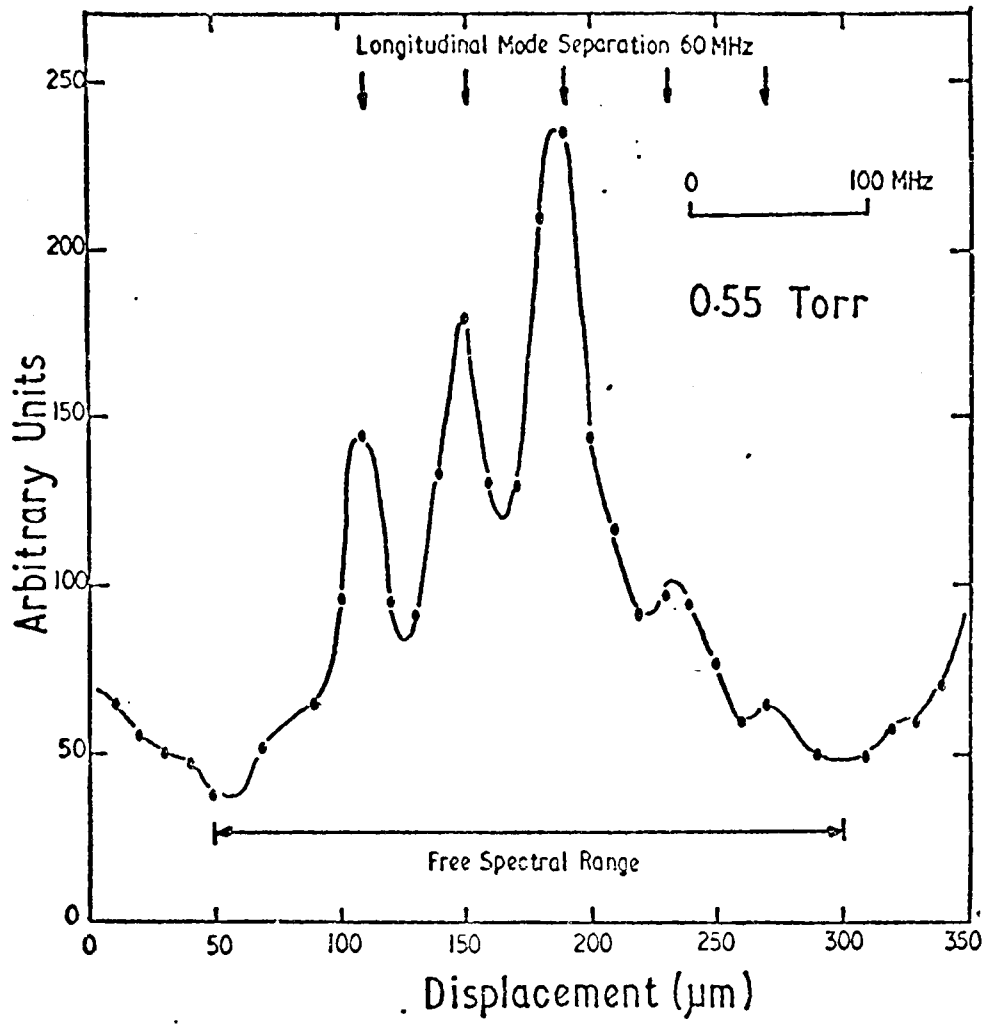
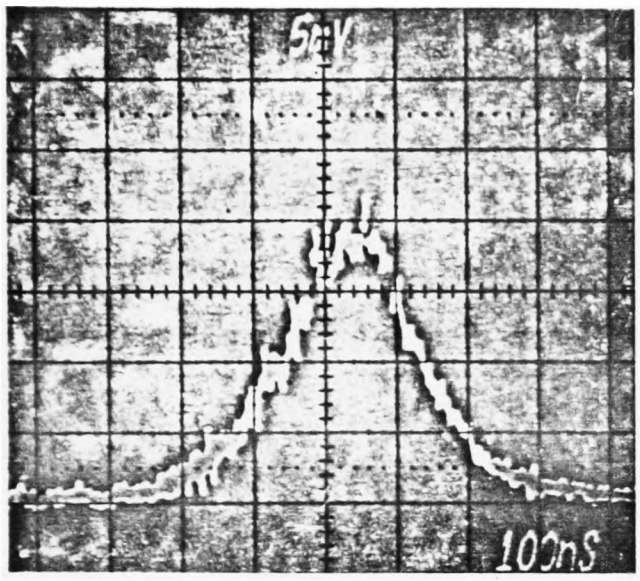


Fig.4.9
Fabry-Perot interferometer scan showing several longitudinal cavity modes separated by about 60 MHz

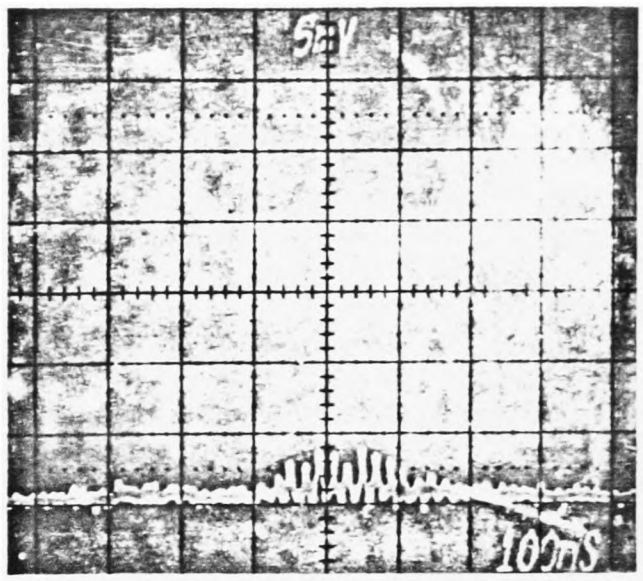
strong peaks, separated by about 60 MHz, were found in the F I R output spectrum, the overall bandwidth being about 140 MHz.

The behaviour of the F I R output as a function of the position of the interferometer side-arm mirror is shown in Fig.4.10. This figure shows point contact diode traces of the F I R output pulse for six different positions of the side-arm mirror, the side-arm mirror being displaced axially by 50 μm between each trace. The total displacement of 250 μm corresponds to scanning through one free spectral range of the interferometer for the 496 μm F I R radiation. As the side-arm mirror was adjusted, the output pulse from the laser became strongly modulated at 60 MHz, suggesting that the laser cavity was oscillating on two or more longitudinal modes. Further adjustment of this mirror resulted in complete suppression of oscillation in the cavity, until single longitudinal mode operation was regained, after the side-arm mirror had been moved through 250 μm.

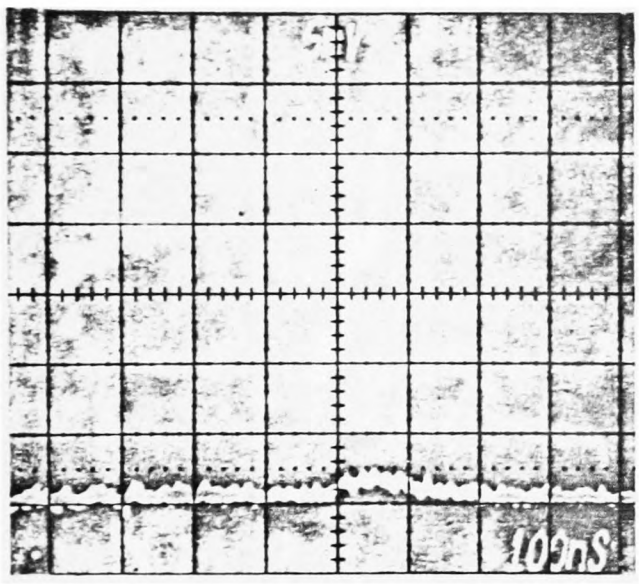
(a)



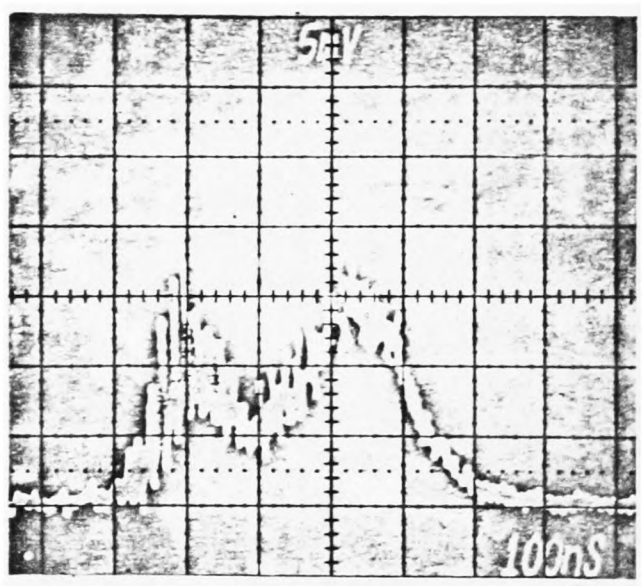
(b)



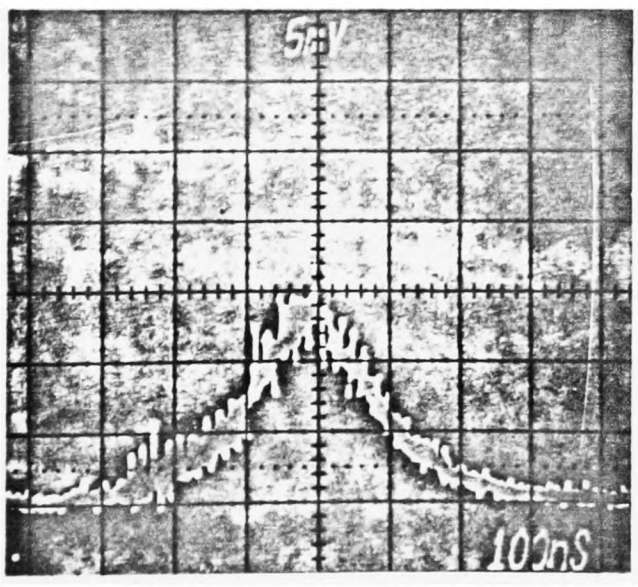
(c)



(d)



(e)



(f)

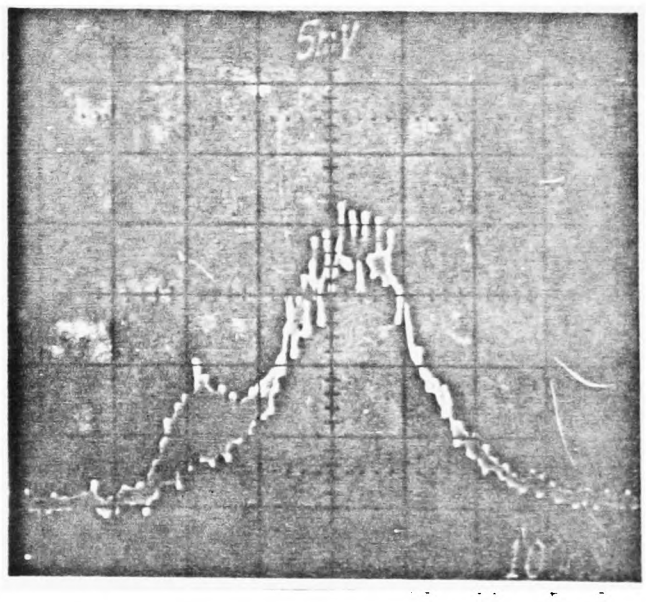


Fig.4.10

Point contact diode signals of the FIR cavity output for several positions of the Fox-Smith interferometer side arm mirror. Signals are shown for mirror displacements of (a) 0, (b) 50, (c) 100, (d) 150, (e) 200 and (f) 250 μm. (The transverse mode limiting stop was about 3 cms in diameter for all the signals shown. The horizontal scale is 100 nsecs/division)

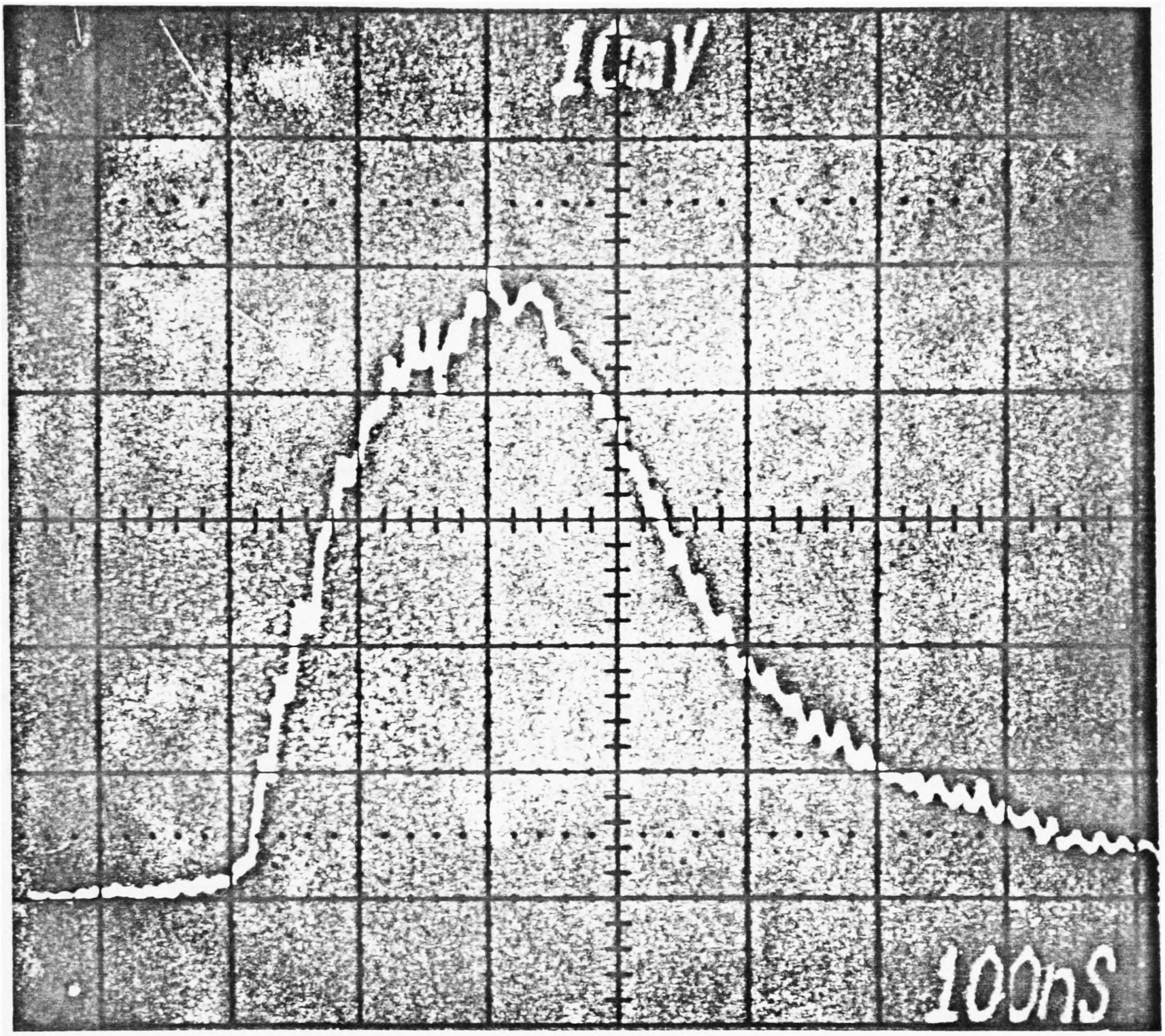


Fig.4.11

Point contact diode trace of the output of the single mode cavity with longitudinal and transverse mode selection fully optimized (Horizontal scale is 100 nsecs/division)

Figure 4.11 illustrates the pulse shape obtained from the F I R cavity when both transverse and longitudinal mode selection had been optimized in the F I R cavity. The F I R pulse waveform was nearly smooth with a duration of nearly 600 ns. Since the detection system used had an overall bandwidth of 100 MHz, the smoothness of the F I R pulse shape suggests that the spectrum is transform limited, so that the spectral width is approximately the reciprocal of the pulse width (i.e. ~ MHz). Fig. 4.12 shows a Fabry-Perot interferometer scan of the single mode laser output. The curve drawn through the experimental points is the instrumental Airy function for a finesse of 14 (see Appendix 'C'). The close fit of this function suggests a laser line width which is considerably narrower than the instrumental width of 27 MHz.

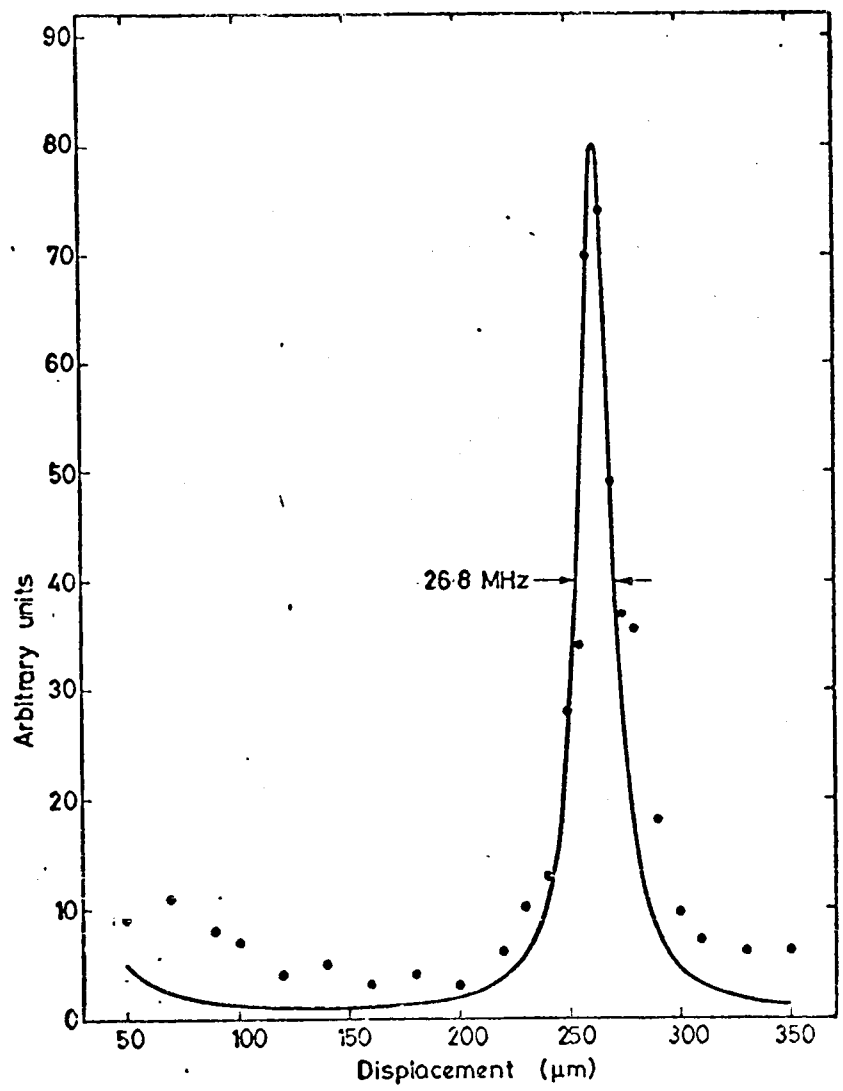


Fig.4.12
Fabry-Perot interferometer scan of the single mode output showing an instrumentally limited bandwidth of about 27 MHz. The curve drawn here is the Airy function for a finesse of 14

The total F I R pulse energy for the single mode cavity laser was 0.3 mJ. This, together with the F I R pulse shape in Fig.4.11, suggests an average pulse power of 500 W and a peak power of 1 kW, substantially less than the power obtained for the multimode cavity laser. The F I R output energy was measured at 0.5 cm intervals both horizontally and vertically across the F I R output of the single mode laser with a 14 BT Laser Instrumentation calorimeter†, (see Fig.4.13). This calorimeter had a 1 cm diameter

† Calibrated to an accuracy of better than 10% at the National Physical Laboratory, U.K.

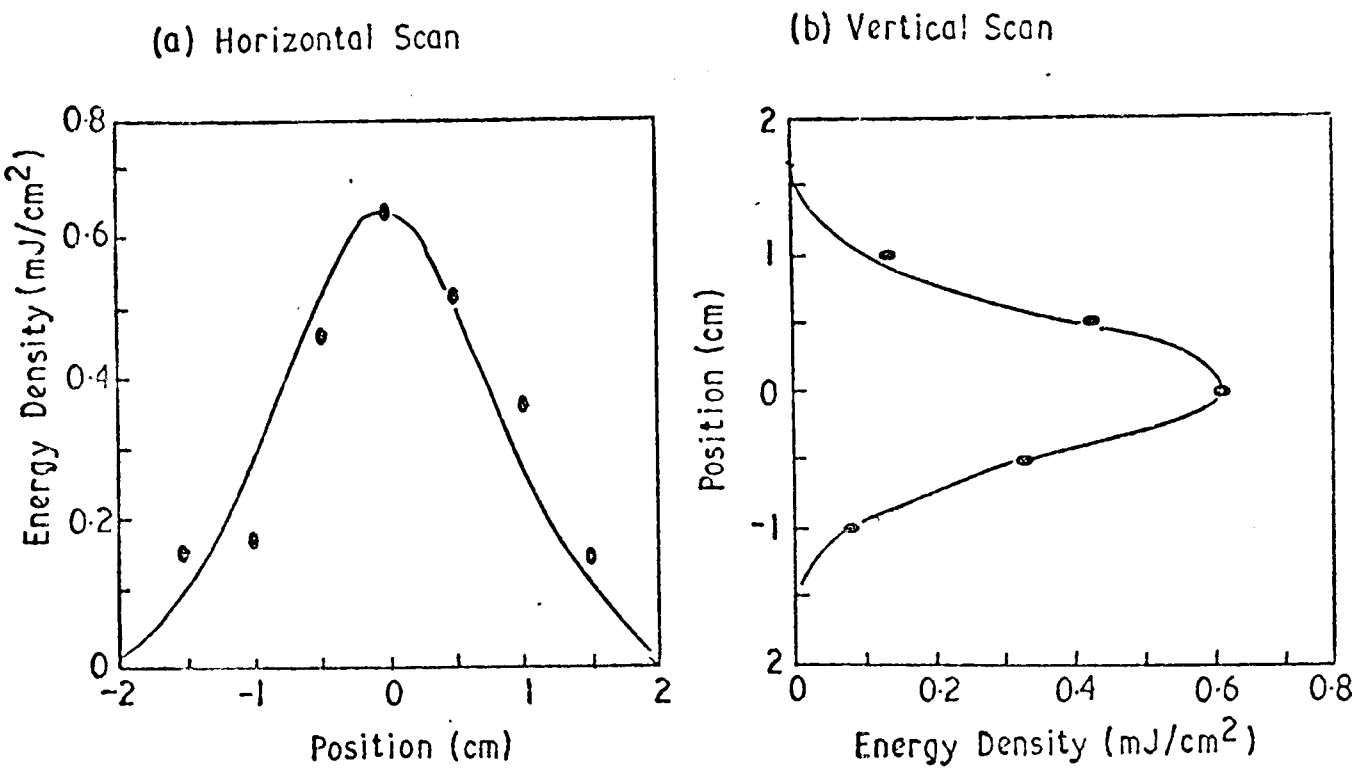


Fig.4.13
Beam energy profile for the single mode FIR laser output.
The curves are best fit Gaussians

sensitive area. The beam width was found to be about 2.5 cms horizontally and about 2 cms vertically, the maximum energy density being about 0.7 mJ/cm^2. The beam profile was nearly Gaussian as expected for a TEM_{oo} mode pattern.

4.5 SUMMARY OF THE PROPERTIES OF THE 496 μm CH_3F CAVITY LASER

To summarize, the performance of the 496 μm CH_3F cavity laser was as follows: (Results were obtained for a total CO_2 pump energy of 30 J.)

	Multimode Cavity	Single Mode Cavity
Wavelength	496 μm	496 μm
CH_3F Operating Pressure	0.8 torr	0.8 torr
Pulse Length	600 ns	600 ns
Pulse Energy	2 mJ	0.3 mJ
Average Power	3.5 kW	500 W
Peak Power	7 kW	1 kW
Bandwidth	140 MHz	< 30 MHz *
Polarization	Vertical †	Vertical †
Conversion Efficiency ≠	8.6×10^{-5}	1.5×10^{-5}

* Si-W diode traces suggest bandwidth ~ MHz

† Polarization perpendicular to CO_2 laser polarization

≠ The conversion efficiency is defined as FIR output energy divided by the total CO_2 pump energy.

CHAPTER V

THE SUPER-RADIANT F I R LASER

In the previous chapter we presented experimental results concerning the operation of a F I R cavity laser, which satisfied both the wavelength and the bandwidth requirements for collective Thomson scattering derived in Chapter I. However, even the comparatively broadband ($\gtrsim$ 100 MHz) multimode cavity produced only a few kilowatts of 496 μm radiation, which is several orders of magnitude less than the minimum required power for Thomson scattering (see section 1.3).

In this chapter we discuss the performance of mirror-less, D_2O and CH_3F super-radiant lasers, which produce intense F I R radiation at several different wavelengths between 50 and 496 μm. The pulse powers of most of the laser emissions investigated were found to satisfy and in some cases to exceed the minimum power requirement for Thomson scattering.

Section 5.1 describes the layout of the super-radiant laser used in this work. In section 5.2 we consider the performance of a super-radiant CH_3F laser pumped by the P(20) (9.6 μm band) CO_2 laser line. In sections 5.3, 5.4 and 5.5, we present results for a D_2O super-radiant laser, pumped by the R(22), R(12) and P(32) 9.6 μm band CO_2 laser lines, respectively. Finally, in section 5.6 we summarize and compare the performance of the super-radiant lasers investigated here.

5.1 THE SUPER-RADIANT LASER

Figure 5.1 shows a schematic diagram of the super-radiant laser used in the work described in the following sections of this chapter. A 4.2 m long, 10 cm diameter glass pipe was used to contain the laser medium. The CO_2 laser pump radiation entered one end of this pipe via a 15 mm thick KCl window. The F I R radiation left the gas cell at the opposite end of

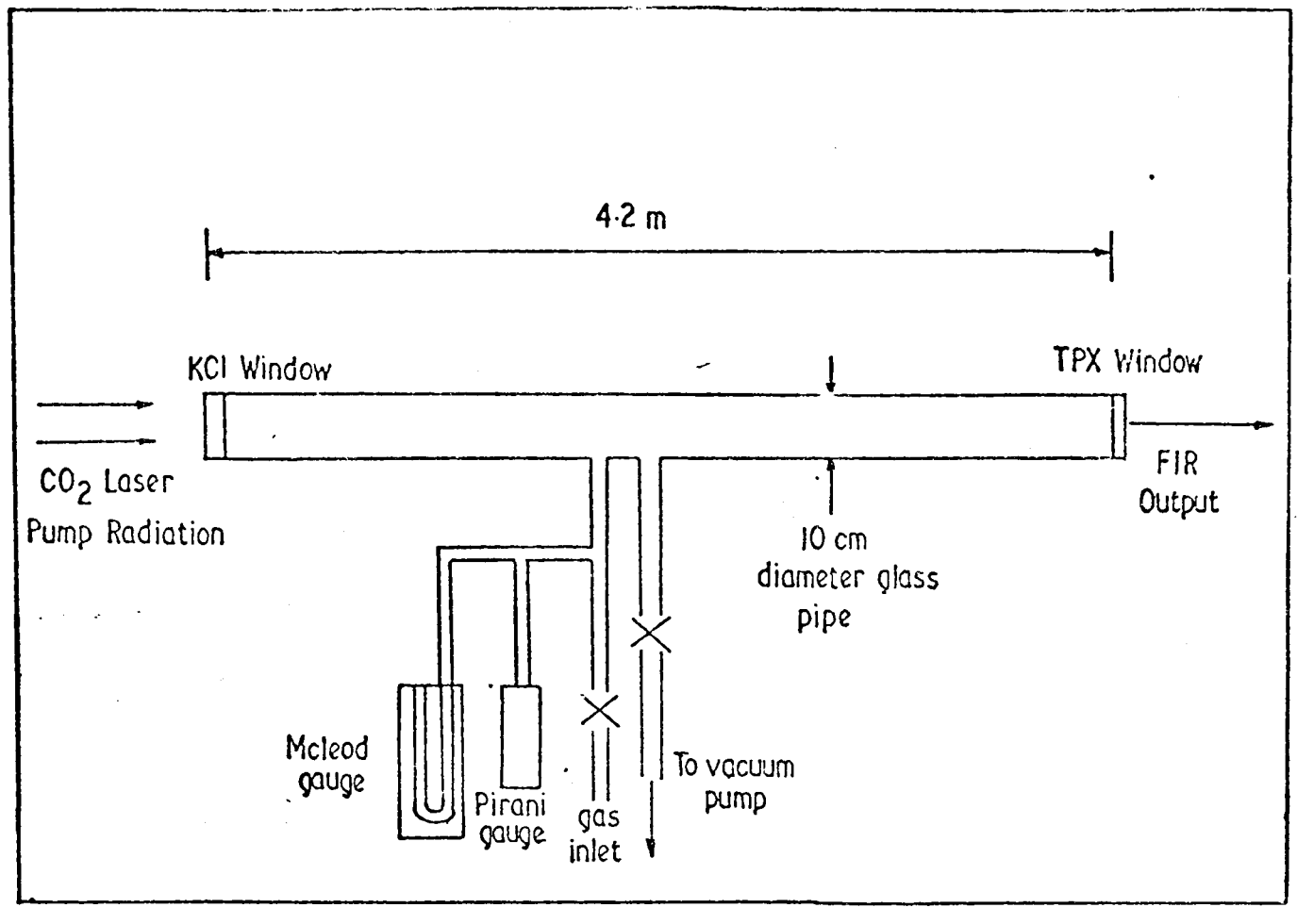


Fig.5.1
Layout of the superradiant laser apparatus

the pipe via a 9.6 mm thick TPX window. A single stage rotary pump was used to evacuate the glass pipe and the pressure was monitored with McLeod and Pirani gauges.

Prior to filling the gas cell with several torr of CH_3F the pipe was evacuated to 10^{-2} torr. When the laser was operated with D_2O a small flask containing about 50 cm^3 of heavy water was connected to the system via a needle valve. The super-radiant cell was first pumped down to 10^{-2} torr before the needle valve was opened. The flask was then pumped for about 5 minutes, in order to evacuate as much air as possible, whilst allowing the water vapour to evaporate and fill the vacuum vessel. The pump was then sealed off from the rest of the vacuum system and the flask left connected to the gas cell, until sufficient water vapour had evaporated to reach the required operating pressure (normally $\sim$ 4 torr). However, since the vapour pressure of water at 20°C is about 15 torr, it was not possible to operate above about 10 torr.

The glass pipe was constructed from several sections which were relatively easy to assemble, so that the tube length could be varied as required. Gas cells longer than 4.2 metres were tried but, owing to the restricted size of the laboratory, this required one or more mirrors to deflect the pump and FIR radiation through 90° or 180°.

The CO_2 pump radiation was produced by the system B laser described in Chapter III, which was operated as a 4.5 m long oscillator. Initially we used the laser in an oscillator-amplifier configuration, but feedback from the KCl window at the entrance to the super-radiant laser caused the CO_2 amplifier to oscillate at 10.6 μm.

5.2 THE 496/452 μm CH_3F LASER

Using the gas cell described in the previous section the FIR output from CH_3F gas pumped by the P(20), 9.55 μm, CO_2 laser line was measured as a function of gas pressure and CO_2 pump energy. The results of these measurements are shown in Fig.5.2 and 5.3.

The FIR output from the gas cell was measured directly in front of the TPX window with a calorimeter (Laser Instrumentation Model 14 BT). The CO_2 laser beam was attenuated by calibrated polythene sheets immediately before it entered the gas cell. Fig.5.2 shows the FIR output energy as a function of CH_3F gas pressure. The curves obtained for the super-radiant laser were found to be similar to those obtained for the CH_3F cavity laser (see Chapter IV). In particular the pressure at which the maximum FIR output was obtained was found to increase with increasing pump energy. The maximum FIR output, 33 mJ, was obtained with a CH_3F gas pressure of 2.2 torr and a total CO_2 pump energy of 43 J.

The pump to FIR energy conversion efficiency was about 0.08% which is nearly an order of magnitude better than that achieved with the multimode CH_3F cavity laser (see section 4.2). However later in this section we

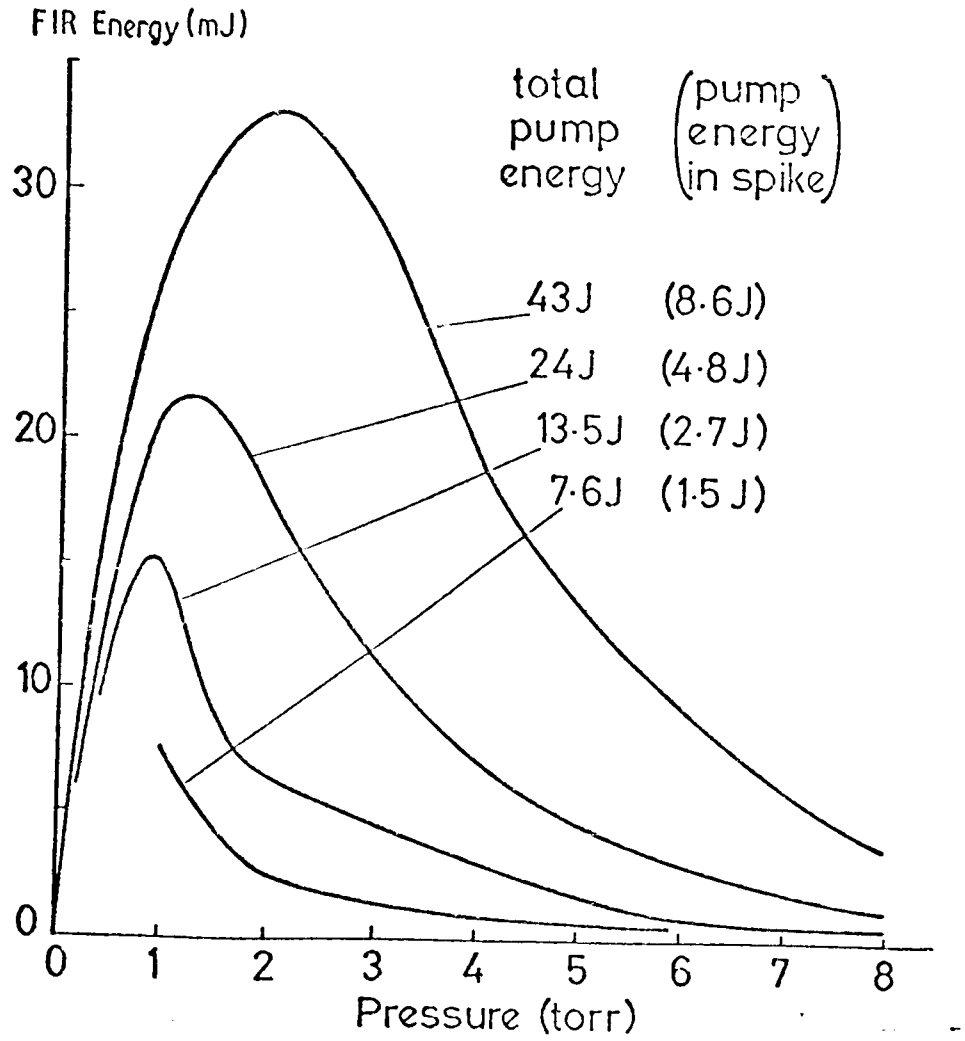


Fig.5.2

FIR output energy against CH_3F pressure for the 496/452 μm emission. Several cases are shown, each for a different CO_2 laser pump energy

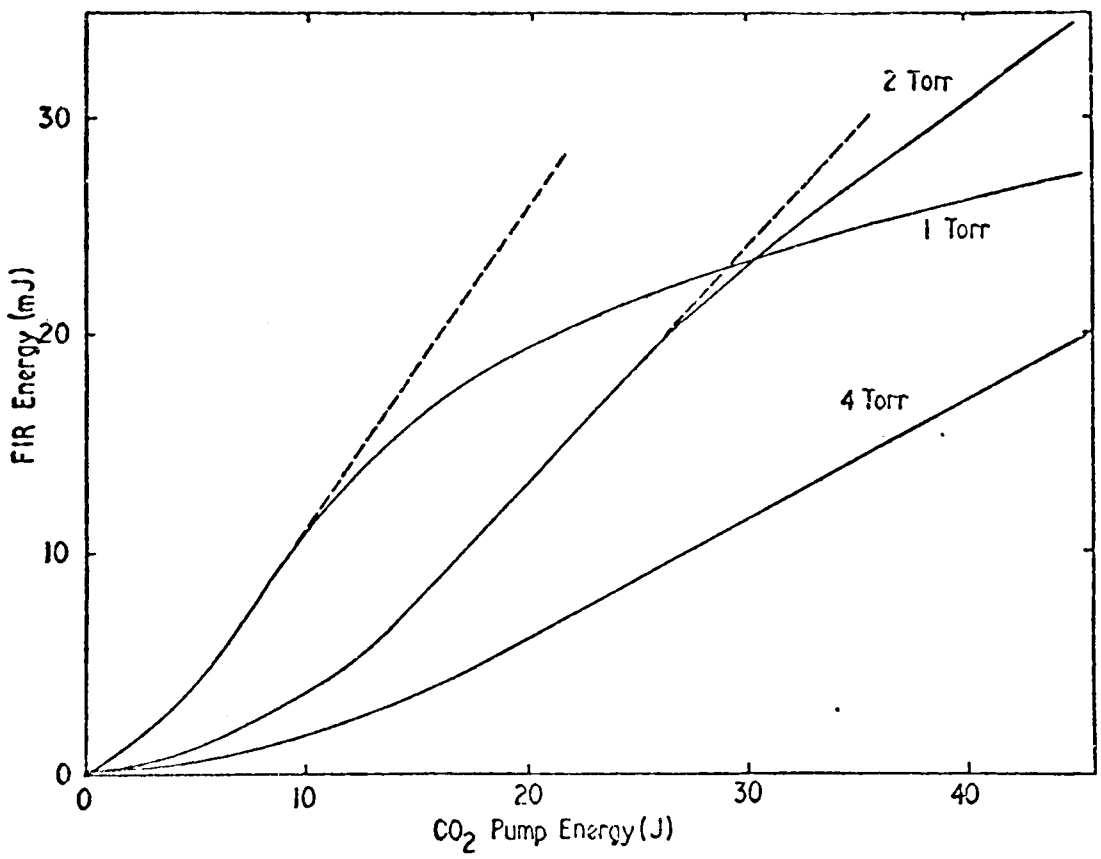


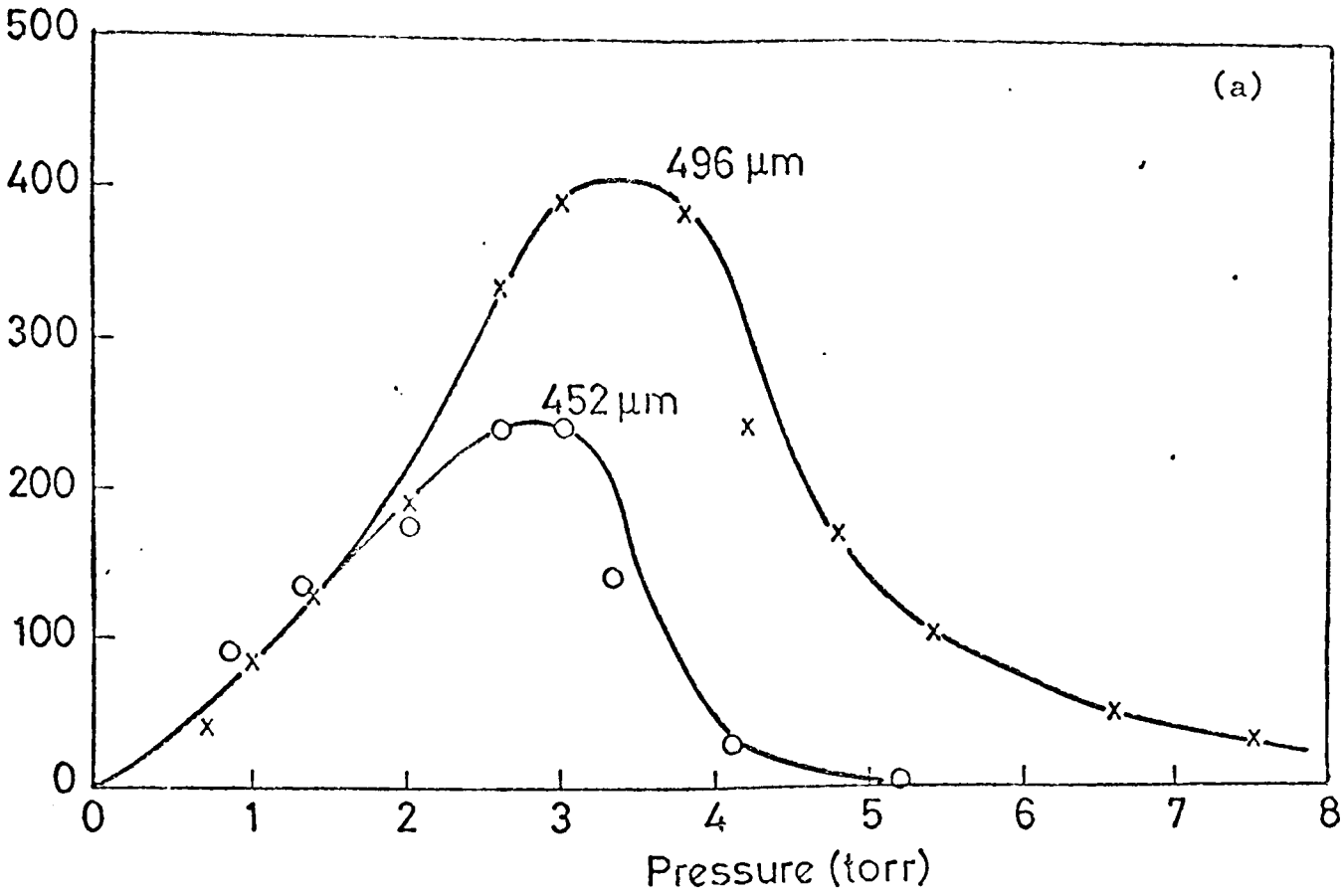
Fig.5.3

FIR output energy against CO_2 laser pump energy for the 496/452 μm emission. Several curves are shown each for a different CH_3F gas pressure

present evidence which strongly suggests that only the gain-switched spike of the CO_2 laser pulse generates F I R super-radiant laser radiation. Therefore since only 20% of the CO_2 laser pulse energy resides in the spike (see for example the photon drag detector signal in Fig.3.5(a)) the true conversion efficiency is about 0.4%, which compares favourably with the Manley-Rowe photon conversion limit of 2%.

The dependence of F I R output energy on CO_2 pump energy is shown in Fig.5.3. For all the CH_3F gas pressures investigated in the present work the F I R output was found to rise faster than linearly with CO_2 pump energy up to a CO_2 pump energy of about 15 J (i.e. about 3 J in the gain-switched spike). As the pump energy was increased above this value, the F I R energy was found to increase linearly with pump energy. However, at high pump energies and low pressures ($\leqslant$ 1.5 torr) the pump to F I R energy conversion efficiency fell steadily with increasing pressure; we interpret this effect as the result of saturation of the F I R laser medium by the pump radiation. (The dashed lines in Fig.5.3 indicate the slope of the linear region.)

A Fabry-Perot interferometer with 250 line/inch Cu mesh plates (see Appendix 'C') was used to determine the wavelength of the F I R output radiation, from the frequency of repetition of fringes as the plate separation was increased by several wavelengths. Normally two lines were observed, with wavelengths of 496 and 452 μm. (These lines correspond to the ν_3, $J = 12 \rightarrow 11$ transition and the ground vibrational state, $J = 13 \rightarrow 12$ transition, as shown in Fig.E.2(a)). Fig.5.4(a) shows a plot of the relative F I R energy of these components against pressure, which was obtained with a CO_2 pump energy of 45 J. At 2.5 torr the 452 μm line was about 60% as intense as the 496 μm emission. As the CH_3F pressure was increased the 452 μm line rapidly diminished relative to the 496 μm line, until at 5 torr it had virtually vanished. On several occasions, notably when the system B CO_2 laser was found to



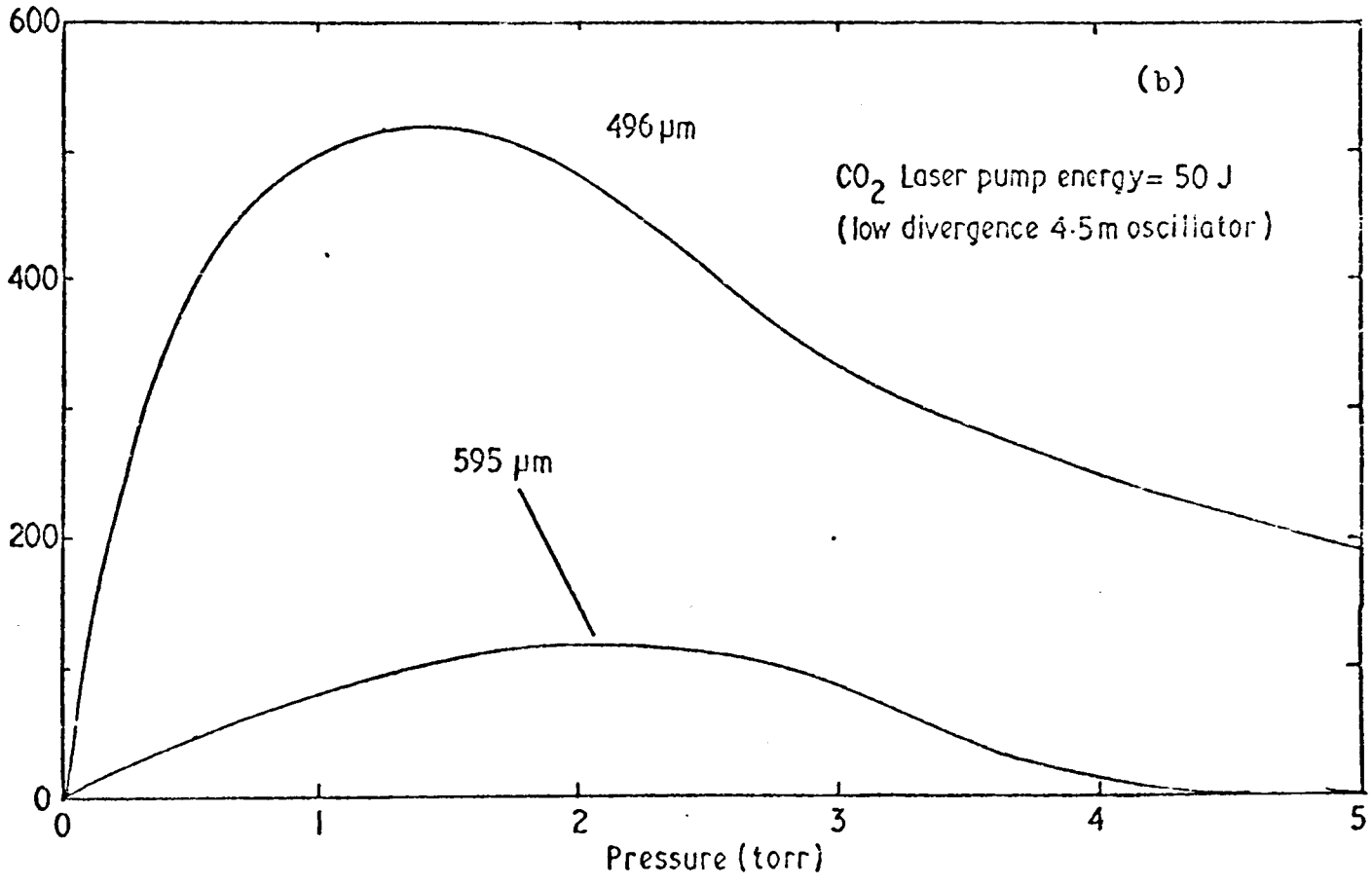


Fig.5.4

(a) Relative energy of the 496 and 452 µm emission lines as a function of CH_3F pressure for a CO_2 laser pump energy of 45 J
(b) Relative energy of the 595 and 496 µm emission lines produced under intense pumping conditions as a function of CH_3F pressure

produce a very low divergence, intense beam, an additional line was observed with a wavelength of 595 μm. The pressure dependence of the intensity of this line relative to the 496 μm emission is shown in Fig.5.4(b). This line has also been observed by BROWN et al (1974) under intense pumping conditions, in a transverse optically pumped (TOP), super-radiant laser (see section 2.5). They assign the 595 μm line to the ν_3, $J = 10 \rightarrow 9$ transition. Brown et al also observed simultaneous emission at 541 μm, corresponding to the ν_3, $J = 11 \rightarrow 10$ transition. However we have never observed the emission at 541 μm, which would be expected to occur if the 595 μm emission arose as a result of a three stage radiative cascade from the $J = 12$ to the $J = 9$ state.

The time dependence of the 496/452 μm output pulse is illustrated in Fig.5.5. The FIR pulse shape was measured with a silicon-tungsten (Si-W) point contact diode and recorded on a 100 MHz storage oscilloscope. The power scale shown in the figure was calculated by equating the area under the FIR pulse to the total measured FIR energy of 33 mJ. The FIR output pulse width was between 60 and 100 ns, with an average power of about 500 kW, and consisted of several randomly spaced spikes each a few nanoseconds wide, with peak powers of up to 1.0 MW. The time delay between the beginning of the gain switched spike of the CO_2 pulse, used to pump the super-radiant tube, and the start of the FIR pulse, was about 25 to 30 ns, for the pressure range investigated here (i.e. 1 to 10 torr). No FIR radiation was detected during the period corresponding to pumping by the tail of the CO_2 laser; it therefore appears that only the gain-switched spike has sufficient intensity to produce super-radiance in the single pass CH_3F laser.

Figure 5.6 summarizes the results obtained for FIR output and CO_2 pump attenuation as a function of CH_3F gas pressure for tube lengths of 1.46, 2.66, 4.2 and 7.3 metres. For these measurements the system B CO_2 laser

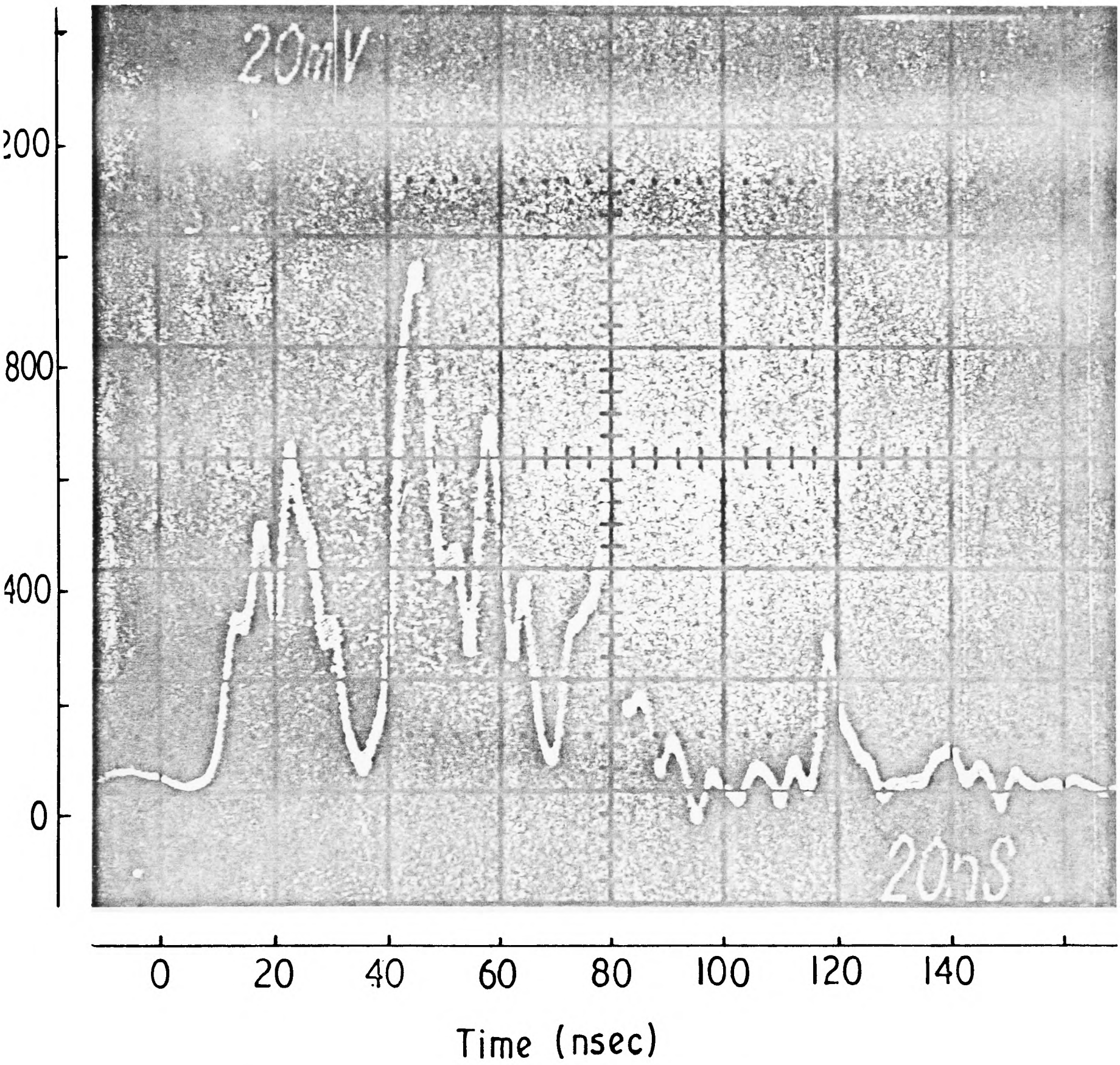


Fig.5.5

Time resolved output pulse for the 496/452 μm emission showing the peak FIR power as a function of time

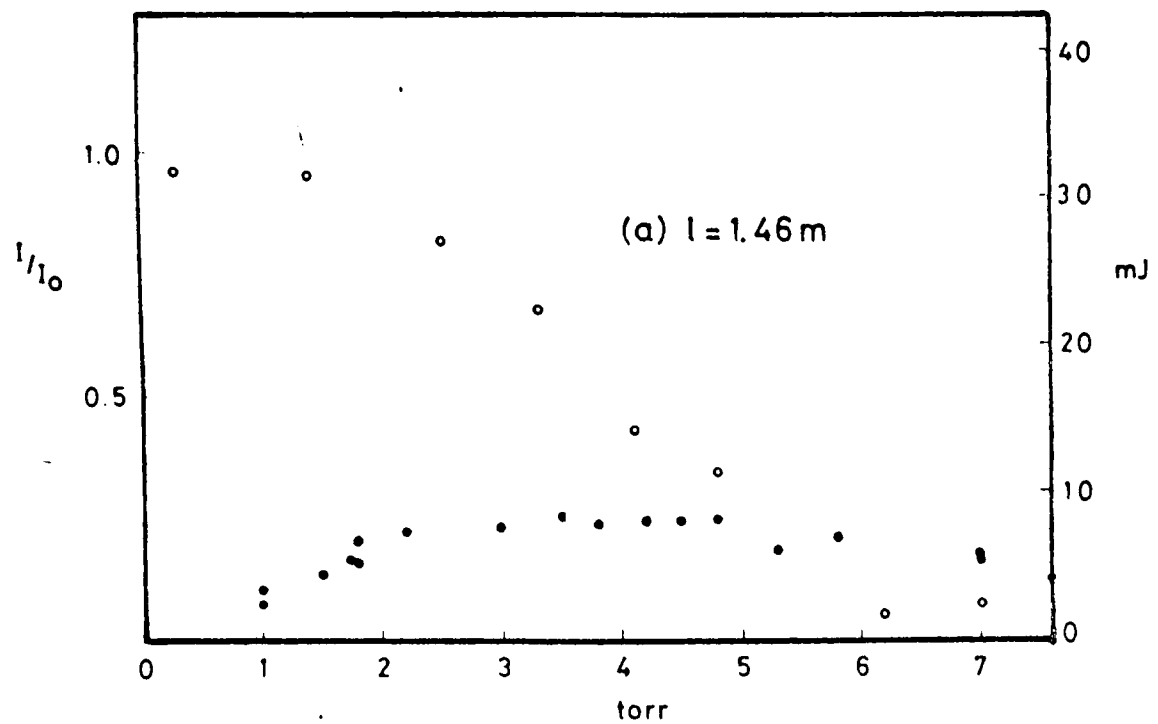


Fig.5.6

The CO_2 laser absorption and the FIR output at 496/452 μm as a function of CH_3F pressure for superradiant cell lengths of (a) 1.46, (b) 2.66, (c) 4.2 and (d) 7.3 m
(● - FIR output o - attenuation of CO_2 radiation)

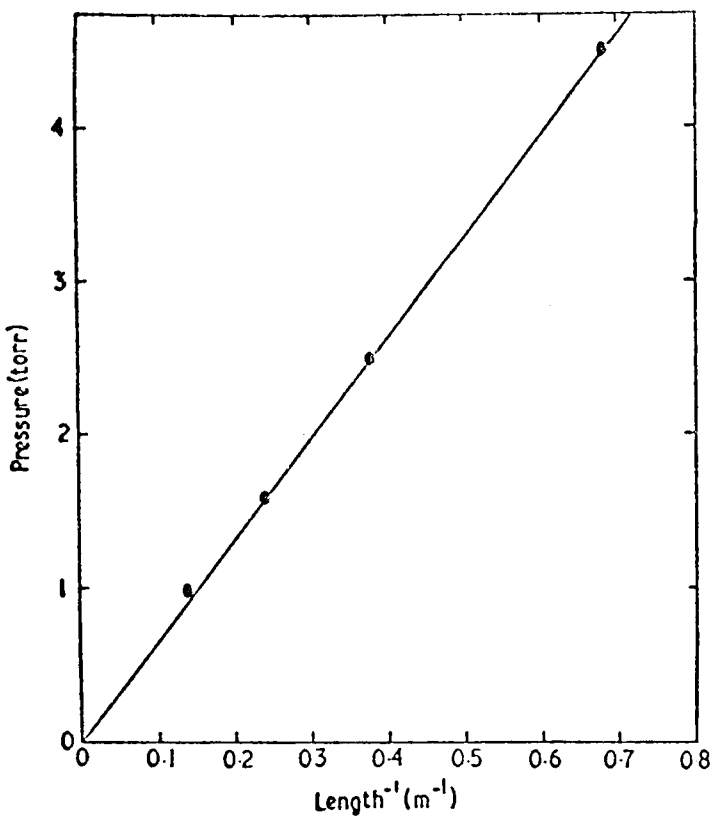


Fig.5.6(c)
CH_3F pressure for maximum F I R output against length^{-1}

was operated as a 3 metre oscillator and only two of the CO_2 laser modules in system B were used. This configuration produced a total CO_2 laser pulse energy of 30 J of which approximately 6 J was generated in the gain switched spike.†

For all the tube lengths investigated here, the F I R output was found to be maximum when the CH_3F pressure was adjusted so that approximately 70% of the CO_2 pump energy had been absorbed. The pressure at which the F I R output peaked, decreased with increasing tube length, so that the maximum F I R energy was generated for the same number of CH_3F molecules, regardless of tube length, as illustrated in Fig.5.6(e).

Most of the CO_2 laser energy was absorbed at comparatively low pressures (< 6 torr). Since the frequency of the CO_2 laser pulse is situated between the K = 1 and K = 2 components of the $0 \rightarrow \nu_3$, J = 12 → 12 absorption in CH_3F (INGUSCIO et al, 1976) (see Fig.E.2(b)) and the CO_2 laser pulse has a bandwidth of about 1 GHz (see Chapter III), at least 40% of the pump energy is several hundred MHz away from the absorption in CH_3F.

At high pump intensities* ($\geqslant 100\,kW/cm^2$) the high frequency electric field generated by the CO_2 laser would be expected to produce off-resonant

---

† The CO_2 laser attenuation was determined with a Photon Drag detector in order to isolate the gain switched spike.

* The pump intensity in the experiments discussed here was approximately $1.3\,MW/cm^2$, assuming that the 6 J CO_2 spike has a half width of 60 ns and the pump radiation is uniform over the cross-section ($\sim 80\,cm^2$) of the gas cell.

pumping, similar to that observed by FETTERMAN et al (1972). In order to determine whether this was indeed the case, we carried out CO_2 laser absorption measurements for the 4.2 m CH_3F gas cell at low pump intensities (i.e. $\leqslant 50\,kW/cm^2$). Attenuation in CH_3F remained high even at $10\,kW/cm^2$, where the linewidth due to a.c. Stark broadening would be less than 25 MHz. We must therefore conclude that a.c. Stark broadening is not the only process contributing to the absorption of the off-resonant CO_2 pump radiation. A possible mechanism for the absorption of the off-resonant pump radiation, at both low and high intensities, may lie in the coincidence of the pump frequency with a strong absorption other than the $0 \rightarrow \nu_3$, $J = 12 \rightarrow 12$ transition. We discuss this possibility in Appendix 'D'.

A calorimeter with a $1\,cm^2$ sensitive area was used to measure the F I R energy as a function of position across the diameter of the superradiant tube. The calorimeter was scanned both vertically and horizontally across the TPX output window, and the results are shown in Fig.5.7. The

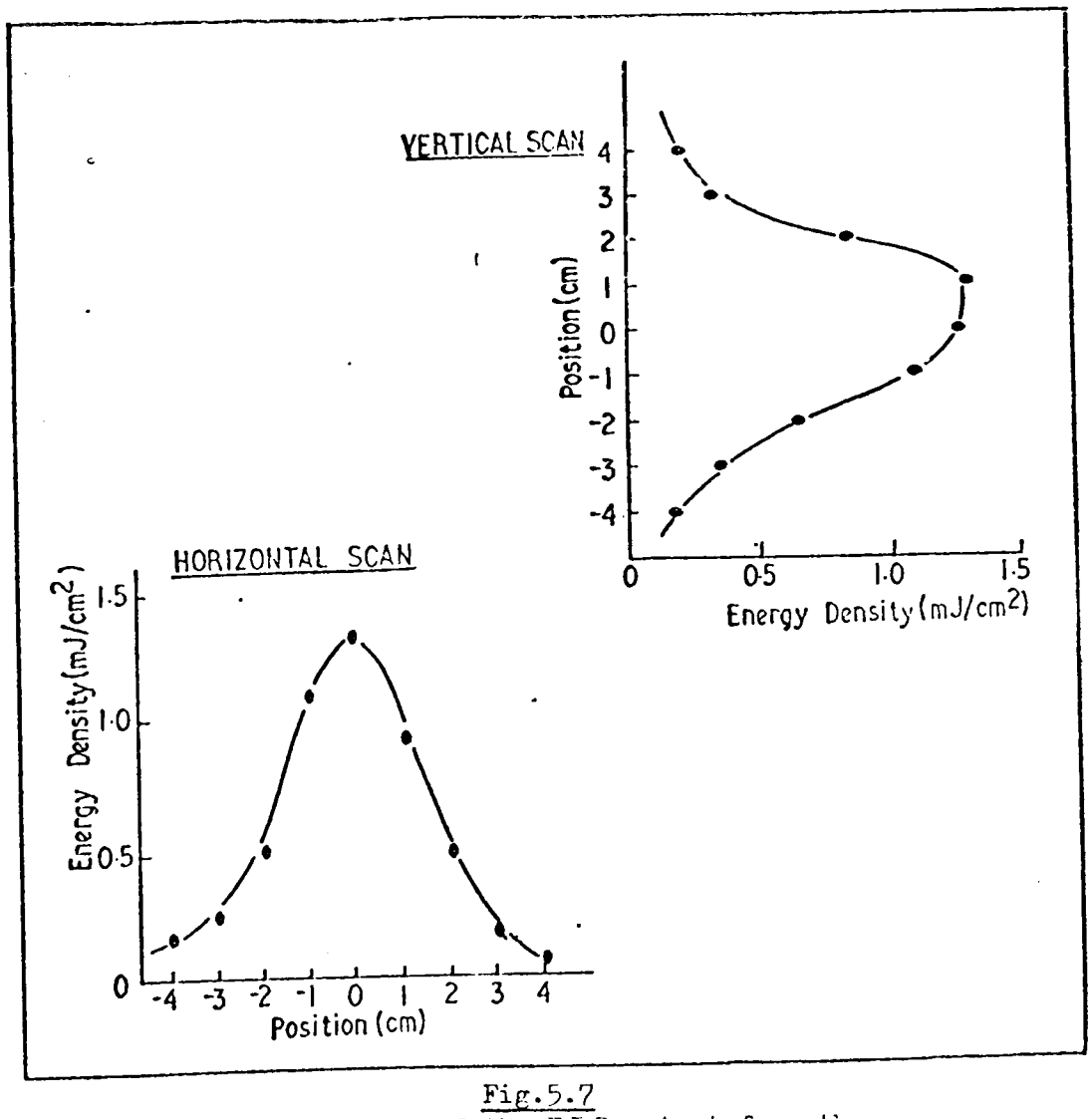


Fig.5.7
Beam profile of the F I R output from the 496/452 μm superradiant laser

beam profile was symmetric about the tube axis and roughly Gaussian in shape, with a peak energy density of $1.3\,mJ/cm^2$. (The total FIR energy was 33 mJ.)

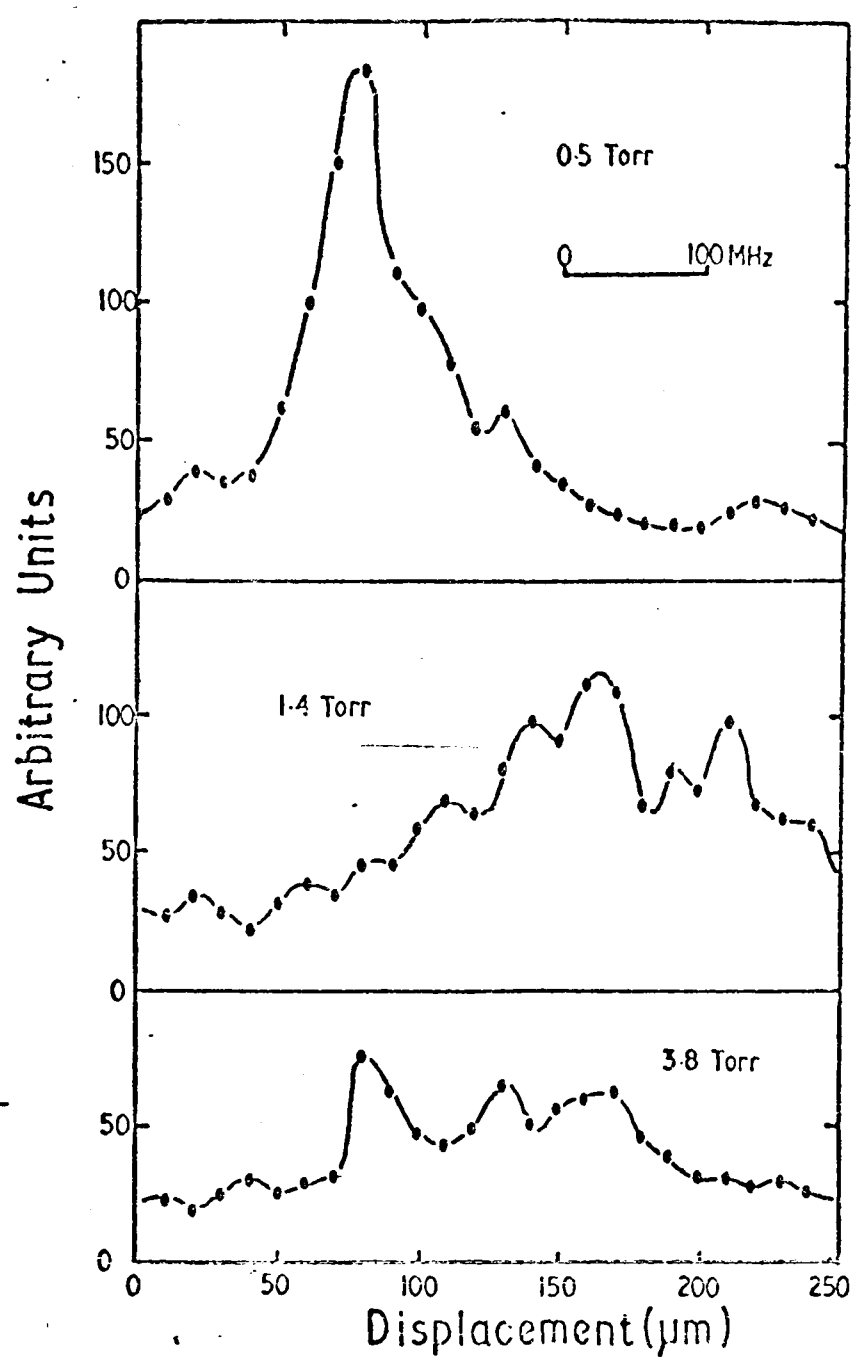


Fig.5.8
Fabry-Perot interferometer scan of the 496 μm superradiant laser pulse for CH_3F gas pressures of 0.5, 1.4 and 3.8 torr. (NB: The vertical scales are different for each scan)

The electric vector of the FIR radiation was found to be perpendicular to the CO_2 pump radiation, in agreement with similar measurements made on the CH_3F cavity laser (see Chapter IV), although the FIR beam was only 80 to 90% plane polarized for the super-radiant assembly. Theoretically (CHANG, 1974), if $|\Delta J|_{absorption}$ and $|\Delta J|_{emission}$ are the difference in J values for the molecular states involved in the pump absorption and FIR emission, the the FIR output should be linearly polarized parallel or perpendicular to the polarization of the pump, depending on whether $|\Delta J|_{absorption} - |\Delta J|_{emission}$ is zero or ± 1, respectively. For the 496 μm CH_3F laser, the observed polarization is in agreement with this theory.

A Fabry-Perot interferometer was used to measure the bandwidth of the 496 μm radiation emitted by the super-radiant laser. Fig.5.8 summarizes the results obtained for three different CH_3F pressures. The bandwidth was found to increase from 100 MHz at 0.5 torr to 300 MHz at 1.4 torr, and remained approximately constant above this pressure. A frequency shift phenomenon similar to that observed in the CH_3F multimode cavity (see Chapter IV) was seen with the CH_3F super-radiant laser. When the CH_3F pressure

was increased from 0.5 to 1.4 torr the centre frequency moved about 200 MHz towards longer wavelengths. We consider a possible explanation for this effect in Appendix 'B'.

Finally, we modified the 4.2 m super-radiant tube by replacing the 15 mm thick KCl flat with an uncoated, 8 mm thick, 150 mm diameter, germanium window, mounted at 45° to the tube axis. F I R radiation generated in the super-radiant tube and travelling in the opposite direction to the pump photons was reflected from the inside face of the germanium and through a TPX window. Since the CO_2 laser radiation was horizontally polarized only about 25% of it was lost by reflection at the germanium window, while about 60% of the 'backward' travelling F I R radiation, which was vertically polarized, was reflected out of the tube. By this method we were able to measure the proportion of F I R photons being radiated in the opposite direction to the pump photons. We found the forward to backward ratio for the F I R radiation to be 2:1 for a total CO_2 energy of 30 J (after transmission through the Ge window). (This ratio was found to be independent of CH_3F gas pressure.) In a similar experiment carried out by PLANT et al (1974), a forward to backward anisotropy of $\sim 10^4$ was observed for both optically pumped CH_3F and D_2O.

5.3 THE 385/359 μm D_2O LASER

In this section we present results obtained for D_2O vapour optically pumped by the R(22), 9.26 μm, CO_2 laser line. Fig.5.9 summarizes the results obtained for the total F I R output as a function of D_2O pressure. The pressure at which the maximum F I R energy was generated increased with increasing pump energy, in a similar fashion to the F I R output for the CH_3F laser (see section 5.2 and Chapter IV). The maximum F I R energy obtained for a D_2O pressure of 4.8 torr and a total CO_2 pump energy of 60 J (12 J in the CO_2 spike) was 120 mJ. The energy conversion efficiency (i.e. CO_2

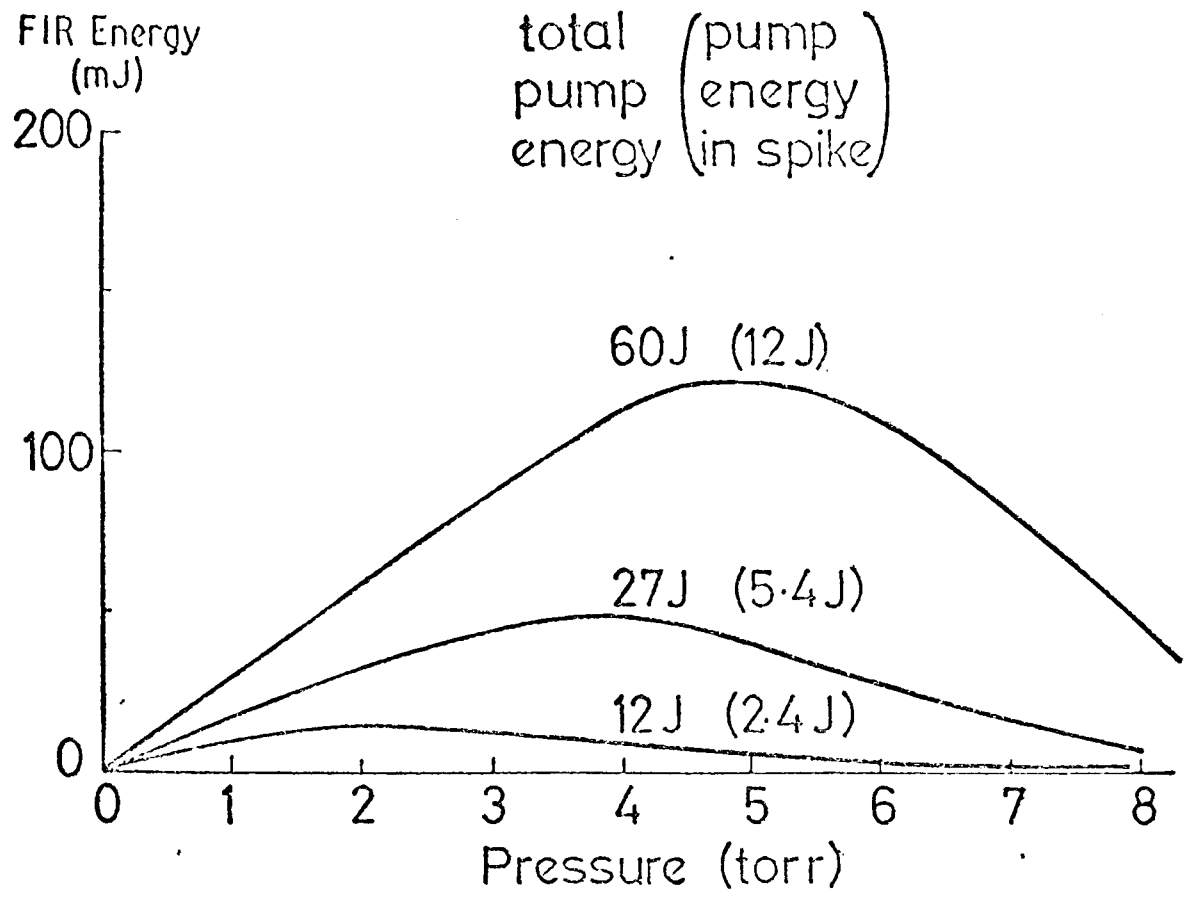


Fig.5.9

FIR output energy against D_2O pressure for the 385/359 μm emission. Several curves are shown each for a different CO_2 laser pump energy

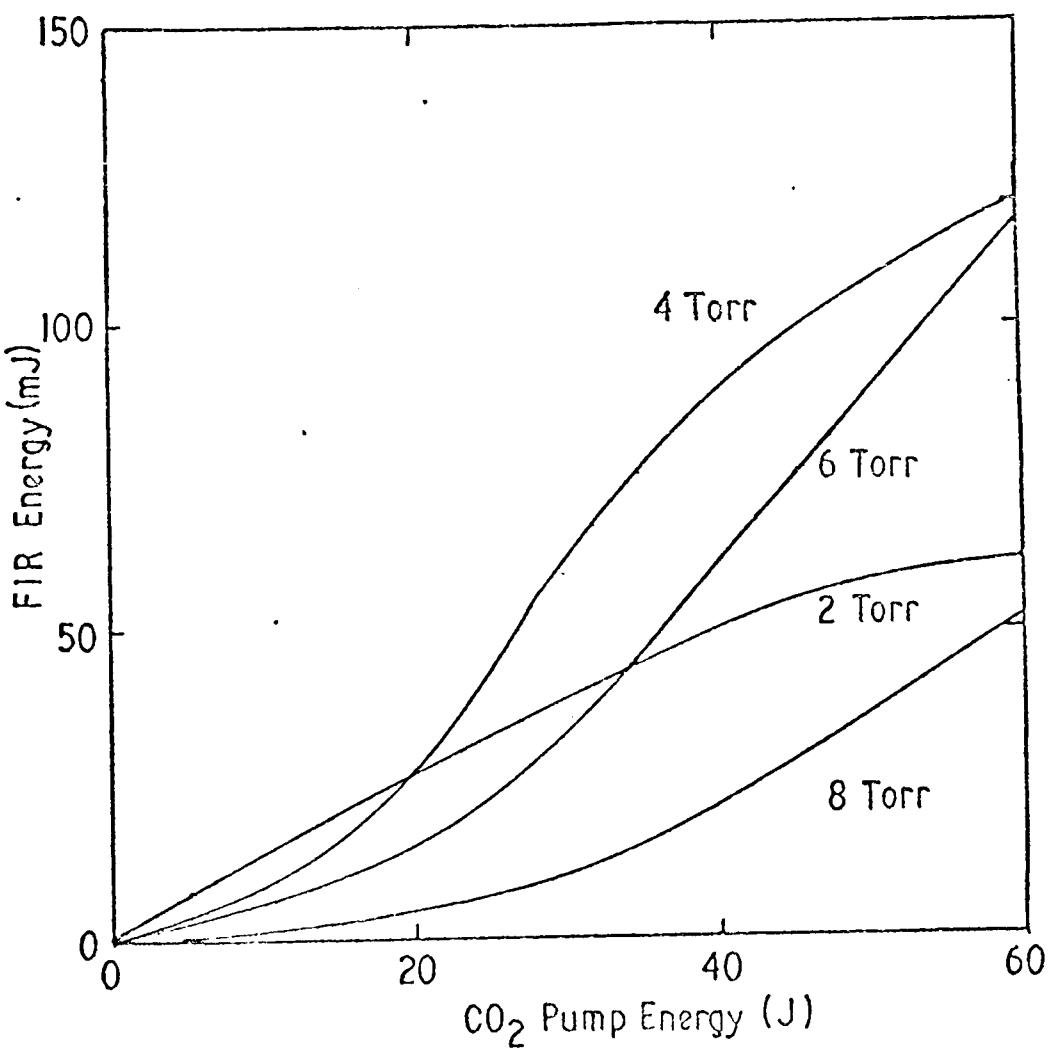


Fig.5.10

FIR output energy against CO_2 laser pump energy for 385/359 μm emission. Several curves are shown each for a different D_2O pressure

spike energy to F I R output energy) increased from 0.04%, for a total CO_2 pump energy of 12 J, to 1% for a total CO_2 pump energy of 60 J.

In Fig.5.10 we have plotted the F I R energy as a function of CO_2 pump energy. For D_2O pressures below 4 torr, the F I R output was found to saturate at the highest CO_2 pump energies. In particular at 2 torr the F I R energy was enhanced by only 15% when the total CO_2 pump energy was increased from 40 to 60 J.

Two components were observed in the F I R output, with wavelengths of 385 and 359 μm (measured with a Fabry-Perot etalon equipped with 400 line/inch plates.) The pulse energy of these components was found to be in the ratio of 2:1, independent of D_2O pressure (see Fig.5.11). These wavelengths have been assigned (WILLIAMSON, 1969; LIN and SHAW, 1976) to the $0104_{22} \rightarrow 0104_{13}$ transition and the cascade transition $0104_{13} \rightarrow 0104_{04}$ (using the nomenclature described in Appendix 'E'). The CO_2, R(22) pump line absorption has been assigned to the $0005_{33} \rightarrow 0104_{22}$ transition (see Fig.E.4).†

Figure 5.12 shows a time resolved oscillogram of the F I R output pulse. The power scale in this figure has been derived by equating the total area under the pulse to the pulse energy of 120 mJ. The laser pulse is similar to that observed for the CH_3F super-radiant laser (see Fig.5.5). The average power, however, is over 2 MW and spikes within the pulse reach peak powers above 4.5 MW (i.e. considerably more power than the 496 μm line in CH_3F.)

A scan of the beam profile at the output of the 385/359 μm D_2O laser (see Fig.5.13) revealed a similar beam cross-section to that observed for the CH_3F laser (see Fig.5.7). The peak energy density was about 2 mJ/cm^2. Polarization measurements of the output pulse showed the electric vector of

---

† The CO_2 pump line centre frequency is in fact 300 MHz higher than the frequency of the absorbing transition in D_2O (KEILMANN et al, 1975)

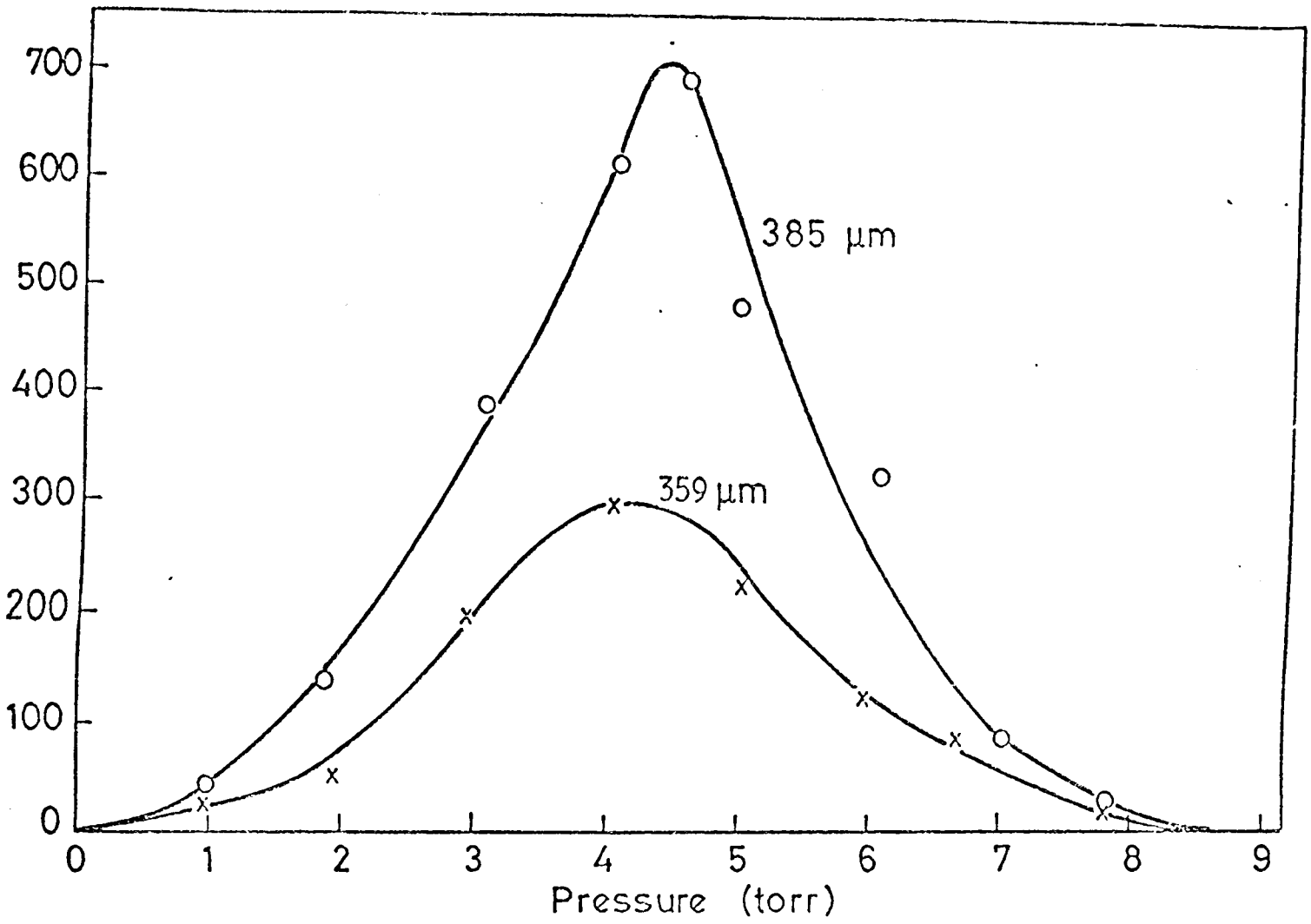


Fig.5.11

Relative energy of the 385 and 359 µm emission as a function of D_2O pressure for a CO_2 laser pump energy of 50 J

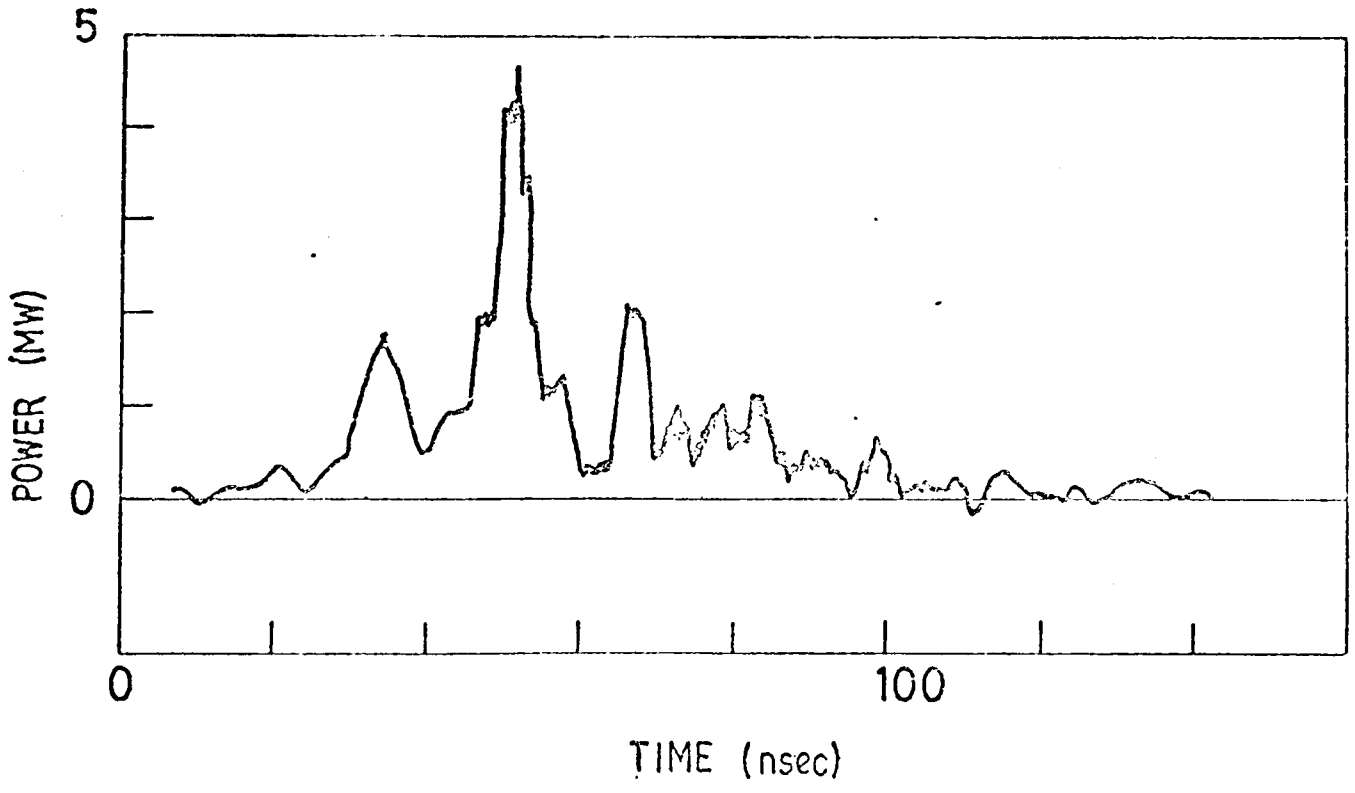


Fig.5.12

Time resolved output pulse for the 385/359 µm emission showing the peak F I R power as a function of time

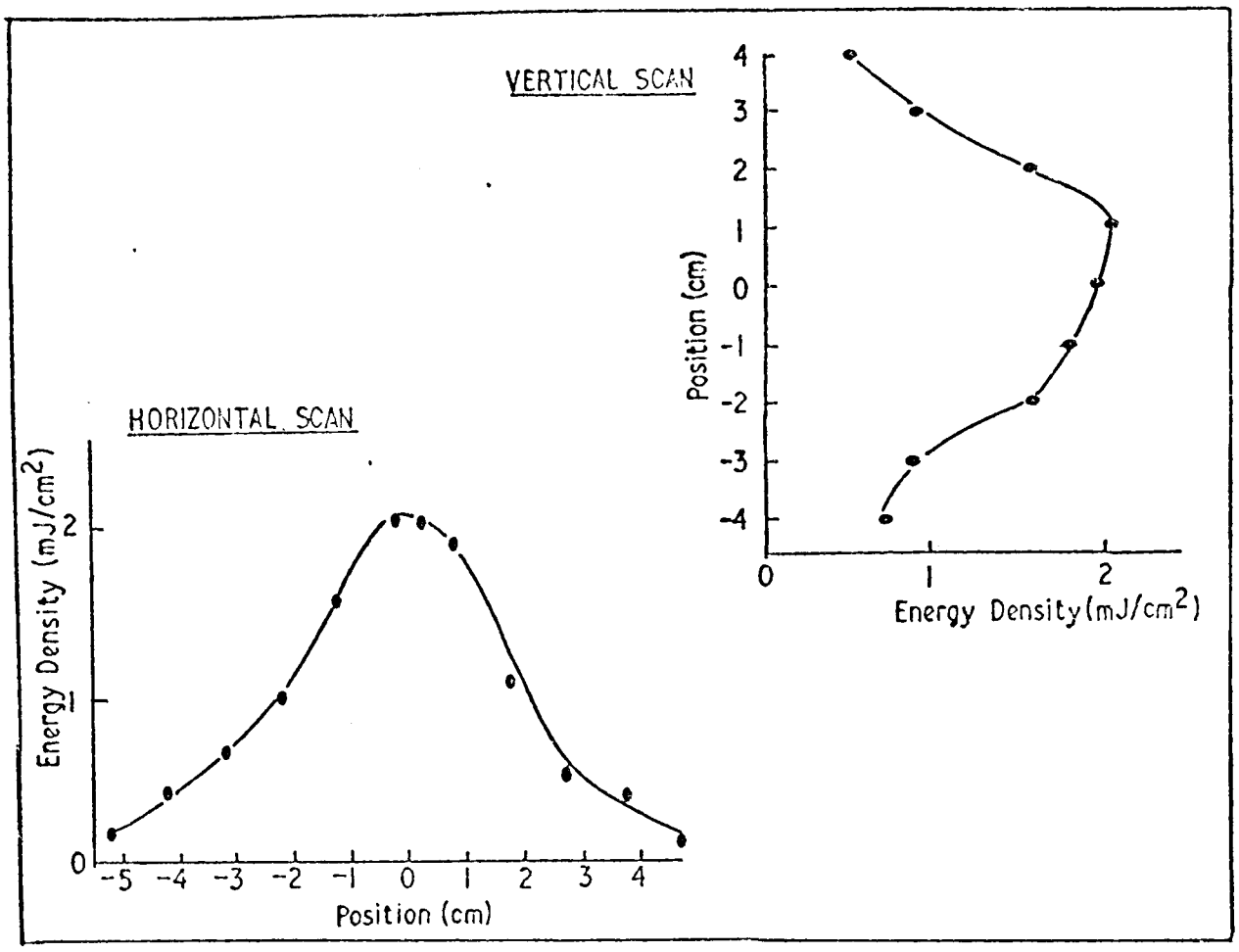


Fig.5.13
Beam profile of the FIR output from the 385/359μm superradiant laser

the FIR radiation to be perpendicular to the polarization of the CO_2 pump photons, consistent with the transition assignment (CHANG, 1974) (the degree of polarization being about 80%).

Figure 5.14 shows a Fabry-Perot interferometer scan of the FIR output. The two components display significantly different bandwidths of 370 and 180 MHz, respectively. SHIMODA and SHIMIZU (1972) have shown theoretically that it is possible to obtain broadening of molecular transitions optically pumped off resonance. We therefore attribute the broader bandwidth of the 385 μm transition (whose

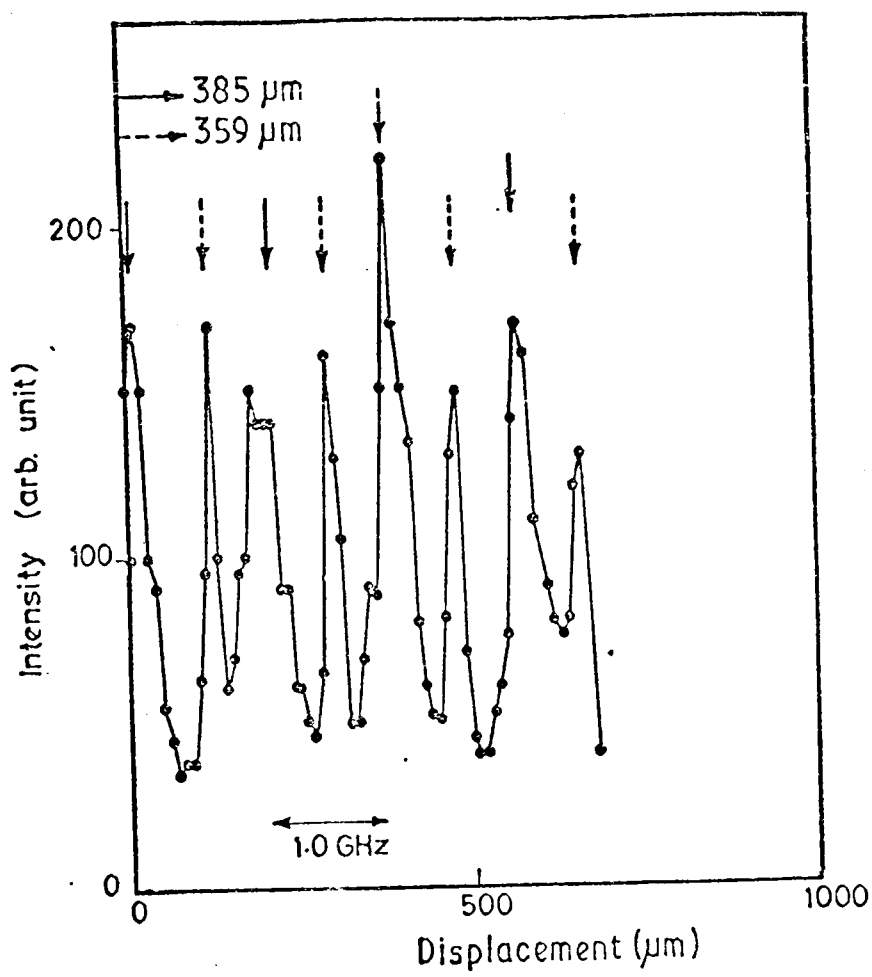


Fig.5.14
Fabry-Perot interferometer scan of the 385 and 359μm superradiant laser emission lines

upper level, 0104_{22}, is also the upper level of the pump photon transition, see Fig.E.4) to broadening of the 0104_{22} level by the 1 GHz bandwidth CO_2 pump laser.

The dependence of the frequency of the 385 μm emission with D_2O pressure was investigated from 0.5 to 8 Torr and, within the resolution of the Fabry-Perot interferometer (i.e. ≤50 MHz), no frequency shift, similar to that observed for the 496 μm CH_3F laser, was measured. The absence of a frequency shift in D_2O would appear to support the interpretation of the shift in the frequency of the 496 μm CH_3F laser (see section 5.2), as due to a change in K component of the F I R emission (see Appendix 'B'), since the 385 μm emission has only one possible K component (see Appendix 'E').

5.4 THE 114 μm D_2O LASER

The dependence of F I R output with CO_2 pump energy and D_2O pressure was determined for D_2O, optically pumped by the 9.32 μm, R(12), CO_2 laser line. The results of these measurements are summarized in Figs. 5.15 and 5.16. The 9.6 mm thick TPX output window of the super-radiant laser was found to attenuate the F I R output by a factor of 2.1. The maximum F I R energy was found to be 550 mJ (when corrected for attenuation by the TPX output window), which was obtained for a D_2O pressure of 5 torr and a CO_2 pump energy of 51 J (i.e. about 10 J in the CO_2 laser spike). If we consider only the CO_2 spike energy, the CO_2 pump to

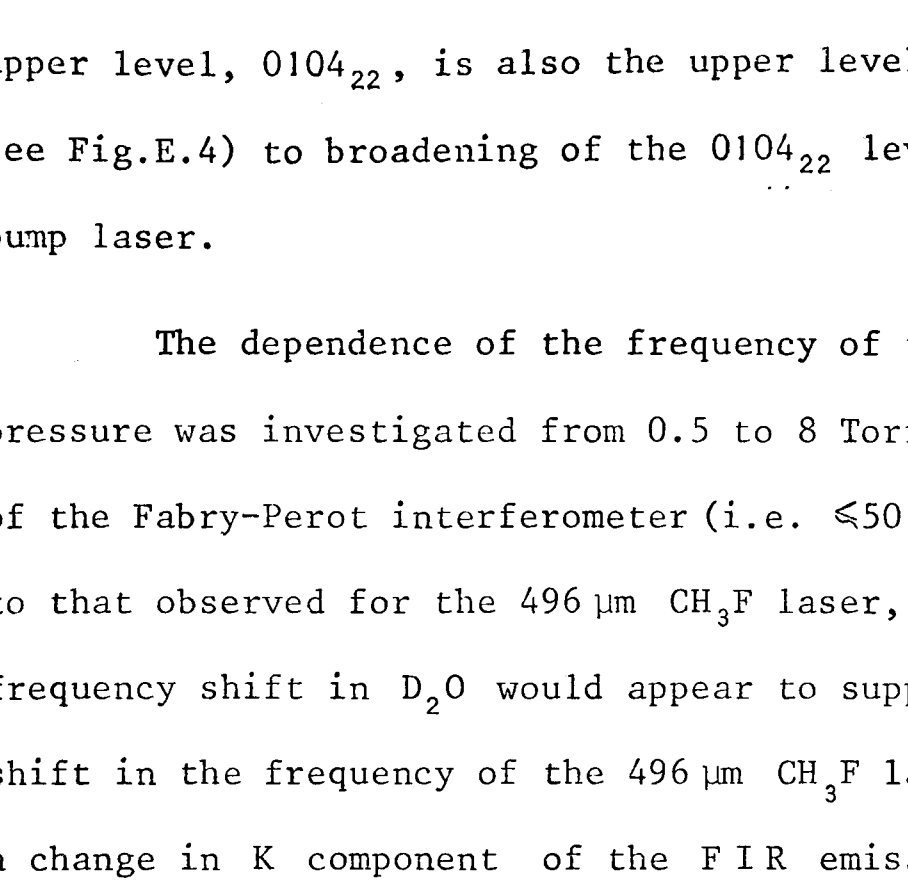


Fig.5.15

F I R output energy against D_2O pressure for the 114 μm emission. Several curves are shown each for a different CO_2 laser pump energy

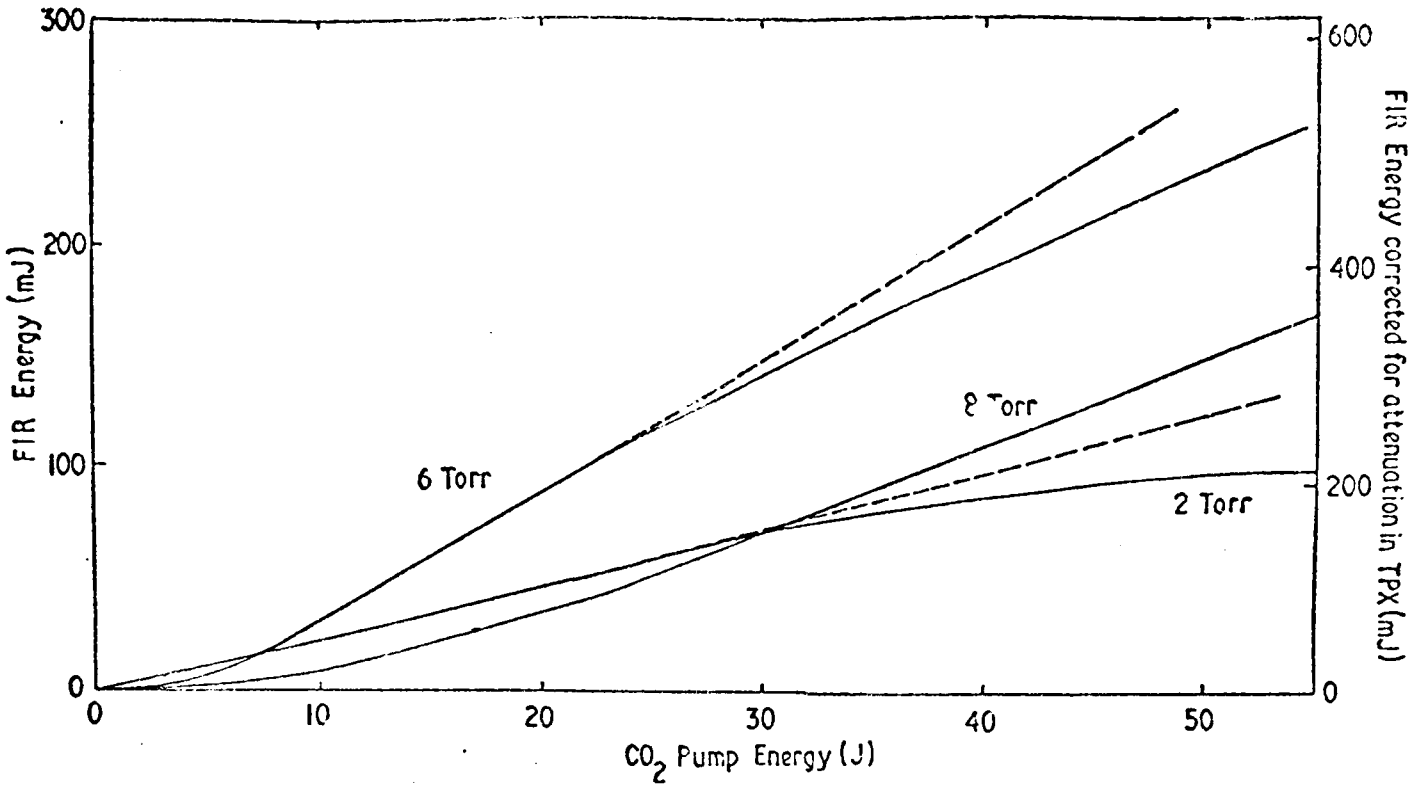


Fig.5.16
FIR output energy against CO_2 laser pump energy for the 114 μm emission. Several curves are shown each for a different D_2O pressure

FIR energy conversion efficiency increased with increasing pump energy from 3.7% to 5.4%, when the total pump energy was increased from 10 to 51 J, which corresponds to a maximum photon conversion efficiency of 66%.

Time resolved traces of the FIR output generated by D_2O optically excited by the R(12), 9.6 μm band, CO_2 laser line were recorded using a gallium doped germanium (Ge:Ga) photo-conductive detector (MOORE and SHENKER, 1965 and MOORE, 1976), cooled to liquid helium temperatures. This detector was adopted because the Si-W point contact diode used to detect 496 and 385 μm radiation proved insensitive at wavelengths $\leqslant$ 300 μm.† The chip of Ge:Ga was 2 mm × 2 mm × 5 mm and its resistance at 6°K was 40 kΩ. A bias current of 0.1 mA was passed through it and signals of a few millivolts amplitude were generated. These signals were then amplified by an Avantek 400 MHz bandwidth amplifier and displayed on a R 7912 Tektronix oscilloscope, which had a bandwidth of 500 MHz. A typical oscillogram is illustrated in Fig. 5.17. Two power scales are shown in the figure, the left hand scale being

† A fast pyroelectric element was also tried but the response time of this detector was found to be more than an order of magnitude inferior to Ge:Ga.

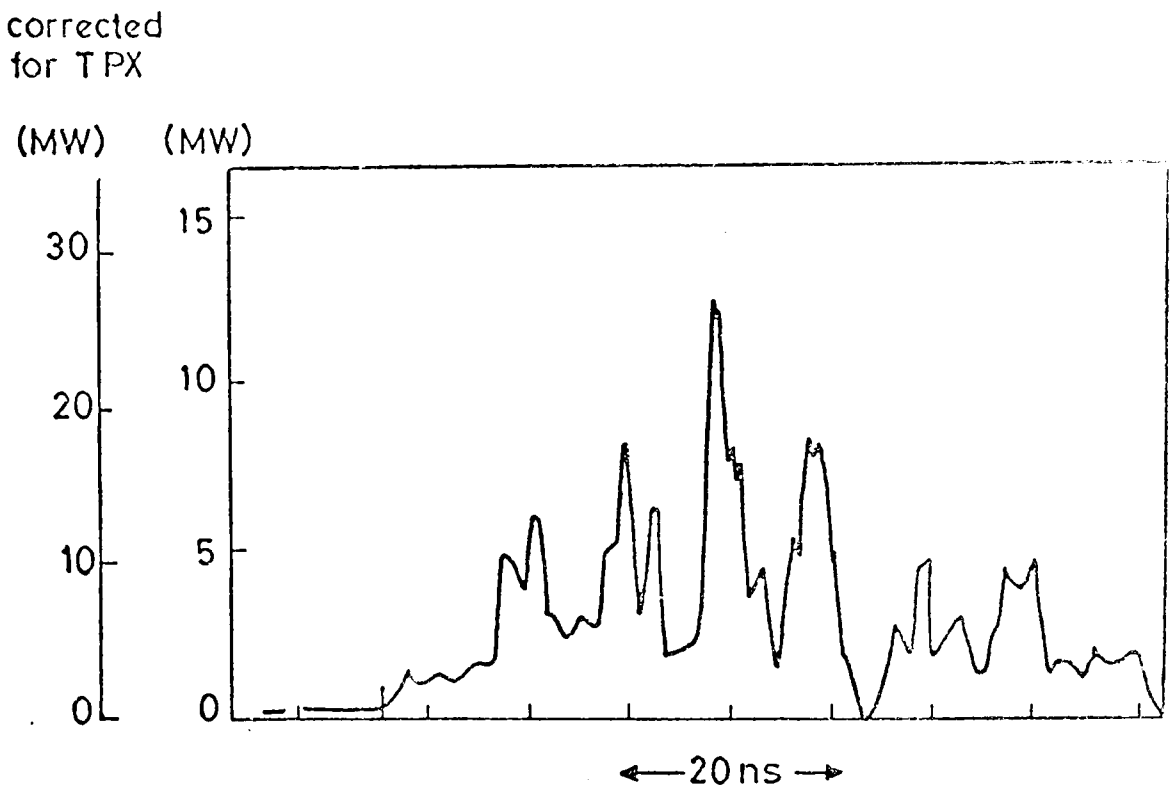


Fig.5.17
Time resolved output pulse for the 114 μm emission. The left hand power scale has been corrected for attenuation in the 9.6 mm thick TPX laser output window

the power corrected for absorption in the TPX output window. Pulse powers of 9.2 MW were measured, whilst peak powers exceeded 25 MW.

Figure 5.18 shows the result of a Fabry-Perot interferometer scan of the FIR output from the super-radiant laser, the etalon being formed from 1000 line/inch copper mesh. Since the output from the FIR laser was found to suffer strong attenuation in air, the interferometer and Golay detector were located immediately beyond the TPX output window and were enclosed in an argon atmosphere. The main constituent of the spectrum was identified as the 114 μm emission in D_2O, corresponding to the $0109_{28} \rightarrow 0109_{19}$ transition (see Fig.E.4). The low intensity line appearing beside the strong fringes in the figure is not the expected 94 μm

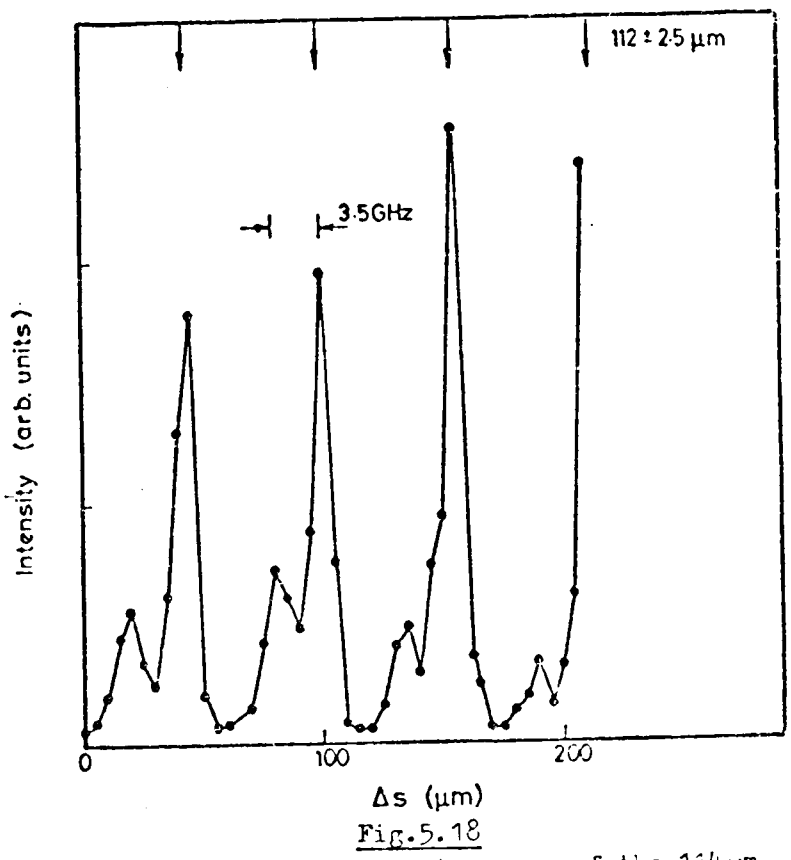


Fig.5.18
Fabry-Perot interferometer scan of the 114 μm superradiant laser emission line

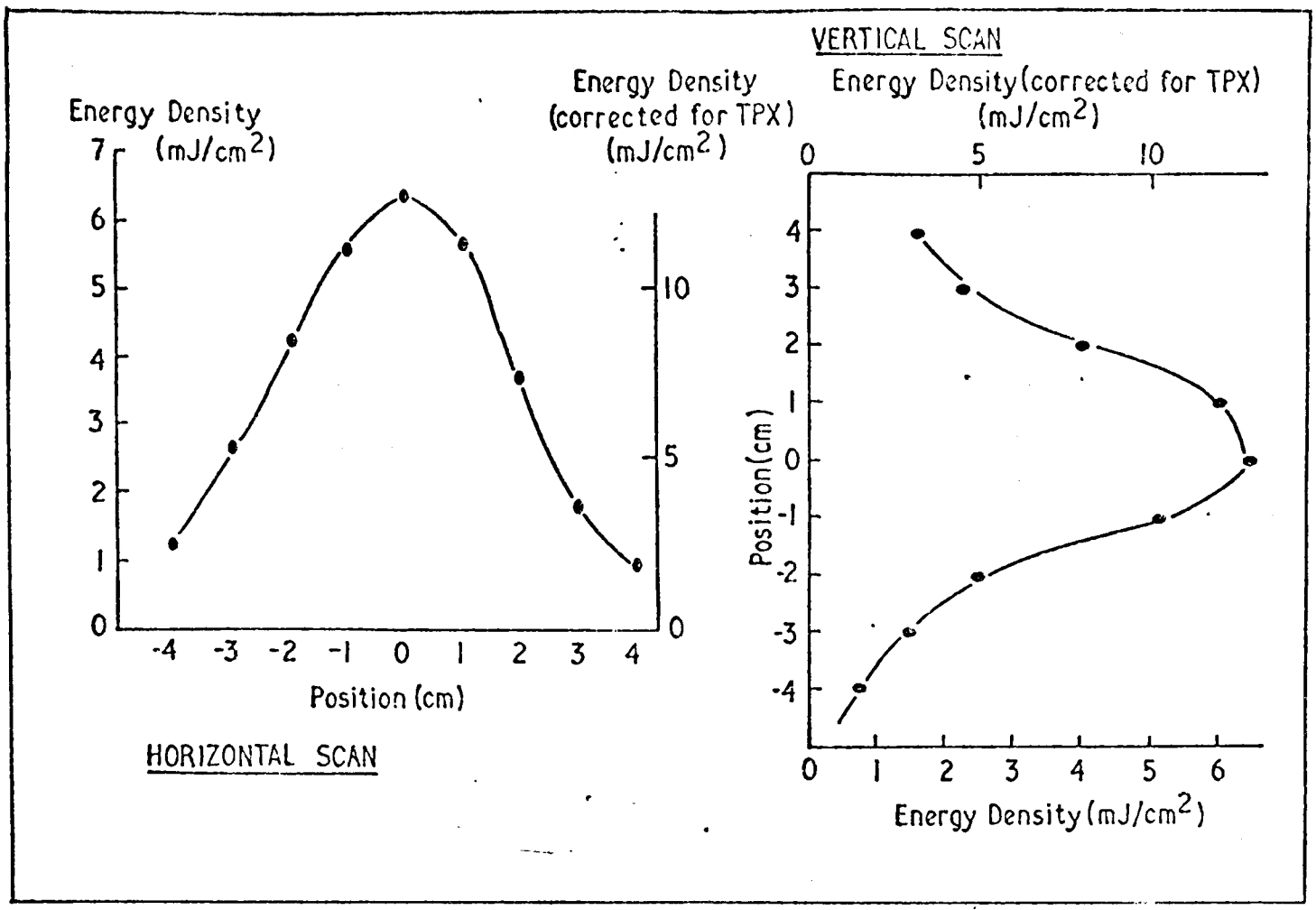


Fig.5.19
Beam profile of the FIR output from the 114 μm superradiant laser. Two energy density scales are shown, one with and one without correction for the 9.6 mm thick TPX laser output window

component (see Appendix 'E' and Fig.E.4), but instead appears to be a satellite of the 114 μm line, separated from it by about 3.5 GHz.

The beam profile of the 114 μm emission is shown in Fig.5.19. The energy density at the centre of the beam was about 12.5 mJ/cm^2. The 114 μm radiation was found to be plane polarized and parallel to the electric vector of the CO_2 pump radiation, which is in disagreement with the assignment of the transitions involved in the operation of the laser (CHANG, 1974). This observation, together with the high photon conversion efficiency of 66%, may indicate that Raman scattering is the dominant process in this laser (see section 5.6).

5.5 THE 66/119/50 μm D_2O LASER

The FIR output for D_2O optically pumped by the P(32), 9.66 μm, CO_2 laser line was measured as a function of D_2O pressure and CO_2 pump energy. The results are summarized in Figs.5.20 and 5.21. The maximum FIR

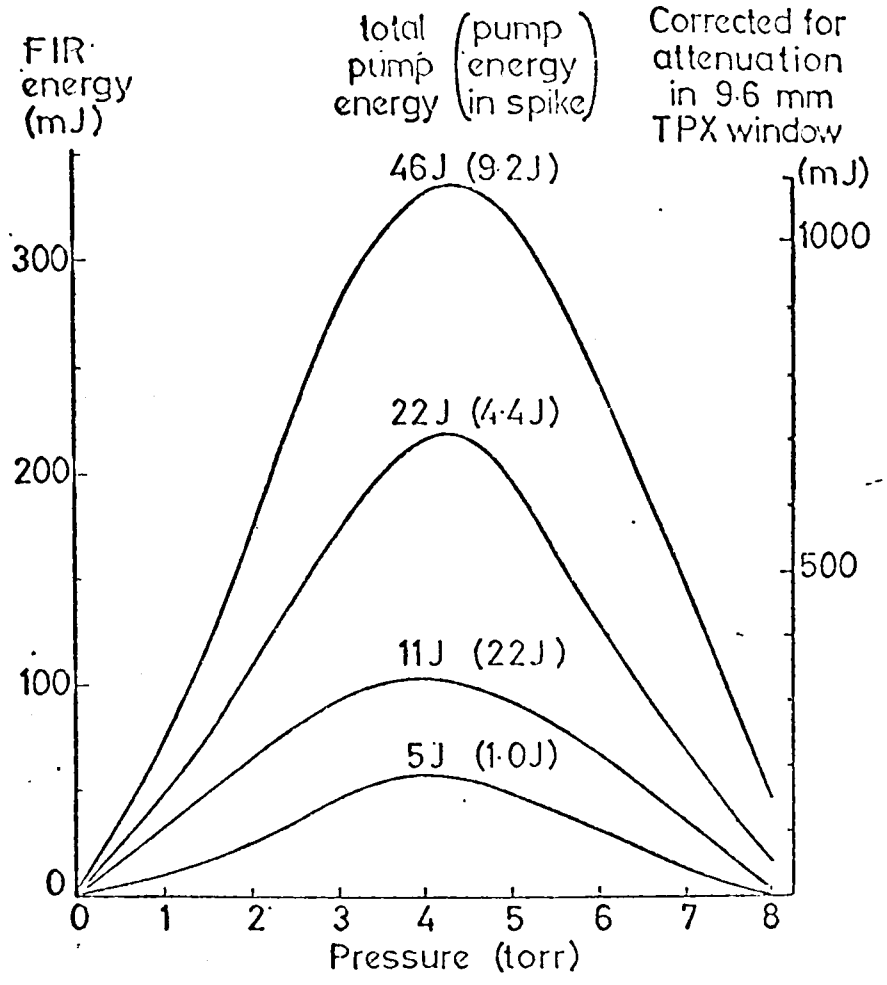


Fig.5.20

FIR output energy against D_2O pressure for the 66/119/50μm emission. Several curves are shown each for a different CO_2 laser pump energy

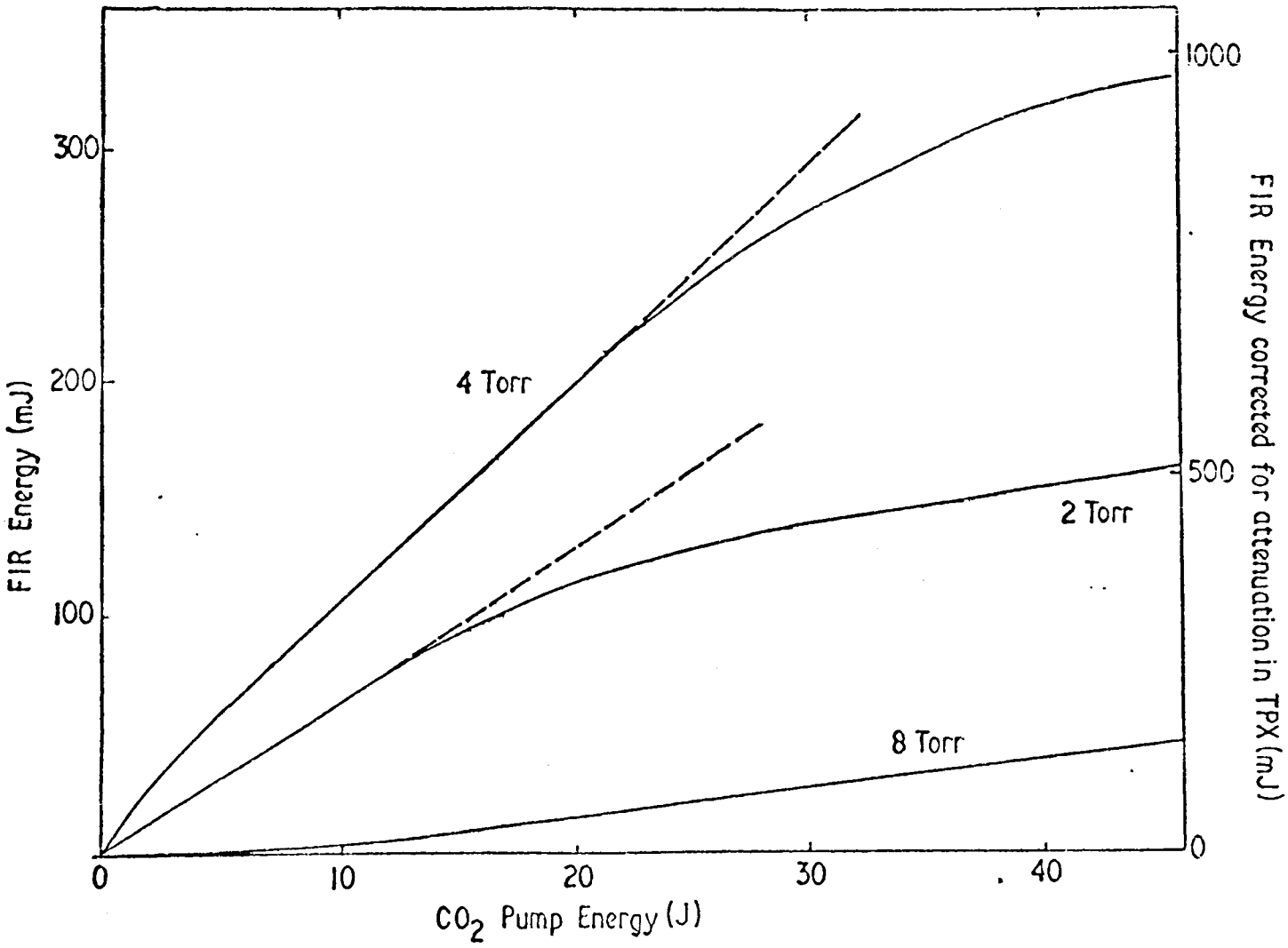


Fig.5.21

FIR output energy against CO_2 laser pump energy for the 66/119/50μm emission. Several curves are shown each for a different D_2O pressure

output energy of 330 mJ was obtained for 46 J of CO_2 pump energy and a D_2O pressure of 4.5 torr. However, the 9.6 mm thick TPX output window of the super-radiant laser was found to attenuate the F I R output by a factor of 3.3. We have, therefore, included an additional power scale in Figs.5.20 and 5.21 which takes account of this attenuation. With this correction the maximum F I R energy was calculated to be 1.06 J. The pump* to F I R energy conversion efficiency decreased with increasing pump energy from 16.5% to 11.8%, when the total CO_2 pump energy was increased from 5 to 46 J.

Three components with wavelengths of 66, 119 and 50 μm were observed and the relative energy of each of these components as a function of D_2O pressure, at the output of the F I R laser, is shown in Fig.5.22. The results shown in the figure were obtained for a total CO_2 pump energy of 46 J. The 66 and 50 μm components have been identified as arising from the $0105_{51}, 5_{50} \rightarrow 0104_{41}, 4_{40}$ and the $0007_{71}, 7_{70} \rightarrow 0006_{61}, 6_{60}$ transitions in D_2O, respectively (see Appendix 'E' and Fig.E.4). Both these emissions arise as a result of excitation of the $0006_{61}, 6_{60} \rightarrow 0105_{51}, 5_{50}$ transition in D_2O by the P(32) CO_2 laser radiation. However, this absorption is about 1.5 GHz away from the P(32) centre frequency (see Table E.1) and PETUCHOWSKI et al (1977) have suggested that both the 66 and 50 μm lines are generated by Raman scattering. Unfortunately the bandwidth of the CO_2 pump laser used here is too wide (≈ 1 GHz) to allow measurement of the expected frequency shift (~ 1.5 GHz) in the F I R output due to Raman scattering of the pump radiation.

The 119 μm component has been assigned to the $0106_{25} \rightarrow 0105_{14}$ emission in D_2O (see Fig.E.4). This F I R emission line arises from a different absorption† from that involved in the generation of the 66 and 50 μm

---

* The CO_2 laser energy used here is the spike energy only.

† LIPTON et al (1977) have recently confirmed the existence of two separate absorbing transitions for the P(32) CO_2 laser line in D_2O.

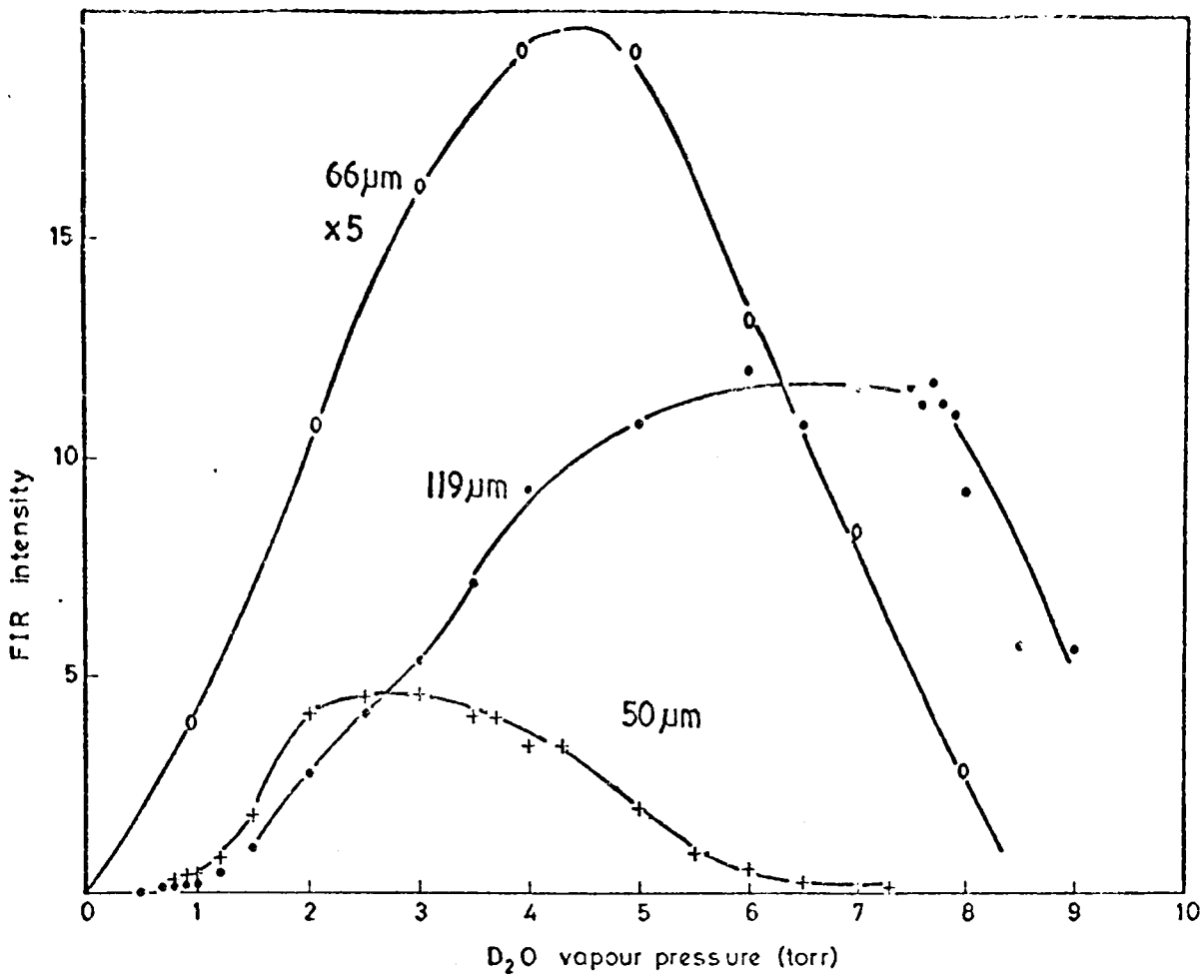


Fig.5.22

Relative energy of the 66, 119 and 50μm emissions as a function of D_2O pressure for a CO_2 laser pump energy of 45J. (The curve for the 66μm emission has been reduced by a factor of 5 in energy to allow all three emissions to be shown on the same figure.)

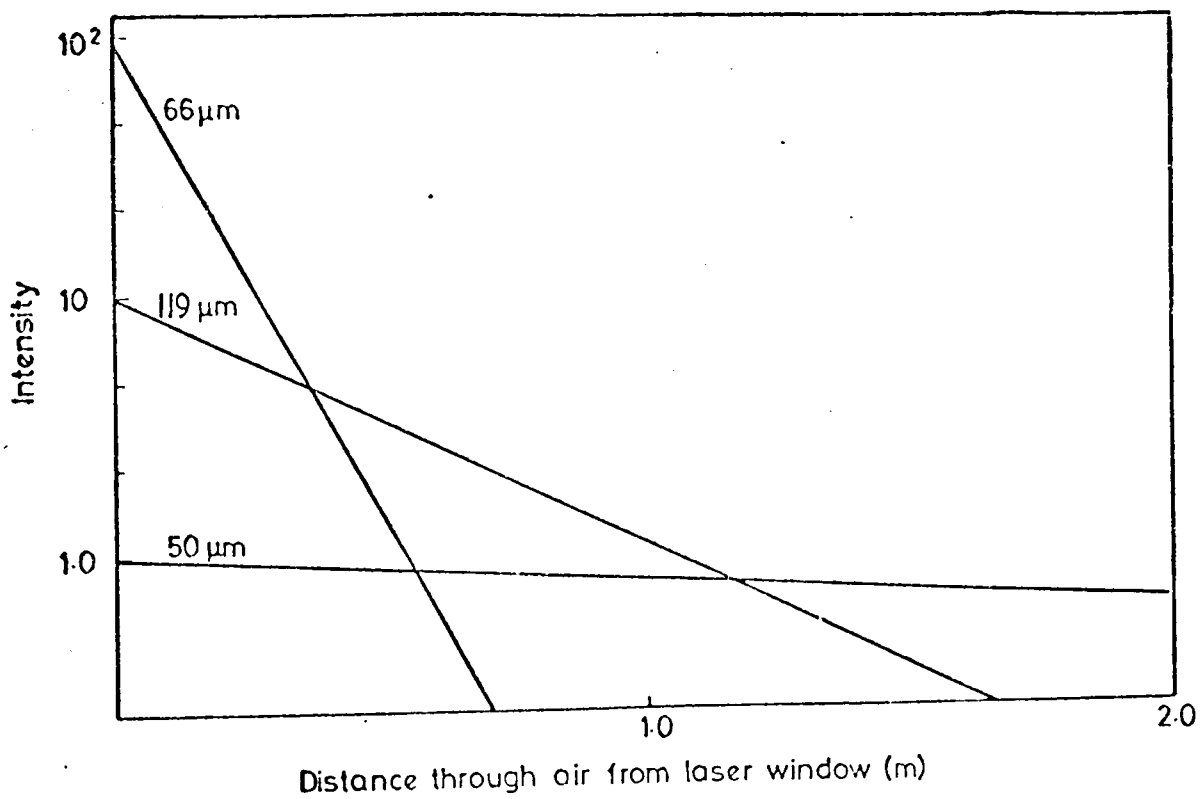


Fig.5.23

Absorption in atmospheric air as a function of distance from the FIR laser output window for the 66, 119 and 50 μm laser emission lines in D_2O

lines, namely the $0007_{34} \rightarrow 0106_{25}$ transition.

The relative intensities of the 66, 119 and 50 μm lines as a function of distance from the end of the super-radiant tube is shown in Fig.5.23. The 66 μm component was found to absorb strongly in air, being undetectable 1 metre from the end of the super-radiant laser. The 119 μm component was absorbed slightly less than the 66 μm component, the 50 μm line being the only wavelength to propagate further than 2 m from the super-radiant laser. (GALLAGHER et al (1977) have compared the atmospheric absorption of a large proportion of the F I R laser lines known at present.)

The beam profile of the F I R output at the TPX window of the laser is shown in Fig.5.24. The peak energy density was about 26 mJ/cm^2, about 90% being at 66 μm, 9% at 119 μm and 1% at 50 μm. All three wavelengths were found to be plane polarized parallel to the electric vector of the CO_2 pump radiation, which is consistent with the assignment of the transitions involved in the generation of these wavelengths.

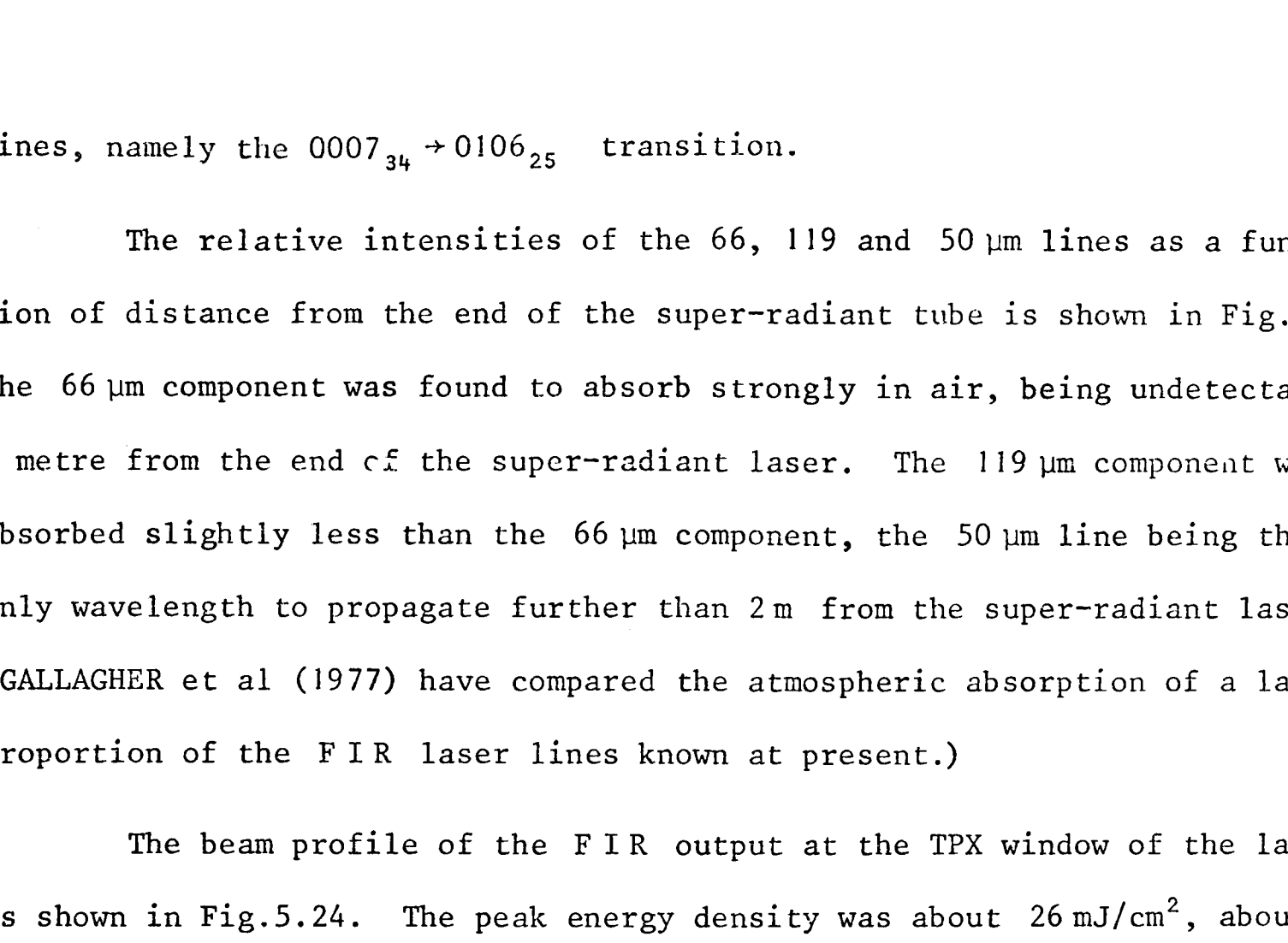


Fig.5.24

Beam profile for the 66 μm emission line of D_2O. Two energy density scales are shown, one with and one without correction for the 9.6 mm TPX laser output window

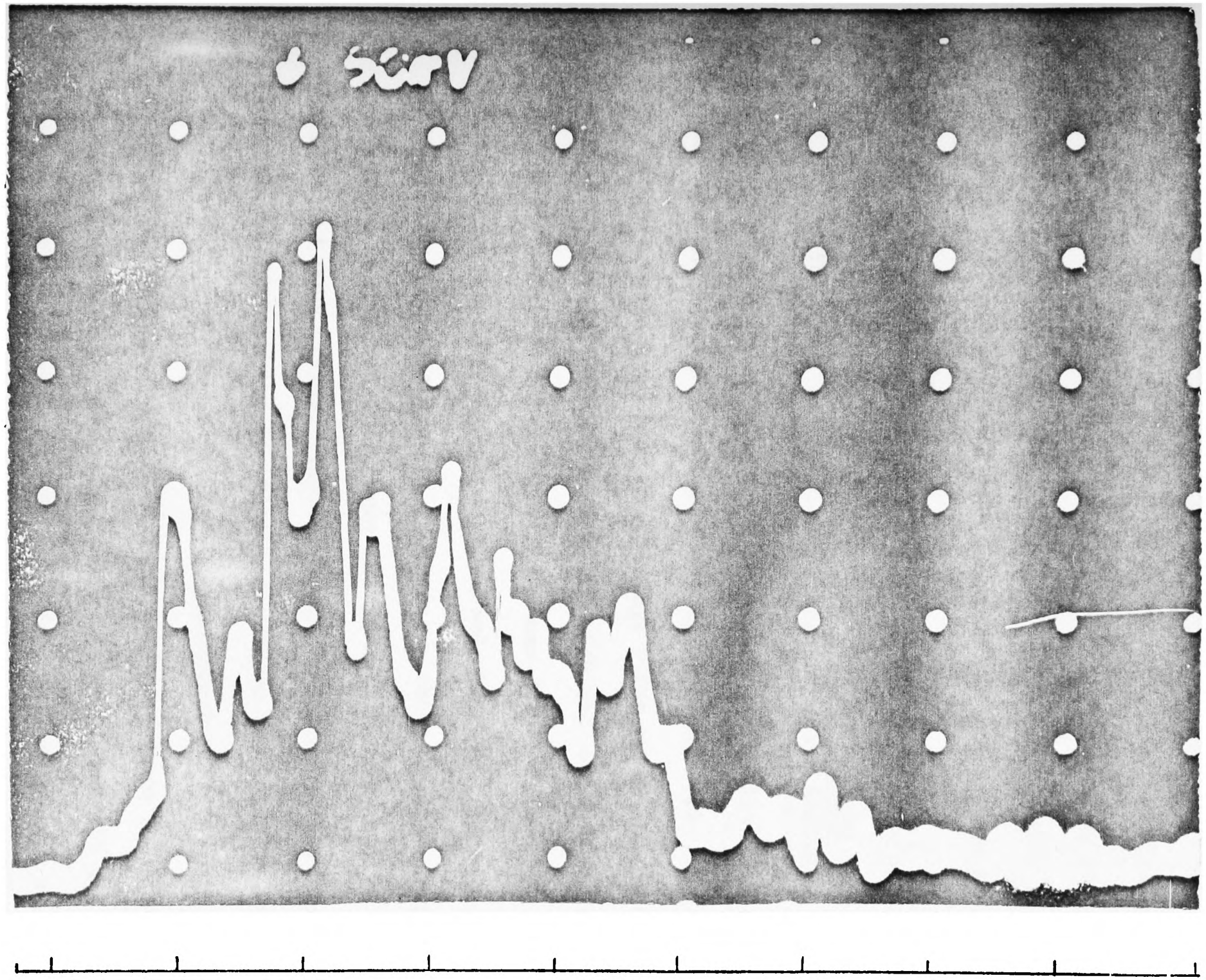


Fig.5.25

The rise time of the Ga:Ge detector used in the present work is illustrated by this oscillogram of a superradiant pulse of 50 μm radiation from the D_2O laser

Finally Fig.5.25 shows an oscillogram of the laser output 4 metres from the laser (i.e. predominantly 50 μm radiation). This was obtained with the Ge:Ga detector described in the previous section. The response time of the Ge:Ga detector is indicated by the rise-time of this trace, i.e. < 2 ns. If the 66 μm radiation is generated in a pulse of similar duration and shape to the 50 μm radiation, then the measured F I R energies would imply an average power of 15.8 MW and a peak power of 40 MW at 66 μm (allowing for attenuation in the TPX window).

5.6 SUMMARY OF THE PERFORMANCE AND CHARACTERISTICS OF THE CH_3F AND D_2O SUPER-RADIANT F I R LASERS

Table 5.1 summarizes the main characteristics of the CH_3F and D_2O super-radiant lasers investigated in the present work. For half the laser emissions investigated here the average pulse power exceeded 1 MW, the highest average power, 15.8 MW being obtained with the 66 μm D_2O laser. For each pump photon there can be no more than one F I R photon, and the highest photon conversion efficiency is obtained when both the pump and the F I R transitions become saturated. However, without strong collisional recycling the photon conversion efficiency can be no more than 50% in this case. (TEMKIN and COHN, 1976). Therefore, in order to justify the measured photon conversion efficiencies of 72% for the 66 μm laser and 66% for the 114 μm laser we must invoke either strong collisional recycling or Raman scattering†. Indeed, PETUCHOWSKI et al (1977) have recently shown the 66 μm emission to arise from stimulated Raman scattering. Since the R(12) CO_2 line used to pump the 114 μm laser is 680 MHz away from the absorption in D_2O (see Table E.1), the interpretation that the high photon conversion efficiency of the

---

† Stimulated Raman scattering does not involve absorption of the pump photons to an intermediate molecular state prior to the F I R emission, since the intermediate state in this case is a virtual one. Thus the maximum photon-conversion efficiency is 100%.

TABLE 5.1

SUMMARY OF THE MAIN CHARACTERISTICS OF THE CH_3F AND D_2O LASERS INVESTIGATED IN THE PRESENT WORK

FIR Wavelength	496 μm	452 μm	385 μm	359 μm	114 μm	66 μm	119 μm	50 μm
9.6 μm Band CO_2 Laser Pump Line	P(20)	P(20)	R(22)	R(22)	R(12)	P(32)	P(32)	P(32)
CO_2 Laser Wavelength	9.55 μm	9.55 μm	9.26 μm	9.26 μm	9.[illegible] μm	9.66 μm	9.66 μm	9.66 μm
Peak FIR Power (see note 5)	0.64 MW	0.36 MW	3.0 MW	1.5 MW	25 MW	40 MW	4 MW	0.5 MW
Average FIR Power (see note 5)	0.32 MW	0.18 MW	1.32 MW	0.68 MW	9.2 MW	15.8 MW	1.6 MW	0.2 MW
Total FIR Energy (see note 5)	21 mJ	12 mJ	80 mJ	40 mJ	550 mJ	950 mJ	95 mJ	11 mJ
Pulse Width FWHM	60 ns	60 ns	60 ns	60 ns	60 ns	60 ns	60 ns	60 ns
Bandwidth	300 MHz	300 MHz	370 MHz	180 MHz	see note 1	see note 1	see note 1	see note 1
Conversion Efficiency (see note 4)	0.27%	0.13%	0.66%	0.33%	5.4%	10.6%	1.1%	0.1%
FIR Polarization (see note 2)	⊥	⊥	⊥	⊥	∥	∥	∥	∥
Total CO_2 Laser Pump Energy	43 J	43 J	60 J	60 J	51 J	46 J	46 J	46 J
Divergence	30 mrad	30 mrad	see note 3	see note 3	see note 3	see note 3	see note 3	see note 3
Operating Pressure	3.4 torr	2.7 torr	4.8 torr	4.8 torr	5.2 torr	4.5 torr	7.0 torr	2.7 torr
Laser Medium	CH_3F	CH_3F	D_2O	D_2O	D_2O	D_2O	D_2O	D_2O
Absorption in Atmospheric Air	Low	Low	Low	Low	V. High	V. High	High	Mod.
Photon Conversion Efficiency	14%	6%	27%	13%	66%	72%	13%	0.5%

NOTES

1. The bandwidth for the 114, 66, 119 and 50 μm emissions was not measured, however the high frequency structure of the FIR pulses measured with the Ge:Ga detector suggests bandwidths $\geq$ 200 MHz.
2. The notation used for the FIR polarization measurements is as follows:
   ⊥ perpendicular to the electric vector of the CO_2 laser pump radiation
   ∥ parallel to the electric vector of the CO_2 laser pump radiation.
3. The divergence of the radiation at these wavelengths has not been measured, however an upper limit of 45 mrad is set by the diameter of the tube in relation to its length.
4. The conversion efficiencies quoted here were corrected for absorption in the TPX output window and calculated assuming that only the CO_2 laser pulse spike drives the super-radiance.
5. The powers and energies quoted are corrected for absorption in the TPX output window.

114 μm line results from stimulated Raman scattering does not seem unreasonable. This may explain the measured polarization of the 114 μm emission, which was found to be parallel to the direction of polarization of the pump radiation rather than perpendicular, as predicted for a 'conventional' process, involving the absorption of a pump photon followed by emission of a F I R photon.

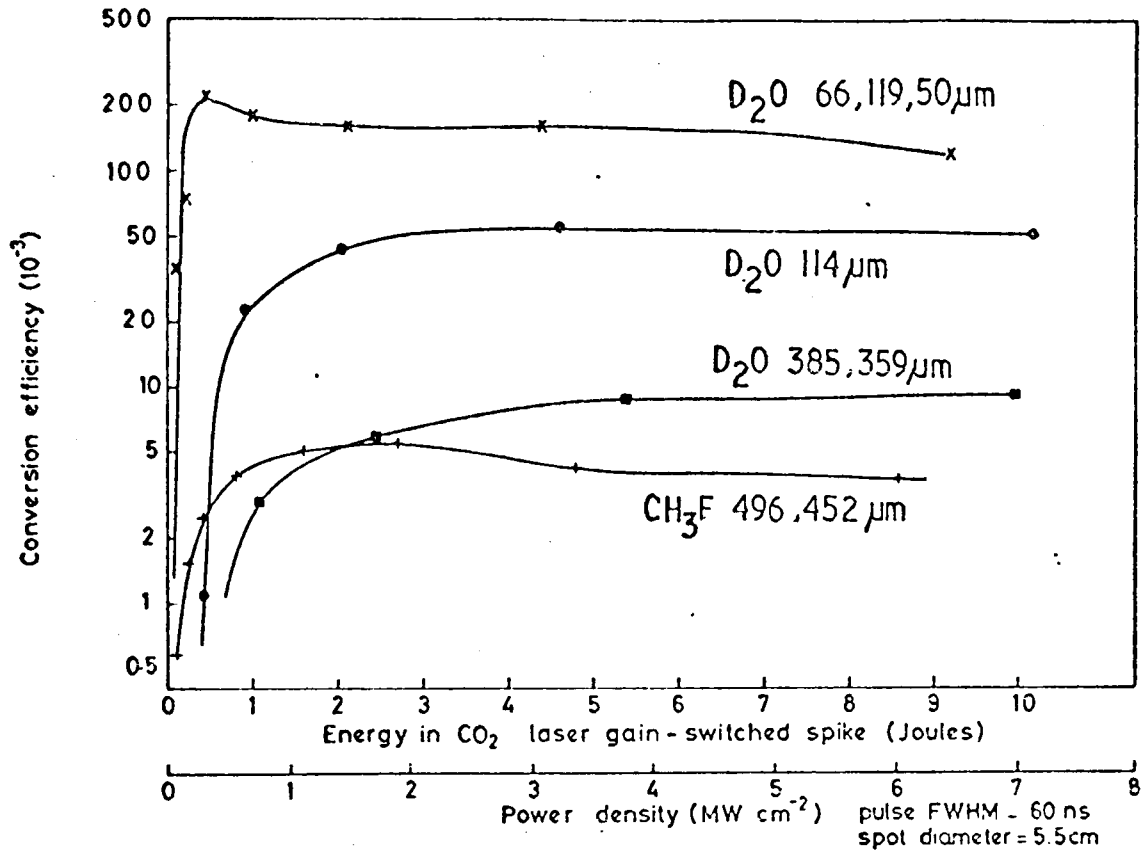


Fig.5.26
F I R to pump photon energy conversion efficiency as a function of CO_2 laser pump energy for the 496/452 μm CH_3F laser and the 114, 385/359 and 56/119/50 μm D_2O lasers

Figure 5.26 shows the conversion efficiency (defined as F I R energy generated per unit pump energy in the CO_2 laser pulse spike) for each of the CO_2 pump lines used in this work, plotted as a function of the energy in the CO_2 pulse spike and the pump power per unit area. (We have assumed here a CO_2 spike duration of 60 ns (F W H M) and a pump radiation beam diameter of 5.5 cms). In each case the measurement was made at the optimum pressure and correction for attenuation in the TPX window has been applied. The curve corresponding to the 66, 119 and 50 μm emission lines of D_2O exhibits a rapid switch-on at pump energies of about 0.3 J (i.e. 200 kW/cm^2). In the light of the identification, by PETUCHOWSKI et al (1977), of the 66 and 50 μm lines as arising from a stimulated Raman process we can interpret this behaviour as indicating the threshold for this effect.

In summary, optically pumped super-radiant lasers offer a comparitively simple solution to the generation of megawatt pulses of F I R radiation. However, the bandwidth of all lines investigated here was more than 180 MHz. Although it might be possible to determine the width of the ion feature and hence the plasma ion temperature with these devices, a much narrower bandwidth would be needed in order to determine the shape of the ion feature (e.g. for the determination of impurity concentrations, see Chapter I).

The D_2O super-radiant laser is particularly attractive since it is possible to obtain wavelengths between 50 and 385 μm simply by tuning the CO_2 laser to a different pump line. In a Thomson scattering experiment this would allow the observation of several different scale lengths in the plasma, without moving the laser or collection optics in order to change the scattering angle. In particular the 385 μm D_2O laser has a long wavelength allowing the use of Schottky diodes (which can be operated at room temperature in a sensitive heterodyne system) and is capable of generating average F I R powers in excess of 1 MW with photon conversion efficiencies of about 30%.

CHAPTER VI

THE F I R OSCILLATOR INJECTED SUPER-RADIANT LASER

The single mode CH_3F oscillator discussed in Chapter IV had a bandwidth of a few MHz but produced comparatively low power, ~ 500 W, pulses of 496 μm radiation. In contrast the super-radiant lasers described in Chapter V produced megawatt pulses of F I R radiation but with bandwidths of over 200 MHz. However, in order to satisfy the requirements for collective Thomson scattering derived in Chapter I, we need both high power and narrow bandwidth simultaneously.

Injection lasers have already been used with considerable success to mode lock high power, pulsed, CO_2 laser oscillators (IZATT and BUDHIRAJA, 1975 and CORKUM et al, 1976). Recently (ALCOCK et al, 1977), for example, 1 - 2 mW of narrow bandwidth CW laser power has been used to mode-lock a 1 GW pulsed CO_2 oscillator. This represents an effective power gain of $\sim 10^{12}$. However, the injection principle has been used hitherto with cavity lasers; in the present chapter we investigate the effect of injecting low power, narrow bandwidth, F I R oscillator pulses into a high gain, mirror-less super-radiant laser.

6.1 DESCRIPTION OF THE OSCILLATOR INJECTED SUPER-RADIANT LASER

A schematic diagram of the F I R injection laser assembly is shown in Fig.6.1 and a photograph of the apparatus is shown in Fig.6.2. The single mode F I R oscillator used here was the same as that described in Chapter IV (see Fig.4.6), and was optically pumped by the system A CO_2 laser (see Chapter III). The 4.2 metre long F I R super-radiant assembly was similar to that described in the previous chapter, except for the addition of a 250 line/inch copper mesh beam mixer at the front of the super-radiant tube. The mesh reflected approximately 90% of the vertically polarized

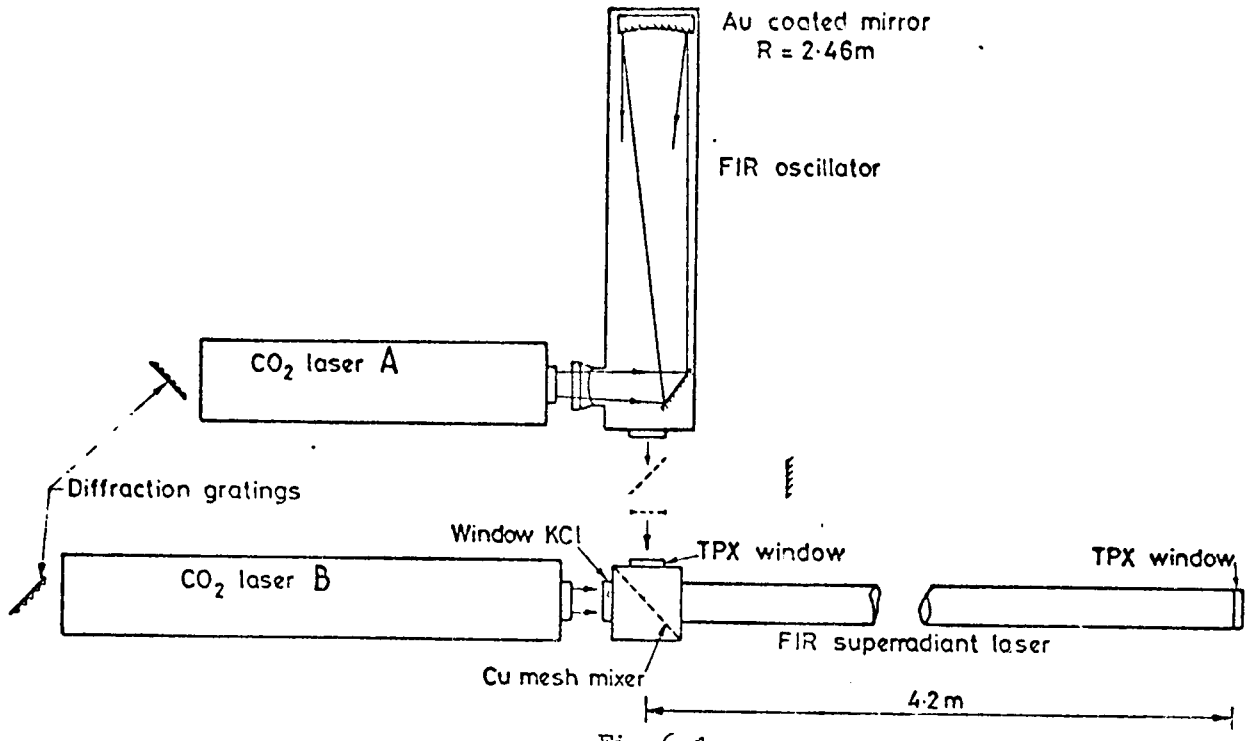


Fig.6.1

Schematic diagram of the FIR oscillator injected superradiant laser

radiation from the FIR oscillator into the super-radiant laser, while transmitting 55% of the horizontally polarized 9.55 μm pump radiation from the system B CO_2 laser (which was operated in the oscillator-amplifier configuration described in Chapter III).

The mesh was mounted inside the vacuum system, the CO_2 pump radiation entering the super-radiant assembly via a 15 mm thick, 100 mm diameter KCl window, while the FIR oscillator radiation entered via a 7 mm thick, 100 mm diameter TPX window.

The FIR injection system has also been successfully operated with a 5 mm thick, 120 mm diameter germanium flat (anti-reflection coated for 9.55 μm radiation) in place of the mesh mixer. Since the germanium mixer can also act as a vacuum window for the pump radiation, this eliminates the need for a KCl flat at the front of the super-radiant laser. In addition the anti-reflection coated germanium has a far higher transmission (~ 95%) for the CO_2 pump radiation than the 250 line per inch copper mesh. Finally, because the FIR oscillator radiation is more than 90% vertically polarized (see Chapter IV), it is strongly reflected from the inside surface of the germanium window, measured reflectivities exceeding 60%.

Two independently operated CO_2 pump lasers were used here to allow flexibility in the firing time of the FIR oscillator and super-radiant

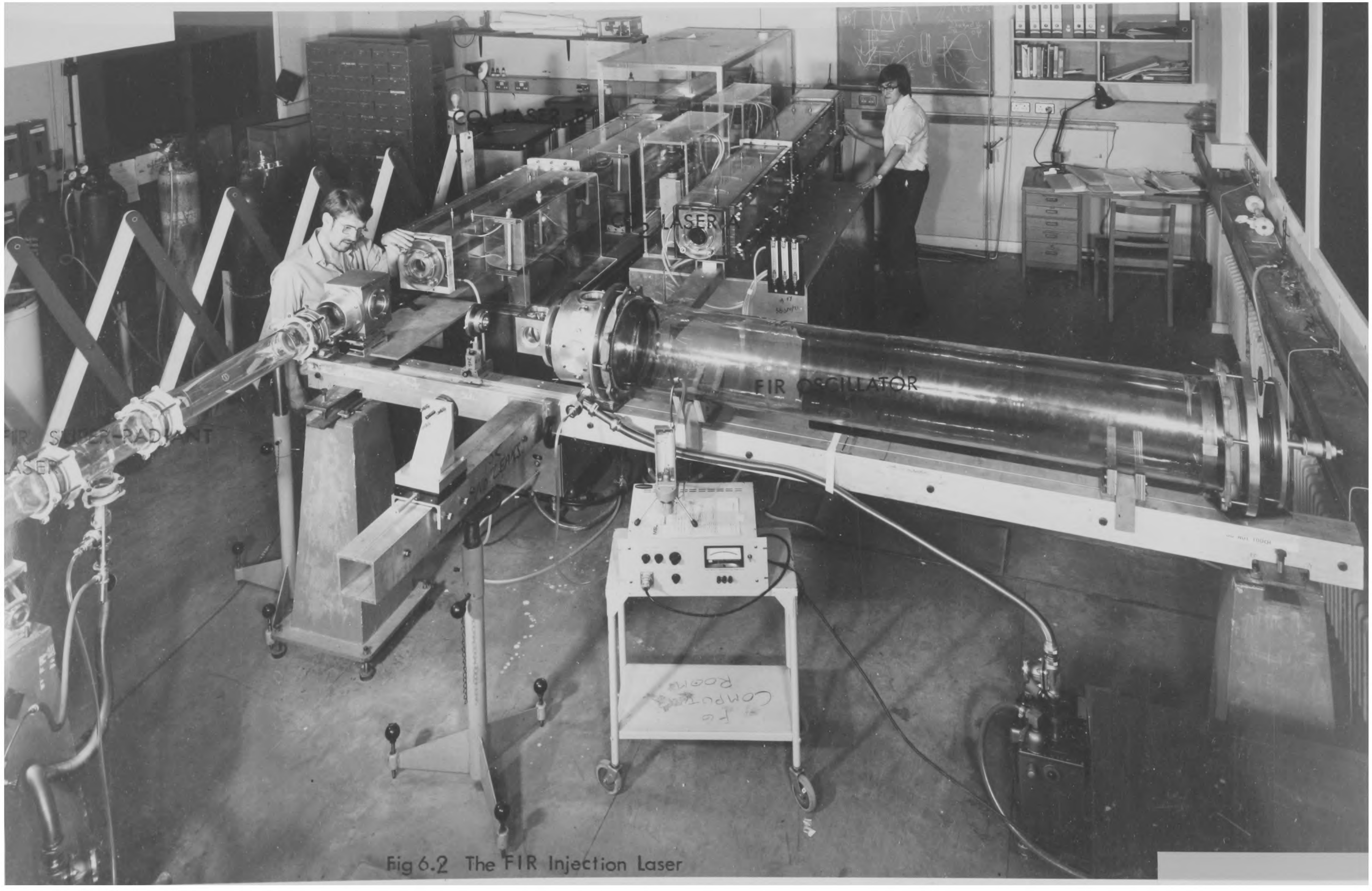
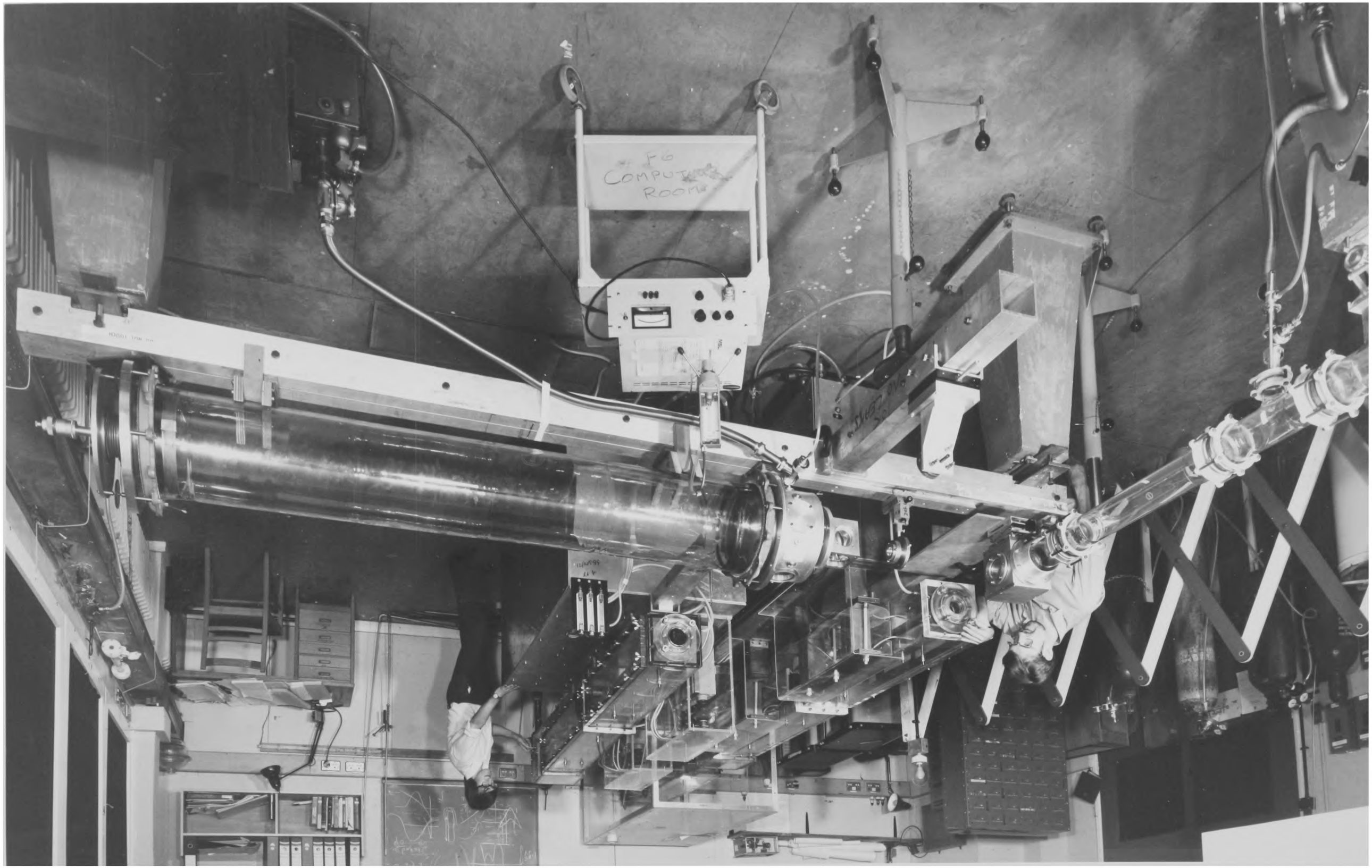


Fig 6.2 The FIR Injection Laser


F6
COMPUTER
ROOM

assembly. This has a further advantage, since in the F I R oscillator the tail of the CO_2 pulse contributes > 50% of the effective pumping energy (see Chapter IV), whereas in the super-radiant laser it contributes very little (see Chapter V), and it is therefore advantageous to be able to vary independently the spike-to-tail ratio for each CO_2 laser. (The spike-to-tail ratio is adjusted by varying the $N_2 : CO_2$ ratio, see appendix 'F').

The firing sequence for the F I R injection laser is illustrated in Fig.6.3. The system A laser was fired about 200 ns before the system B oscillator. The 500 ns long F I R oscillator pulse had therefore risen to nearly maximum power at the time the system B CO_2 pump initiated the growth of the F I R super-radiant pulse. The whole of the super-radiant tube was therefore filled with radiation from the narrow bandwidth F I R oscillator at the time the super-radiant pulse began to grow. If the intensity of injected F I R radiation is sufficiently high to compete with spontaneous emission at the front of the super-radiant tube (which would otherwise result in the generation of broadband super-radiance), the injected F I R photons can deplete the available gain in the super-radiant tube before wideband super-radiance is generated.

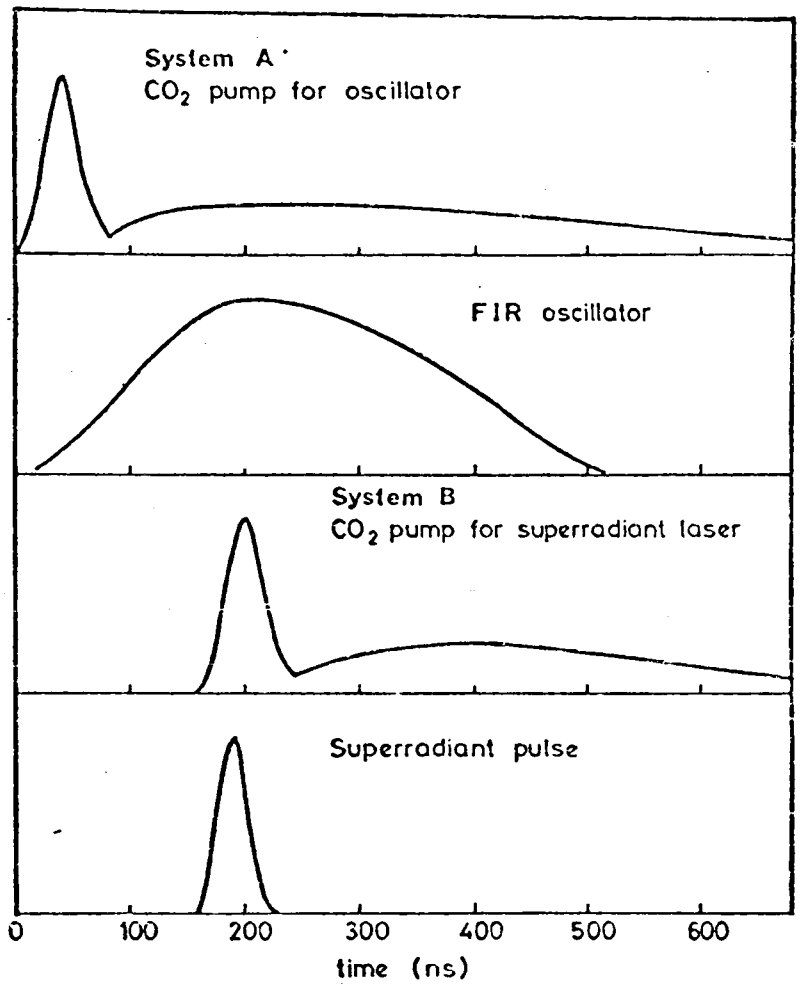


Fig.6.3
The firing sequence for the CO_2 pump lasers, the F I R oscillator and F I R superradiant laser in the oscillator injected superradiant system

6.2 THE DEPENDENCE OF THE INJECTION LASER BANDWIDTH ON THE INTENSITY OF THE INJECTED F I R RADIATION

Initially we carried out a series of experiments with a low power, narrow band CH_3F injection laser operated at 496 μm. For these experiments we used only the oscillator of CO_2 system B to pump the F I R super-radiant assembly. This generated about 6 J of 9.55 μm pump radiation of which only 1.2 J was in the gain-switched spike*.

In order to investigate the dependence of the injection laser bandwidth on the power of the F I R oscillator pulse, the output from the F I R oscillator was progressively attenuated from 300 to 1 μJ. For each F I R oscillator energy the bandwidth of the super-radiant injection laser was measured with the Fabry-Perot interferometer (see Appendix 'C') and the F I R pulse shape was measured with as Si-W point contact diode. (The signals being displayed on a 400 MHz bandwidth oscilloscope).

Without narrow-band injection the super-radiant laser generated about 0.3 mJ of broad-band super-radiance for a CH_3F pressure of 2.5 torr. The F I R pulse shape, obtained under those conditions, is shown in Fig.6.4(a). The super-radiant output can be seen to consist of a random sequence of spikes, the average power being about 7.5 kW with the spikes rising to about 15 kW.

When the single mode F I R oscillator was operated in synchronism with the super-radiant laser, as illustrated in Fig.6.3, the pulse shape exhibited a smooth variation upon which spikes (similar to, but smaller than, those observed without injection) were superimposed, as shown in Fig.6.4(b). This alteration in pulse shape is consistent with narrowing of the bandwidth in the injection laser. Measured F I R energies for injection laser operation were about 1 mJ corresponding to an average power of about 17 kW. Interferograms of the F I R output, both with and without injection, are shown in

---

* Only about 0.7 J actually entered the super-radiant tube, due to the 55% transmission of the mesh mixer.

(a)

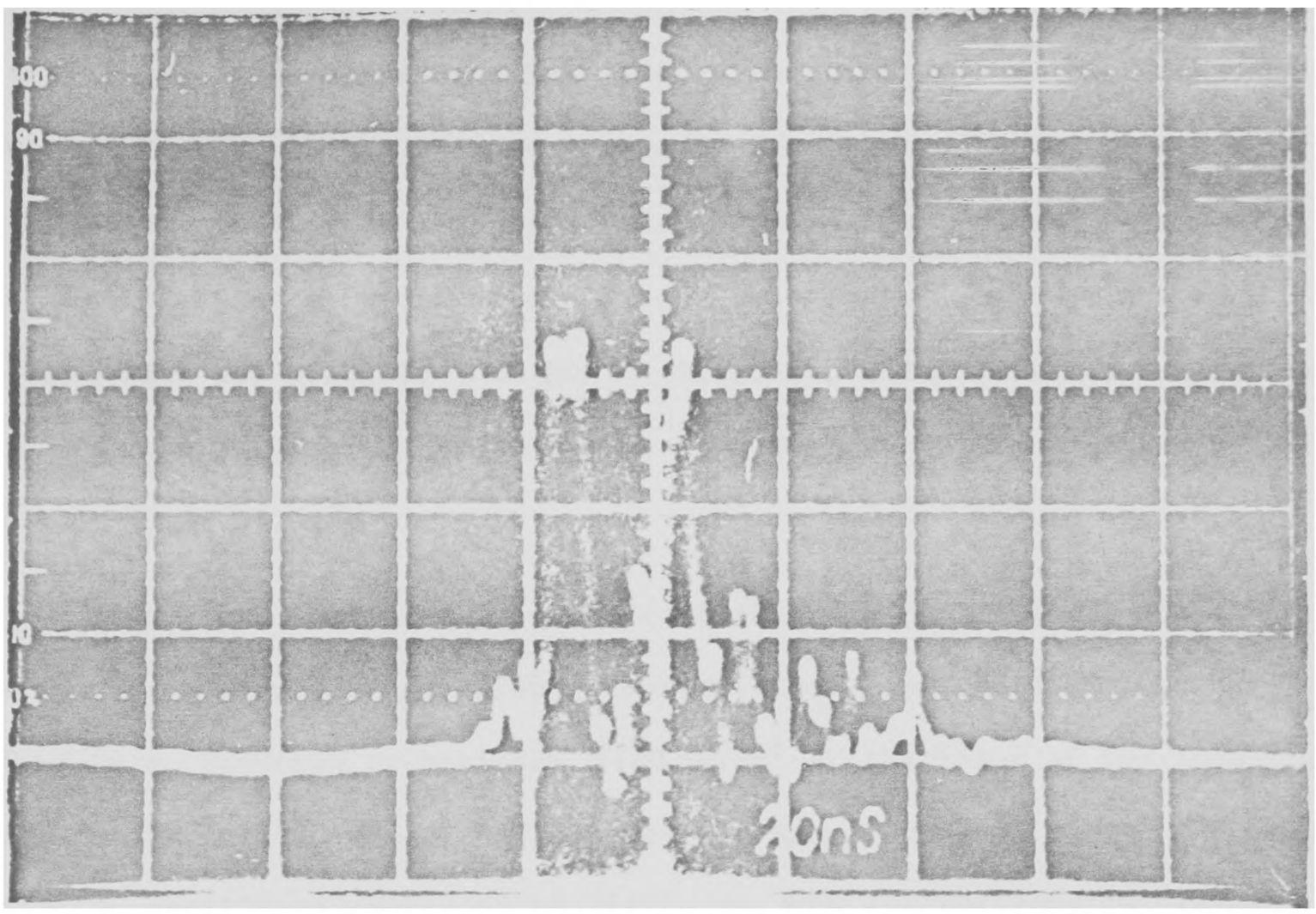


Fig.6.4
Point contact diode signals for
(a) Superradiant operation (horizontal scale = 20 nsec/div)
(b) Narrow bandwidth oscillator injected
superradiant operation (horizontal scale = 20 nsec/div)

(b)

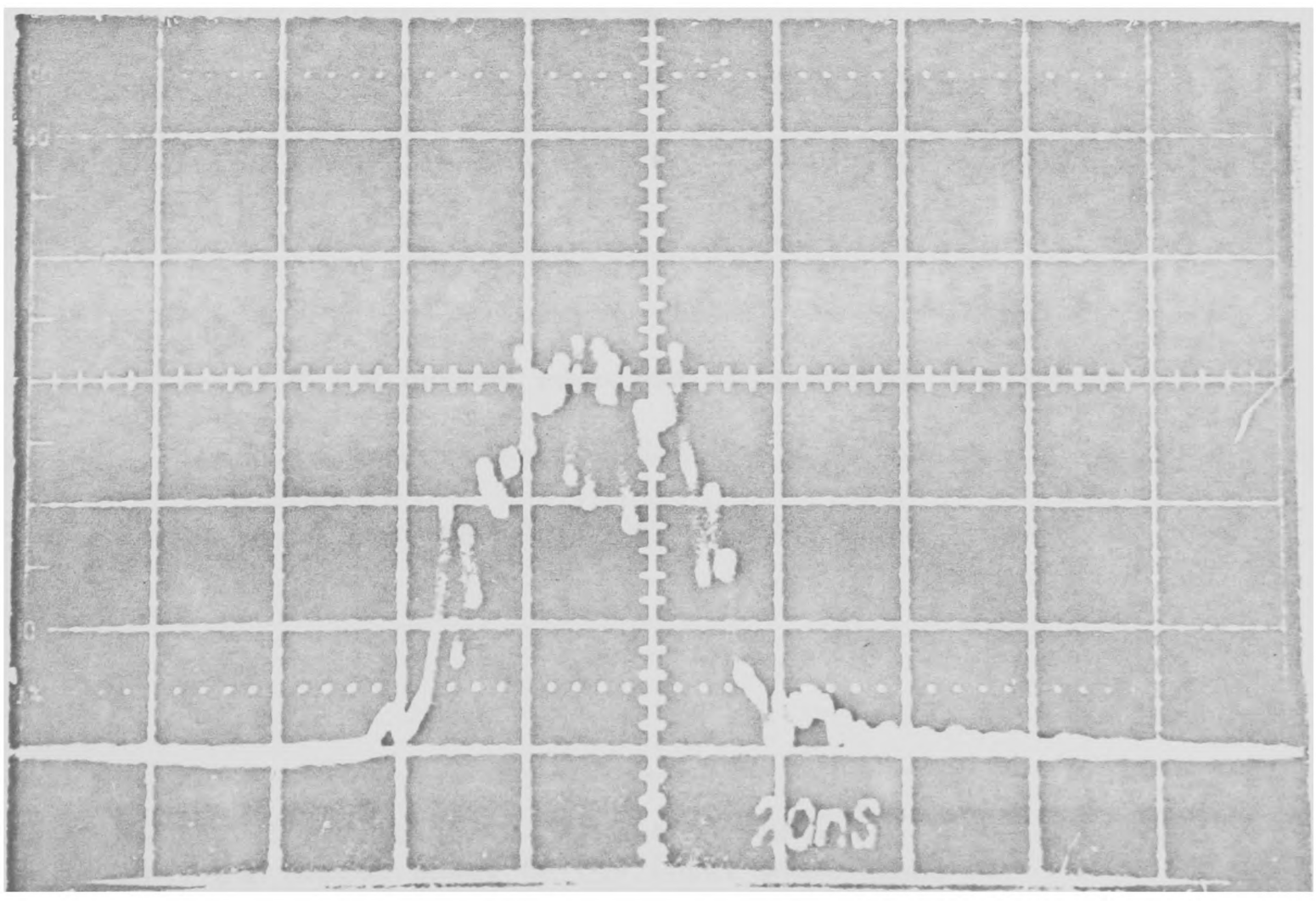


Fig.6.5, these confirm the bandwidth reduction inferred from the change in the observed pulse shape. Without injection the bandwidth is seen to be about 200 MHz, while with injection this falls to about 40 MHz. (However, since the instrumental width of the Fabry-Perot etalon was ~30 MHz, the true bandwidth was probably < 40 MHz.) Since the F I R oscillator used here had an average power of about 500 watts (see Chapter IV), the effective power gain† is about 34.

Figure 6.6 shows the dependence of the injection laser bandwidth with the injected F I R radiation intensity. For injected F I R energies $\geqslant 10\,\mu J$ (i.e. injected intensities $\geqslant 700\,mW/cm^2$ at the input of the injection laser) the injection laser bandwidth was $\leqslant 40$ MHz. It would appear therefore that F I R oscillator powers of as little as 80 W are required to produce 17 kW of narrow-band ($\leqslant 60$ MHz) radiation, representing an effective power gain of over 200. If this effective gain can be obtained in a scaled-up system, the 500 W F I R oscillator should be capable of driving over 100 kW of narrow-band F I R radiation.

Using the expression given by JUDD (1975) for the saturation energy density, namely $E_s = h\nu/2\sigma_f$ (where ν is the frequency of the F I R transition and σ_f is the stimulated emission cross-section for the F I R) , we obtain $E_s \approx 9 \times 10^{-4}$ J m^{-2}. Since the diameter of the pump beam at the front of the super-radiant tube is about 6 cm, the minimum injected F I R energy required to saturate the super-radiant laser (and hence to produce narrowband F I R radiation) is approximately 2.5 μJ. Which is in good agreement with the observed threshold (see figure 6.6).

---

† We define the effective power gain as the ratio of the narrow-band (e.g. $\leqslant$ 60 MHz) F I R output power to the input power from the F I R oscillator.

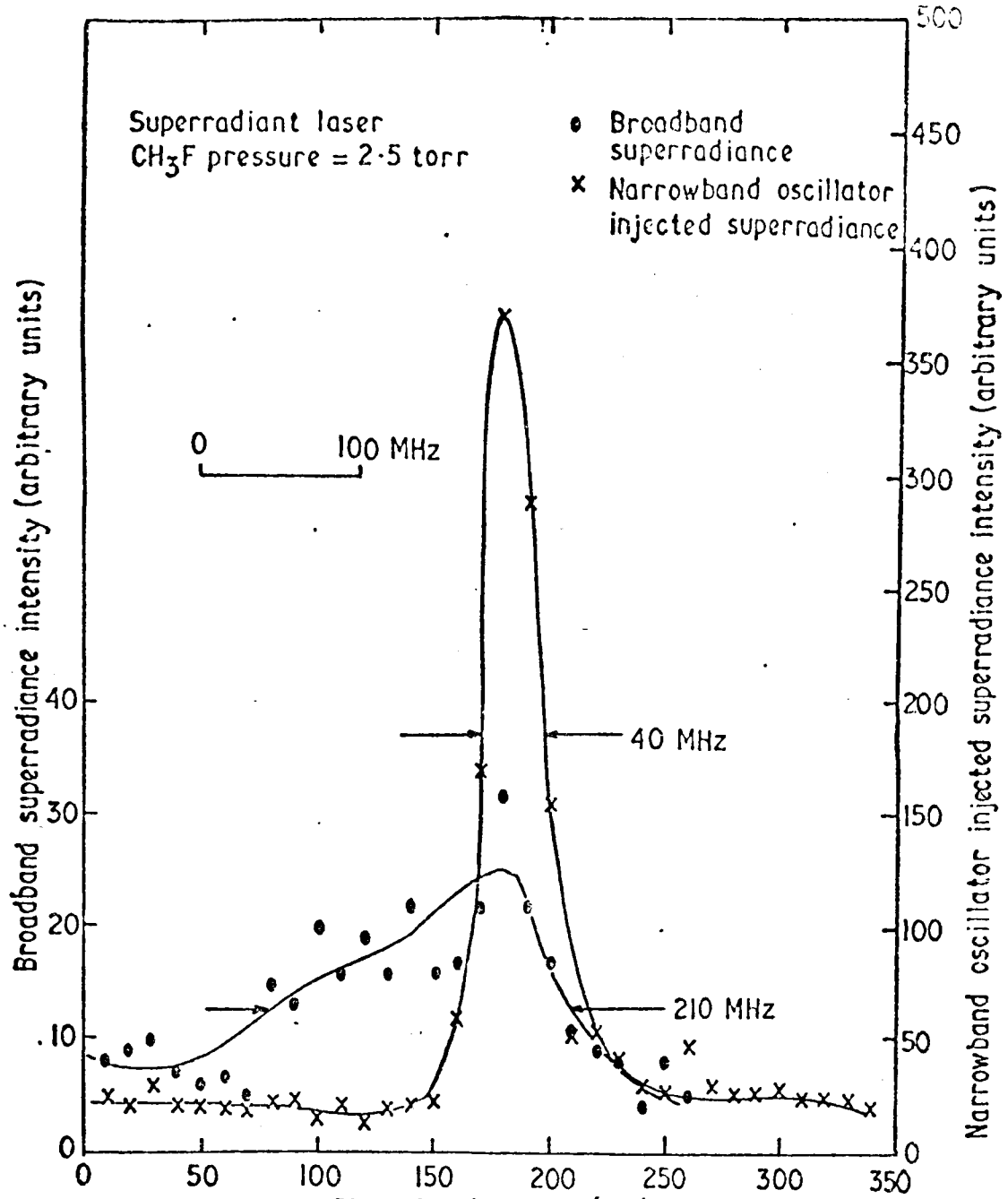


Fig.6.5
Fabry-Perot interferometer scans for the 7.5kW FIR superradiant laser, and the 17kW oscillator injected superradiant laser

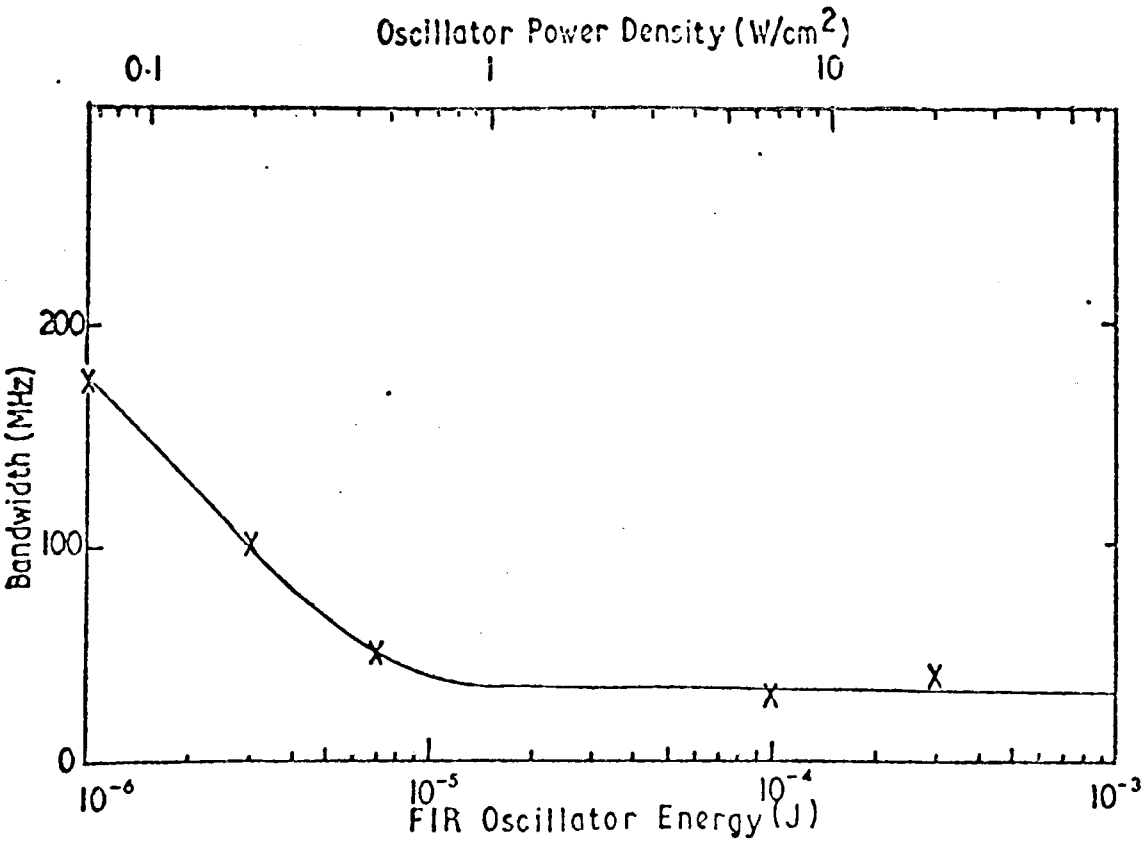


Fig.6.6
The bandwidth of the 17kW oscillator injected superradiant system as a function of the FIR pulse energy of the oscillator

6.3 OPTIMIZATION OF THE POWER OUTPUT OF THE F I R INJECTION LASER

In the experiments described in this section both the oscillator and the amplifiers of CO_2 system B were used to pump the F I R super-radiant laser. With 500 W of injected power from the single mode F I R oscillator, the CO_2 pump energy from the system B laser was increased until narrow-band operation of the injection system was no longer obtained. The injection laser output was optimized (i.e. the maximum F I R power with a bandwidth $\leqslant$60 MHz) for a CO_2 spike energy of 7 J, of which about 4 J remained after transmission through the mesh mixer. The F I R super-radiant pulse generated, without injection, for this pump energy and a CH_3F pressure of 2.5 torr[†], had a total energy of 8 mJ, which corresponds to an average power of 160 kW. An interferogram of the F I R output from the super-radiant laser revealed a bandwidth of about 300 MHz, as shown in Fig.6.7(a).

When the super-radiant laser was injected with the 500 W single mode F I R oscillator pulse (an interferogram of the F I R oscillator output is shown in Fig.6.7(b)), the super-radiant laser energy increased to 12.5 mJ, corresponding to an average pulse power of 250 kW and interferograms similar to that shown in Fig.6.7(c) were obtained.

Thus for the 496 μm CH_3F injection laser effective power gains of up to 500 are possible, if bandwidths $\leqslant$60 MHz are required.

[†] We will discuss the constraints on the operating pressure in section 6.4.

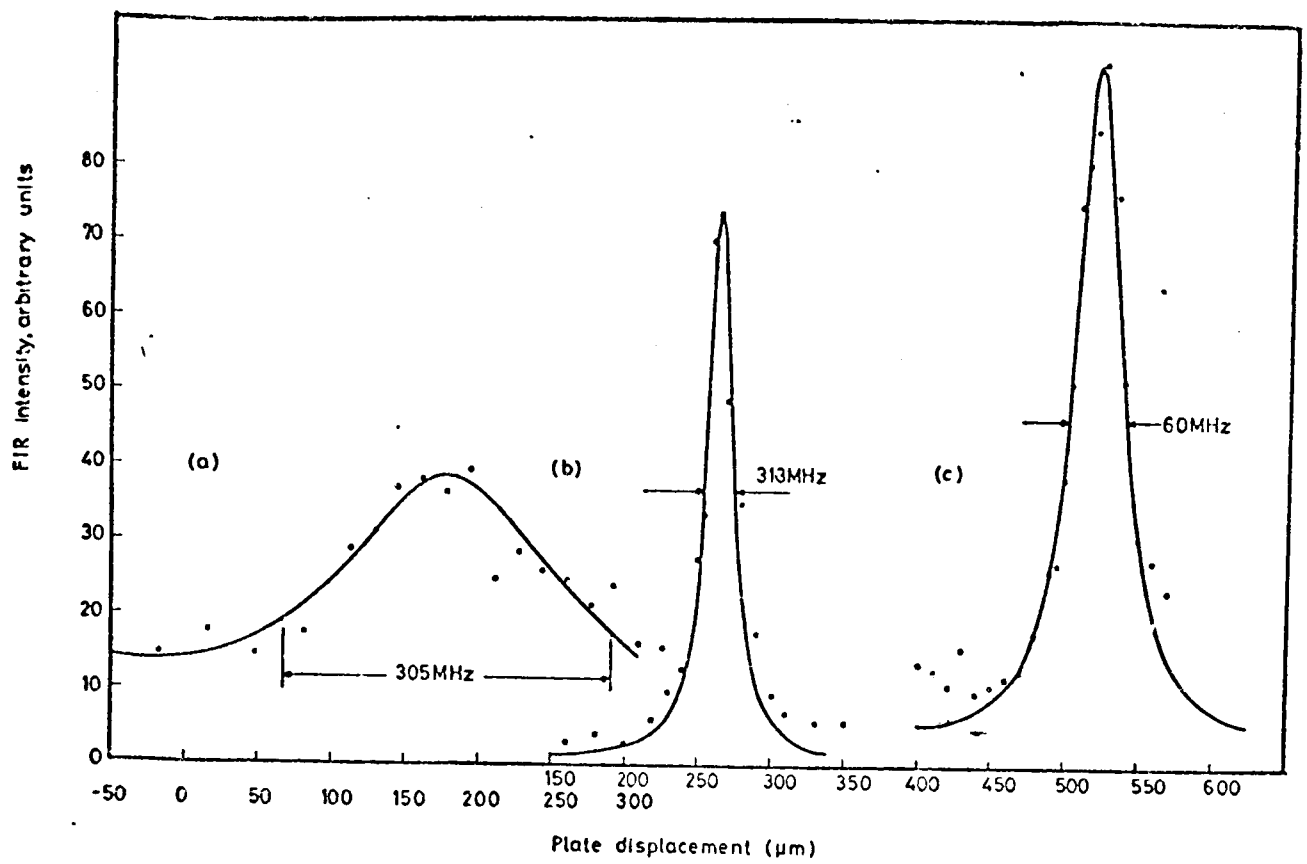


Fig.6.7
Fabry-Perot Interferometer scans of
(a) the 160kW FIR superradiant laser
(b) the 500 W FIR oscillator
(c) the 250kW oscillator injected super-radiant system

6.4 CONSTRAINTS ON THE OPERATING PRESSURE IN THE 496 μm CH_3F INJECTION LASER

A major constraint on the operating pressure of the 496 μm, CH_3F injection laser was imposed by the pressure dependent frequency shift phenomenon (see Appendix 'B'), which has been observed to take place in both the CH_3F oscillator (see Chapter IV) and the CH_3F super-radiant laser (see Chapter V). If the CH_3F super-radiant laser is operated below 1.5 torr, while the FIR oscillator is run at its optimum CH_3F pressure of about 0.8 Torr, only broad-band super-radiance is generated in the injection assembly, due to the mismatch between the output frequency of the FIR oscillator and the super-radiant laser (This frequency mismatch can become as great as 200 MHz for super-radiant laser pressures less than 1 Torr, see Chapter V). In order to obtain frequency matching between the FIR oscillator and the super-radiant laser it is necessary to operate at CH_3F pressures $\geqslant$ 2 Torr in the super-radiant assembly.

A second constraint on the operating pressure is imposed by the K level substructure of the $0 \rightarrow \nu_3$, $J = 12 \rightarrow 12$ pump absorption, which is very closely spaced for low K values (see Appendix 'E'). The CO_2 pump laser, which has a bandwidth of about 1 GHz (see Chapter III), can therefore produce a population inversion on energy levels with several different K values simultaneously, (CHANG, 1977). As a result, 496 μm super-radiance generated by the broad-band CO_2 pump consists of several frequencies (corresponding to F I R transitions with different K values), each separated by between 50 and 150 MHz and broadened due to collisions in the CH_3F gas. Since the F I R radiation from the single mode CH_3F cavity laser can arise only for a transition with a single K value (as a consequence of its narrow bandwidth) it can affect only one component of the K substructure in the super-radiant laser. However, since collisions in the CH_3F gas produce a pressure broadening of about 40 MHz $torr^{-1}$,† above about 2 torr we would expect strong collisional transfer between adjacent energy levels within the K sub-structure of the ν_3, $J = 12$ level. Thus, by injecting narrow-band radiation corresponding to a F I R transition with one K value we can also deplete the inversion on adjacent energy levels with different K values. For this reason, together with the pressure dependent frequency shift, it is necessary to operate the super-radiant laser at CH_3F pressures above 2 torr, where collisional losses become increasingly severe, resulting in poor photon conversion efficiencies.

6.5 SUMMARY OF THE PERFORMANCE OF THE 496 μm, CH_3F INJECTION LASER

Table 6.1 lists the main characteristics of the injection laser investigated here.

---

† The collisional broadening has been calculated by CHANG and BRIDGES (1970) using the theory of ANDERSON (1949).

TABLE 6.1

Summary of the Characteristics of the 496 μm CH_3F Injection Laser Investigated in the Present Work (see Note 6)

CO_2 Pump Energy for the Super-Radiant Laser (see Note 1)	0.66 J		3.9 J	
	Without Injection	With Injection	Without Injection	With Injection
F I R Output Energy	0.3 mJ	1.0 mJ	8.0 mJ	12.5 mJ
Average F I R Pulse Power	7.5 kW	17 kW	160 kW	250 kW
Bandwidth	~200 MHz	30 MHz	300 MHz	60 MHz
Maximum Effective Power Gain (see Note 2)	-	⩾200	-	500
F I R Single Mode Oscillator Power (see Note 3)	-	⩽ 80 W	-	500 W
Energy Conversion Efficiency (see Note 4)	0.05%	0.15%	0.2%	0.3%
Photon Conversion Efficiency (see Note 5)	2.6%	8%	10.7%	17%

NOTES

1. The energy quoted here refers to the CO_2 spike, allowing for transmission loss in the copper mesh beam mixer.
2. The effective power gain is defined as the ratio of the injection laser output power to F I R oscillator power.
3. The characteristics of the F I R single mode oscillator used here are the same as those given in Table 4.1.
4. The energy conversion efficiency is defined as the ratio of the F I R output energy to the CO_2 spike pump energy, allowing for transmission through the copper mesh mixer.
5. The photon conversion efficiency is the ratio of the F I R photons generated to the pump photons used. Without recycling or Raman scattering the maximum possible efficiency is 50% (see Chapter V).
6. The results quoted here were obtained for a CH_3F gas pressure of 2.5 torr and a super-radiant tube length of 4.2 m.

CHAPTER VII

COMPUTER SIMULATION OF THE 496 μm CH_3F SUPER-RADIANT LASER

This chapter presents a simulation of the 'super-radiant'[†] laser system, based upon a three level rate equation model (BLOEMBERGEN, 1956) as a first step towards predicting the behaviour of the injection assembly described in Chapter VI.

Since the discovery of the first optically pumped F I R laser by CHANG and BRIDGES in 1970, considerable effort has been expended on the development of a theoretical description of pulsed optically pumped F I R lasers (TUCKER, 1976; TEMKIN and COHN, 1976 and BLUYSSEN et al, 1975). A detailed theory of the F I R injection system must correctly treat both the molecular dynamics of the laser medium (e.g. relaxation rates), and the optical transitions of the medium at the pump and F I R frequencies.

In a pulsed F I R laser the rate of optical pumping is in equilibrium with the rate of relaxation and stimulated emission within the excited vibrational level, and both the pump and emitting transitions are usually homogeneously (i.e. pressure) broadened. TEMKIN and COHN (1976) and TUCKER (1976) have used a rate equation model, which assumes homogeneously broadened transitions, to describe a F I R laser. In particular, TUCKER (1976) has derived an expression for the pump absorption which agrees well with experimental data for a CH_3F, 496 μm, super-radiant laser.

[†] The term 'super-radiance' was first used by Dicke in 1954 when describing the phenomenon of cooperative spontaneous emission, where an assembly of atoms are coupled by their common radiation field. The intensity emitted by N atoms under this condition is proportional to N^2, instead of N, and thus super-radiance is a fundamental effect. (MacGILLIVRAY and FELD, 1976). However, in this work we use the term 'super-radiance' to refer to all the radiating processes which take place in mirrorless single-pass, F I R lasers and not specifically to the effect described by Dicke in 1954.

However, the three-level rate equation model is insufficient to describe the detailed behaviour of a super-radiant laser, where the F I R laser field is strong. PANOCK and TEMKIN (1977) and CHANG (1977) have obtained analytic expressions for pump absorption and F I R laser gain, which are valid for strong F I R laser fields, by employing a quantum mechanical treatment. In the rate equation model, molecules are excited by means of two successive single photon transitions, whilst the quantum theory also allows two photon transitions, in which a photon is, simultaneously, absorbed at the frequency of the pump laser and a photon emitted at the frequency of the F I R laser (i.e. Raman scattering). This two photon process can give rise to a frequency splitting of the small signal gain of the F I R laser into two symmetric peaks, if either the pump frequency is far from resonance, or the pump transition is strongly saturated (SHIMODA and SHIMIZU, 1972).

In order to model a mirrorless, super-radiant laser we need to derive the F I R output and the pump intensity as functions of time and distance along the super-radiant tube axis. This is in contrast to the modelling of optically pumped, F I R cavity lasers, where it is normally possible to assume spatial uniformity of both the pump radiation and the laser emission, so that only the temporal dependence of these quantities is required (BLUYSSEN et al, 1975). In addition, a detailed quantum mechanical model of the super-radiant assembly would require frequency dependence. To run a quantum mechanical model of the super-radiant laser would require many hours of computation time on a modern computer, we have, therefore, used a simpler three level rate equation model, without frequency dependence. (Even this simple model requires 10-15 minutes of computer time on an ICL 4/70 machine).

The theory of pulse propagation in laser amplifiers has been considered by several authors (FRANTZ and NODVIK*, 1963; BELLMAN et al, 1963;

* see also ICSEVGI and LAMB , Phys. Rev. 185 , 517 (1969)

DAVIS and SOOY, 1964 and AVIZONIS and GROTBECK, 1966), who have obtained analytic solutions of the radiative transfer and rate equations which describe these devices. Also, YARIV (1967) has obtained analytic solutions for the equations describing the generation of photon noise in laser amplifiers. However, these analytic solutions either neglect spontaneous emission or assume that pumping is uniform and occurs only before the laser pulse is amplified. Although these are valid constraints for conventional laser amplifiers (e.g. ruby or neodymium), they are not applicable to super-radiant lasers.

In the following sections we consider the first computational model for a F I R, optically pumped, super-radiant laser, which retains both temporal and spatial dependence and involves none of the foregoing assumptions.

7.1 THE SLAB MODEL FOR AN OPTICALLY PUMPED SUPER-RADIANT LASER

Figure 7.1 illustrates the model used here to describe the operation of a F I R super-radiant laser. The super-radiant tube has a total length L and is divided into a number of thin slabs, each of thickness Δx. Within a slab the pump radiation, the F I R emission and the population densities of the states involved in the laser process, are assumed to be uniform. The absorption of pump photons in the laser medium and the subsequent emission of F I R laser radiation, is represented by a three level model. This is illustrated in Fig.7.2; the pump photons excite the molecules in the laser medium from level C to level A, whilst the F I R laser emission occurs between level A and level B. The equations describing the rates for these processes are:

$$\frac{\partial N_A}{\partial t} = -\sigma_p (N_A - N_C) \frac{I_p}{h\nu_p} - \sigma_f (N_A - N_B) \frac{I}{h\nu} - \frac{(N_A - N_{A_o})}{\tau} \quad \ldots (7.1)$$

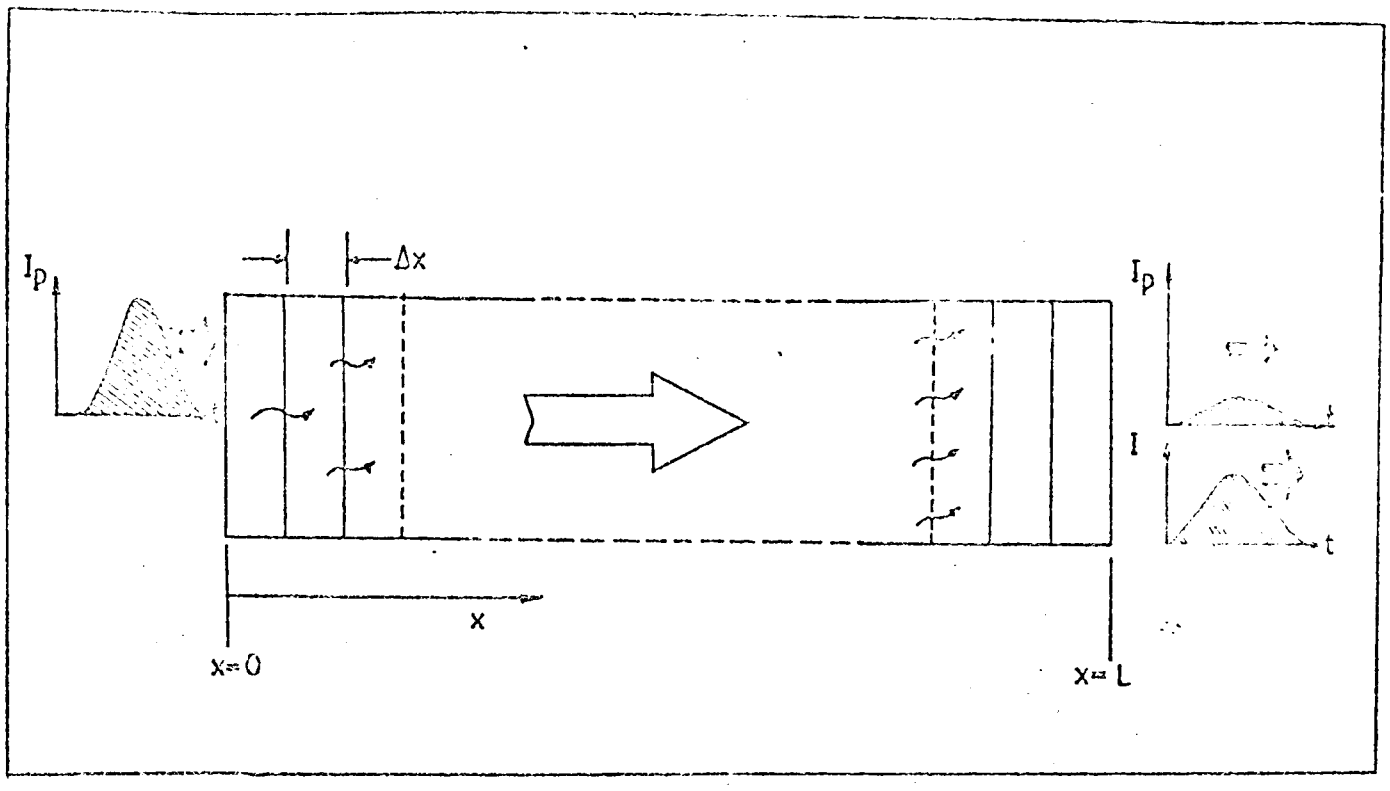


Fig.7.1
Schematic diagram of the slab model for an optically pumped superradiant laser

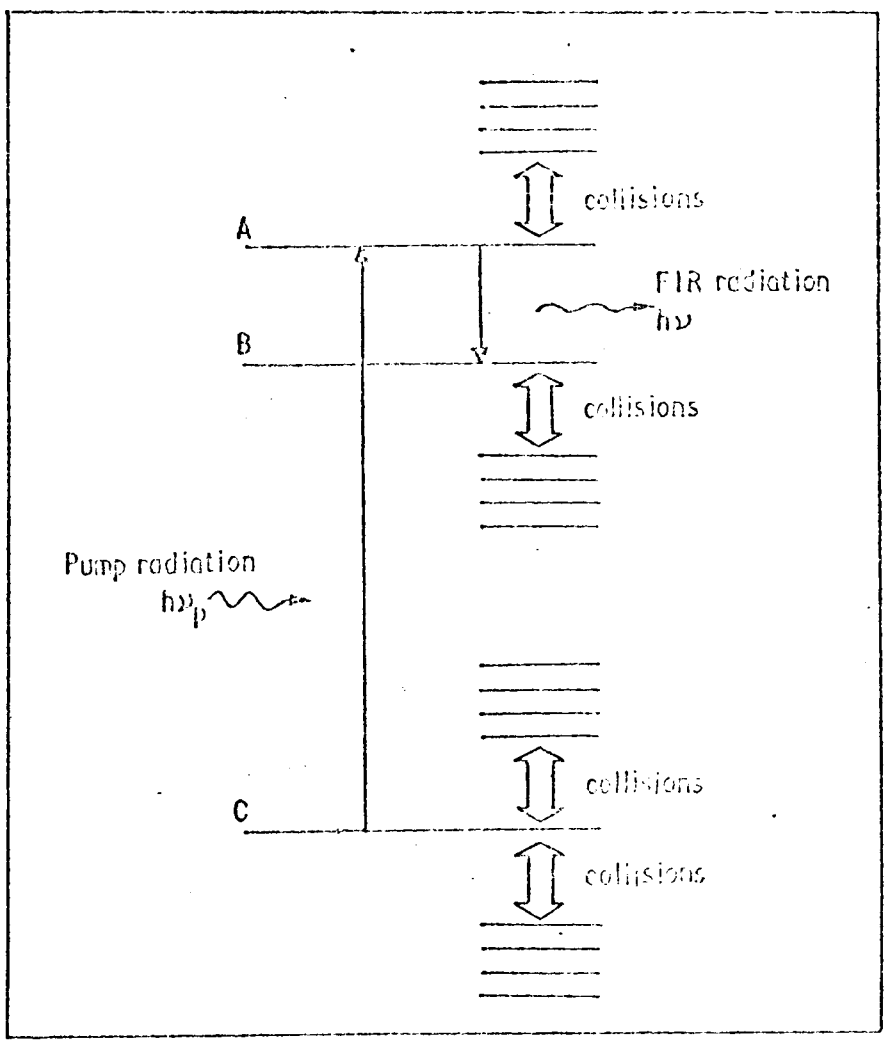


Fig.7.2
Partial energy level diagram to illustrate the three level rate equation model

$$\frac{\partial N_B}{\partial t} = \sigma_f (N_A - N_B) \frac{I}{h\nu} - \frac{(N_B - N_{B_o})}{\tau} \quad \ldots (7.2)$$

$$\frac{\partial N_C}{\partial t} = \sigma_p (N_A - N_C) \frac{I_p}{h\nu_p} - \frac{(N_C - N_{C_o})}{\tau} \quad \ldots (7.3)$$

where the parameters used here are listed in Table 7.1.

TABLE 7.1

Physical Parameters for the Computer Model of the F I R CH_3F Laser

Physical Parameter	Symbol	Value
Population density of level A	N_A	-
Population density of level B	N_B	-
Population density of level C	N_C	-
Equilibrium population density of level A	N_{A_o}	3.19×10^{18} m^{-3} ‡
Equilibrium population density of level B	N_{B_o}	3.24×10^{18} m^{-3} ‡
Equilibrium population density of level C	N_{C_o}	4.91×10^{20} m^{-3} ‡
Intensity of the pump radiation	I_p	-
Intensity of the F I R radiation	I	-
Cross-section for F I R stimulated emission	σ_f	1.1×10^{-19} m^2 ≠
Cross-section for pump absorption	σ_p	2.5×10^{-23} m^2 *
Frequency of the pump radiation	ν_p	3.138×10^{13} Hz
Frequency of the F I R radiation	ν	6.043×10^{11} Hz
The rotational-rotational collision time	τ	8×10^{-9} sec †‡
F I R spontaneous emission time	t_{sp}	2.3×10^{2} sec †
Pump energy density	I_{p_o}	-

NOTES:
‡ Values quoted for a pressure of 1 torr
† CHANG and BRIDGES, 1970
≠ BROWN and COHN, 1974
* CHANG, WANG and CHEO (1969), derived from their measurement of the pump absorption coefficient, α_p (measured to be 1.8 m^{-1}).

The first term in equation (7.1) and (7.3) describes the population of level A and the depopulation of level C by the pump radiation, whilst the second term of equations 7.1 and 7.2 describes the depopulation of level A and the population of level B as a result of FIR emission. Finally, the last term in each of these equations describes the collisional transfer between levels A, B and C, and other rotational energy levels in the molecule.

We assume here that the FIR super-radiance, generated by pumping the laser medium, is emitted only in the forward direction (i.e. from left to right in Fig.7.1). This is not entirely true experimentally, since for the 496 μm CH_3F laser we have measured the forward to backward ratio to be about 2 : 1 (see Chapter V). However, PLANT et al (1974) have measured ratios as high as 10^4 : 1.

The radiative transfer equations which describe the propagation of both pump and FIR radiation along the super-radiant tube are:

$$\frac{\partial I_p}{\partial t} + c\,\frac{\partial I_p}{\partial x} = \sigma_p\, c(N_A - N_C)\, I_p \qquad \ldots (7.4)$$

$$\frac{\partial I}{\partial t} + c\,\frac{\partial I}{\partial x} = \sigma_f\, c\,(N_A - N_B)\, I + \frac{ch\nu_f}{t_{sp}}\, N_A \qquad \ldots (7.5)$$

where t_{sp} is the FIR spontaneous emission time. We have ignored a spontaneous emission term in equation (7.4), since it should be negligibly small. The second term on the right hand side of equation (7.5) is the spontaneous emission, which is the source of the FIR radiation. Strictly speaking this spontaneous emission term should be multiplied by a solid angle $\sim r^2/4L^2$, where r is the radius of the super-radiant tube. However, the growth of FIR radiation in the super-radiant laser is dominated by stimulated emission and is therefore relatively insensitive to the magnitude of the spontaneous emission term.

To make the left hand side of equation (7.4) and (7.5) derivatives in time only, we choose a frame (x', t') such that $x' = x - ct$, $t' = t$. Equations (7.4) and (7.5) now become:

$$\frac{\partial I_p}{\partial t'} = \sigma_p\, c(N_A - N_C)\, I_p \qquad \ldots (7.6)$$

$$\frac{\partial I}{\partial t'} = \sigma_f\, c(N_A - N_B)\, I + \frac{ch\nu_f}{t_{sp}}\, N_A\,. \qquad \ldots (7.7)$$

7.2 THE COMPUTER PROGRAM

In this section we discuss the computer program used to solve the rate and radiative transfer equations given in section 7.1. A flow diagram, summarizing the main steps in the program, is shown in Fig.7.3. Given a time dependence for the pump pulse entering the first slab, the program calculates N_A, N_B and N_C as a function of time, using equations (7.1), (7.2) and (7.3). The time step used here, Δt, is determined by Δx since we have chosen $\Delta x/\Delta t = c$ (see section 7.1). The rate equations are solved by a Kutta-Merson iteration process† (FOX, 1962). When the program has calculated N_A, N_B and N_C as functions of time for the first slab, the time dependence of I_p and I leaving the slab is then determined by solving equations (7.6) and (7.7). I and I_p are then integrated with respect to time to produce the total F I R and pump energy leaving the slab.

The program steps to the next slab and, using the newly calculated time dependence of I_p and I, it repeats the process carried out for the first slab. This sequence continues until x satisfies the condition $x \geq L$, at which point the program is terminated. Note that in the program flow chart in Fig.7.3, the time counter (t) is reset to zero at the beginning of the calculation for each slab. In reality there is a time delay $\Delta x/c$ which should be added for each additional slab, but this only shifts the pulse in time, it does not affect the calculated pulse shape.

As the F I R pulse grows along the super-radiant tube it was found necessary to reduce Δt to maintain the accuracy of the calculation. For this reason two lengths were specified, at which the mesh spacing, Δt, could be halved.

---

† A simple finite difference method was used initially, but this method was found to be inefficient and suffered from severe numerical instabilities.

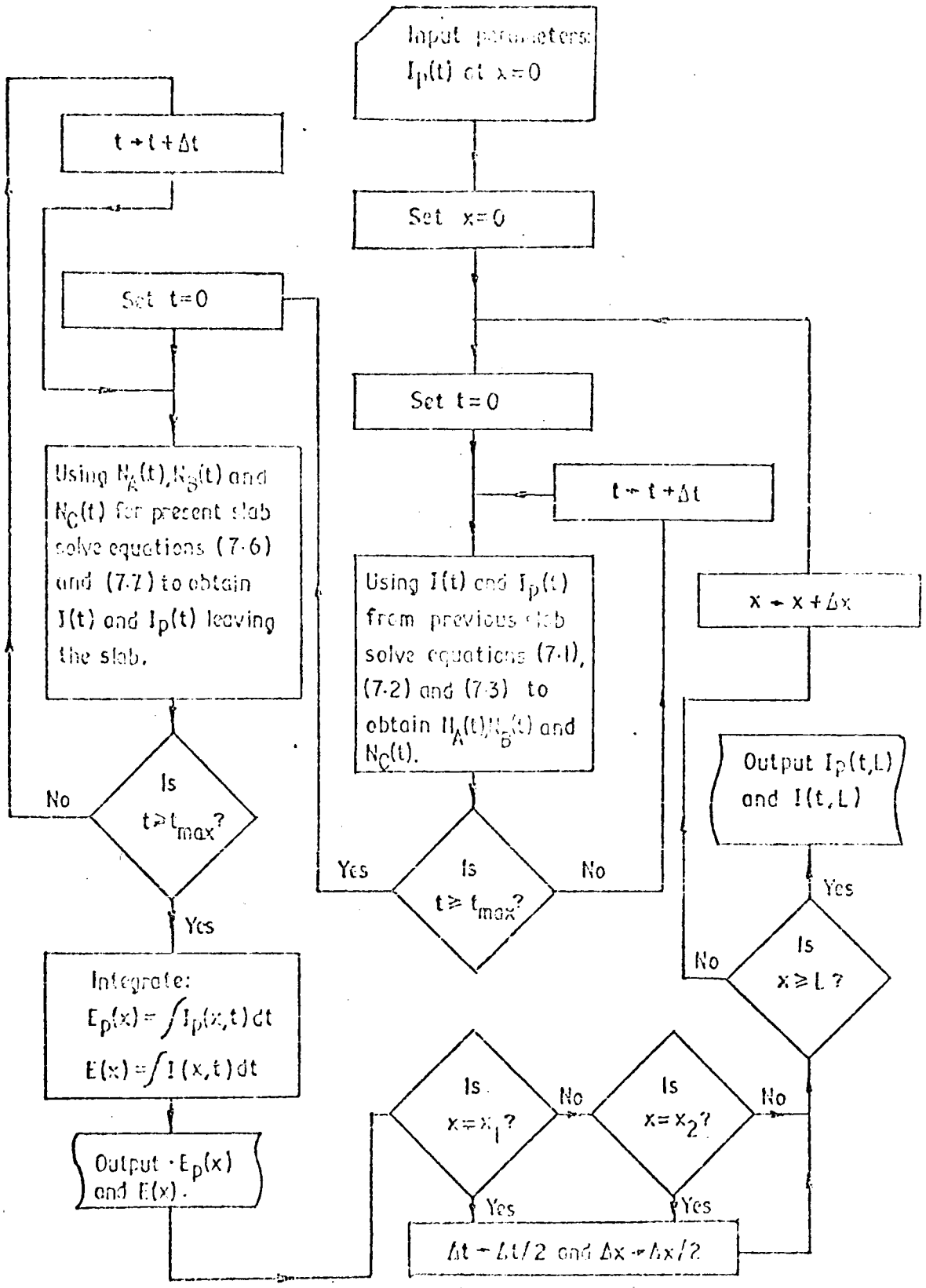


Fig.7.3
Flow diagram of the computer program for the simulation of a superradiant laser

7.3 COMPARISON OF THE COMPUTER SIMULATION WITH EXPERIMENTAL DATA FROM THE 496 μm, CH_3F, SUPER-RADIANT LASER

The program described in section 7.2 was used to simulate the operation of the 496 μm, CH_3F, super-radiant laser discussed in section 5.2. Initially the parameters in the model were set equal to the values listed in Table 7.1. For the 496 μm CH_3F laser, level A (in the three level model illustrated in Fig.7.2) is the ν_3, J = 12 state, level B is the ν_3, J = 11 state and level C is the J = 12 level of the ground vibrational manifold. In order to calculate N_{A_o}, N_{B_o} and N_{C_o} we substituted the vibrational and rotational constants given by FREUND et al (1974) into the relevant formulae, which can be found in TOWNES and SCHAWLOW (1955), to obtain the statistical weights for each of the states in the model. These calculations gave the equilibrium number densities shown in Table 7.1.

The pump pulse used in the model had a Gaussian temporal profile with a FWHM of 60 ns, in order to simulate the spike of the CO_2 laser pulse (see Chapter 3).

Figure 7.4 shows the results computed for the input data given in Table 7.1, with pump energy density, $I_{po} = 600\ J/m^2$ and tube length, L = 4.2 m. The model is found to predict much lower pump absorption than observed experimentally and FIR output peaking at a much higher CH_3F pressure. However, it is known that acceptable agreement between computed pressure dependence and experimental data can be secured by a suitable modification of the physical parameters specifying the curves. Thus BLUYSSEN et al (1975) achieved a respectable fit to their data in a three level, time only-dependent, rate equation model by altering one parameter, namely the effective number of molecules taking part in the laser action. In the present calculation, modification of two parameters proved necessary to obtain satisfactory agreement between computed curves and experimental points. It was found that varying the collision time, τ, produced a significant change in the FIR emission curve, mainly at pressures higher than that at which the

F I R output was maximum, while at lower pressures the curve was influenced chiefly by variations in the absorption cross-section, σ_p .

The value of σ_p used initially was that measured by CHANG, WANG and CHEO in 1969, for low pump intensity conditions. However, recently CHANG (1977) and PANOCK and TEMKIN (1977) have shown that the number of K levels excited in the CH_3F laser depends on the intensity of the pump, so that at high pump intensities more K levels are excited. Since σ_p is proportional to K^2 for the $J = 12 \rightarrow 12$, $0 \rightarrow \nu_3$ absorption (TOWNES and SCHAWLOW, 1955), it therefore depends strongly on the pump intensity.

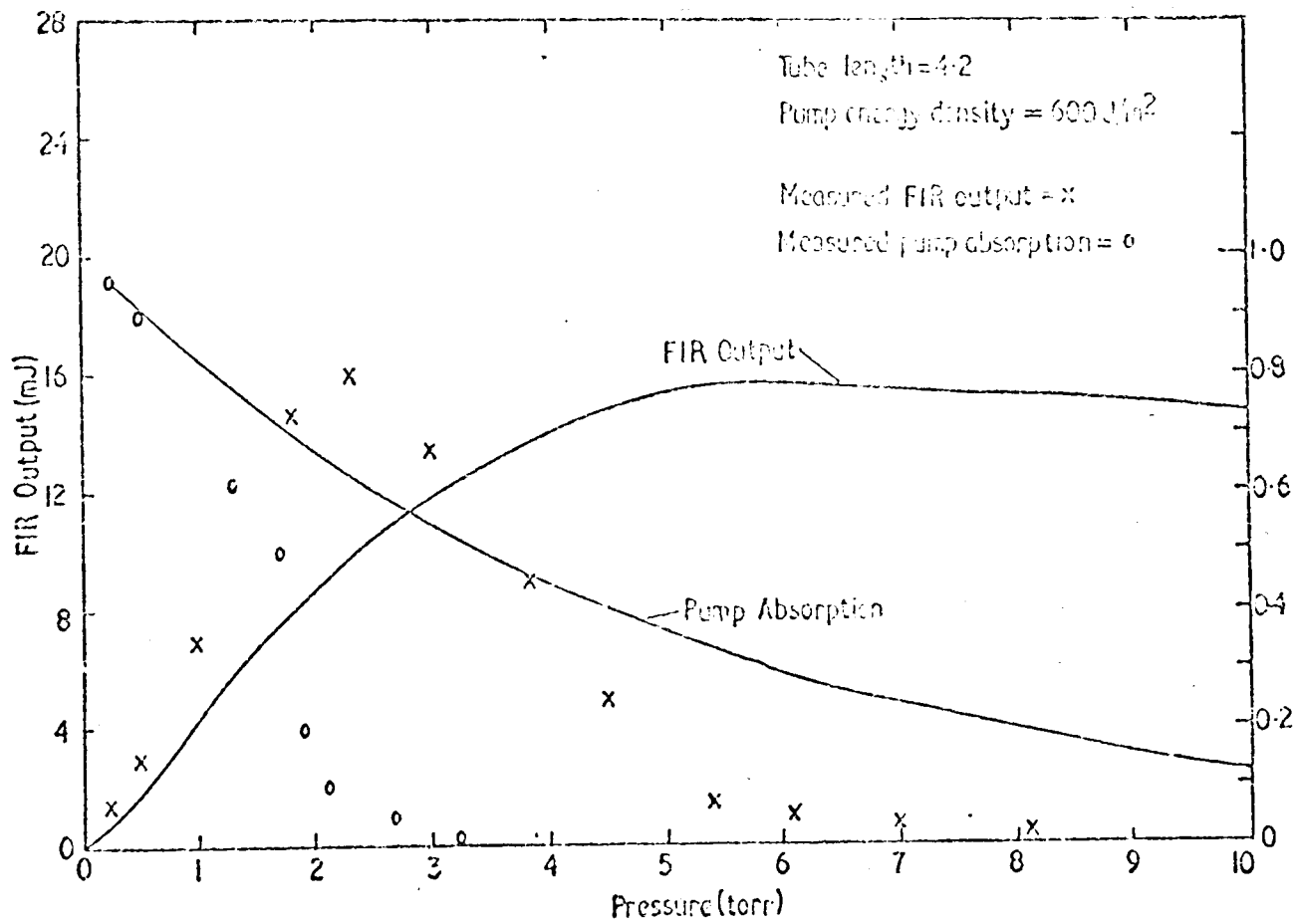


Fig.7.4
Computer results for pump energy density of 600 J/m^2 and a tube length of 4.2 m
[$\sigma_p = 2.5 \times 10^{-23}$ m^2, $\tau = 8 \times 10^{-9}$ p^{-1} (torr) sec]

The value of τ was deduced from the pressure broadened width of the 496 μm emission line of CH_3F (CHANG and BRIDGES, 1970), but the effective relaxation rate is, in practice, different for each level in the model and is influenced by processes other than collisions. For example, the relaxation rate for level C will be enhanced by the generation of 452 μm radiation, which rapidly populates this level.

Thus, both σ_p and τ may be reasonably increased to fit the observed data. The choice of $\sigma_p = \quad 10^{-22}\,m^2$ and $\tau = 2 \times 10^{-9}\,p^{-1}$ (torr) sec, i.e. a four-fold increase in both the rotational-rotational collision frequency and the pump absorption cross-section, resulted in the fit to experimental points illustrated in Fig.7.5(a) Notice that this modification leads to both the emission and the absorption curves displayed, no other normalization being necessary.

The scaling of pump absorption and F I R emission with tube length was investigated, no other normalization or modification of parameters beyond those already mentioned being introduced. Nevertheless, the model predicts reasonably closely the results observed for $L = 2.66\,m$, as shown in Fig.7.5(b). The predicted F I R emission peaks at slightly lower pressures and fails to reach quite the measured intensity; however, only a small adjustment in σ_p and τ will remove this disagreement.

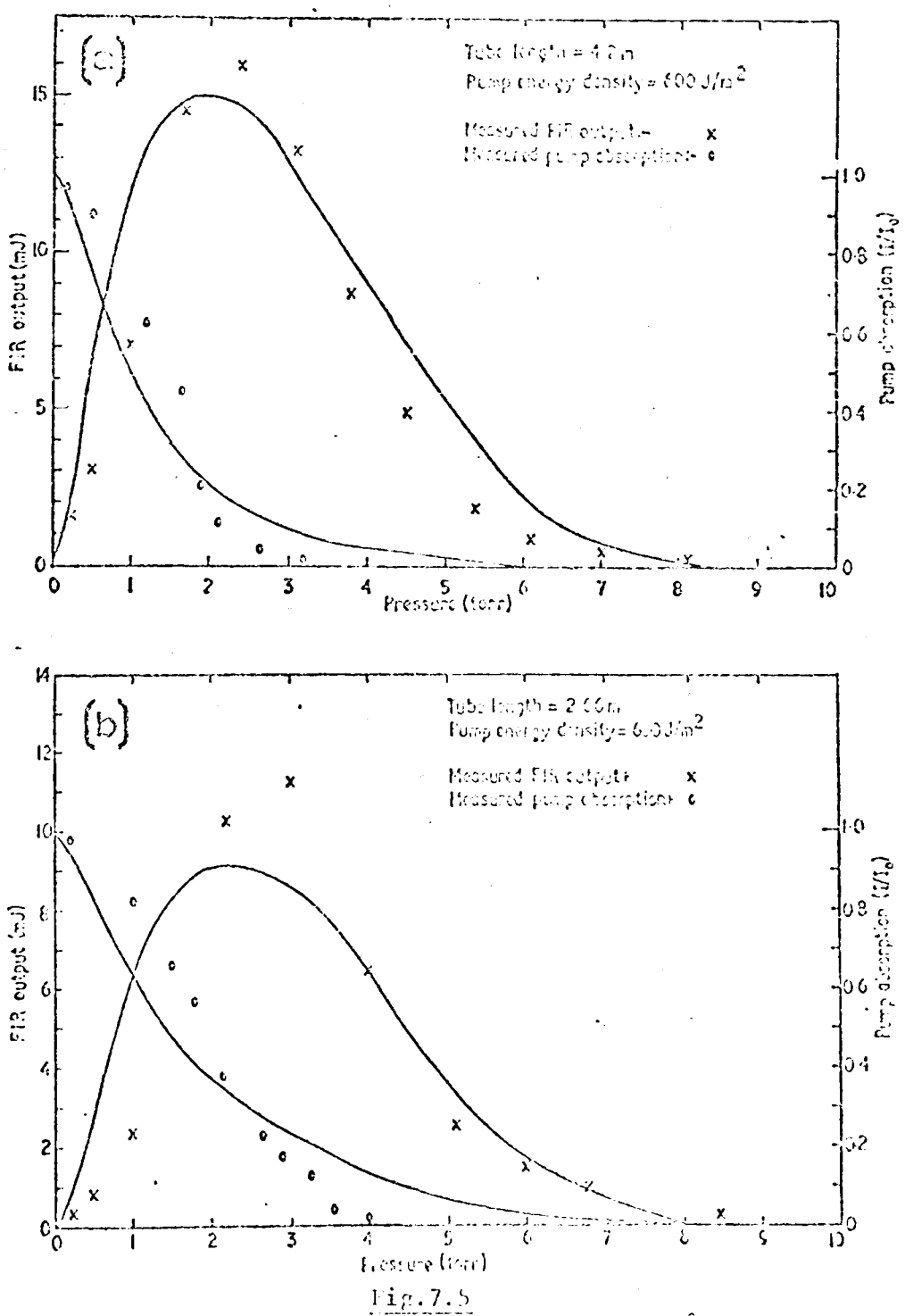


Fig.7.5
Results for a pump energy density of 600 J/m², (a) for a 4.2 metre long tube, and (b) a 2.66m long tube. [$\sigma_p = \quad 10^{-22}\,m^2$, $\tau = 2 \times 10^{-9}\,p^{-1}$ (torr) sec]

The scaling of F I R emission with pump energy density proved less satisfactory. In Fig.7.6

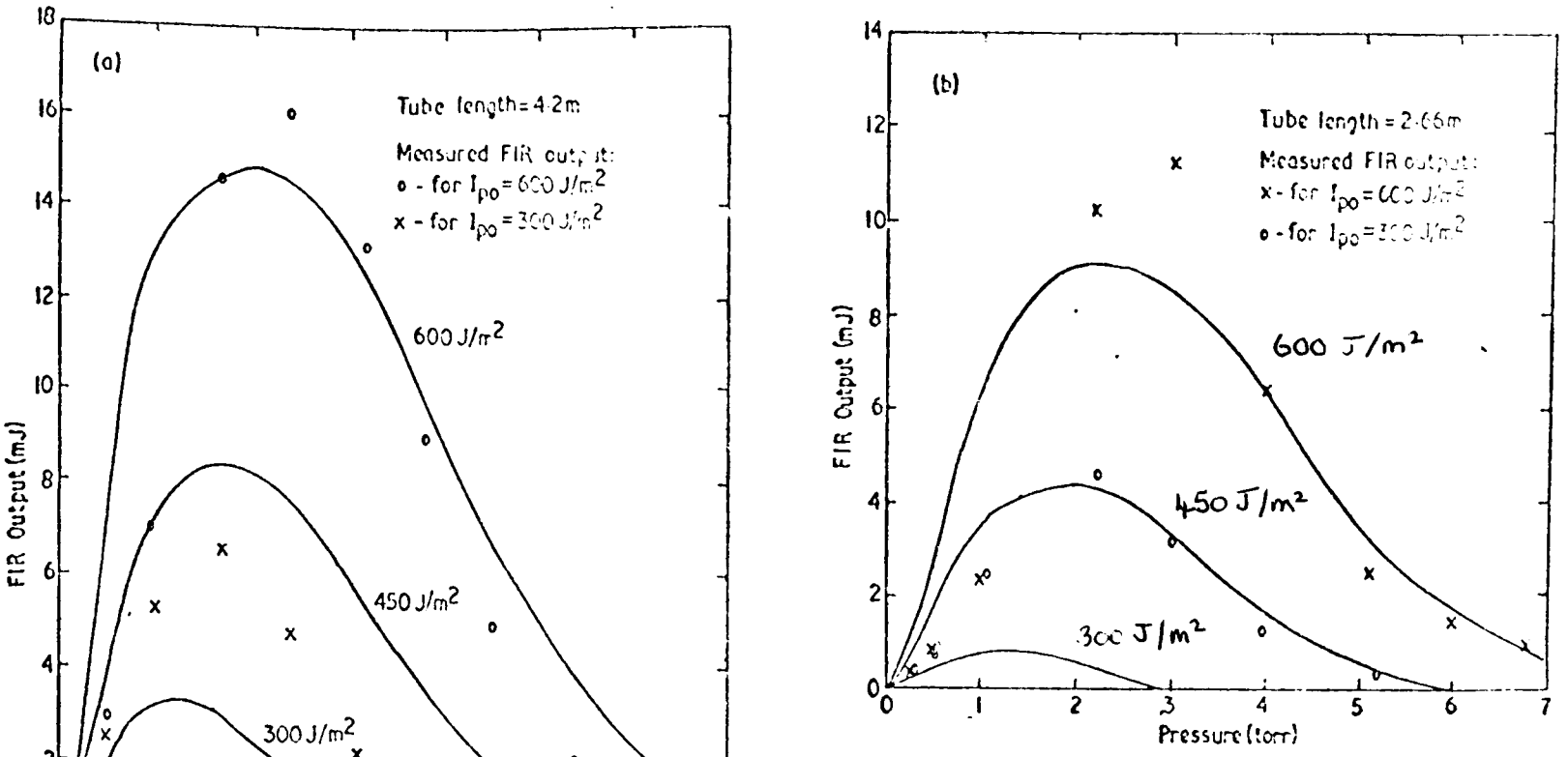


Fig.7.6

Experimental results for pump energy densities of 300 and 600 J/m^2, and computational results for pump energy densities of 600, 450 and 300 J/m^2: (a) for a 4.2 m tube and (b) for a 2.66 m tube.
[σ_p = 10^{-22} m^2, τ = 2 10^{-8} p^{-1} (torr) sec]

we compare measured data for $I_{po} = 600$ and $300\,J/m^2$ with curves computed for $I_{po} = 600$, 450 and $300\,J/m^2$ and tube lengths, $L = 4.2\,m$ and $2.66\,m$. The model predicts a more rapid decrease in output as the pump energy density is reduced than actually occurs, this effect becoming more exaggerated at shorter tube lengths.

Fig.7.7 summarizes the computational results obtained for the FIR output as a function of super-radiant tube length for a CH_3F pressure of 2 torr. (Curves are shown for $I_{po} = 300$, 450 and $600\,J/m^2$.) The curves are characterized by a region of exponential growth for $L < 2\,m$, corresponding to the region of small signal gain, whilst for $L > 4\,m$ the FIR output saturates, being particularly noticeable at $600\,J/m^2$.

To summarize, the computational model was found to fit reasonably well the observed dependence of FIR output on super-radiant tube length and CH_3F gas pressure. However, the model predicts a more rapid decrease in FIR output with falling pump energy density than is observed experimentally, and this is particularly noticeable at shorter tube lengths.

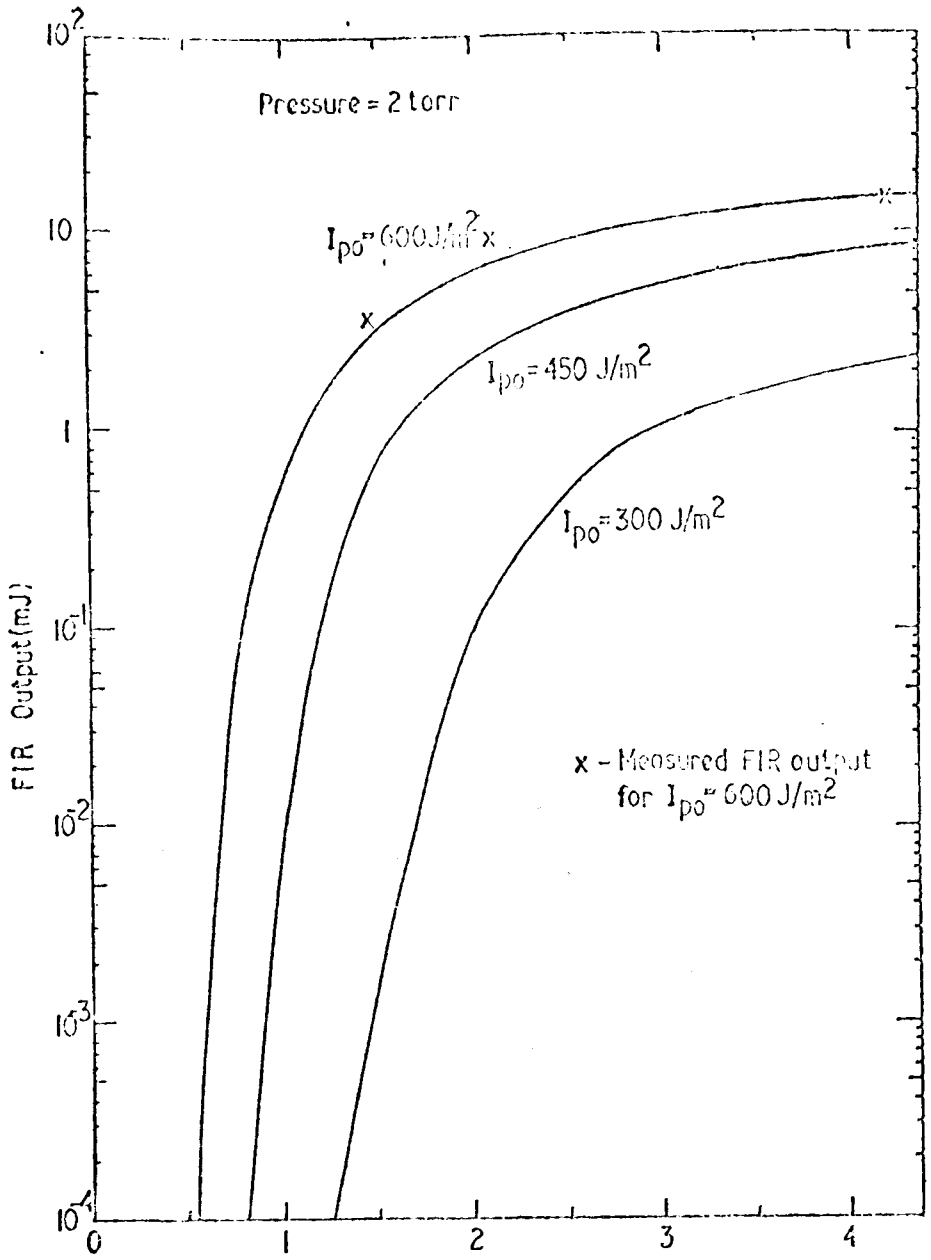


Fig.7.7

FIR output as a function of tube length (predicted by the computer model) for pump energy densities of 600, 450 and 300 J/m^2. Results are shown for a CH_3F pressure of 2 torr. [σ_p = 10^{-22} m^2, $\tau = 2 \times 10^{-9} p^{-1}$ (torr) sec].

It is clear from this preliminary study that σ_p, and probably τ, depend on pump intensity, and that by ignoring the K substructure of the rotational levels and the 452 μm emission, we introduce significant inaccuracies into the model. In retrospect, the 385 and 359 μm emissions of D_2O would have been better candidates for our model, since only one K level is involved in each of these transitions (see Appendix 'E'). However, until recently, the spectroscopy relevant to this laser was not known sufficiently well to allow calculations of its behaviour.

Despite these shortcomings, the agreement with experiment is remarkably good, considering the comparative simplicity of the rate equation model used here, which excludes the Raman scattering and a.c. Stark broadening predicted by the, more complex, quantum mechanical model.

CHAPTER VIII

CONCLUSIONS AND SUGGESTIONS FOR FUTURE WORK

In this final chapter we summarize the main conclusions drawn from the work discussed in this thesis, and compare the performance of the laser systems investigated here with the wavelength, power and bandwidth requirements for collective Thomson scattering calculated in Chapter I. Finally, we consider the design of a F I R laser configuration which is suitable for the measurement of T_i and the shape of the ion feature (e.g. for the determination of plasma impurity concentrations) for a typical tokamak plasma (i.e. with $T_e \sim 1\,\text{keV}$, $n_e \sim 5 \times 10^{13}\,\text{cm}^{-3}$).

8.1 SUMMARY OF THE MAIN CONCLUSIONS ARISING FROM THE PRESENT WORK

In Table 8.1 we compare the performance of the 496 μm CH_3F injection laser discussed in Chapter VI with the radiation source requirements derived in Chapter I.

TABLE 8.1

Comparison of the Parameters Required for Collective Thomson Scattering with those Obtained for the Injection Laser

	Requirement Calculated in Chapter I	Performance Obtained for the Injection Laser (see Chapter VI)
Wavelength	$30\,\mu\text{m} \leq \lambda \leq 1\,\text{mm}$	496 μm
Power	$\geqslant 1\,\text{MW}$	250 kW
Bandwidth	$\leqslant 60\,\text{MHz}$	$\leqslant 60\,\text{MHz}$

The success of the 496 μm CH_3F injection laser suggests that the injected super-radiance concept is a viable solution to the production of megawatt pulses of narrow-band F I R radiation. However, we conclude from this work that CH_3F is not the best available laser medium for an injection system. The performance of optically pumped D_2O, and in particular the 385 μm D_2O laser, suggests that it would be superior to the 496 μm

CH_3F laser in a collective Thomson scattering system. Our reasons for this conclusion are as follows:

(1) With the D_2O laser it is possible to generate three widely separated wavelengths, namely 66, 114 and 385 μm (see Chapter V), merely by pumping with the appropriate 9.6 μm band CO_2 laser lines, P(32), R(12) and R(22), respectively. This capacity for changing wavelength is particularly desirable in a scattering experiment because the scale length can be varied by more than a factor of five simply by altering the CO_2 pump wavelength.

(2) The photon conversion efficiency for the production of 385, 114 and 66 μm radiation in the D_2O laser is far superior to that for the 496 μm CH_3F laser (see Table 5.1).

(3) The envelope of the cyclotron emission from tokamak plasmas generally falls rapidly between wavelengths of about 500 and 300 μm. Thus the plasma emission at 385 μm might be 5 to 10 times less than at 496 μm. This is particularly significant since the sensitivity of F I R detectors (e.g. Schottky diodes) has been improved to the point where the minimum power requirement for collective Thomson scattering will be largely determined by the plasma emission (see section 1.3). It is therefore advantageous to use a 385 μm D_2O laser rather than a 496 μm CH_3F laser.

(4) In the 496 μm, CH_3F, super-radiant laser several K components can be excited simultaneously (CHANG, 1977). Since the F I R radiation from the narrow-band CH_3F oscillator can arise only for a transition with a single K value, it can only affect more than one K component if there is strong collisional transfer between adjacent energy levels in the K substructure (i.e. by operating at pressures > 2 torr). However, collisional losses become severe under those conditions, resulting in poor pump to F I R conversion efficiencies (see Chapter VI). In D_2O on the other hand, the K components are widely spaced (see Appendix 'E') so this problem does not arise.

To summarize, although the 496 μm CH_3F injection laser would appear to be capable of satisfying the requirements for collective Thomson scattering in Chapter I, our results for the D_2O laser suggest that D_2O would be a far superior medium for the injection system.

8.2 SUGGESTIONS FOR FUTURE WORK

In this final section we look at some possible improvements to the injection laser system described earlier.

8.2.1 An Improved FIR Oscillator Stage

The photon conversion efficiency of the 496 μm single mode CH_3F oscillator described in Chapter IV, was only 0.1%, in contrast to the super-radiant CH_3F laser which had an efficiency of 14% (see Chapter V). A major contributory factor to the low conversion efficiency of the single mode laser was the limitation on the mode volume of the near hemispherical cavity used in the present work. However, in an unstable cavity the fundamental transverse mode volume can be arranged to occupy the whole volume of the active medium and off-axis transverse modes can be rejected without the need for aperture stops. (The advantages of unstable resonators are discussed by SIEGMAN (1971a).) In this section we discuss the design of an improved FIR oscillator incorporating an unstable resonator, based on principles similar to those used by STAMATAKIS and SELDEN (1976), for a pulsed, discharge excited, single mode CO_2 laser. Some additional optical components have been added to their design to allow optical pumping of the laser medium whilst retaining efficient coupling of the FIR radiation.

Figure 8.1 shows the layout of the oscillator. Two unstable cavities are coupled by a small convex mirror M_1. Each resonator is designed with the cavity losses greater than the available gain, so that neither cavity can oscillate independently. The diffraction losses for the two cavities are matched so that the nett loss for a resonant mode is less than that of the independent modes for each cavity. If the separation between mirrors M_2 and M_3 is ΔL, the longitudinal modes for each cavity differ in frequency by $c/2\Delta L$. M_3 is mounted on a micrometer so that ΔL can be adjusted to make $c/2\Delta L$ equal to the gain-width of the three mirror cavity and a single longitudinal mode can be selected. For the 496 μm, CH_3F laser $\Delta L \approx 75$ cms since the gain width ≈ 200 MHz (see Chapter IV).

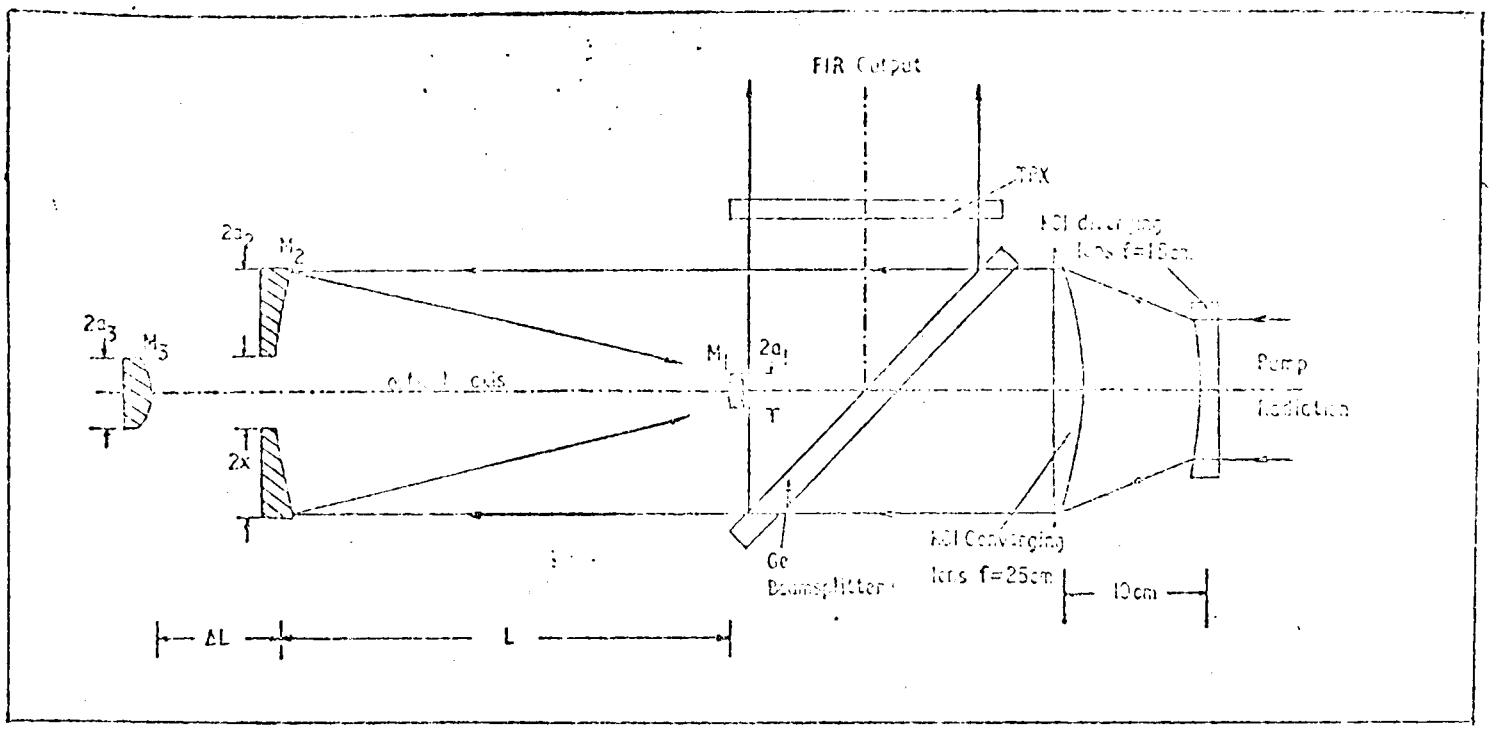


Fig.8.1
The proposed FIR, unstable cavity design

The CO_2 pump radiation passes through a beam expander so that it fills the large concave cavity mirror M_2, which then focuses the pump beam towards the small convex mirror, M_1. Prior to entering the FIR cavity the pump radiation passes through a germanium beam splitter, anti-reflection coated to allow over 95% of the pump radiation to be transmitted. The FIR output is diffraction coupled past M_1 and reflected at 90° to the CO_2 pump by the Ge beamsplitter. (If the beamsplitter is orientated parallel to the electric vector of the FIR output, the reflectivity should be >60%.)

For an unstable resonator with a magnification M the loss per pass, δ, is given by (SIEGMAN, 1971a)

$$\delta \approx \frac{M^2 - 1}{M^2} \qquad \ldots (8.1)$$

In order to maximise the diffraction output coupling at M_1 whilst retaining practical dimensions for the diameters of M_2 and M_1 we have chosen $M_{12} = 10$ (M_{12} being the magnification for the cavity M_2, M_1), so that over 90% of the FIR radiation is coupled out of the cavity for each pass. The diameter of M_2 is constrained by the size of the Ge beamsplitter which is required to intercept the FIR radiation reflected from M_2. A practical diameter for the Ge beamsplitter is about 15 cm, so that the required diameter of M_2 ($2a_2$) is about 11 cm. The diameter of M_1 ($2a_1$) is then given

by the requirement $a_1 = a_2/M_{12} = 1.1$ cm.

The nett round trip gain in a cavity of length L is $(1-\delta)e^{2\alpha_0 L}$, where α_0 is the small signal gain. To just suppress self oscillation in the laser cavity we require:

$$(1-\delta)e^{2\alpha_0 L} \leq 1 \ . \qquad \ldots (8.2)$$

ANAN'EV and SHERSTOBITOV (1974) have investigated the losses in an unstable resonator with a central hole coupling aperture. They define a quantity $|\gamma|$ which determines the diffraction loss δ, where:

$$\delta = 1 - |\gamma|^2 \ , \qquad \ldots (8.3)$$

and they derive the dependence of $\ell n|\gamma|$ on the geometry of the unstable resonator. According to LITTLE et al (1976), who have investigated the performance of a CO_2 laser with a telescopic amplifier, $\ell n|\gamma|$ is given by

$$\ell n|\gamma| = \frac{\ell n(M)\ \ell n\left\{\dfrac{\lambda LM}{\pi a_1^2 (M^2-1)\ (M-1)}\right\}}{\ell n\left(\dfrac{4a_1^2}{x^2} M\right)} \qquad \ldots (8.4)$$

for a confocal resonator. Where λ is the wavelength of the FIR radiation and x is the radius of the central coupling hole. Substituting (8.3) into (8.2) we have the condition $\ell n|\gamma| = \alpha_0 L$ for self oscillation. SEMET, OBENSCHAIN and LUHMANN Jr. (1976) have measured α_0 as a function of pressure for the 496 μm CH_3F laser. At 1 torr they found the small signal gain to be 30 dB/m† which implies a value of -6.9 for $\ell n|\gamma|$ when L = 1 metre. Because of this high gain it is necessary either to use a short cavity or lossy mirrors to prevent self oscillation. In the present treatment we will calculate the design specifications of a short, L = 1 metre cavity, however it has been suggested (STAMATAKIS, 1977) that by making M_1 of poor reflectivity material, the losses of both cavities could be kept equal whilst suppressing self oscillation.

---

† A small signal gain of 27 - 30 dB/m was also obtained as a result of indirect measurements by CHANG and BRIDGES (1970) and BROWN et at (1973).

From telescope theory the constraints $M_{12} = 10$, $L = 100$ cms infer a radius of curvature for M_1 (r_1) of 222 cm[†] and for M_2 (r_2) of -22 cm. Substituting for M, L, a_1, λ and $\ell n|\gamma|$ in equation (8.4) gives $x = 2.1$ cm. The radius of curvature of M_3 (r_3) is determined by the need to match the losses of the cavity M_1, M_2 with those of the cavity M_1, M_3. Substituting equation (8.1) in (8.2) we have the condition $e^{\alpha_0 L} \leq M$ and since $e^{\alpha_0 L} = 10^3$ the magnification of the cavity M_1, M_3 (M_{13}) must be 10^3 to match the losses of this cavity with those of the cavity M_1, M_2. The asymmetric round-trip magnification for an unstable resonator is given by (SIEGMAN, 1971a):

$$M_{13} = 2g_1g_3 + 2\sqrt{g_1g_3(g_1g_3 - 1)} - 1 \qquad \ldots (8.5)$$

where g_1 and g_2 are defined as:

$$g_1 = 1 - \frac{(L + \Delta L)}{r_1}$$

$$g_3 = 1 - \frac{(L + \Delta L)}{r_3}$$

and on substituting for L, ΔL, r_1 and M_{13} into equation (8.5) we obtain $r_3 = -10$ cms. In order to fill mirror M_2 with the 6 cm diameter CO_2 pump beam from the system A CO_2 laser (see Chapter III), the KCl beam expander in Fig.8.1 would be constructed from a 15 cm focal length concave lens positioned 10 cm from a 25 cm focal length convex lens. We summarize the geometrical parameters for the unstable F I R oscillator in Table 8.2.

TABLE 8.2

Summary of the Geometrical Parameters for the F I R Unstable Oscillator

$a_1 = 0.55$ cm	$\Delta L = 75$ cm
$a_2 = 5.5$ cm	$x = 2.1$ cm
$a_3 \approx 3$ cm	$L = 100$ cm
$r_1 = 222$ cm	$M_{12} = 10$
$r_2 = -22$ cm	$M_{13} = 10^3$
$r_3 = -10$ cm	

[†] The radius of curvature of each mirror is considered positive if the mirror is concave inward towards the resonator.

8.2.2 *A Two Stage F I R Injection Laser System*

It is clear from Table 8.1 that at least a four-fold improvement in F I R output power is required. In this final section we consider a two stage injection system which should easily satisfy this power requirement.

The proposed two stage F I R injection laser is shown schematically in Fig.8.2. The system shown in the figure includes a stable hemispherical oscillator similar to that discussed in Chapter IV, or, if the unstable resonator proposed in the previous section were shown to be more efficient this could be used instead.

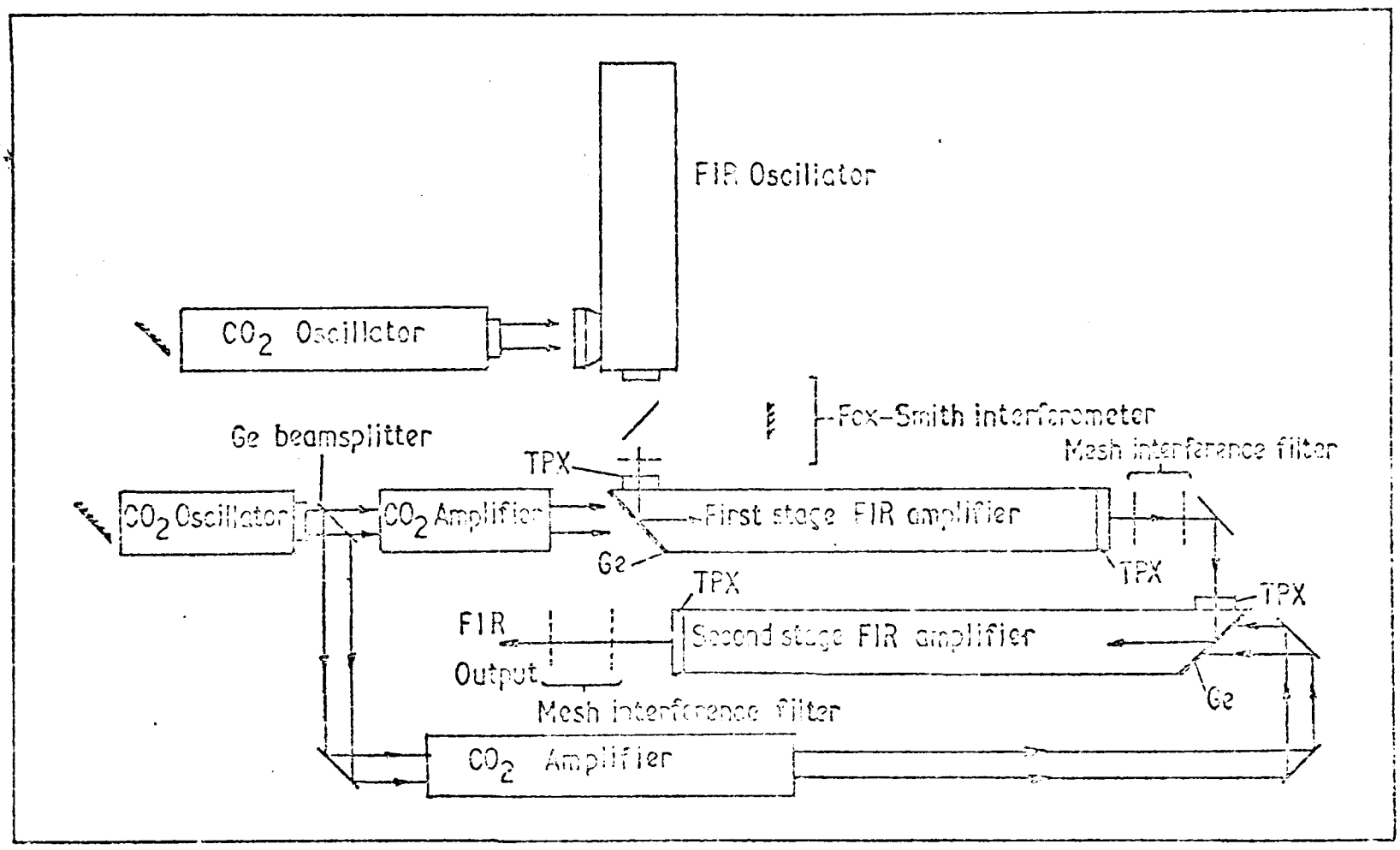


Fig.8.2
Schematic diagram of the proposed two stage F I R injection laser

In the proposed system CO_2 laser B (see Chapter III) would be modified so that the 1.5 metre CO_2 oscillator output is directed, via an uncoated Ge beamsplitter, so that 40% of the oscillator output enters a 1.5 m CO_2 amplifier and 60% enters a 3 m CO_2 amplifier. The 1.5 m CO_2 amplifier would then be used to optically excite the first stage F I R injection amplifier. This F I R amplifier would be constructed in a similar fashion to the super-radiant stage described in Chapter VI, the Ge entrance window for the

CO_2 pump being oriented at 45° to the super-radiant tube axis and anti-reflection coated on both faces for the CO_2 laser wavelength. The CO_2 pump energy entering the first stage F I R amplifier would be about 25 to 30 Joules, so that from the CH_3F injection laser experiments discussed in Chapter VI, we would expect about 200 kW of 60 MHz bandwidth, 496 μm radiation to be transmitted through the T P X exit window of the first F I R amplifier stage. The F I R output could then be filtered by a mesh Fabry-Perot interferometer with a free spectral range of 500 MHz and a pass-band of about 35 MHz (i.e. a finesse of about 14). This should remove broad-band super-radiance from the F I R output.† Thus we might expect approximately 100 kW of 496 μm radiation within a bandwidth of 40 MHz, to be injected into the second stage F I R amplifier, which would be similar in construction to the first stage. The 3 m CO_2 amplifier should produce about 60 J of CO_2 pump radiation so that, from our measurements on high power CH_3F super-radiant lasers (see Chapter V), we expect about 2 MW of narrow-band 496 μm radiation to be generated in the second F I R amplifier. If necessary broad-band super-radiance generated in the final amplifier could be removed by another 40 MHz pass-band interference filter; this might reduce the F I R output power to between 1 and 1.5 MW within a bandwidth of 40 MHz.

Notice that although our proposed design has been expressed in terms of a 496 μm CH_3F system we would stress that D_2O appears to be a superior laser medium, as discussed in section 8.1. In particular, from our measurements on the 385 μm super-radiant D_2O laser (see Chapter V) we could expect 3 to 4 MW of narrow-band 385 μm radiation from such a two-stage injection system, which is more than sufficient to satisfy the laser requirements in Table 8.1.

---

† Such an interference filter would have a rejection ratio (i.e. the ratio of the peak to trough heights of the Airy distribution) of $1 + (4F^2)/\pi^2$, where F is the finesse. For F = 14 this gives a rejection ratio of about 80:1, but if a higher rejection ratio were required, two or more interference filters could be used in series.

APPENDIX 'A'

CALCULATION OF THE TRANSVERSE MODE SPACING FOR A HEMISPHERICAL LASER CAVITY

The resonance frequency of the q^{th} axial mode in the mn^{th} transverse mode pattern for a cavity mirror separation L is given by (SIEGMAN, 1971b)

$$f_{qmn} = \left\{ \frac{q + (m+n+1)\cos^{-1}(g_1 g_2)^{\frac{1}{2}}}{\pi} \right\} \frac{c}{2L} \qquad \ldots (A.1)$$

where c is the velocity of electromagnetic radiation in vacuo, and g_1 and g_2 are the cavity mirror parameters which are defined by

$$g_1 = 1 - \frac{L}{R_1}$$

$$g_2 = 1 - \frac{L}{R_2}$$

R_1 and R_2 are the radii of curvature of the cavity mirrors. For a near hemispherical cavity $R_1 \approx L$ and $R_2 = \infty$, thus $g_1 \to 0$ and $g_2 \to 1$. Substituting these conditions in equation (A.1) gives

$$\cos^{-1}(g_1 g_2)^{\frac{1}{2}} \to \frac{\pi}{2} .$$

Therefore

$$f_{qmn} = q\Delta f_{long} + (m+n+1)\ \Delta f_{trans}$$

where $\Delta f_{long} = c/2L$, is the longitudinal mode spacing, and $\Delta f_{trans} = \frac{c}{4L}$, is the transverse mode spacing. Therefore, for the laser cavity described in Chapter IV, where $L = 243$ cms, $\Delta f_{long} = 61$ MHz and $\Delta f_{trans} = 30.5$ MHz.

APPENDIX 'B'

POSSIBLE MECHANISMS FOR THE PRESSURE DEPENDENT FREQUENCY SHIFT IN THE 496 μm, CH_3F, LASER

We have only an incomplete picture of the mechanisms leading to the pressure dependent frequency shift in the FIR emission line of the 496 μm CH_3F laser, but for completeness we summarize our thoughts on this problem in the present appendix.

The experimental observations we must seek to explain are:

(1) In the 496 μm CH_3F super-radiant laser the FIR frequency shifted by 200 MHz towards longer wavelengths, when the CH_3F pressure was increased from 0.5 to 2.0 torr (see section 5.2) and remained constant above this pressure.

(2) In the 385 μm D_2O super-radiant laser, no frequency shift was observed (within the experimental limits of our measurements, i.e. $\lesssim$ 50 MHz), when the D_2O pressure was increased from 0.5 to 8.0 torr (see section 5.3).

The shift of the 496 μm line towards longer wavelengths with increasing pressure might be explained by a change in the K component of the ν_3 $J = 12 \rightarrow 11$, FIR transition, as illustrated schematically in Fig.B.1. 9.55 μm CO_2 pump radiation excites the CH_3F to ν_3, $J = 12$ levels with low K values (e.g. $K \leqslant 3$). Due to collisional broadening each K level has a width $\Delta\nu_{coll}$ and energy can therefore be transferred to higher K levels when adjacent levels 'overlap' each other (as shown in Fig.B.1). This would result in the observed shift towards longer wavelengths (see Fig. E.2(b)). It would also explain the absence of a frequency shift in D_2O, since the K levels are too widely spaced in this molecule (WILLIAMSON, 1969 and LIN and SHAW, 1976) to allow the above effect to take place. However, the dipole matrix element for a $J \rightarrow J-1$ $K \rightarrow K$ transition in a symmetric top molecule is given by:

$$|\mu_{ij}|^2 = \mu^2 \frac{J^2 - K^2}{J(2J+1)} ,$$

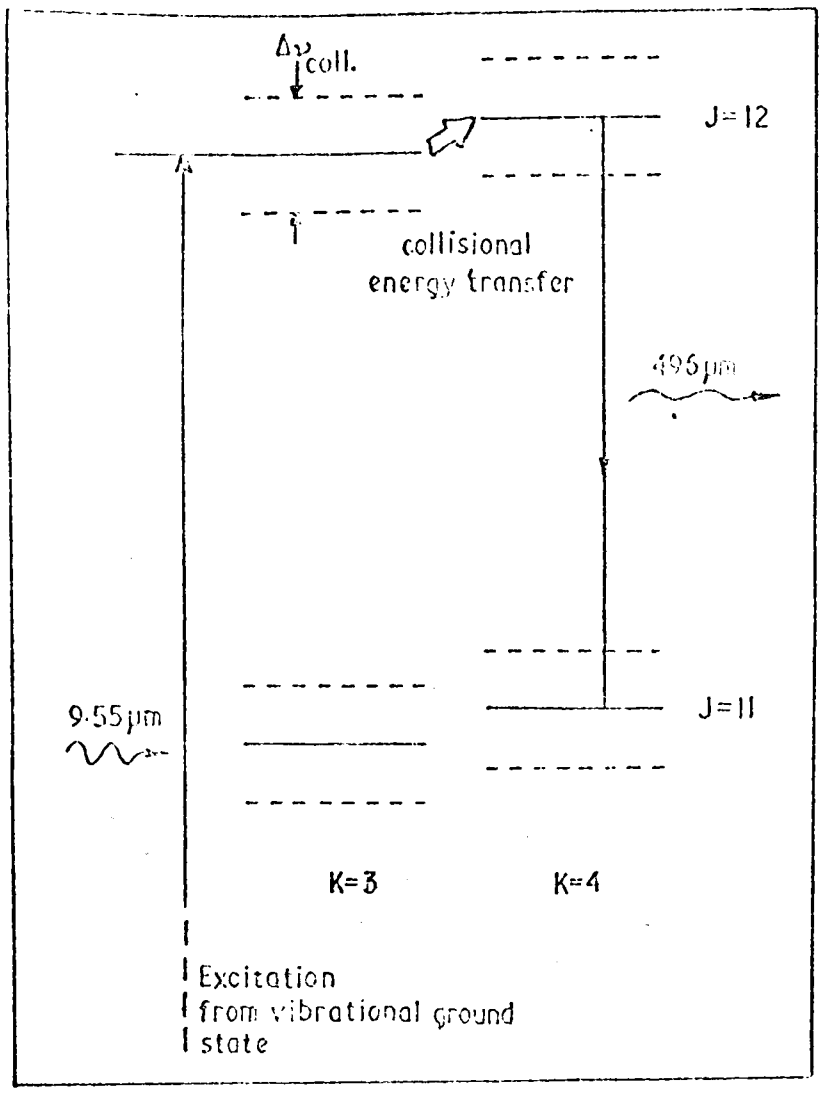


Fig.B.1
Partial energy level diagram of the CH_3F, ν_3 state to illustrate the K level shift discussed in the text

where μ is the permanent dipole moment (TOWNES and SCHAWLOW, 1955). We would therefore, expect laser action on transitions with high values of K to be weaker than transitions with low values of K, in disagreement with the requirements for our model.

Another interpretation of the frequency shift, which seems more plausible, is that it is brought about by a change from a predominantly two photon, Raman scattering, process at high pressures (i.e. $\geqslant 1.0$ torr) to a single photon absorption process at low pressures ($\leqslant 1.0$ torr). Our reasons for supporting this explanation are as follows: Because of the three-fold symmetry of CH_3F with three identical atoms of spin $\frac{1}{2}$, the components with K = 3, 6, 9 and 12 have twice the statistical weight of all other K components (TOWNES and SCHAWLOW, 1955). Thus, the K = 3 component, which is the closest of these favoured states to the CO_2 pump line centre (see Fig.E.2(b)), might be expected to result in a significant two photon gain at sufficiently high pressures (PANOCK and TEMKIN, 1977). Since the K = 3 component is about 200 MHz away from the CO_2 pump line centre, this frequency switching effect would result in a 200 MHz frequency shift at high pressures.

This explanation could be criticised on the grounds that it does not explain the absence of a frequency shift in the 385 μm, D_2O laser. However, TEMKIN (1977) has recently published results which show a pressure dependent

frequency shift of 390 MHz in the D_2O, 385 μm laser (corresponding to the difference between the CO_2 pump line centre and the D_2O absorption frequency) at D_2O pressures ~0.5 torr (i.e. below the pressure range investigated in the present work). In addition, WIGGINS et al (1977) have found no frequency shift in the 447 μm CH_3I laser, which has only one K level and is pumped at the centre frequency of the CH_3I absorption.

APPENDIX 'C'

THE METAL MESH FABRY-PEROT INTERFEROMETER

The Fabry-Perot interferometer used in the present work was a standard optical interferometer, which was converted to F I R operation by replacing the etalon mirrors with copper or nickel electroformed mesh reflectors. This mesh can be obtained with several different grid spacings and its transmission and reflection properties have been studied by both RENK and GENZEL (1962) and ULRICH (1967). The interferometer used here was scanned manually from one laser shot to the next, the transmitted F I R intensity being measured with a Golay Cell detector, as shown in Fig.C.1.†

Three factors effect the measured finesse of a Fabry-Perot etalon (JACQUINOT, 1960):

(a) The plate reflectivity.
(b) Surface imperfections.
(c) Divergence of the incident radiation.

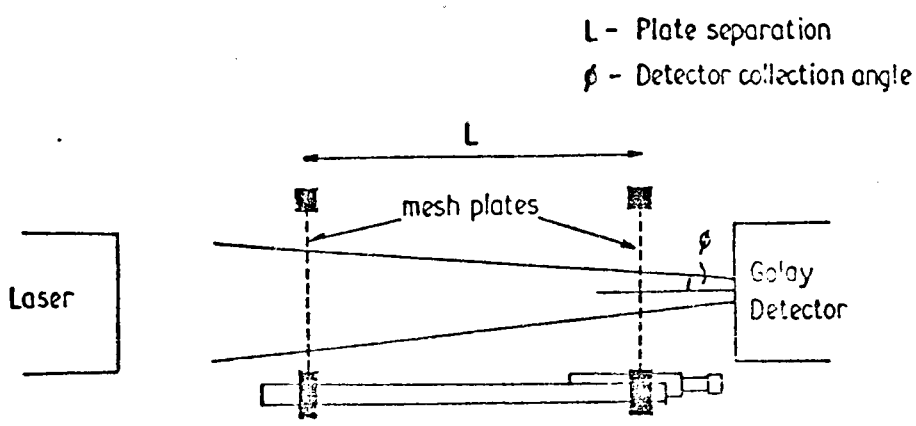


Fig.C.1 Layout of the Fabry-Perot Etalon

For the Fabry-Perot etalon used here, the mesh plates were about 5 cms in diameter and they were aligned with a He Ne laser to be parallel to within about 10 μm over the effective area of the plates. The experimental finesse was obtained for a plate separation of 10 mm, which corresponds to a free spectral range of about 15 GHz. Since the CH_3F laser line has a maximum width of a few hundred MHz (see section 4.2), it was possible to obtain the etalon finesse under these conditions. The measured finesse was close to that which would be expected if

---

† It is important to note that we do not use a lens to focus the F I R radiation on to the Golay cell, so that the Golay detector is effectively receiving radiation from only a small area of the Fabry-Perot plate. In order to use this method it is necessary that the divergence of the radiation source is sufficiently small not to effect the measured finesse.

only the plate reflectivity was important. For example, for 250 line/inch plates and a radiation wavelength of 496 μm, the measured finesse was about 14. The reflectivity finesse = $\pi\sqrt{R}/(1-R)$, where R is the plate reflectivity, thus, since the transmission of one of the plates had been measured to be 20%, we would expect a reflection finesse of about 14. in agreement with the measured value. We can, therefore, neglect divergence and surface imperfection effects. Finally, since the laser beam divergence is negligible the finesse is independent of the plate separation.

APPENDIX 'D'

POSSIBLE PROCESS FOR THE ABSORPTION OF OFF-RESONANT P(20) CO_2 PUMP RADIATION IN CH_3F

Calculated frequencies* for the hot band, $\nu_3 \rightarrow 2\nu_3$, absorption in CH_3F give a value of 3.13845×10^{13} Hz for the $\nu_3 \rightarrow 2\nu_3$, $J = 8 \rightarrow 9$ absorption, which is within 2.7 GHz of the P(20) CO_2 laser line centre at 3.13818×10^{13} Hz. SMITH and MILLS (1963) have measured the frequencies of several P and R branch absorptions† in the $\nu_3 \rightarrow 2\nu_3$ band and some of their results are tabulated in Table D.1. The error on the experimental values is less than ± 0.6 GHz and thus the disagreement with the calculated frequencies would seem to be real and not due to systematic error.

TABLE D.1

Line Frequencies of the $^{12}CH_3F$ ($\nu_3 \rightarrow 2\nu_3$) Hot Band Absorption — R Branch Transitions. (After SMITH and MILLS, 1963)

J	Observed Frequency (Hz)	Calculated (Hz)	$-\Delta$ (Hz)
7		3.13405×10^{13}	
8	(3.13812×10^{13})	3.13845×10^{13}	(3.3×10^{9})
9		3.14283×10^{13}	
10	3.14688×10^{13}	3.14715×10^{13}	2.7×10^{9}
11	3.15116×10^{13}	3.15140×10^{13}	2.4×10^{9}
12	3.15536×10^{13}	3.15554×10^{13}	1.8×10^{9}
13	3.15944×10^{13}	3.15965×10^{13}	2.1×10^{9}
14		3.16265×10^{13}	
15		3.16768×10^{13}	
16	3.17149×10^{13}	3.17161×10^{13}	1.2×10^{9}
17	3.17533×10^{13}	3.17542×10^{13}	0.9×10^{9}

The numbers shown in brackets in the 'observed frequency' column and the column for Δ (the difference frequency between the observed and calculated values) are derived values obtained by extrapolating the systematic

---

* Using constants given by FREUND et al (1974)

† But not the $J = 8 \rightarrow 9$ transition, since this is obscured by the stronger $0 \rightarrow \nu_3$ $J = 12 \rightarrow 12$, fundamental, absorption.

disagreement between the observed and calculated frequencies. This extrapolation gives 3.13812×10^{13} Hz for the $\nu_3 \rightarrow 2\nu_3$, $J = 8 \rightarrow 9$ absorption frequency, which is only 600 MHz away from the centre of the P(20) CO_2 pump line.

The matrix element for the $0 \rightarrow \nu_3$, $J = 12 \rightarrow 12$ absorption is given by (TOWNES and SCHAWLOW, 1955):

$$|\mu_{ij}|^2 = \frac{\mu^2 K^2}{J(J+1)}$$

where μ is the molecular dipole moment. So that for the $K = 1$ component $|\mu_{ij}|^2 \approx 0.006\,\mu^2$. The dipole matrix element for the $\nu_3 \rightarrow 2\nu_3$, $J = 8 \rightarrow 9$ absorption is given by

$$|\mu_{ij}|^2 = \mu^2 \left\{ \frac{(J+1)^2 - K^2}{(J+1)(2J+1)} \right\} .$$

For the $K = 1$ component we therefore have $|\mu_{ij}|^2 \simeq 0.52\,\mu^2$. Therefore the ratio of the probabilities for inducing absorption is $\sim$ 90:1 in favour of the $J = 8 \rightarrow 9$, $\nu_3 \rightarrow 2\nu_3$ transition. So despite the large disparity between the thermal populations of the ν_3, $J = 8$ and $\nu = 0$, $J = 12$ states (i.e. $\sim$ 50:1), we might expect the $\nu_3 \rightarrow 2\nu_3$, $J = 8 \rightarrow 9$ transition to be a significant process for the absorption of 9.55 μm, P(20) CO_2 pump radiation. We must, of course, postulate rapid refilling of the $J = 8$, ν_3 state, but collision rates between the $J = 11$ and $J = 8$ levels of the ν_3 manifold are sufficiently rapid (the rotational-rotational relaxation time for the CH_3F molecule is $\sim$ 10 ns at 1 torr (CHANG, WANG and CHEO, 1969)) to allow collisional refilling of the ν_3, $J = 8$ level, as shown in Fig.D.1.

If hot band absorption is a major contributory factor to the absorption of CO_2 radiation, then this could be an important loss mechanism limiting the efficiency of the CH_3F laser.

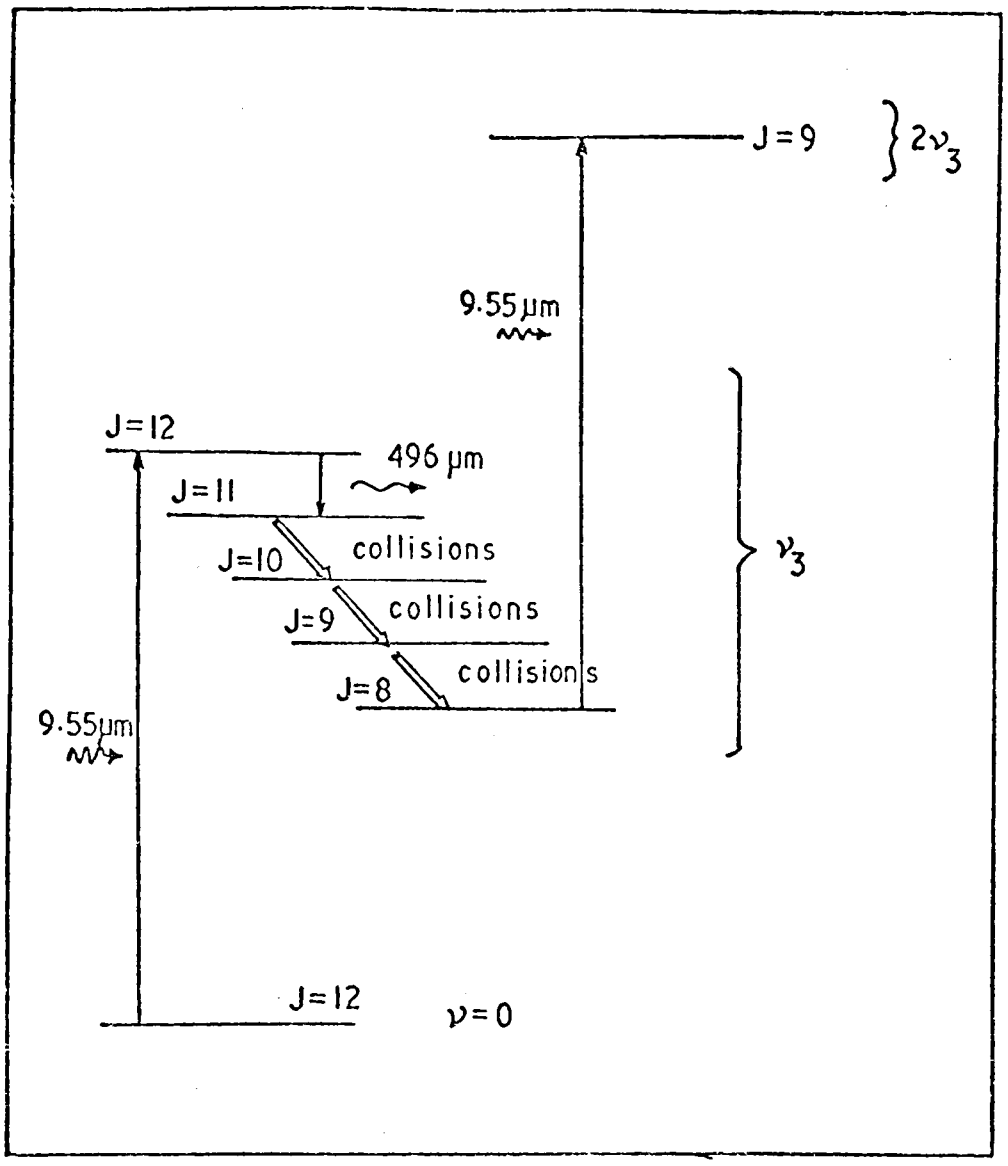


Fig.D.1
Schematic diagram of the energy levels of CH_3F involved in the absorption of off resonant CO_2 pump radiation by the 'hot band' $\nu_3 \rightarrow 2\nu_3$, $J = 8 \rightarrow 9$ transition

APPENDIX 'E'

THE SPECTROSCOPY OF THE OPTICALLY PUMPED D_2O AND CH_3F F I R LASERS

Molecular spectroscopy is a complex and involved subject and several excellent standard works have been written in this field (TOWNES and SCHAWLOW 1955 and HERTZBERG, 1945). We shall, therefore, confine the present discussion to those aspects of molecular spectroscopy which affect the operation of the methyl fluoride (CH_3F) and heavy water vapour (D_2O) F I R lasers, whose study is described in this dissertation. Both these molecules possess excited vibrational states which can be populated by the absorption of radiation at near infrared wavelengths ($\sim$10 μm) that can be readily generated by pulsed CO_2 lasers. This population inversion is the precursor for F I R laser action on rotational transitions in the excited vibrational state. This process therefore effectively transforms the near infrared radiation to F I R photons.

The energy of the various rotational quantum states of a molecule is determined by its three principal moments of inertia, namely I_A, I_B and I_C. For the D_2O molecule these three moments of inertia are different and the molecule is said to be an asymmetric top. No simple closed expression can be written for the molecular energy levels which arise from these rotational states in this case. However, for a symmetric top molecule, such as CH_3F, two of these moments of inertia are equal and the expression for the molecular energy levels can be written in a closed form. We shall, therefore, consider this more straightforward, symmetric case, first.

E.1 THE SPECTROSCOPY OF THE CH_3F F I R LASER

For a symmetric molecule, such as CH_3F, the spectroscopic notation used is of the form J_K, where J is the rotational quantum number and can take the values 0, 1, 2 ... and K, which is the projection of J on the symmetry axis of the molecule, can take the (2J + 1) values, 0, ±1, ±2, ... ±J.

As a result of the molecular symmetry, states which differ only in the sign of K have the same energy and thus there are only J + 1 levels in the K substructure for the J^{th} rotational energy level.

For a symmetric top the expression for the rotational energy levels can be written in the form:

$$E(J,K) = BJ(J+1) + (A-B)K^2 - D_J J^2 (J+1)^2 - D_{JK} J(J+1)K^2 - D_K K^4 \quad \ldots (E.1)$$

where

$$A = \frac{h}{8\pi^2 c I_A} \quad \text{and} \quad B = \frac{h}{8\pi^2 c I_B} \ ,$$

and c and h are the velocity of light and Planck's constant, respectively. The coefficients D_J, D_{JK} and D_K are very small and take account of the centrifugal distortion arising from the non-rigid nature of the molecule. The K levels for a given J state are therefore very nearly degenerate and equation (E.1) can normally be simplified to:

$$E(J) = BJ(J+1) - D_J J^2 (J+1)^2 \quad \ldots (E.2)$$

The molecular geometry of CH_3F is illustrated in Fig.E.1. The CO_2 laser, tuned to the 9.55 μm, P(20), line is in close coincidence with the J = 12 → 12 lowest order stretching mode of the carbon-fluorine bond (ν_3 mode) (SMITH and MILLS, 1963). (FREUND et al (1974) give the constants required for the calculation of the energy levels in the ground vibrational state, and the ν_3 and $2\nu_3$ vibrational states of $^{12}CH_3F$.) The motion of the atoms for this ν_3 vibrational mode is illustrated

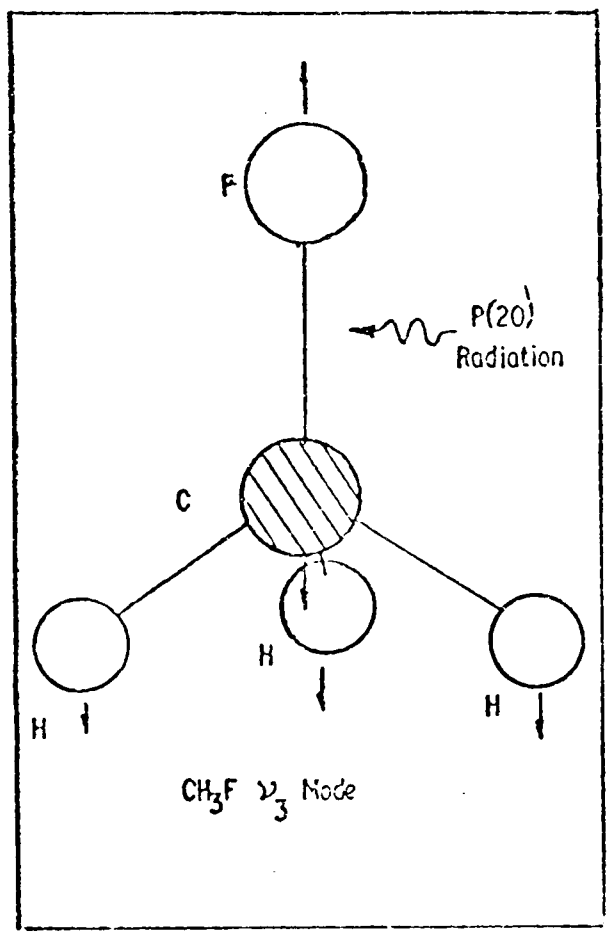
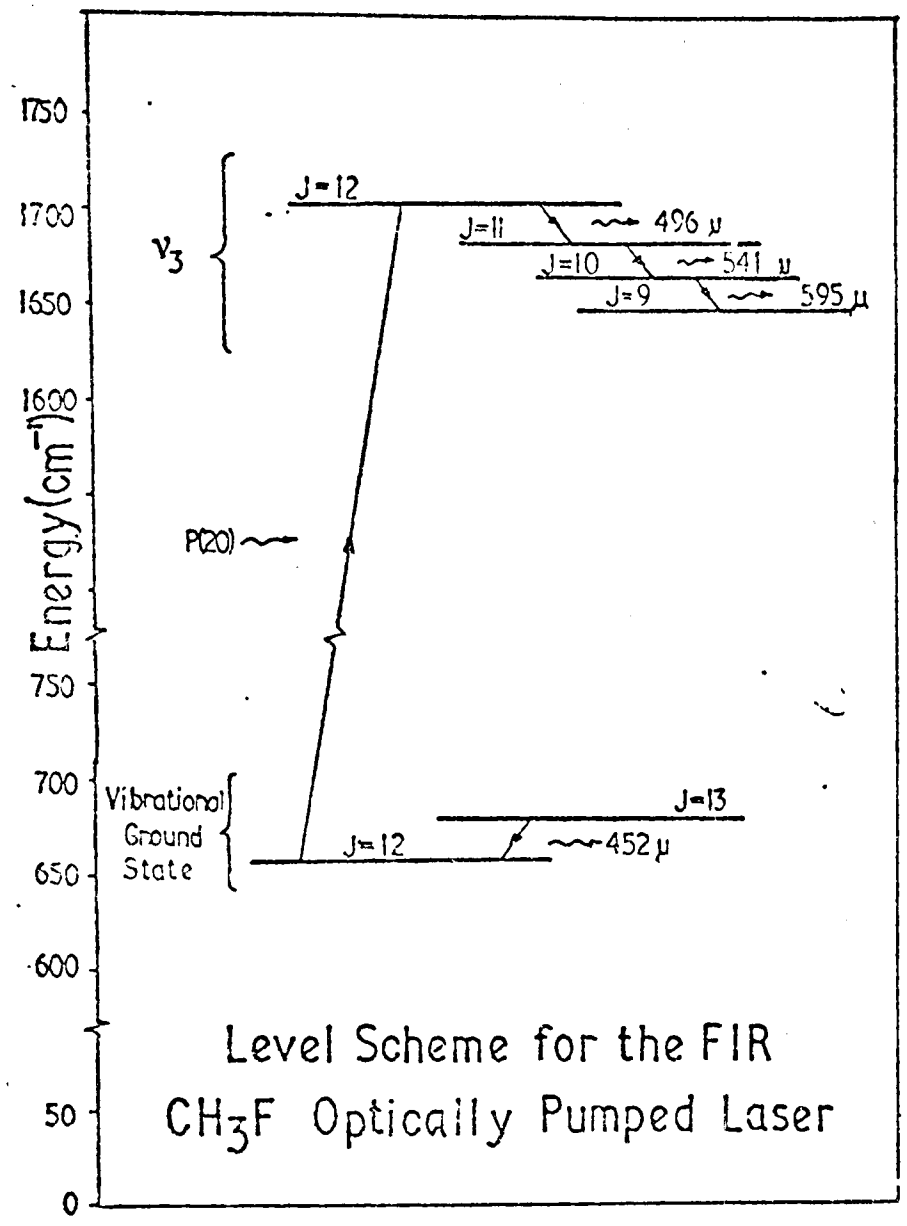


Fig.E.1
Schematic diagram of the CH_3F molecule, the direction of motion of its constituent atoms in the ν_3 stretching mode is illustrated by the arrows



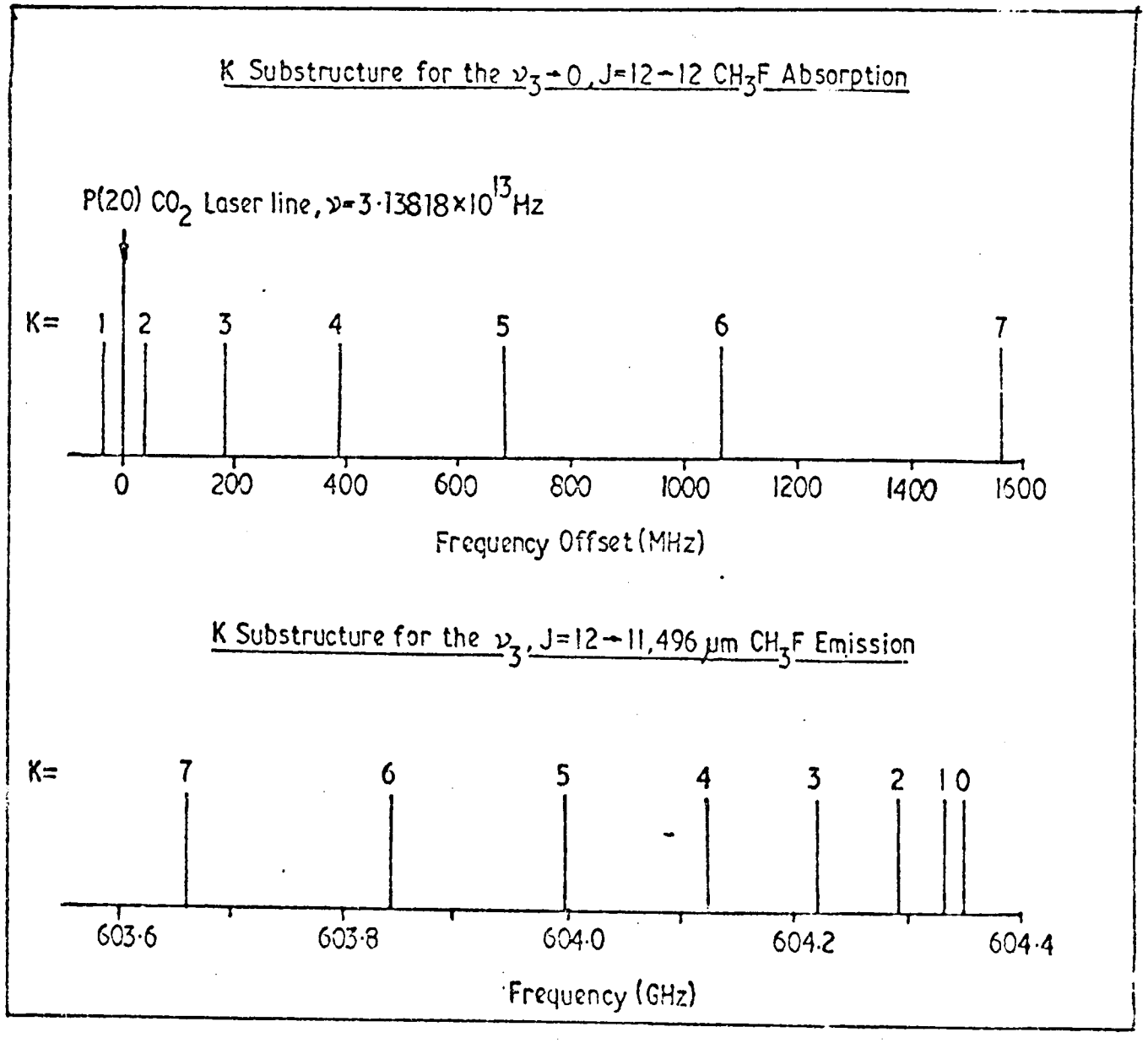


Fig.E.2

(a) Level scheme for the CH_3F laser; (b) K substructure for the P(20)CO_2 line absorption and the $J = 12 \rightarrow 11$, 496 μm emission in CH_3F

in Fig.E.1. This vibrational excitation results in a rapid depopulation of the J = 12 level of the ground vibrational state (Fig.E.2(a)) and a correspondingly rapid inversion between the J = 12 and 11 levels of the ν_3 manifold. If the CH_3F gas is kept at a low pressure (~ torr), the collisional relaxation between adjacent levels is sufficiently slow to allow radiative emission, both in a cascade from several J levels in the ν_3 state and on the J = 13 to 12 transition in the ground vibrational state (as illustrated in Fig.E.2(a)). Fig.E.2(b) illustrates the position of the CO_2 P(20) laser line relative to the K substructure for the $0 \rightarrow \nu_3$, J = 12 → 12 absorption. The K substructure for the J = 12 → 11, 496 μm emission line is also illustrated.

E.2 THE SPECTROSCOPY OF THE D_2O F I R LASER

A schematic diagram of the D_2O molecule is shown in Fig.E.3, unlike CH_3F it has no unique axis of symmetry and therefore no two principal moments of inertia are equal. This complicates considerably the determination of the molecular energy levels and a closed expression similar to equation (E.1) can no longer be used. One consequence of this asymmetry is that the K levels greater than zero lose their double degeneracy. We therefore define two pseudo quantum numbers, K_{-1} and K_1 to replace K, where K_{-1} and K_1 are the limiting values of K for a prolate and oblate symmetric top, respectively. The energy levels are then calculated with the use of an expression of the form

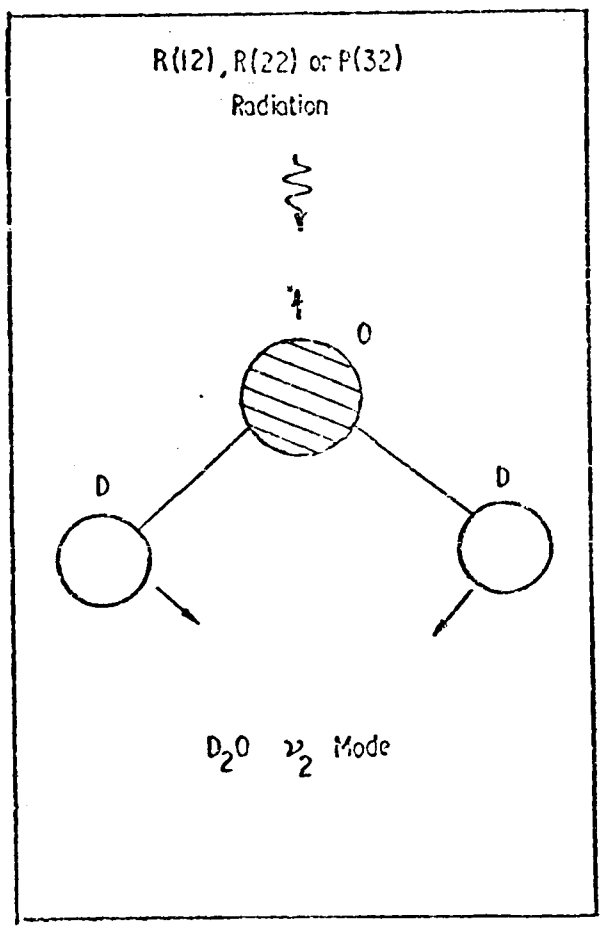


Fig.E.3
Schematic diagram of the D_2O molecule, the direction of motion of its constituent atoms in the ν_2 bending mode is illustrated by the arrows

$$E(J,K_{-1},K_1) = \tfrac{1}{2}(A+C)J(J+1) + \tfrac{1}{2}(A-C)E_{K_{-1}K_1} \quad \ldots (E.3)$$

where

$$C = \frac{h}{8\pi^2 c I_c} \quad .$$

$E_{K_{-1}K_1}$ is a complicated dimensionless function of the asymmetry parameter, κ, given by

$$\kappa = \frac{(2B - A - C)}{(A - C)} \quad \ldots (E.4)$$

The limiting values of κ, namely $\kappa = -1$ and $\kappa = 1$, correspond to a prolate and oblate symmetric top, respectively, whilst $\kappa = 0$ is sometimes called the most symmetric case.

The molecular energy levels involved in the D_2O FIR laser have been tabulated by WILLIAMSON (1969) and more recently by LIN and SHAW (1976). In the present work three different CO_2 laser lines in the 9.6 μm band, namely R(12), R(22) and P(32), have been used to produce excitation of the ν_2 bending mode (which is illustrated schematically by arrows in Fig.E.3). Unlike the CH_3F laser, the D_2O FIR laser lines all arise from rotational transitions generally involving only one K component, since in D_2O the K levels are generally widely spaced in energy. Fig.E.4 shows all the levels involved in the D_2O FIR lasers discussed in the present work,

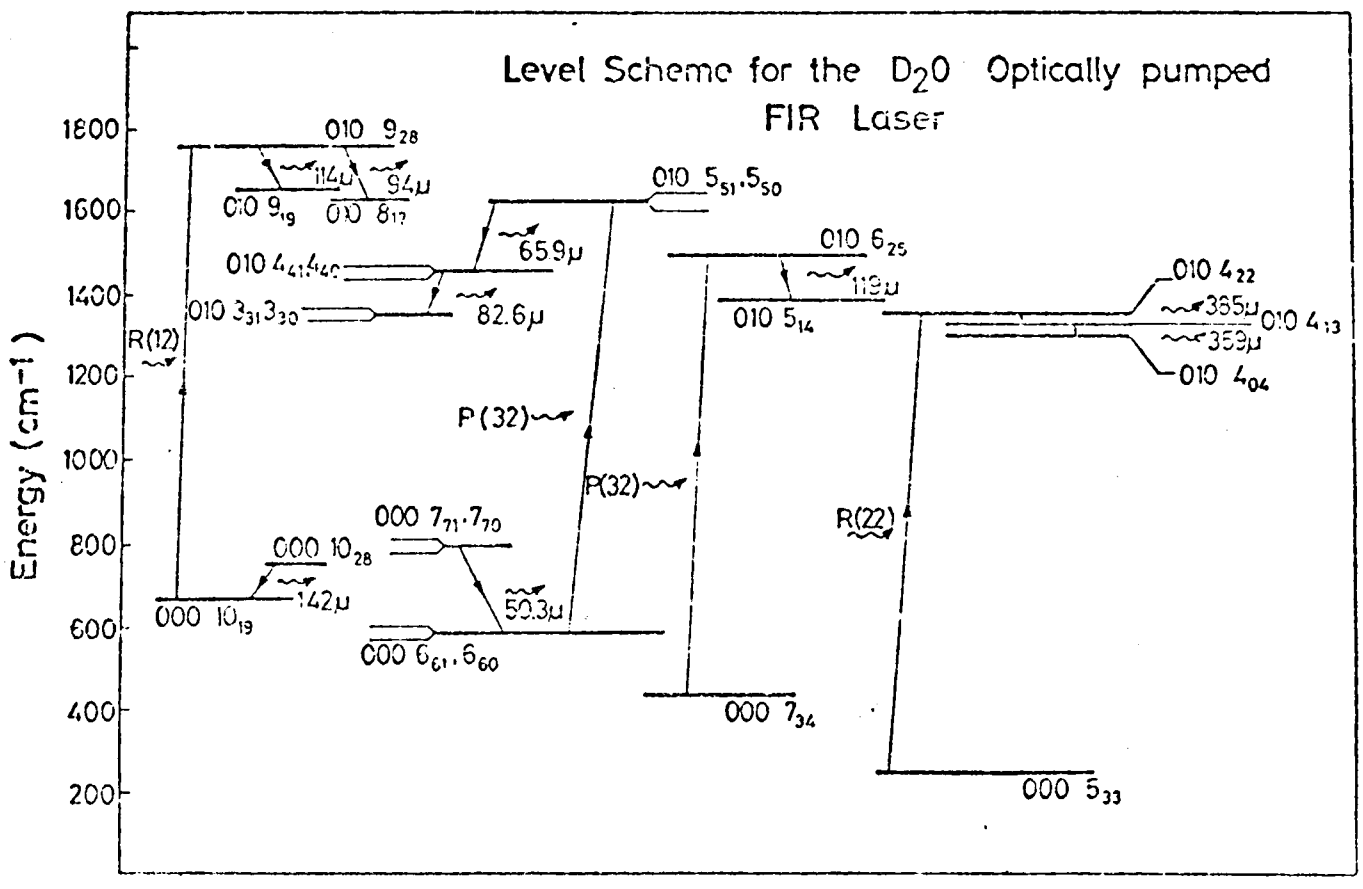


Fig.E.4 Level scheme for the D_2O laser

the notation used for each level is of the form $\nu_1\nu_2\nu_3 J_{K_{-1}K_1}$ where ν_1, ν_2 and ν_3 represent the three vibrational quantum numbers for the normal modes of the D_2O molecule. Not all the CO_2 pump lines used to excite the D_2O molecule are in close coincidence, for example, Table E.1 lists the measured detunings for the CO_2 pump lines used here. In particular, PETUCHOWSKI et al (1977) have recently identified the F I R emission at 65.9 μm and 50.3 μm as arising from stimulated Raman scattering of the P(32) pump line, rather than a molecular absorption followed by an emission in the F I R.

TABLE E.1

Measured Pump Line Detunings for the D_2O F I R LASER

(after PETUCHOWSKI et al, 1977)

CO_2 Pump	D_2O Transition	Detuning $(\nu - \nu_0)$ †
P(32)	$0006_{61},6_{60} \rightarrow 0105_{51},5_{50}$	1.5 GHz
	$0007_{34} \rightarrow 0106_{25}$	-500 MHz
R(12)	$00010_{19} \rightarrow 0109_{28}$	680 MHz
R(22)	$0005_{33} \rightarrow 0104_{22}$	318 MHz

NOTE: † ν = CO_2 pump frequency, and
ν_0 = molecular frequency.

APPENDIX 'F'

THE SPECTROSCOPY OF THE CO_2 LASER

In this appendix we discuss the spectroscopy of the CO_2 laser and the influence of N_2 and He on its behaviour. Fig.F.1 shows a partial energy level diagram for the CO_2 laser, the levels shown in this diagram are those involved in the generation of the 9.6 and 10.6 μm laser emission bands. The CO_2 molecule is a linear symmetric triatomic molecule, the outer atoms being the two oxygen atoms. It has three normal modes of vibration; a symmetric stretching mode, an asymmetric stretching mode and a bending mode. Level A in Fig.F.1 is the vibrational energy level corresponding to the asymmetric stretching mode. In the discharge excited CO_2 laser this is populated by exciting N_2 to its fundamental vibrational state, the energy of this state is very close to that of level A in CO_2 and there is therefore a strong collisional energy transfer between the two species. The inversion created as a result of this selective population of level A can then result in laser emission arising from two alternative transitions, namely A to B_1 (the fundamental symmetric stretching mode) or A to B_2 (the second order bending mode).

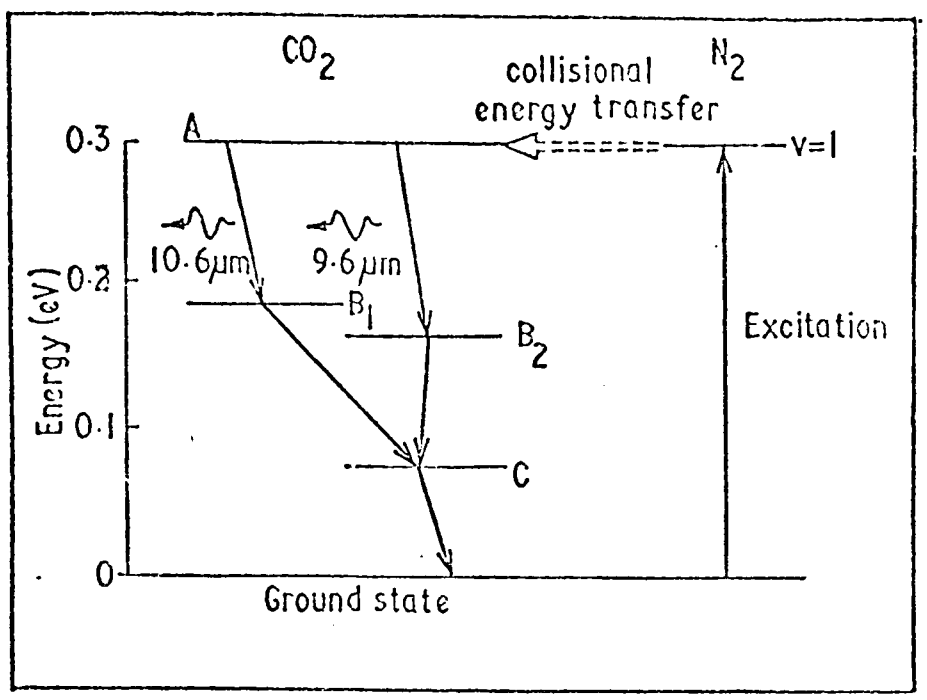


Fig.F.1
Partial energy level diagram to illustrate the operation of the CO_2 laser

Since each vibrational level consists of a large number of rotational levels, the A to B_1 and A to B_2 transitions, result in two broad-bands of laser radiation, which have wavelengths about 10.6 and 9.6 μm respectively. A detailed laser transition diagram for the A to B_2, 9.6 μm, band is shown in Fig.F.2. This band consists of about 50 possible laser transitions with

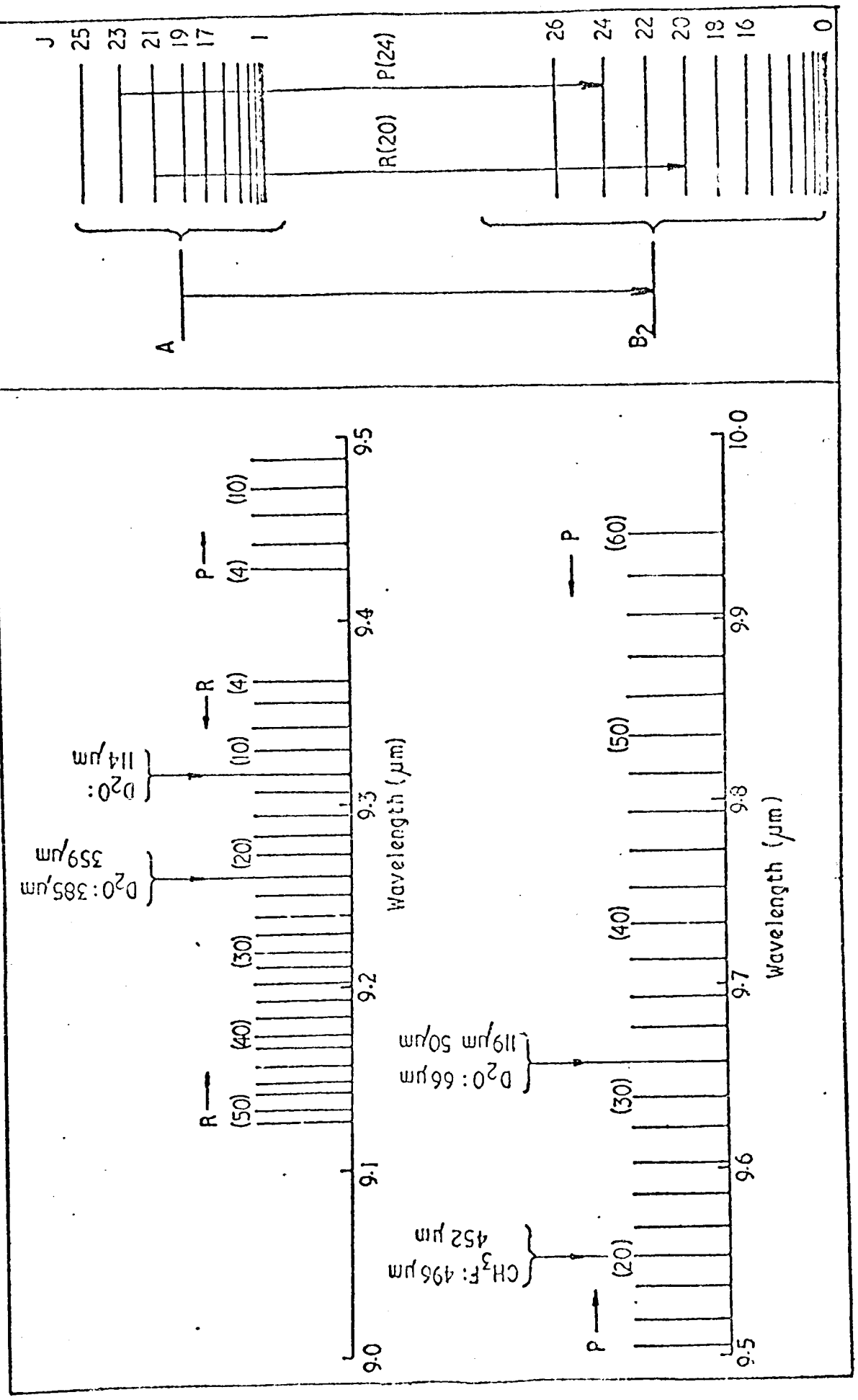


Fig.F.2

Schematic diagram of the 9.6μm emission band of the CO_2 laser. Lines used in the present work are indicated by arrows together with the molecule pumped by them and the FIR wavelengths generated as a result of optical pumping

wavelengths between 9.13 and 9.95 μm. The selection rules for vibrational rotational transitions in the CO_2 molecule are $\Delta J = +1$, giving the so-called P branch transitions; and $\Delta J = -1$, giving the R branch transitions. Individual transitions are denoted by the letter P or R for either branch and include the J value of the lower level. In Fig.F.2, the wavelengths used in the present work are indicated by arrows. The A to B_1 band centred around 10.6 μm has a similar number of transitions to the 9.6 μm band, so that in total there are about 100 possible CO_2 laser emissions between 9 and 11 μm. In order to select a particular wavelength component it is therefore necessary to use a frequency selective device in the laser cavity, such as a diffraction grating, with a resolution of better than 10^3.

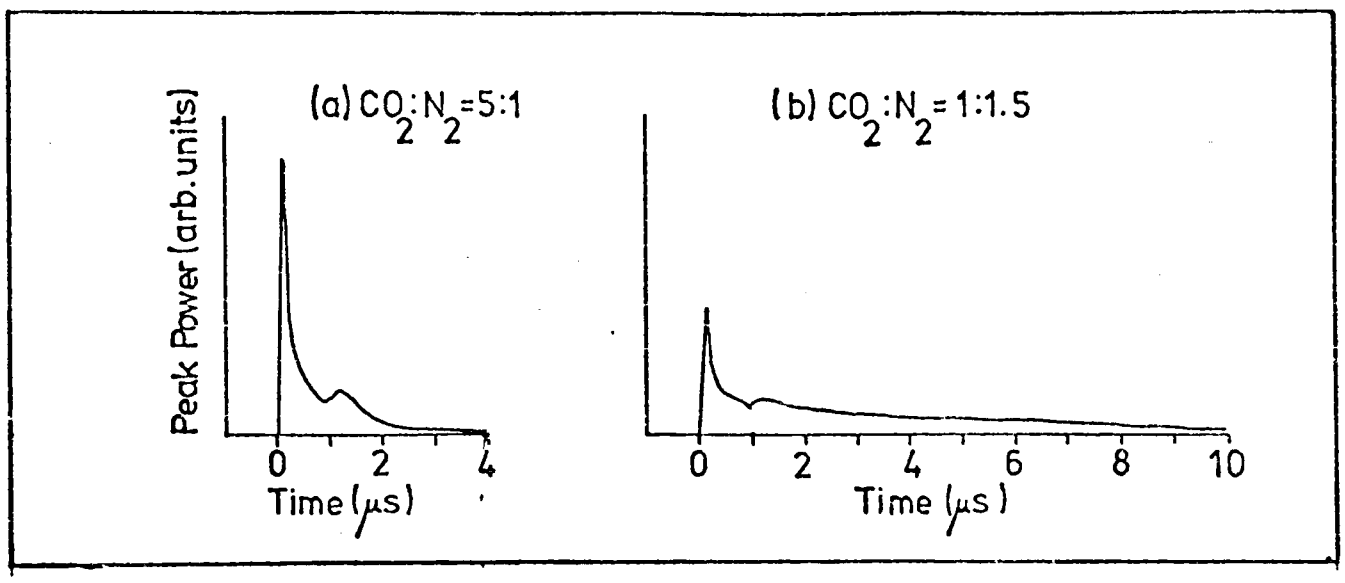


Fig.F.3
CO_2 pulse shape for (a) $CO_2:N_2$ = 5.1; (b) $CO_2:N_2$= 1:1.5

The CO_2 laser pulse shape (see for example, Fig.3.5) consists of a gain switched spike (of about 60 ns FWHM) and a long (~ μs) tail, which is due largely to the presence of N_2 in the laser medium (GILBERT et al, 1972). The N_2 gas behaves as an energy store which refills level A of the CO_2 molecule as it is depleted as a result of the laser action. Thus by removing the N_2 from the laser medium, the tail will vanish, as shown in Fig.F.3.

Finally, He is added to the laser medium in order to increase the thermal conductivity and hence to depopulate levels B_1 and B_2 of the CO_2 molecule. By depopulating these levels He helps to maintain the population inversion between level A, and levels B_1 and B_2.

REFERENCES

ALCOCK, A.J., CORKUM, P.B. and JAMES, D.J., Appl. Phys. Lett., 30, 148 (1977).

ANAN'EV, Yu.A. and SHERSTOBITOV, V.E., Soviet Phys. Tech. Phys., 18. 640 (1974).

ANDERSON, P.W., Phys. Rev., 76, 647 (1949).

AVIZONIS P.V. and GROTBECK, R.L., J. Appl. Phys., 37, 687 (1966).

BEAULIEU, J.A., Proc. of the IEEE, 59, 667 (1971).

BELLMAN, R., BIRNBAUM, G. and WAGNER, W., J. Appl. Phys., 34, 780 (1963).

BERRY, L.A., BUSH, C.E., CALLEN, J.D. and others, Proc. 6th Int. Conf. on Plasma Physics and Controlled Nuclear Fusion Research, Berchtesgaden, 1976, Paper CN 35/A4/1.

BLOEMBERGEN, N., Phys Rev., 104 324 (1956)

BLUYSSEN, H.J.A., McINTOSH, R.E., van ETTEGER, A.F. and WYDER, P., IEEE J. Quant. Elect., QE-11, 341 (1975).

BOYD, G.D. and KOGELNIK, H., Bell Systems Tech. J., 41, 1347 (1962).

BROSSIER, P. and BLANKEN, R.A., IEEE Trans. Microwave Theory and Tech., MTT-22, 1053 (1974).

BROSSIER, P., COSTLEY, A.E., KOMM, D.S., RAMPONI, G. and TAMOR, S., 6th Int. Conf. on Plasma Physics and Controlled Nuclear Fusion Research, Berchtesgaden, 1976, Paper CN 35/A13-2.

BROWN, F. and COHN, D.R., IEEE Trans. Microwave Theory and Tech., MTT-22, 1112 (1974).

BROWN, F., HISLOP, P.D. and KRONHEIM, S.R., Appl. Phys. Lett., 28, 654 (1976).

BROWN, F., HISLOP, P.D. and TURPINIAN, J.O., 2nd Int. Conf. on Submillimetre Waves, San Juan, 1976, Also IEEE J. Quant. Elect., QE-13, 445 (1977).

BROWN, F., HORMAN, S.R., PALEVSKY, A. and BUTTON, K.J., Optics Comm., 9, 28 (1973).

BROWN, F., KRONHEIM, S. and SILVER, E., Appl. Phys. Lett., 25, 394 (1974).

CHANG, T.Y., IEEE Trans. Microwave Theory and Tech., MTT-22, 983 (1974).

CHANG, T.Y., IEEE J. Quantum. Elect., (to be published) (1977).

CHANG, T.Y. and BRIDGES, T.J., Optics Comm., 1, 423 (1970).

CHANG, T.Y. and McGEE, J.D., Appl. Phys. Lett., 29, 725 (1976).

CHANG, T.Y., WANG, C.H. and CHEO, P.K., Appl. Phys. Lett., 15, 157 (1969).

COHN, D.R., FUSE, T., BUTTON, K.J., LAX, B. and DROZDOWICZ, Z., Appl. Phys. Lett., 27, 280 (1975).

CORKUM, P.B., ALCOCK, A.J., JAMES, D.J., ANDREWS, K.J., LEOPOLD, K.E., ROLLIN, D.F. and SAMSON, J.C., 4th Workshop on Laser Interactions and Related Plasma Phenomena, Troy, New York, 1976.

COSTLEY, A.E., BROSSIER, P. and HASTIE, R.J., Workshop on Diagnostics and Data Acquisition for JET, Fontenay-aux-Roses, 1975. Paper E 23.

CROCKER, A., GEBBIE, H.A., KIMMITT, M.F. and MATHIAS, L.E.S., Nature, London, 201, 250 (1964).

DAVIS, J.I. and SOOY, W.R., Appl. Optics, 3, 715 (1964).

DeSILVA, A.W. and GOLDENBAUM, G.C., 'Methods of Experimental Physics', 9A, (Edited by L. Morton), Academic Press, New York, 1970, Chpt.3.

DeTEMPLE, T.A., PLANT, T.K. and COLEMAN, P.D., Appl. Phys. Lett., 22, 644 (1973).

DICKE, R.H., Phys. Rev., 93, 99 (1954).

DROZDOWICZ, Z., TEMKIN, R.J., BUTTON, K.J. and COHN, D.R., Appl. Phys. Lett., 28, 328 (1976).

DULEY, W.W., 'CO_2 Lasers - Effects and Applications', Academic Press, New York (1976).

DUMANCHIN, R., MICHON, M., FARCY, J.C., BOUDINET, G. and ROCCA-SERRA, J., IEEE J. Quant. Elect., QE-8, 163 (1972).

EVANS, D.E. and KATZENSTEIN, J., Rep. Prog. Phys., 32, 207 (1969).

EVANS, D.E., SHARP, L.E., JAMES, B.W. and PEEBLES, W.A., Appl. Phys. Lett., 26. 630 (1975).

EVANS, D.E., SHARP, L.E., PEEBLES, W.A. and TAYLOR, G., Optics Comm., 18, 479 (1976).

EVANS, D.E., SHARP, L.E., PEEBLES, W.A. and TAYLOR, G., IEEE J. Quant. Elect., QE-13, 54 (1977).

EVANS, D.E. and YEOMAN, M.L., Phys. Rev. Lett., 33, 76 (1974).

FETTERMAN, H.R., SCHLOSSBERG, H.R. and PARKER, C.D., Appl. Phys. Lett., 23, 684 (1973).

FETTERMAN, H.R., SCHLOSSBERG, H.R. and WALDMAN, J., Optics Comm., 6, 156 (1972).

FOSTER, H., Optics and Laser Tech., 121, June 1972.

FOX, L., 'Numerical Solution of Ordinary and Partial Differential Equations', Pergamon, Oxford, 1962.

FRANTZ, L.M. and NODVIK, J.S., J. Appl. Phys., 34, 2346 (1963).

FREUND, S.M., DUXBURY, G., RÖMHELD, M., TIEDJE, J.T. and OKA, T., J. Mol. Spectroscopy, 52, 38 (1974).

GALLAGHER, J.J., BLUE, M.D., BEAN, B. and PERKOWITZ, S., Infrared Phys., 17, 43 (1977).

GEBBIE, H.A., Stone, N.W.B. and FINDLAY, F.D., Nature, London, 202, 685 (1964).

GIBSON, A.F., KIMMITT, M.F. and WALKER, A.C., Appl. Phys. Lett., 17, 75 (1970).

GILBERT, J., LACHAMBRE, J.L., RHEAULT, F. and FORTIN, R., Canadian J. Phys., 50, 2523 (1972).

HACKER, M.P., DROZDOWICZ, Z., COHN, D.R., ISOBE, K. and TEMKIN, R.J., Phys. Letts., 57A, 328 (1976).

HERTZBERG, G., 'Infrared and Raman Spectra', van Nostrand, New York, 1945.

INCUSCIO, M., MINGUZZI, P. and STURMIA, F., Infrared Phys., 16, 453 (1976).

IZATT, J.R. and BUDHIRAJA, C.J., Physics in Canada, 31, 19 (1975).

JACQUINOT, P., Rep. Prog. Phys., 23, 268 (1960).

JASSBY, D.L., COHN, D.R., LAX, B. and HALVERSON, W., Nucl. Fusion, 14, 745 (1974).

JUDD, O. "High Power Gas Lasers 1975" (edited by E.R. Pike) page 47, I O P conference Series 29,, 1975.

KEILMANN, F., SHEFFIELD, R.L., LEITE, J.R.R., FELD, M.S. and JAVAN, A., Appl. Phys. Lett., 26, 19 (1975).

KOGELNIK, H., 'Lasers: A Series of Advances', (edited by A.K. Levine), 1, 330 (1966).

LAX, B. and COHN, D.R., Trans. Microwave Theory and Tech., MTT-22, 1049 (1974).

LIN, C.L. and SHAW, J.H., 31st Symposium on Molecular Spectroscopy, Columbus, Ohio, 1976, Paper FC 10.

LIPTON, K., NICHOLSON, J.P. and ILLINGWORTH, R., Optics Comm., 21, 42 (1977).

LITTLE, V.I., SELDEN, A.C. and STAMATAKIS, T., J. Appl. Phys., 47, 1295 (1976).

MacGILLIVRAY, J.C. and FELD, M.S., Phys. Rev., A14, 1169 (1976).

MAGYAR, G., Optics Comm., 20, 271 (1977).

MOORE, W.J., 'One Hundred Micron Detector Development Program', Cornell University, Centre for Radio Physics and Space Research Report, CRSR 642, (1976).

MOORE, W.J. and SHENKER, H., Infrared Phys., 5, 99 (1965).

PANOCK, R. and TEMKIN, R.J., I E E E J. Quant. Elect., QE-13, 425 (1977).

PANTELL, R.H. and PUTHOFF, H.E., 'Fundamentals of Quantum Electronics', Wiley, New York, 1969.

PETUCHOWSKI, S.J., ROSENBERG, A.T. and DeTEMPLE, T.A., I E E E J. Quant. Elect., QE-13, 476 (1977).

PLANT, T.K., NEWMAN, L.A., DANIELEWICZ, E.J., DeTEMPLE, T.A. and COLMAN, P.D., I E E E Trans. Microwave Theory and Tech., MTT-22, 988 (1974).

RENK, K.F. and GENZEL, L., Appl. Optics, 1, 643 (1962).

ROSENBLUH, M., TEMKIN, R.J. and BUTTON, K.J., Appl. Opt., 15, 2635 (1976).

SEMET, A. and LUHMANN, Jr., N.C., Appl. Phys. Lett., 28, 659 (1976).

SEMET, A., OBENSCHAIN, S. and LUHMANN, Jr., N.C., Infrared Phys., 16, 189 (1976).

SHARP, L.E., PEEBLES, W.A., JAMES, B.W. and EVANS, D.E., Optics Comm., 14, 215 (1975).

SHARP, L.E. and WETHERALL, A.T., Appl. Optics, 11, 1737 (1972).

SHEFFIELD, J., 'Plasma Scattering of Electromagnetic Waves', Academic Press, New York, 1975.

SHIMODA, K. and SHIMIZU, T., 'Nonlinear Spectroscopy of Molecules', Progress in Quantum Electronics, 2, Pergamon Press, Oxford, 1972.

SIEGMAN, A.E., Laser Focus, 7, 42 (1971a).

SIEGMAN , A.E., 'An Introduction to Lasers and Masers', McGraw-Hill, New York, 1971b.

SMITH, W.L. and MILLS, I.M., J. Mol. Spect., 11, 11 (1963).

SMITH, P.W., I E E E J. Quant. Elect., QE-1, 343 (1965).

STAMATAKIS, T., Private Communication, (1977).

STAMATAKIS, T. and SELDEN, A.C., Phys. Letts., 58A, 221 (1976).

TEMKIN, R.J., I E E E J. Quant. Elect., QE-13, 450 (1977).

TEMKIN, R.J. and COHN, D.R., Optics Comm., 16, 213 (1976).

TEMKIN, R.J., COHN, D.R. and DROZDOWICZ, Z., Optics Comm., 14, 314 (1975).

T F R Group, Proc. 6th Int. Conf. on Plasma Physics and Controlled Nuclear Fusion Research, Berchtesgaden, 1976, Paper CN 35/A3.

TOWNES, C.H. and SHAWLOW, A.L., 'Microwave Spectroscopy', McGraw-Hill, New York, 1955.

TUCKER, J.R., Optics Comm., 16, 209 (1976).

ULRICH, R., Infrared Phys., 7, 37 (1967).

WIGGINS, J., DROZDOWICZ, Z. and TEMKIN, R.J. (To be published), (1977).

WILLET, C.S. and GLEASON, T.J., Laser Focus, 7, 30 (1971).

WILLIAMSON, J.G., Ph.D. Thesis, Ohio State University, (1969) (Available from: University Microfilm Inc., Ann Arbor, Michigan).

WOSKOBOINIKOW, P., DROZDOWICZ, Z., ISOBE, K., COHN, D.R. and TEMKIN, R.J., Phys. Lett., 59A, 264 (1976).

YAMANAKA, M., The Review of Laser Engineering, 3, 253 (1976).

YARIV, A., 'Quantum Electronics', Wiley, New York, 1967.